IMPERIAL

IMPERIAL COLLEGE LONDON
DEPARTMENT OF MECHANICAL ENGINEERING

Sensorimotor Control of Stability–Movement Transitions: Impedance Control Dynamics at the Human Wrist

Nathan Steadman

November 2024

Supervised by:
Dr. Shlomi Haar
Professor Ravi Vaidyanathan
Professor Huiling Tan

Submitted in part fulfilment of the requirements for the degree of Doctor of Philosophy in Neurotechnology of Imperial College London.

Abstract

Mechanical impedance is central to human motor control, supporting postural stability, movement, and adaptation to uncertainty. In healthy motor behaviour it is usually treated as a brief corrective response, while persistence across motor contexts is mainly discussed in pathology. It therefore remains unclear whether impedance in unimpaired motor control is purely transient or can persist as an enduring control state between stabilisation and movement. There is also limited knowledge of the neural correlates, as most evidence is similarly derived in the context of clinical impairments such as Parkinson's disease. This thesis addresses these gaps through a unified framework examining impedance across stability–movement transitions, integrating behavioural, muscular, and beta-band neural dynamics.

Using a robotic wrist manipulandum, impedance was elevated through stabilisation challenges altered in temporal predictability and perturbation amplitude. During stabilisation, impedance rapidly increased beyond passive mechanics and remained stable, indicating early formation of a stabilising control state. Changes in temporal predictability influenced impedance more than amplitude manipulations: uncertain scheduling of perturbations induced greater muscle co-contraction and importantly, this stabilisation-related impedance carried forward into voluntary movement, biasing movement dynamics and motor activity.

Neural analyses revealed strong suppression of beta-band corticomuscular coherence during stabilisation, with beta dynamics tracking stabilising demands and inversely coupling with passive stiffness, linking corticospinal activity to mechanical compliance. Post movement beta rebound showed context-dependent updating, with suppression following uncertain stabilisation. Passive stiffness assessments showed that changes in temporal predictability produced small but reliable shifts in stiffness persisting beyond task completion, whereas amplitude manipulations did not. Extending this analysis to Parkinson's disease demonstrated quantified passive stiffness correlated with clinician-rated rigidity, supporting translational relevance.

Together, these findings provide evidence that impedance regulation in healthy motor control is not purely transient but a context-sensitive motor state persisting across task boundaries, sensitive to changes in temporal predictability, but not mechanical load.

Statement of Originality

I hereby declare that this thesis represents my own original work, conducted as part of my PhD programme in Neurotechnology at Imperial College London. It has not previously been submitted, in whole or in part, for any degree or qualification at this or any other institution. All materials not original to this thesis have been appropriately referenced.

I confirm that I have read the University's current research ethics policy and have exercised due diligence to ensure full adherence to the relevant specifications and guidelines.

Copyright Notice

Acknowledgements

I would like to express my deepest gratitude to my supervisors - Professor Vaidyanathan, Professor Tan and Dr. Haar - for their unwavering support, guidance, and understanding throughout the extended duration of this doctoral program. Their encouragement has been invaluable to the completion of this work. I am also sincerely grateful to Dr Thomas Martineau for his essential contributions in bringing the first robotic device to operational success. Special thanks go to Cosima Graef, Jenna Yun, Emma Burroughs, and Dr. Yen Tai for their assistance with data collection and clinical assessments, which were critical to the project. Lastly, I extend my thanks to Dr. Uri Rosenblum Belzer for his critical feedback and editorial support during the final stages of writing, which greatly improved the clarity of this dissertation.

Table of Contents

Nomenclature

Acronym	Meaning
B-CMC	beta corticomuscular coherence
CCI	co-contraction indices
CMC	corticomuscular coherence
EEG	electroencephalography
EMG	electromyography
FE	flexion/extension
GPe	globus pallidus externa
GPi	globus pallidus interna
IMU	inertial measurement unit
M1	primary motor cortex
LBs	Lewy’s bodies
LLSR	long-latency stretch reflex
LNs	Lewy’s neurites
MRBD	movement-related beta desynchronisation
MVF	maximum voluntary force
PD	Parkinson's disease
PLV	phase-locking value
PMBR	post movement beta rebound
PMC	premotor cortex
PNS	peripheral nervous system
RMSE	root mean square error
ROM	range of motion
RT	reaction time
S1	primary somatosensory cortex
SCBG	sensorimotor cortical-basal ganglia
SD	standard deviation
SNc	substantia nigra pars compacta
SNr	substantia nigra pars reticula
SPS	stiff-person syndrome
STN	subthalamic nucleus
UPDRS	Unified Parkinson's disease rating scale

List of Figures

List of Tables

I. Introduction

1.1. Background

Human movement arises from the continuous interaction between the nervous system and the mechanical properties of the musculoskeletal system. A key feature for understanding this interaction is mechanical impedance, which describes how a joint responds to external forces through the combined effects of stiffness, damping, and inertia [1]. Impedance is not a fixed property of the limb; rather, it is dynamically regulated by the sensorimotor system to balance the competing demands of stability and mobility in unpredictable environments [2], [3], [4]. Through selective modulation of muscle activation - particularly the co-contraction of antagonist muscle pairs - the sensorimotor system adjusts joint impedance to resist disturbances while maintaining the flexibility needed for accurate voluntary movement [5], [6], [7].

Although passive muscle-tendon properties contribute to baseline impedance [8], [9], functional modulation is driven primarily by neural processes [10], [11]. Co-contraction elevates both the resistive and dissipative components of impedance, increasing robustness to perturbations and shaping the joint's dynamic response to external loads [12], [13], [14]. This capacity for flexible impedance regulation is essential for a wide range of everyday behaviours, including maintaining posture on public transport, coping with the instability inherent in contact sports, and performing skilled tool use that requires rapid transitions between stability and movement.

Research on impedance control has historically followed two major trajectories. In upper-limb motor control, impedance is typically examined as a task-dependent, rapidly modulated quantity, often assessed using visuospatial or force-field paradigms that reveal how endpoint impedance adapts during movement or learning [15], [16]. These studies show that humans proactively tune impedance through predictive (feedforward) mechanisms and refine it through sensory feedback based on changing uncertainty or task goals [3], [17], [18]. In contrast, lower-limb research often conceptualises impedance as a baseline or phasic property essential for balance control and gait stability, modulating primarily across postural conditions or gait cycles [19], [20], [21]. Together, these bodies of work underscore the importance of impedance regulation but also reflect differences in theoretical emphasis and experimental approach.

A particularly important functional challenge is the stability–movement trade-off. Many natural behaviours require the maintenance of elevated impedance while simultaneously preserving readiness for rapid, precise movement. These contexts demand not only the up-regulation of impedance but also the ability to release or reconfigure it efficiently as task demands shift. Despite the clear relevance of such transitions, the underlying sensorimotor mechanisms and the temporal dynamics through which impedance is sustained or reversed remain incompletely understood.

Insights into prolonged or maladaptive high-impedance states have come primarily from clinical populations, especially individuals with Parkinson's disease (PD). PD rigidity reflects a persistent elevation of muscle tone and an impaired capacity for impedance modulation [22], [23], [24], associated with excessive beta-band (13-30 Hz) neural oscillations and altered interactions across cortical and subcortical circuits [25], [26], [27], [28]. While such findings provide clues about neural substrates of impedance regulation, they cannot fully explain how impedance is adaptively modulated in healthy individuals, particularly over short timescales and during transitions between stability- and movement-oriented states.

A clearer understanding of these short-term dynamics is necessary to characterise how the healthy sensorimotor system flexibly manages stability demands while enabling voluntary action. This context motivates the questions addressed in the present work.

1.2. Motivation

In the study of human sensorimotor control, the idea that impedance modulation may involve a persistent motor set remains conceptually important yet insufficiently explored. Mechanical and behavioural aspects of impedance control have been extensively documented, particularly in tasks involving posture, perturbation resistance, or skilled movement [14], [20], [29], [30]. However, the neural processes that support these impedance changes - especially their short-term persistence - remain poorly understood. While several studies suggest that optimal joint impedance can be learned to compensate for stability-demanding tasks [3], [17], [31], the field lacks a unified framework describing the underlying sensorimotor mechanisms, time course, or functional significance of this effect. Unlike the well-established neural models for short-term adaptation in kinematics or force-field learning [17], [32], [33], impedance carryover lacks clear neural markers, standardised terminology, and validated computational accounts. As a result, it remains unresolved whether short-term persistence of impedance may reflect residual neural drive, task-set inertia or an active control strategy for maintaining robustness. This gap limits our understanding of how the sensorimotor system shifts between stability-oriented and movement-oriented control states.

A paradigm that first challenges upper-limb postural stability and then requires voluntary movement offers a powerful way to probe this stability–movement transition. During postural stabilisation under unstable forces, the sensorimotor system typically increases co-contraction, reflex gains, and overall impedance to ensure stability [34], [35]. When the task then demands precise, fluid movement, the system must rapidly reduce this heightened impedance to allow efficient action. By sequencing a stability-demanding phase immediately before a movement phase, the design can reveal whether impedance persists as a form of short-term motor adaptation, how effectively the system down-regulates impedance, and whether this transition incurs measurable behavioural costs such as slower reaction times or reduced movement accuracy. Critically, such a paradigm allows examination of neural correlates of impedance modulation, enabling us to ask whether known neural signatures such as sensorimotor beta-band activity track the rise, persistence, and release of impedance across changing task demands. This is a major gap in current research: mechanical impedance has been measured extensively, but the neural dynamics that govern its regulation remain largely uncharacterised.

Bridging this gap is especially important in the context of Parkinson's disease (PD), where impaired transitions between stability and movement [36], [37], elevated beta activity [25], [26], [38], and excessive rigidity [22], [39] are defining clinical features. Despite significant progress in understanding basal ganglia dysfunction [25], [40], [41] and motor execution deficits [42], [43], [44], the mechanisms underlying persistent or context-inappropriate impedance remain poorly explained. Investigating how the healthy sensorimotor system regulates, retains, and releases impedance - and identifying the neural signals associated with these transitions - may clarify why individuals with PD struggle to disengage from high-impedance states, contributing to rigidity, bradykinesia, and movement hesitation. Beyond clinical relevance, this work has broader implications for rehabilitation, where retraining flexible impedance modulation could improve functional mobility, and for prosthetic and exoskeletal device design, where accounting for impedance carryover may facilitate more natural transitions between stability and movement. More generally, a deeper understanding of short-term impedance dynamics may inform the development of adaptive robotic and therapeutic systems that mirror the flexibility of healthy human sensorimotor control. Recent advances in neural recording, wearable sensing, and quantitative motor assessment now make it possible to measure and model these subtle transitions with unprecedented resolution, providing a timely opportunity for the present research.

1.3. Aims and Objectives

1.3.1. Introduction

This thesis aims to characterise the sensorimotor mechanisms that regulate stability–movement transitions, with particular emphasis on the short-term persistence of impedance following externally imposed stability demands. Although the mechanical properties of impedance control have been extensively studied, the neural correlates, temporal dynamics and adaptive processes that support transitions between competing motor control states remain poorly understood. This thesis addresses these gaps by integrating behavioural, muscular, and neural measurements within a novel motor control paradigm that alternates between stability-oriented and movement-oriented task goals.

1.3.2. Research Question 1: Persistence and Functional Role of Impedance

To what extent does impedance modulation induced by externally imposed stability demands persist across transitions into voluntary movement, and does this persistence facilitate movement preparation or interfere with movement execution?

It is hypothesised that impedance induced by externally imposed stability demands persists into subsequent voluntary movement, scaling with the level of complexity or challenge imposed. This persistence is predicted to manifest as elevated joint impedance and muscle co-contraction during stabilisation and to impair subsequent movement efficiency. This work is novel in directly testing impedance persistence across stability–movement transitions, rather than within isolated tasks, and aims to link motor and behavioural findings to clinically relevant phenomena, including rigidity and impaired movement initiation in Parkinson's disease.

1.3.3. Research Question 2: Neural Signatures of Impedance State Transitions

Do sensorimotor beta-band dynamics reliably index the rise, persistence, and release of impedance during transitions between stability-oriented and movement-oriented control states?

It is hypothesised that sensorimotor beta-band activity tracks impedance control state maintenance, with elevated beta accompanying stabilisation and sustained beta reflecting persistence of impedance during transitions to voluntary movement. Beta power is predicted to decrease as impedance is released and movement-oriented control is engaged. This approach presents a targeted evaluation of beta activity as a marker of control-state persistence across task transitions, offering insight into pathological beta synchronisation and impaired motor state switching in Parkinson's disease.

1.3.4. Research Question 3: Adaptation and Flexibility of Impedance Control

How does repeated exposure to variable perturbation dynamics shape the adaptation of impedance control, sensorimotor beta activity, and movement performance across stability–movement transitions?

Repeated exposure to variable perturbations is hypothesised to reduce impedance persistence and accelerate beta-band release during voluntary movement, reflecting refined control-state transitions accompanied by optimised muscle activation and improved movement performance. This work targets learning at stability–movement transitions, exploring the sensorimotor dynamics underlying these transitions and their refinement through practice.

1.3.5. Aim 1: Quantify short-term impedance control dynamics under externally imposed stability demands and under incentives to voluntary movement

To determine whether impedance modulation related to resisting perturbations of different amplitudes and dynamics persist across stability–movement transitions.

Objectives:

A. Quantify impedance modulation when stabilising the wrist against perturbation schedules of differing amplitudes and temporal predictability through behavioural and motor responses.

B. Assess the behavioural and motor activity during voluntary reaching movements following challenges to the postural stability of the wrist.

C. Evaluate impedance control dynamics across stability–movement transitions and whether impedance persists, either as a preparatory mechanism or as a maladaptive residual response, during voluntary movement.

1.3.6. Aim 2: Identify neural signatures underlying the rise, persistence, and release of impedance across stability–movement transitions

To evaluate whether sensorimotor beta-band (13–30 Hz) activity serves as a reliable biomarker of impedance control dynamics as task incentives for motor performance change.

Objectives:

A. Quantify beta-band activity during challenges to postural stability of the wrist and subsequent voluntary movement.

B. Test for short-term beta modulation, assessing whether beta-band dynamics mirror impedance-related behavioural and motor activity during stability–movement transitions.

1.3.7. Aim 3: Examine how impedance control evolves across repeated challenges to postural stability paired with incentives to voluntary movement.

To investigate whether repeated exposure to variable perturbation dynamics leads to systematic adaptation in impedance control, sensorimotor neural activity, or movement performance.

Objectives:

A. Examine beta-band cortical activity, peripheral motor activity, and movement performance around stability–movement transitions for markers of motor adaptation or learning.

B. Examine how changes in task difficulty, driven by variations in perturbation dynamics, shape the sensorimotor system’s ability to adapt across repeated task exposures.

C. Identify behavioural, muscular, and neural predictors of successful or impaired transitions, providing insight into mechanisms that enable or limit sensorimotor flexibility.

1.3.8. Aim 4: Advance an integrative understanding of how interactions between muscular, neural and adaptive dynamics modulate impedance around stability–movement transitions.

To study baseline and experimentally manipulated impedance control in healthy individuals, both as a fundamental feature of intact motor control and as a comparative model for clinical deficits such as those seen in Parkinson's disease.

Objectives:

A. Develop a provisional conceptual framework describing how the sensorimotor system modulates, maintains, and releases impedance during transitions between stability- and movement-oriented control states.

B. Contrast the neural, motor, and behavioural dynamics observed with current clinical understanding of how these features relate to impaired impedance control in Parkinson's disease.

1.3.9. Aim 5: Develop a high-performance robotic experimental architecture capable of precisely manipulating and quantifying neural, motor, and behavioural dynamics

To support the detailed exploration of impedance control dynamics that underlie transitions between stability-oriented and movement-oriented motor states.

Objectives:

A. Develop a one degree-of-freedom (1-DOF) robotic manipulandum capable of delivering controlled, variable perturbations and precisely measuring wrist biomechanics.

B. Implement a supporting software and hardware system for recording kinematic, motor, and neural activity while providing automated delivery of an appropriate motor control paradigm.

C. Explore the diagnostic potential of the platform by applying it to the assessment of Parkinson's disease symptom severity and evaluating its correlation with established clinician-rated clinical scores.

1.3.10. Summary

The research questions and aims outlined provide a systematic and comprehensive framework for probing how the sensorimotor system modulates impedance across conflicting stability-oriented and movement-oriented motor states, and how transitions between these states are shaped by the degree of challenge during stabilisation. Exploring these dynamics constitutes a novel investigation of a largely unexplored yet fundamental component of healthy motor control. The understanding gained through these aims offers a robust characterisation of how impedance-related processes can be altered in healthy individuals, while also establishing a strong baseline from which to investigate analogous dynamics in conditions marked by impaired impedance regulation, such as Parkinson's disease.

1.4. Scope of the Research

This thesis examines how the human motor system transitions from high-impedance postural control to flexible, goal-directed movement, with an emphasis on the short-term persistence of elevated impedance following stability demands. Specifically, the research investigates whether exposure to upper-limb postural instability induces a transient retention of elevated impedance during subsequent voluntary movement, how the dynamics of this instability impact movement execution, and how these processes manifest in associated sensorimotor activation. The work further aims to characterise individual differences in this impedance carryover, determine whether its amplitude depends on the intensity and nature of the preceding stability challenge, and evaluate the extent to which this phenomenon reflects adaptive caution versus suboptimal rigidity.

To address these aims, a novel upper-limb motor control experiment was devised that paired controlled perturbation-based postural tasks with spontaneous incentives to voluntary movement requiring precision, speed, and energetic efficiency. Through this targeted approach, the thesis seeks to define the temporal dynamics and behavioural consequences of short-term impedance retention and to establish empirical foundations for understanding flexible impedance control in human motor control.

In addition to the primary studies conducted with healthy participants, a limited investigation involving individuals with Parkinson's disease is included to explore how the technological infrastructure developed could be utilised for clinical diagnostics. While the thesis incorporates modelling of neural mechanisms and comparative analyses, it does not aim to capture all facets of sensorimotor adaptation, fatigue, or whole-body coordination. Its scope remains focused on the behavioural, sensorimotor and computational principles that govern short-term impedance control and its role in stability–movement transitions.

1.5. Thesis Contributions

1.5.1. Establishing Impedance as a Persistent Sensorimotor Control State

This thesis provides novel evidence that impedance is not confined to online stabilisation or reactive responses but constitutes a persistent sensorimotor control state that spans stabilisation, voluntary movement, and subsequent passive contexts. By demonstrating measurable carryover across the stability–movement transition and into passive limb mechanics, the work extends impedance research beyond within-task dynamics to temporally extended motor states.

1.5.2. Demonstrating that Temporal Predictability Dominates Impedance Regulation

A key original contribution is the demonstration that temporal predictability, rather than perturbation amplitude, governs the engagement, persistence, and release of impedance across both active and passive contexts. These finding challenge force-scaling and gain-scheduling accounts of impedance control and instead positions uncertainty and task structure as primary determinants of how impedance-related control states are organised.

1.5.3. Introducing Passive Stiffness as a Marker of Sustained Sensorimotor State

The thesis introduces passive robotic assessment as a novel methodological approach for isolating sustained impedance-related effects from active control. Passive stiffness was shown to reflect retained sensorimotor configuration rather than residual mechanics or tonic muscle activation, revealing state-dependent mechanical effects that were not detectable from active behaviour alone.

1.5.4. Dissociating Mechanical Impedance from Muscular Co-Contraction

The work provides new mechanistic insight by showing that sustained changes in stiffness are not trivially explained by antagonist co-contraction. Co-contraction primarily reflected load-dependent activation, whereas impedance persistence was shaped by temporal structure. This dissociation refines current interpretations of impedance control and clarifies the distinct roles of muscular activation and mechanical state.

1.5.5. Identifying Beta-Band Corticomuscular Coherence as a Neural Index of Impedance State

A novel neural contribution of the thesis is the identification of a robust inverse relationship between beta-band corticomuscular coherence (β-CMC) and mechanical stiffness across task phases and contexts. This positions β-CMC as a neural marker of impedance-related control state rather than a proxy for force output or tonic muscle activation, extending the interpretation of beta dynamics beyond movement execution.

1.5.6. Providing Preliminary Translational Evidence for Objective Rigidity Assessment

Finally, the thesis offers proof-of-concept evidence that passive stiffness measures align with clinician-rated rigidity in Parkinson's disease, particularly in flexion. While exploratory, this represents a novel step toward objective, continuous quantification of rigidity, demonstrating the translational potential of impedance-based metrics derived from controlled robotic assessment.

1.6. Publications

Steadman, Nathan, et al. "Muscle Co-Contraction of the Forearm Is Increased in Response to Temporal Uncertainty During a Dynamic Stabilization Task." *2025 47th Annual International Conference of the IEEE Engineering in Medicine and Biology Society (EMBC)-Proceedings*. Vol. 2025. Institute of Electrical and Electronics Engineers (IEEE), 2025.

1.7. Thesis Structure

Chapter 2 – Literature Review provides a critical examination of relevant literature in the areas of motor control, Parkinson's Disease and robotics research. This analysis serves to contextualise the significance of the research conducted.

Chapter 3 – Robotic Development presents an overview of the robotic architecture developed for this thesis, detailing the software integrations necessary to replicate the investigative approach and highlighting the critical mechanical and software design decisions made during development.

Chapter 4 – Sensorimotor Modulation of the Stability–Movement Transition in Healthy Motor Control presents the central findings of this thesis through an investigation of how the sensorimotor system manages stability–movement transitions in healthy motor control. Specifically, it explores adaptive impedance regulation, highlighting how motor context, perturbation dynamics and learning processes shape the persistence and modulation of upper-limb impedance between postural stabilisation and voluntary movement.

Chapter 5 – Passive Wrist Stiffness in Healthy Motor Control Following Stability–Movement Transitions and at Baseline in Parkinson's Disease describes the use of the robotic manipulandum to automatically assess wrist stiffness during passive movement. The aim was to develop an automated procedure that replicates clinical assessments of wrist rigidity in Parkinson's disease (PD) and to benchmark this protocol against clinician-provided rigidity ratings. The protocol was also integrated into the main experimental paradigm to determine whether challenges to postural stability induce persistent stiffness changes resembling those observed in PD in healthy participants.

Chapter 6 – Conclusion and Final Remarks evaluates the overall impact of the research presented in this thesis and situates the findings within the current scientific landscape. It synthesises the main results, outlines their theoretical and translational relevance, and discusses how the insights gained can be applied and extended through future research.

II. Literature Review

2.1. Introduction

Understanding how the sensorimotor system regulates transitions between stability and movement requires the integration of insights from biomechanics, neuroscience, motor control theory, and clinical research. Although each of these fields has developed sophisticated models to describe specific aspects of human movement, there remains limited cohesion in how mechanical impedance, neural activity, muscular activation, and behavioural performance are jointly conceptualised. This chapter reviews the interdisciplinary foundations necessary to interpret the experimental and theoretical contributions of this thesis.

The chapter begins by outlining core principles of sensorimotor control, emphasising how neural and muscular processes interact with limb biomechanics to generate and regulate movement. Building on this foundation, mechanical impedance is introduced as a central framework for understanding how the nervous system balances stability and mobility, particularly in environments characterised by uncertainty.

An overview of Parkinson's disease (PD) is then provided, describing the cardinal motor symptoms and framing them in terms of impaired impedance control. A concise summary of PD neuropathology is included to contextualise how these symptoms arise from disruptions to the sensorimotor systems outlined previously. The impact of PD on motor adaptation and learning is also reviewed, highlighting how artificially induced impairments in impedance regulation may mirror these aspects of the clinically impaired state.

Subsequently, the review examines the neural dynamics underlying key behavioural aspects of impedance control and motor learning, with a particular focus on beta-band (13–30 Hz) activity. This section synthesises evidence linking beta oscillations to sensorimotor integration, movement preparation, postural control and the regulation of muscle activation patterns, emphasising their role in maintaining and adapting motor states. Particular attention is given to how beta-band dynamics reflect the balance between stability and flexibility in motor behaviour, how they are modulated by task demands and uncertainty, and how disruptions to these dynamics are associated with impaired motor control and learning.

The review also highlights the growing role of robotic systems in the quantification of motor control, examining how manipulanda and servomotor devices have been used to probe sensorimotor function and how such tools may support future diagnostic and assessment applications. A specific focus is given to prior academic deployments of the robotic manipulanda used in this thesis, with emphasis on how these systems have been used to characterise sensorimotor function in both healthy and clinical populations.

The penultimate section provides an overview of the numerical models of impedance, electromyographic (EMG) co-contraction, and stiffness formulations employed in this thesis. Finally, the review identifies key gaps in the existing literature and defines the research scope of the thesis. Together, these sections establish the conceptual and methodological background for the research presented in this thesis. The literature reviewed here provides the basis for identifying critical gaps in current knowledge, motivating the experimental aims, and informing the interpretation of the results.

2.2. The Sensorimotor Control of Human Movement

2.2.1. Introduction

Human movement arises from the dynamic and continuous interaction of neural, muscular, and biomechanical processes operating across multiple levels of the nervous system. The sensorimotor system comprises interconnected cortical, subcortical, spinal, and peripheral mechanisms that collectively enable the planning, execution, and modulation of both voluntary and involuntary actions. Movement is therefore not the product of a single control centre, but of a distributed network in which perception and action are tightly coupled.

Contemporary perspectives characterise the sensorimotor system not as a purely feedforward controller, but as a closed-loop control architecture that continuously integrates predictive internal models with multisensory feedback. Through this ongoing interplay between expectation and sensory evidence, the system adapts motor output in real time to compensate for internal noise, biomechanical constraints, and environmental uncertainty. Such integration is essential for maintaining postural stability, achieving task-specific goals, and flexibly adjusting behaviour in response to changing contexts. Understanding the principles governing sensorimotor control is thus central to explaining how humans produce robust, adaptive, and goal-directed movement.

2.2.2. The Sensorimotor Motor Cortex and Basal Ganglia

The sensorimotor cortex–basal ganglia (SCBG) network is a primary circuit supporting movement selection, initiation, and regulation [45]. The sensorimotor cortex comprises the primary motor cortex (M1), primary somatosensory cortex (S1), and premotor regions, which together integrate sensory information and generate motor commands [46]. These cortical regions send dense projections to the striatum, the main input nucleus of the basal ganglia, forming the corticostriatal pathways that convey both motor intent and sensorimotor context [47]. Within the basal ganglia, these inputs are integrated and transformed through interactions among the striatum, globus pallidus interna and externa (GPi/GPe), subthalamic nucleus (STN), and substantia nigra pars reticula (SNr) and pars compacta (SNc), modulating activity that is ultimately relayed back to the cortex via the thalamus.

The basal ganglia play a central role in the selection and facilitation of motor programs based on integrated sensorimotor information [45]. They contribute not only to action initiation and suppression but also to motor learning and habit formation, with evidence suggesting cooperative interactions between the dorsal striatum and medial temporal lobe systems during stimulus-response learning [48]. This positions the SCBG network as a critical hub for both flexible goal-directed control and automation of frequently executed actions.

Communication within the SCBG is shaped by three principal pathways [49] (**Figure 2.1**), each with distinct functional consequences:

- The direct pathway reduces inhibitory output from the GPi/SNr to the thalamus, thereby increasing thalamocortical excitation and facilitating movement.
- The indirect pathway increases GPi/SNr inhibition of the thalamus, suppressing thalamocortical drive and inhibiting movement. This pathway contributes to movement termination and the maintenance of existing motor states.
- The hyperdirect pathway provides a fast, monosynaptic cortical projection to the STN, which strongly activates the GPi/SNr and rapidly suppresses thalamocortical signalling. This pathway enables abrupt cancellation or interruption of motor commands.

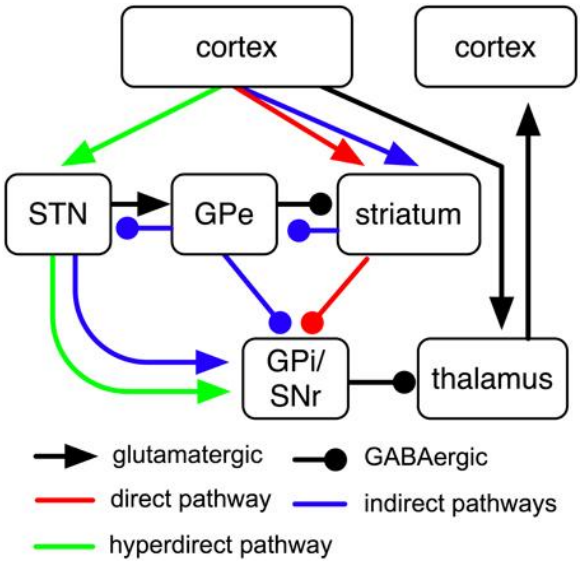

Figure 2.1. Mapping of the pathways in the basal ganglia circuit [50]. Schematic illustrating the direct, indirect, and hyperdirect pathways linking cortex, striatum, globus pallidus, subthalamic nucleus (STN), thalamus, and basal ganglia output nuclei (GPi/SNr). Excitatory glutamatergic and inhibitory GABAergic connections are indicated, highlighting the parallel pathways through which the basal ganglia regulate motor output and action selection.

Together, these pathways implement a dynamic balance of facilitation and inhibition that allows the SCBG network to select appropriate actions, prevent competing or unwanted movements, and adjust to changing task demands.

The SCBG network is also highly relevant to impedance regulation. By shaping motor output and coordinating muscle activation patterns - including co-contraction of antagonist pairs - the basal ganglia contribute to the modulation of joint impedance during both stability maintenance and voluntary movement. Conditions that disrupt SCBG function, such as Parkinson's disease, lead to characteristic impairments in movement initiation, excessive co-contraction, rigidity, and difficulty transitioning between motor states [22], [51], [52]. Understanding the functional organisation of this network is therefore essential for interpreting the neural contributions to impedance control in both healthy and pathological contexts.

At the cortical level, sensorimotor areas (M1, premotor cortex, supplementary motor area) work in concert with basal ganglia and cerebellar circuits to generate, refine, and update motor commands [53]. These descending signals interface with spinal interneurons and reflex pathways, enabling rapid, context-sensitive adjustments of muscle activity. Through this multilayered architecture, the SCBG network ensures that motor actions are appropriately selected, smoothly executed, and modulated according to environmental and internal demands.

2.2.3. Functional Role of Antagonist Muscles in Impedance Regulation

The modulation of joint impedance cannot be understood solely by examining individual muscles in isolation. Most functional movements arise from the coordinated interaction of muscle pairs, particularly antagonist muscles that act in opposition around a joint [54], [55]. Through selective coactivation, these muscles regulate the joint's mechanical behaviour - both its ability to generate movement and its resistance to external forces. In a simplified 1-degree-of-freedom (1-DOF) system, activation of one muscle with concurrent relaxation of its antagonist produces torque in the direction of the active muscle (**Figure 2.2**). Conversely, reversing the activation pattern produces movement in the opposite direction.

When both muscles are simultaneously active, co-contraction increases joint impedance, making the joint more resistant to perturbations or unwanted motion.

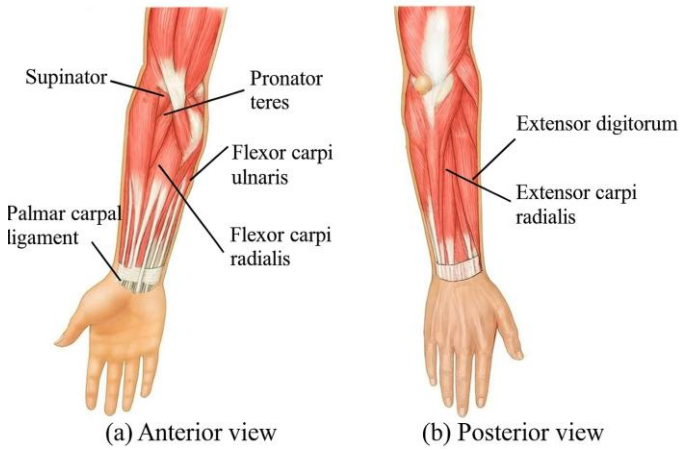

Figure 2.2. Anatomy of the human forearm, highlighting primary flexor and extensor muscles which act as antagonist muscles during wriest flexion/extension movement [56].

This co-contraction strategy plays a central role in stabilising and terminating voluntary movements [57], enabling the motor system to finely tune joint impedance according to task demands. Increased co-contraction enhances stability during postural tasks or when interacting with unstable environments [58], while reductions in co-contraction often accompany improved motor performance or skill acquisition [59]. Thus, antagonist muscle coordination provides a flexible mechanism for shaping both stability and mobility across a wide range of behaviours.

The neural regulation of co-contraction relies on reciprocal inhibition, a spinal mechanism that coordinates activation of agonist and antagonist muscles [60]. When muscle spindles activate Ia afferents, they excite motor neurons of the agonist muscle while simultaneously engaging inhibitory interneurons that suppress activation of the antagonist muscle [57]. Complementary Ib pathways modulate muscle activation based on force feedback, inhibiting α-motor neurons during excessive tension and supporting fine-grained motor control. Together, these interconnected pathways ensure smooth and coordinated movement by preventing inappropriate coactivation when low impedance is desired and enabling well-controlled coactivation when high impedance is required [61].

Understanding the functional role of antagonist muscles is therefore essential for interpreting impedance regulation in human motor control. Antagonist co-contraction represents one of the primary means through which the sensorimotor system shapes joint mechanics in real time, integrating proprioceptive feedback, descending motor commands, and predictive control strategies. By adjusting the balance between agonist and antagonist activation, the system can transition seamlessly between movement-oriented and stability-oriented control states.

2.2.4. Reflex Pathways and Fusimotor Contributions to Sensorimotor Control

The myotatic reflex, or stretch reflex, is a fast-acting (20 - 50 ms) spinal reflex fundamental to impedance regulation [62]. Skeletal muscle contains extrafusal fibres, which generate force, and intrafusal fibres, which form the muscle spindles that detect changes in muscle length and the rate of that change [63]. Muscle spindles are innervated by primary (Ia) afferent neurons, which transmit information to the spinal cord via monosynaptic connections onto alpha motor neurons [64]. Secondary (Type II) afferents also arise from muscle spindles and convey information about sustained muscle

length, contributing to tonic reflex activity and postural control. When a muscle is stretched, Ia afferents increase their firing, leading to reflexive activation of the same muscle [65]. This contraction increases muscle impedance and limits further stretch, functioning both as a protective mechanism and as a means of stabilising posture in the presence of external perturbations.

Muscle spindles contain two principal types of intrafusal fibre: nuclear bag fibres and nuclear chain fibres [66]. Nuclear bag fibres are subdivided into dynamic (bag1) fibres, which are highly sensitive to the rate of muscle stretch and therefore support rapid corrective responses, and static (bag2) fibres, which more reliably encode muscle length, contributing to sustained postural control [67]. Nuclear chain fibres, thinner and arranged linearly, encode the absolute muscle length through tonic firing [67]. The differing sensitivities of these fibres illustrate the range of stretch-related information available to the sensorimotor system and explain how different movement dynamics modulate reflex strength.

While the myotatic reflex provides a rapid, automatic means of regulating baseline impedance, the long-latency stretch reflex (LLSR) - sometimes referred to as the transcortical reflex - provides a more flexible, context-dependent response [68]. Occurring approximately 50 -100 ms after muscle stretch, the LLSR begins with the same Ia afferent activation but is routed via ascending pathways to the sensorimotor cortex. This allows contextual, task-relevant information to modulate the descending response, producing finely tuned adjustments in muscle activation and impedance [69]. Because it integrates sensory evidence with internal models of movement, the LLSR supports adaptive control, enabling rapid modifications to impedance when environmental dynamics or task demands change [70]. The LLSR has been associated with both motor adaptation and skill acquisition, and disruptions to its normal patterning are linked to impaired impedance regulation in clinical conditions such as Parkinson's disease and dystonia [71].

Both the myotatic reflex and the LLSR depend on muscle spindle activity, and their effectiveness relies on the ability of the sensorimotor system to adjust spindle sensitivity according to context. This modulation is achieved by the fusimotor system (**Figure 2.3**), in which gamma motor neurons innervate intrafusal fibres to regulate their tension and thereby their sensitivity to stretch. By adjusting intrafusal fibre length, gamma activation ensures the spindle remains responsive across a wide range of muscle states, particularly during voluntary contraction. Gamma motor neuron activity reflects contributions from both peripheral proprioceptive feedback (from muscle spindles and Golgi tendon organs) and central descending signals originating in the brainstem and motor cortex [70].

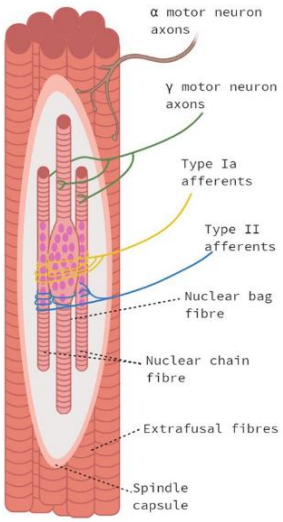

Figure 2.3. Diagram of a muscle spindle illustrating key elements of the fusimotor system [72]. The schematic shows intrafusal fibres (nuclear bag and nuclear chain) within the spindle capsule, innervated by primary (Type Ia) and secondary (Type II) afferents, alongside alpha motor neurons supplying extrafusal muscle fibres and gamma motor neurons regulating spindle sensitivity.

Importantly, alpha-gamma coactivation ensures that intrafusal fibres remain functionally engaged even when the muscle is shortening, preserving the fidelity of proprioceptive information [73]. Disturbances in alpha-gamma coactivation have been associated with pathological conditions such as spasticity, highlighting its importance for normal postural and movement control [74], [75].

The fusimotor system therefore plays a crucial role in impedance regulation by modulating the sensitivity of the muscle spindle - the primary sensor driving both the myotatic reflex and the LLSR. Through this mechanism, the fusimotor system adjusts the gain and responsiveness of reflex pathways, enabling impedance to be tailored to the immediate demands of posture, movement, and environmental uncertainty [76]. Together, these reflexive and fusimotor processes illustrate that impedance modulation is not merely a passive mechanical response, but a highly adaptive and context-sensitive aspect of sensorimotor control.

2.2.5. Mechanical Impedance in Healthy Motor Control

Mechanical impedance refers to the dynamic relationship between force and motion at a joint, governed by the combined contributions of stiffness (resistance to displacement), damping (resistance to velocity), and inertia (resistance to acceleration) [1]. In the context of human motor control, impedance describes how the neuromuscular system regulates the limb's mechanical behaviour to maintain stability, respond to perturbations, and enable precise voluntary movement. Impedance is not a fixed property of the limb; rather, it is actively modulated through changes in muscle activation - particularly co-contraction of antagonist muscles - and through adjustments in reflex pathways and predictive control. Understanding how healthy individuals regulate mechanical impedance is essential for interpreting both the stability–movement transitions and the adaptive processes examined in this thesis.

The current understanding of impedance modulation in healthy motor control has historically emphasised its reactive aspects, particularly how the system responds to external disturbances [2], [4], [31], [34]. Nonetheless, the existing literature provides important insights into how limbs enter and maintain a high-impedance state and how humans regulate impedance proactively in anticipation of task demands.

A central finding is that passive stiffness dominates wrist rotational dynamics, with inertial contributions typically an order of magnitude smaller; this disparity is further amplified when active stiffness resulting from muscle co-contraction is considered [77]. This has implications for experimental modelling. While more complex impedance models may capture additional features, the improvements in accuracy may be limited - especially in systems that lack direct velocity or acceleration measurements, where numerical differentiation can increase noise.

Studies have consistently shown that impedance increases with task accuracy requirements [78], [79], driven primarily by alterations in antagonist muscle co-contraction [55]. When attempting to achieve stability or precision, individuals increase impedance to reduce sensitivity to both internal variability and external perturbations. This modulation follows rational principles: stiffness is increased selectively to minimise uncertainty in the presence of unpredictable or unstable environments [31], [80], and often scales in proportion to the level of uncertainty [81]. Conversely, predictable perturbations do not always elicit increased stiffness [82], [83], indicating that impedance regulation reflects a trade-off between robustness and energetic cost rather than an indiscriminate stiffening strategy.

Impedance control is not solely reactive. Ball-catching and load-handling studies demonstrate anticipatory co-contraction, where individuals adjust impedance before contact based on the expected amplitude or variability of incoming forces [84], [85]. These findings reveal the role of feedforward processes and internal models in shaping impedance in advance of sensory feedback.

Recent work has examined how wrist impedance varies as a function of the variability of external loads. In tasks involving unpredictable force perturbations, most participants showed a monotonic increase in

stiffness with increasing variability [86]. For those who did not, the authors suggested that differing priorities, such as energetic efficiency or movement accuracy, may underlie individual strategies, highlighting inherent trade-offs in motor control.

Together, these findings illustrate that mechanical impedance in healthy motor control emerges from a multilayered interplay of passive biomechanics, reactive feedback, and predictive sensorimotor processes. The ability to modulate impedance flexibly is central to achieving stable yet adaptable movement and underpins the transitions between stability- and movement-oriented control states that are central to this thesis.

2.2.6. Summary

The neuroanatomy involved in impedance control highlights the multilayered dynamics underlying human motor function. While the basic mechanisms mediated by the myotatic reflex are relatively direct, incorporating the contributions of the LLSR and the fusimotor system reveals a far more complex interplay between spinal, subcortical, and cortical processes. These intricacies are further emphasised when considering the dynamics of the SCBG network, which engages multiple interacting pathways that collectively facilitate, modulate, and terminate movement.

The current literature on impedance control underscores the critical importance of stiffness and more broadly, impedance modulation to achieving effective joint movement, particularly through the coordinated activity of antagonist muscle pairs. Empirical studies consistently show that stiffness is most strongly elevated under conditions of uncertainty, with irregular perturbations or variable force requirements eliciting the most robust increases in impedance. Furthermore, the literature provides multiple approaches to quantifying stiffness, ranging from direct measurement of mechanical responses to sophisticated integrated models that incorporate neuromuscular and reflex contributions.

Despite these advances, a substantial gap remains in understanding how the sensorimotor system orchestrates stability–movement transitions specifically and how neural and mechanical subsystems co-ordinate during this critical shift. This lack of clarity motivates the investigation undertaken in the present thesis.

2.3. Parkinson's Disease

2.3.1. Introduction

Parkinson's disorder (PD) is a progressive neurodegenerative condition affecting over 8 million people worldwide, with a prevalence exceeding 1% in individuals over the age of 60 [87], [88]. It is a disorder of the sensorimotor cortex-basal ganglia (SCBG) network caused by the degeneration of the dopaminergic neurons in the substantia nigra pars compacta (SNc) [40]. PD can cause significant reductions in quality of life [89] and, although not directly terminal, increases the mortality rate of affected individuals when compared to unaffected peers [90]. The cardinal motor features include bradykinesia [91], rigidity [22], [39], [92], resting tremor [93], and postural instability, though individuals may manifest these symptoms to varying degrees. Bradykinesia - slowness and reduced amplitude of movement - is typically the most disabling symptom and is central to PD diagnosis [91]. Non-motor symptoms such as cognitive decline [94], mood disorders [95], [96], and autonomic dysfunction [97] also contribute significantly to disease burden but fall outside the primary scope of this thesis.

A key attribute of PD is its heterogeneity. Individuals differ substantially in their symptom progression, medication response, and functional impairment. However, the degree of impairment often correlates with the complexity of the motor task - fine motor tasks, such as buttoning a shirt, are typically more affected than larger, less precise movements [98]. Despite this variability, a consistent theme across PD motor symptoms is difficulty regulating and transitioning between motor control states, especially those involving posture or movement initiation. Understanding the mechanisms underlying these deficits provides critical context for examining how the sensorimotor system, both healthy and impaired, manages transitions between stability and movement.

2.3.2. Neuropathology and Impact on Reflex Pathways

PD is caused by the degeneration of dopaminergic neurons in the basal ganglia leading to dysfunction of its circuits (i.e., cognitive, affective and motor) [40]. This cell degeneration is caused by the aggregation of misfolded α-synuclein protein into Lewy's bodies (LBs) [99], [100] that progressively build up within the affected neuron, impairing its function before leading to cell death [101].

The motor symptoms associated with PD are primarily caused by dopaminergic depletion within the SNc [102]. This in turn reduces the availability of dopamine to the striatum, dysregulating both the direct and indirect motor pathways (**Figure 2.1**). The lack of dopamine availability causes underactivity in the direct pathway, increasing the difficulty of movement initiation while the indirect pathway becomes overactive, resulting in reduced motor output from the cortex.

While the primary motor impairments are associated with the presence of LBs within the SNc, the progression of these build ups is not limited to this brain region. The progression of LBs can be classed based on Braak staging [103] (**Figure 2.4**). During stages 1 and 2, LBs are not present but instead preceded by Lewy neurites (LNs). This is a preclinical stage mainly effecting the PNS and brainstem. At stages 3 and 4, LBs begin to spread through the basal ganglia and midbrain [103] and PD-related motor symptoms begin. In the final stages of α-synuclein pathology, the mesocortex and neocortex develop LBs, resulting in the cognitive symptoms associated with PD. Despite this clear trajectory of neuropathology, the correlation between Braak staging and individual symptomatic presentation is relatively weak.

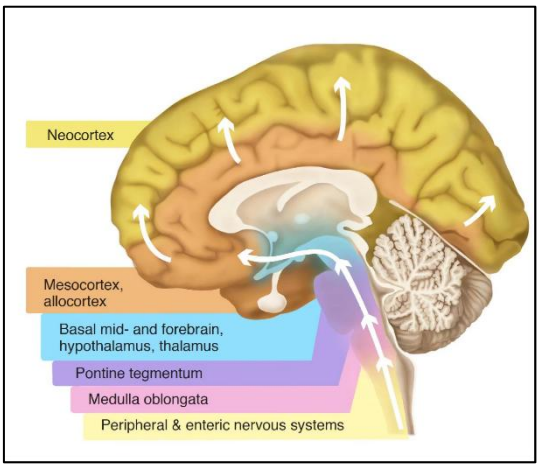

Figure 2.4. Visualisation of the spread of α-synuclein aggresomes by Braak Staging [104]

Reprinted under CC BY 4.0, https://creativecommons.org/licenses/by/2.0/.

The motor impairments observed in PD extend beyond central nervous system dysfunction and may include alterations in the viscoelastic and neuromuscular properties of peripheral tissues [105]. For example, PD has been shown to reduce the efficacy of Ib interneurons, impairing the ability to down-regulate muscle tone appropriately [106]. Similarly, Ia afferent activity is diminished in the upper limbs of individuals with PD, leading to reduced recurrent inhibition and compromised proprioceptive signalling [107]. These findings indicate that although basal ganglia dysfunction remains the primary pathology in PD, secondary alterations within the peripheral nervous system may also contribute to abnormal impedance control.

Changes in reflex pathways also play a significant role in the motor deficits associated with PD. Abnormal gain in the long-latency stretch reflex (LLSR) [71], [108], impaired integration of proprioceptive feedback [109], [110], and potential alterations in fusimotor drive [111] have all been reported. Such disruptions interfere with the rapid, context-sensitive adjustments required for impedance regulation, resulting in irregular responses to perturbations. These abnormalities compromise the system's ability to adapt reflexively to changes in environmental or task dynamics.

Impaired reflex modulation may also hinder the transition between stability-oriented and movement-oriented motor states. If reflex pathways remain tuned for heightened stability demands - for example, through increased spindle sensitivity or elevated LLSR gain - the neuromuscular system may remain locked in a high-impedance state even when flexibility is required for voluntary movement. This can exacerbate bradykinesia and postural instability by preventing timely reductions in impedance. Understanding how these reflex-level alterations contribute to impaired impedance regulation and difficulty transitioning between motor states therefore provides an important link between peripheral mechanisms and central neural control in PD.

2.3.3. Rigidity, Bradykinesia, and Postural Instability in Parkinson's Disease

Rigidity, defined as increased resistance to passive joint movement independent of movement speed, is a hallmark motor symptom of PD [22], [39]. Unlike spasticity, which is velocity-dependent and typically associated with upper motor neuron lesions [74], [112], PD rigidity presents as either uniform resistance throughout the full range of motion ("lead-pipe rigidity") or as intermittent, ratcheted resistance ("cogwheel rigidity") [92]. This heightened muscle tone is thought to arise from abnormal central neural drive rather than purely mechanical factors [27], [113]. Increased background activation in both agonist and antagonist muscles contributes to an overall elevation of joint impedance, raising resistance even during passive displacement.

Mechanistic explanations for rigidity include increased tonic activation of alpha motor neurons, abnormal facilitation of polysynaptic spinal pathways, and impaired integration of sensory feedback within basal ganglia circuits [109], [110]. Altered reflex excitability, including enhanced LLSR, has also been implicated in some individuals [114]. Functionally, rigidity reduces the ability to modulate impedance according to task requirements, forcing the limb into a persistently high-impedance state that restricts fluidity, increases energetic cost, and introduces mechanical resistance during voluntary movement [39].

Bradykinesia, another core symptom of PD, is characterised by slowness of movement, reduced movement amplitude, and impaired initiation of voluntary actions [115]. While rigidity manifests as elevated muscle tone, bradykinesia reflects deficits in movement scaling and initiation, often linked to excessive beta synchrony within cortico-basal ganglia circuits and an impaired ability to suppress stability-oriented neural activity [27], [116]. These neural abnormalities can hinder the appropriate down-regulation of impedance at movement onset, leading to slowed and effortful motion. Bradykinesia therefore represents both a neural and biomechanical deficit, in which insufficient modulation of muscle activation and inadequate release from high-impedance states impair dynamic motor flexibility.

Postural instability is a third major motor symptom of PD, marked by impaired balance and difficulty responding to destabilising forces [117]. It typically emerges in later disease stages and contributes significantly to falls. Disrupted sensory integration, delayed corrective reactions, and impaired scaling of postural responses all play a role [118]. From a mechanical standpoint, individuals with PD often struggle to modulate impedance rapidly in response to perturbations, either failing to increase impedance sufficiently to resist disturbances or maintaining excessively high impedance that restricts compensatory movement [119].

Together, rigidity, bradykinesia, and postural instability reflect impaired motor regulation in PD, highlighting how disrupted neural and reflex pathways compromise flexible impedance modulation. Tremor, although a cardinal PD symptom, does not reflect specific impairment of impedance control and therefore lies outside the scope of this thesis. These PD motor impairments are used as a contrasting clinical phenotype indexing impaired impedance control, illustrating behavioural deficits that healthy individuals may exhibit across stability–movement transitions.

2.3.4. Clinical Assessment in Parkinson's Disease

The severity of PD is typically assessed using semiquantitative clinical rating scales, the most widely used being the Unified Parkinson's Disease Rating Scale (UPDRS) [120], [121]. This scale aims to provide a comprehensive evaluation of disease impact, encompassing motor and non-motor symptoms, functional impairment in daily living, and overall quality of life. Non-motor symptoms are assessed primarily through patient-reported questionnaires, with items scored on a 0 to 4 scale based on severity. Motor symptoms are also rated on a 0 to 4 scale but rely on clinician-led examination of the patient performing specific motor tasks.

Rigidity is evaluated clinically by passively mobilising the patient's joints while instructing the patient to remain relaxed (**Table 2.1**). If no rigidity is detected under isolated passive movement, the clinician may introduce an activation manoeuvre (such as tapping the foot) to amplify subtle rigidity. The assessment focuses on the degree of resistance to passive motion, the presence or absence of cogwheeling, and whether full range of motion can be achieved.

Table 2.1. The UPDRS subitem detailing how to assess rigidity [120].

UPDRS Subitem 3.3. Rigidity		
0	Normal	No rigidity.
1	Slight	Rigidity only detected with activation maneuver.
2	Mild	Rigidity detected without the activation maneuver, but full range of motion is easily achieved.
3	Moderate	Rigidity detected without the activation maneuver; full range of motion is achieved with effort.
4	Severe	Rigidity detected without the activation maneuver and fill range of motion not achieved.

In addition to rigidity, the UPDRS evaluates bradykinesia, which is assessed through repetitive and alternating movement tasks such as finger tapping [122] (**Table 2.2**), hand opening and closing, forearm pronation-supination, and foot tapping. Clinicians observe and score reductions in speed, amplitude, rhythmicity, and decrement over time. These assessments provide a semiquantitative measure of the slowness and scaling deficits that characterise bradykinesia.

Table 2.2. The UPDRS subitem detailing how to assess bradykinesia through finger tapping [120].

UPDRS Subitem 3.4. Finger Tapping		
0	Normal	Normal speed and amplitude; no decrement.
1	Slight	Slight slowing and/or reduction in amplitude; minimal decrement.
2	Mild	Mild slowing; early fatigue or obvious decrement in amplitude.
3	Moderate	Moderate slowing; prominent and progressive decrement; movement may be interrupted.
4	Severe	Severe bradykinesia; barely able to perform the movement.

Postural instability is assessed through tasks such as the pull test, where the clinician applies a sudden backwards pull to the patient's shoulders and evaluates the patient's ability to regain balance. Postural responses are scored according to step size, latency, and the need for external support. Additional gait and stability items assess freezing episodes, turning ability, and general steadiness during ambulation.

Although the UPDRS remains the gold standard, clinical motor assessments are unavoidably limited by the subjectivity and precision of manual examination. Scoring relies on the clinician's perception of resistance, speed, or steadiness, introducing considerable inter- and intra-rater [123], [124], [125]. The five-point scale has been criticised for its limited granularity, which can mask subtle progression or underrepresent early-stage motor deficits [126]. Variability in assessment technique, physical strength of the examiner, and patient fatigue can further confound results.

While clinician-led examination remains the standard of care, these limitations highlight the clear need for objective, and replicable methods for quantifying PD motor symptoms. Developing reliable quantitative measures of rigidity, bradykinesia, and postural instability is essential not only for clinical diagnostics but also for tracking disease progression, evaluating treatment efficacy, and improving the sensitivity of research tools. This motivation underpins the technological and methodological contributions of the present thesis.

2.3.5. Impaired Modulation of Impedance in Parkinson's Disease

Effective motor control relies on the flexible modulation of mechanical impedance to meet changing task demands. Healthy individuals increase impedance to stabilise posture or counteract unpredictable forces, and reduce it when transitioning into fluid, goal-directed movement [3], [4], [17], [34]. In PD, this flexibility is markedly disrupted. The three principal motor symptoms discussed previously - rigidity, bradykinesia, and postural instability - can all be interpreted, at least in part, as consequences of impaired impedance regulation.

Rigidity reflects an abnormally elevated baseline impedance that persists even during passive movement [22], [127]. Increased co-contraction of agonist and antagonist muscles [127], [128], combined with altered reflex excitability [114], [129], results in a chronically stiff limb that fails to down-regulate impedance when lower resistance is required. Consequently, movement initiation becomes mechanically and metabolically costly, and the limb remains locked in a high-impedance state regardless of behavioural context. This pathological persistence contrasts sharply with healthy control, where impedance is increased only when needed [17], [55].

Bradykinesia, although distinct from rigidity, also reflects impaired modulation of impedance. To initiate quick and efficient movement, the nervous system must transiently reduce impedance by decreasing co-contraction and appropriately scaling motor commands. Individuals with PD often struggle to release the stability-oriented motor state associated with elevated beta synchrony [27], [28], leading to insufficient reduction in impedance at movement onset. This results in slower, smaller, and less forceful movements. Even when reaction times are preserved, the movement itself is executed at reduced speed and amplitude, consistent with an inability to transition out of a high-impedance regime.

Postural instability further illustrates failures in the dynamic regulation of impedance. In healthy individuals, sudden perturbations evoke rapid increases in impedance through reflexive and voluntary mechanisms. In PD, both the timing and amplitude of these adjustments are impaired. Some individuals fail to elevate impedance sufficiently to resist destabilising forces, resulting in exaggerated sway or loss of balance [118], [119]. Others exhibit excessive or poorly timed stiffness, limiting the flexibility required for effective corrective movements [36], [37]. These deficits reflect impaired integration of sensory feedback and delayed activation of context-appropriate motor responses.

Taken together, these symptoms indicate that PD does not simply elevate impedance but disrupts the ability to modulate impedance appropriately over time. The neural systems that normally shift the motor state between stability-oriented and movement-oriented modes malfunction in PD. This results in an impaired ability to adjust impedance to match environmental uncertainty, task demands, or behavioural goals. While the present thesis does not aim to dissect the pathological mechanisms underlying PD, understanding these impairments provides valuable context. PD exemplifies what occurs when the transitional mechanics between stability and movement fail. The disorder highlights the importance of flexible, context-sensitive impedance regulation in healthy motor control - the very process investigated in the experimental work of this thesis.

2.3.6. Motor Learning and Adaptation in Parkinson's Disease

Motor learning and adaptation in PD present a complex interplay of preserved abilities and specific impairments. Although PD primarily affects the basal ganglia, certain forms of sensorimotor adaptation

that depend more heavily on cerebellar circuits can remain relatively intact [48], [130], [131]. For example, PD patients are often able to adjust their movements in response to predictable perturbations or stable force fields, demonstrating that some aspects of internal model updating can still occur [32], [132]. However, these preserved capacities tend to break down when learning requires the integration of noisy or unpredictable sensory environments, or when the task demands rapid, trial-by-trial recalibration.

Deficits in PD become more apparent in contexts that rely on the basal ganglia's contribution to reinforcement learning, error sensitivity, and movement scaling. Individuals with PD frequently show impaired updating of internal models [133], reduced retention of newly acquired motor skills [134], and diminished ability to transfer learning across tasks [135]. Trial-by-trial error correction is slowed, and patients often compensate by relying more heavily on explicit cognitive strategies, which are less efficient and more susceptible to fatigue [133] . In tasks requiring rapid recalibration of motor output, PD patients sometimes show inflexible or stereotyped response patterns, reflecting a difficulty escaping from stability-oriented motor states [136].

These learning and adaptation deficits have direct implications for impedance regulation. Efficient modulation of impedance requires the sensorimotor system to integrate sensory feedback with internal predictions across repeated movements. Through learning, healthy individuals refine their co-contraction patterns, adjust reflex gains, and optimise the timing of transitions between high- and low-impedance states. However, in PD, slowed adaptation and reduced error sensitivity could hinder this refinement process, contributing to persistent high-impedance tendencies. If the system cannot efficiently learn when and how to reduce co-contraction or modify joint stiffness, the individual may remain inappropriately anchored in stability-oriented motor modes, exacerbating rigidity-like behaviour and postural control difficulties.

In addition, PD-related changes in beta oscillations may interfere with the neural mechanisms that support learning. Elevated or poorly modulated beta activity has been associated with reduced sensitivity to prediction error [137], impaired motor adaptation [138], and difficulty disengaging from previous motor states [139]. These oscillatory abnormalities may therefore interact with basal ganglia dysfunction to constrain adaptive processes at both the neural and behavioural levels.

The present thesis examines motor adaptation in healthy individuals using repeated blocks of perturbation-based trials. This provides a normative benchmark for understanding how impedance modulation evolves across repeated exposure to instability, how the system learns to manage transitions between stability and movement, and how these adaptations manifest in beta activity, co-contraction, and movement performance. Although PD is not the primary focus of this thesis, the findings from healthy participants offer a clear comparative framework for interpreting how adaptive processes may fail in individuals with PD and how technological approaches developed here could be applied in future diagnostic or rehabilitation contexts.

2.3.7. Summary

PD is a neurodegenerative disorder whose pathology and characteristic motor symptoms offer valuable insights into the neuromotor dynamics associated with high-impedance states. Dysfunction of the basal ganglia, combined with secondary alterations in peripheral and reflex pathways, highlights the importance of these systems for healthy impedance regulation. In addition, the clinical assessments used to evaluate rigidity, bradykinesia, and postural instability provide methodological guidance for the quantitative evaluation of motor function. However, because PD represents a pathological condition, it does not fully reflect the mechanisms of healthy motor control, and findings drawn from PD must be interpreted with caution. Evidence from the disorder can inform hypotheses about normal impedance regulation, but direct study of healthy individuals remains essential.

Individuals with PD typically experience difficulty transitioning from stable postures to voluntary movement, a core requirement of everyday motor behaviour. These deficits manifest as delayed movement initiation, hesitations, and freezing episodes, reflecting impairments in both motor planning and disengagement from stability-oriented control states. Effective movement requires a reduction in impedance and a controlled release of co-contraction, yet PD is characterised by persistently elevated impedance that hinders this shift. Postural instability further illustrates how impaired impedance regulation affects responsiveness to perturbations and the scaling of corrective actions.

Deficits in stability–movement transitions may also involve cognitive components, as PD patients often show slowed task-set switching and increased reliance on attentional processes during motor preparation. Nonetheless, at a sensorimotor level, the inability to rapidly adjust impedance and neural state appears central. This view aligns with the thesis focus on understanding how healthy individuals manage such transitions and how neural dynamics, particularly within the beta-band, support or obstruct the required reconfiguration of motor control.

Overall, PD disrupts the sensorimotor processes required for flexible and efficient movement transitions. Elevated rigidity, impaired modulation of co-contraction, altered reflex pathways, excessive beta-band activity, and deficits in motor learning collectively limit the ability to shift from stability-oriented to movement-oriented control states. This thesis examines the sensorimotor mechanisms underlying stability–movement transitions in healthy individuals, identifying neural and mechanical signatures of impedance regulation. Characterising how these dynamics are impaired in PD therefore provides a clinically relevant contrast for interpreting the transition dynamics elicited by the experimental paradigm.

2.4. Beta Oscillations in Motor Control

2.4.1. Introduction

Neural oscillations are patterns of electrical activity generated by the synchronous firing of neuronal ensembles. Examination of their spectral features combined with synchronisation to cognitive or motor function can provide insight into the neural dynamics associated with changing behaviour. Neural oscillations are contextualised by their neuroanatomical location as well as the frequency of their oscillatory behaviour [140].

Beta (13 - 30 Hz) oscillations have been associated with cognitive processes such as visual processing [141], attentional focus [142] and working memory [143], [144]. However, beta oscillatory features within the sensorimotor cortical-basal ganglia (SCBG) are more commonly linked to motor function, such as movement-related amplitude changes correlating with movement termination accuracy [145], or the frequency of cortical bursting events synchronising with the level of motor activity [10]. These oscillations occur throughout the SCBG [22] [146] and divergence in their dynamics from normative function is considered a putative biomarker of PD [147]. Understanding the role of beta oscillations in motor control is essential to understanding impedance control, as these oscillations are highly correlated with key functions such as motor execution and learning.

2.4.2. During Posture and Stability Control

Beta oscillations (13 - 30 Hz) within the sensorimotor system are associated with the maintenance of stable motor states [148], [149]. During periods of postural holding or low-movement demands, beta activity is typically elevated, reflecting a neural regime oriented towards preserving the status quo of the motor system [150]. This characteristic pattern has led to the proposal that beta oscillations index a state of motor stability, in which ongoing sensorimotor activity is reinforced and deviations from the current posture are minimised.

Studies have demonstrated that beta power increases during isometric contraction [151], [152], sustained postural maintenance [10], [153], and steady force production [154]. In these contexts, the motor system prioritises robustness to perturbations and the suppression of unnecessary movement - behavioural demands that parallel the mechanical requirement for higher joint impedance. Elevated beta is therefore frequently interpreted as a neural signature of a control state reflecting stability rather than flexibility.

The functional role of beta during postural control is further supported by perturbation studies [155]. When the limb is subjected to unpredictable mechanical disturbances, beta activity often remains high or shows only modest reductions, suggesting that it may contribute to stabilising the motor state or maintaining readiness to resist displacement. In contrast, conditions demanding rapid changes in motor output are typically associated with prominent beta suppression [156]. This inverse relationship underscores the idea that beta oscillations help to reinforce stability but inhibit movement initiation.

Importantly, beta is not simply a correlate of muscle activation. Studies controlling for EMG, force level, or co-contraction show that beta power does not scale linearly with peripheral activation [151], [157]. Instead, beta appears more closely related to sensorimotor confidence, state estimation, or the maintenance of an internally predicted model of the limb [158]. Under this view, high beta reflects a neural system that is committed to its current state and less willing to update or reconfigure its control strategy.

This interpretation aligns naturally with impedance regulation. When individuals maintain posture or prepare to counter unpredictable forces, the sensorimotor system often increases impedance through co-contraction and reflex tuning. Elevated beta may reflect the neural counterpart of this high-

impedance state: a cortical-subcortical configuration that promotes stability and resists change. Such coupling between neural stability signals and mechanical impedance is especially relevant for tasks involving postural challenges, load anticipation, or unpredictable dynamics.

In summary, beta oscillations during posture and stability control appear to signal a neural mode in which the motor system favours resistance to change, maintenance of ongoing activity, and robustness to perturbation. This makes beta a compelling candidate for indexing the neural dimension of high-impedance states and provides essential context for understanding the stability–movement transitions explored in this thesis.

2.4.3. Movement Initiation and Termination

Motor actions are accompanied by a characteristic pattern of beta oscillatory dynamics that unfolds across the preparation, execution, and termination of movement. Approximately 500 ms before movement onset, beta amplitude typically begins to decrease due to a desynchronisation of sensorimotor neuronal populations, producing the movement-related beta decrease (MRBD) [53]. This reduction continues throughout movement execution and is followed, shortly after movement completion (typically 300–1500 ms), by a pronounced increase in beta amplitude known as the post-movement beta rebound (PMBR) [159], [160]. Together, these phases form a canonical signature of beta modulation during voluntary action (**Figure 2.5**).

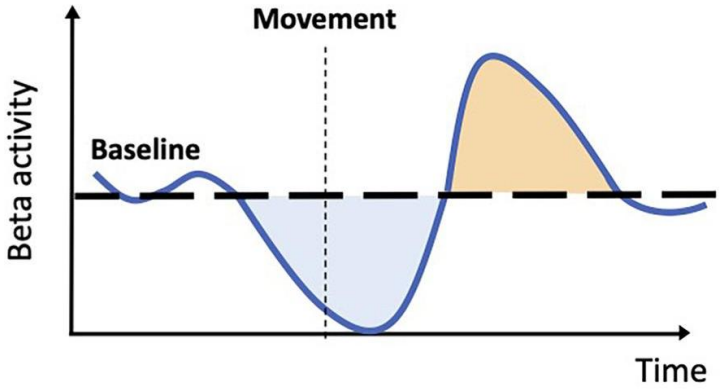

Figure 2.5. A visual representation of beta amplitude around a movement event [148]. The Blue line represents the magnitude of the beta activity. The blue shaded zone highlights the movement related beta decrease (MRBD) while the orange shaded highlights the post movement beta rebound (PMBR).

The amplitude and timing of both the MRBD and PMBR are sensitive to the dynamics of the movement being performed. Slower voluntary movements are associated with reduced MRBD amplitude [145], [161], as well as a decreased PMBR [162]. These attenuated responses have been interpreted as reflecting a “slowed movement state” in healthy individuals [163]. More broadly, elevated beta oscillations have been linked to slower, less precise voluntary movement [164] and to reduced movement speed without affecting reaction time [165], reinforcing the notion that high beta may oppose rapid or flexible motor output.

However, changes in beta are not driven solely by movement speed. PMBR amplitude has been shown to increase with force output, whereas the MRBD does not scale in the same manner [154]. More generally, beta-band modulation correlates with force generation during isometric contraction [152], [166], suggesting that beta dynamics reflect both motor output and the sensorimotor context in which movement is generated. The anticipatory nature of the MRBD is further supported by evidence that

similar decreases in beta power occur during motor imagery - that is, visualisation or mental rehearsal of a movement without overt execution [167]. This indicates that beta suppression reflects not only physical movement but also the intent to move and the associated reconfiguration of sensorimotor networks.

The complementary dynamics of MRBD and PMBR have been widely interpreted as evidence for an anti-kinetic role of beta oscillations. Under this framework, the reduction of beta synchrony through MRBD facilitates the initiation and execution of movement by releasing the motor system from a stabilising, status-quo-preserving state. Conversely, the subsequent PMBR is thought to reflect a return to a more stable sensorimotor configuration, re-establishing the motor set after movement termination. Earlier theories proposed that beta represented an “idling” rhythm of the motor system during rest [168], but contemporary perspectives suggest a more nuanced interpretation: elevated beta activity may signal preservation of the existing motor state or a resistance to change [150]. Consistent with this, beta amplitude has been shown to increase when individuals resist movement or maintain posture against external forces [120].

Despite this compelling theoretical framework, the hypothesis that beta-band activity specifically encodes a motor stability state and that transitions into or out of movement require systematic modulation of this state has not been directly tested in the literature. Understanding whether beta activity tracks changes in impedance, co-contraction, or motor set inertia remains a key open question.

2.4.4. Sensory Feedback and Error Processing

Beyond their role in movement preparation and execution, beta oscillations are deeply involved in processing sensory feedback and evaluating deviations between predicted and actual motor outcomes [38], [169]. A key feature of beta dynamics in this context is the PMBR, which is consistently observed following voluntary movement or externally imposed perturbations [155]. The PMBR has been interpreted as reflecting the integration of sensory feedback with internal models, signalling a return to a stable sensorimotor state after the transient disruption caused by movement or external forces [158].

During tasks involving mechanical perturbations, beta oscillations often display rapid, context-dependent modulation [155], [170]. Sudden or unpredictable disturbances typically evoke transient reductions in beta power, reflecting an increased reliance on sensorimotor feedback to update internal state estimates and adjust corrective responses. This beta suppression is thought to facilitate rapid error processing by enabling flexible reconfiguration of motor output [171]. Following correction, the PMBR marks a reinstatement of synchronised activity across sensorimotor networks, potentially signalling that updated predictions have been consolidated.

Several studies have argued that beta activity supports a form of predictive coding within the motor system [172], [173], [174]. Under this framework, the brain continuously generates predictions about expected sensory consequences of movement. When actual sensory input deviates from these predictions, beta power decreases, indicating a greater need for feedback-driven updating. Conversely, when sensory outcomes match expectations, beta activity tends to remain elevated or returns quickly to baseline via the PMBR, suggesting confidence in the internal model. This interpretation aligns with evidence that beta suppression is proportional to the amplitude of sensory prediction error during force-field adaptation and proprioceptive distortion tasks.

Beta oscillations also modulate the precision and gain of sensory feedback pathways. Elevated beta has been associated with reduced sensitivity to incoming sensory information, consistent with a motor state favouring stability and resistance to change [175]. In contrast, beta suppression enhances the influence of sensory feedback, enabling rapid adjustments to unanticipated disturbances. This dynamic modulation of sensory weighting mirrors the behavioural trade-off between stability and adaptability, and it parallels the mechanical modulation of impedance through changes in reflex gain and co-contraction.

In tasks requiring postural control or resistance to unpredictable forces, beta oscillations have been shown to coordinate with long-latency stretch responses (LLSRs), suggesting a close coupling between cortical processing and reflexive motor adjustments [176], [177]. This relationship supports the notion that beta activity helps regulate how sensory information shapes motor corrections, particularly under conditions of uncertainty or instability.

Taken together, these findings position beta oscillations as a central mechanism for integrating sensory feedback, signalling prediction error, and stabilising internal models of the limb and environment. This perspective is directly relevant to the present thesis, which examines how beta dynamics evolve during perturbation-driven postural challenges and subsequent voluntary movement. Understanding beta's role in sensory feedback processing provides essential context for interpreting how the nervous system manages stability–movement transitions and how these processes may become impaired in neurological conditions such as Parkinson's disease.

2.4.5. Motor Learning and Adaptation

Motor adaptation refers to the process by which the sensorimotor system updates its internal model of movement dynamics in response to discrepancies between expected and actual outcomes [139]. The aim of adaptation is to adjust rapidly to task demands or environmental uncertainty using sensorimotor feedback [178]. The internal, feedforward model generates predictions about the sensory consequences of motor actions, and when these predictions are violated, a sensory prediction error occurs [179]. This error drives updates to the internal model, influencing the execution of subsequent actions.

Adaptation is commonly studied using forcefield or visuomotor perturbation paradigms. In these experiments, participants adjust their movements while a manipulation is applied, gradually compensating for the altered dynamics. When the perturbation is removed or altered, the adapted behaviour initially persists - typically revealed through after-effects - before the system recalibrates to the new conditions. These paradigms have been instrumental in demonstrating the role of beta oscillatory dynamics in adaptation. Specifically, the amplitude of the PMBR has been shown to be inversely proportional to uncertainty in the feedforward model [179], indicating that PMBR may index the degree of confidence in the updated internal model. Similarly, beta oscillations increase with the amount of corrective response required following postural perturbations [158], suggesting a role for beta in encoding corrective effort or prediction error.

Motor learning, while related to adaptation, reflects a broader and more enduring process in which neural dynamics change alongside improvements in motor performance [180]. Learning can occur through error-based mechanisms, driven by the minimisation of performance errors without explicit reinforcement [138], or through reward-based mechanisms, in which successful outcomes serve as reinforcement signals guiding future behaviour [181]. The distinction between adaptation and learning is often one of timescale and purpose: adaptation involves rapid, short-term adjustments to environmental dynamics, whereas learning reflects longer-term acquisition or refinement of motor skills. These processes also rely on partially distinct neural substrates; adaptation relies heavily on the cerebellum, while longer-term motor learning involves sustained plasticity within cortical regions [182].

The role of PMBR in motor learning remains an active area of debate. PMBR amplitude has been observed to increase following motor errors [183], suggesting a potential involvement in error evaluation or the resetting of motor predictions. However, emerging evidence indicates that the relationship between PMBR and learning may be more complex. A recent study of novice billiards players identified two distinct learner subgroups differentiated by the direction of PMBR change as performance improved [184], implying that PMBR modulation may reflect divergent learning strategies or neural mechanisms. Additionally, PMBR amplitude has been associated with future performance upon returning to a previously practised task [185], raising the possibility that beta rebound strength may signal consolidation or readiness to re-engage with a learned skill.

Together, these findings indicate that beta oscillations, and PMBR in particular, play a significant but multifaceted role in motor adaptation, error processing, and long-term learning. Beta activity appears sensitive to uncertainty and the confidence of internal models - properties that are intimately connected to the regulation of motor impedance and the stability–movement transitions explored in this thesis. Understanding how beta reflects or influences learning processes provides an important foundation for interpreting the neural signatures observed in tasks that require repeated exposure to variable perturbations or changes in motor context.

2.4.6. Pathological Alterations of Beta: Insights from Parkinson's Disease

Understanding the neural dynamics of motor impairment in Parkinson's disease (PD) has highlighted beta oscillations as a compelling candidate biomarker of pathological motor control. Numerous studies report elevated beta activity within the SCBG that corresponds closely with the core motor symptoms of PD, including rigidity and bradykinesia [27], [147], [186]. These abnormalities extend to well-established movement-related beta dynamics: both the MRBD and PMBR are consistently dampened in individuals with PD [187], [188], [189]. In addition, PD is associated with an increased occurrence and duration of high-amplitude beta bursts [25], [190], suggesting that pathological beta may manifest not only as sustained oscillatory power but also as aberrant transient events.

Broadly, PD symptoms are linked to excessive beta synchrony across the SCBG [191], [192], reinforcing the view that heightened beta reflects a neural state biased towards stability and resistance to change. Conversely, reductions in beta power within the subthalamic nucleus (STN) correlate with reduced motor impairment [193], [194], indicating that modulation of beta activity is closely tied to the severity of motor dysfunction. Alterations in beta–gamma coupling have also been associated with PD symptom severity [187], suggesting that disruptions in cross-frequency communication may further compromise flexible motor control.

Although PD is principally a disorder of dopaminergic deficiency, beta abnormalities are not exclusively modulated by dopamine. Administration of the GABAergic drug zolpidem has been shown to reduce the amplitude of the PMBR following movement [195], demonstrating that beta dynamics are also sensitive to changes in inhibitory neurotransmission. This underscores the broader neurochemical basis of oscillatory dysfunction in PD.

Deep brain stimulation (DBS) provides further insight into the relationship between beta dynamics and motor impairment. DBS is a second-line treatment reserved for cases where pharmacological therapy becomes insufficient and symptoms are severe [196], [197]. Electrodes are implanted into specific nuclei within the basal ganglia, selected according to the patient's dominant symptoms [198]. High-frequency current delivered through these electrodes influences local and downstream basal ganglia circuits. Despite ongoing debate, three primary mechanistic theories have been proposed. The inhibition theory suggests that DBS reduces pathological firing or mimics the effects of lesioning within the target nucleus [40], [199]. The excitation theory argues that DBS elevates firing rates in a way that regularises aberrant activity [200]. The disruption theory proposes that DBS interferes with pathological synchronisation, partially uncoupling input and output signals [196]. Regardless of the precise mechanism, DBS reliably interrupts high-amplitude, long-duration beta bursts and alleviates motor impairment [201]. The therapeutic reduction in rigidity and related symptoms seen following DBS, together with its suppression of pathological beta activity, provides strong convergent evidence for the importance of beta dynamics in impedance and stiffness regulation.

Studying beta oscillatory behaviour in PD therefore provides valuable insight into the potential role of beta in regulating impedance, as elevated beta frequently co-occurs with increased rigidity and impaired movement initiation. However, as with the symptom of rigidity itself, it is essential to interpret these findings within the context of disease pathology. Neural dynamics observed in PD may reflect compensatory mechanisms, maladaptive circuit changes, or downstream consequences of dopamine depletion, and therefore may not fully represent beta's functional role in healthy motor control. For this

reason, caution is needed when extrapolating from pathological data to normative sensorimotor processes. Nevertheless, the convergent evidence from PD, together with the therapeutic effects of DBS, strongly supports the hypothesis that beta oscillations help regulate transitions between stability-oriented and movement-oriented motor states. Disruptions to this regulatory system may lead to diminished adaptability and impaired modulation of impedance processes that lie at the heart of motor impairment in PD,

2.4.7. Beta Oscillations in Other Disorders Affecting Impedance

While PD is the predominant disorder when considering pathological impairment of impedance control, other conditions impair normal motor impedance modulation and can be explored to gain understanding of healthy stiffness control through comparison.

Stiff-person syndrome (SPS) is a rare autoimmune disorder in which the immune system attacks proteins necessary to produce the neurotransmitter GABA [202]. The impairs the reciprocal inhibition of antagonist muscles, resulting in rigidity, particularly of the trunk and limbs. SPS presents a case where the primary source of stiffness dysregulation is from dysfunction of peripheral rather than central contributions.

Huntington's disease is a hereditary genetic disorder that affects the basal ganglia, primarily the striatum [203]. Mutated huntingtin proteins accumulate and cause neuronal degeneration. This results in dysregulation of the indirect pathway resulting in chorea – involuntary, jerky movements. However, as the disease progresses, the direct pathway can become affected causing rigidity [204].

Dystonia is class of neurological disorder that has different specific types of dependent on the body part affected. However, each is defined by the common symptom of sustained involuntary muscle contraction. Dystonia is associated with basal ganglia disfunction and hyperexcitability of the motor cortex [205], [206]. Dystonia acts as a contrast to PD where PD motor symptoms are associated with excessive beta synchrony, dystonia is associated with reduced inhibition and excessive movement.

These conditions affecting impedance provide further evidence for the role of the SCBG circuit in regulating impedance, demonstrating how distinct impairments within this critical network can lead to related but mechanistically different forms of impedance dysregulation. SPS additionally highlights the importance of dysfunction within the peripheral nervous system, showing that peripheral mechanisms can also drive impairments in impedance control. Taken together, these pathologies illustrate that both central and peripheral abnormalities can disrupt the sensorimotor processes required for flexible impedance regulation.

2.4.8. Other Frequency Ranges and Corticomuscular Coherence

Although beta oscillations are the most widely studied frequency range in motor neuroscience, other oscillatory bands also contribute to sensorimotor processing and may influence aspects of impedance regulation and motor control. These include theta (4-8 Hz), alpha (9-12 Hz), and gamma (31-100 Hz) bands, each of which has been associated with distinct functional roles in movement preparation, execution, and adaptation.

Theta oscillations in the motor cortex have been linked to motor planning and motor learning, particularly during processes involving error detection or performance monitoring [207]. Elevated theta activity commonly accompanies tasks in which individuals evaluate discrepancies between intended and actual movement outcomes, suggesting a role in updating internal models and guiding corrective responses.

Alpha oscillations are prominent in the sensorimotor cortex during movement preparation and are thought to modulate the flow of sensorimotor information [208], [209]. Increases or decreases in alpha power can reflect shifts in attentional engagement, sensory gating, or preparatory inhibition, all of which influence how the motor system transitions between postural stability and voluntary action.

Gamma oscillations, in contrast, are associated with higher-level processing, including sensory integration, attention, and the co-ordination of complex movements. Gamma activity differs in synchronisation properties from beta oscillations [210]. In the sensorimotor system, gamma power reliably increases during movement execution, suggesting involvement in the fine modulation of muscle activity and rapid adjustments to motor demands [210], [211]. These properties make gamma oscillations a potential contributor to the high-frequency control mechanisms underlying rapid force modulation or corrective responses.

The relationship between oscillatory activity and motor function can be further understood through corticomuscular coherence (CMC), a measure of synchrony between cortical rhythms and muscle activity. CMC reflects the degree of functional coupling between the sensorimotor cortex and the periphery, providing insight into how neural oscillations influence motor output [212]. CMC is generally thought to arise from the top-down projection of cortical oscillations to motor units, synchronising descending commands with muscle activation patterns [211], [213].

Beta-band corticomuscular coherence (β-CMC) is particularly well characterised. β-CMC is observed during steady isometric contractions [211] and is modulated during transitions between movement planning and execution [214]. It is most evident in tasks requiring consistent force output or sustained muscle tone [151], [214], aligning closely with contexts in which joint impedance must be stabilised. Experimental manipulation of cortical activity through 20 Hz transcranial alternating-current stimulation has been shown to increase β-CMC and slow voluntary movements, implying that excessive coherence may over-constrain or “over-regulate” motor output [215]. These findings support the idea that β-CMC contributes to stabilising the motor system but may limit flexibility in actions requiring rapid change.

CMC is not restricted to the beta band. Gamma-band CMC is commonly observed during movements requiring rapid or precise adjustments, and appears to reflect fast, adaptive modulation of motor output [211]. This aligns with the role of gamma oscillations in supporting fine-grained sensorimotor integration and the rapid dynamics required for responsive motor control.

Taken together, these oscillatory and coherence patterns reveal that the neural control of movement operates across multiple frequency bands, each contributing distinct functional capabilities. While beta oscillations dominate the stability-oriented aspects of motor control, theta, alpha, and gamma frequencies - as well as their coupling with muscle activity - support complementary processes related to planning, feedback integration, and rapid adjustment. Understanding these interactions provides a broader neurophysiological context for interpreting the oscillatory signatures observed during stability–movement transitions and impedance regulation, forming an important foundation for the empirical work in this thesis.

2.4.9. Summary

Beta oscillations occupy a central role in the neural control of human movement, with consistent evidence linking elevated beta activity to motor stability and preservation of the current motor state while beta suppression is integral to movement initiation and flexibility. Across a range of behaviours, beta activity is increased during postural maintenance, sustained force production, and resistance to perturbation, and is reduced during movement preparation and execution. The complementary dynamics of the MRBD and PMBR reflect transitions between stability-oriented and movement-oriented control states.

These beta dynamics closely parallel the mechanical requirements of impedance regulation. High-impedance states that support stability are characterised by increased co-contraction and heightened reflex gains, coinciding with elevated beta activity and reduced sensory responsiveness. In contrast, beta suppression prior to movement may facilitate the release of these stability mechanisms, allowing impedance to be lowered and movement to proceed. Following movement, PMBR may reflect the re-establishment of a stable motor set through feedback integration and updating of internal models. In this way, beta oscillations are well positioned to coordinate the neural components of impedance control.

Despite these converging observations, direct empirical links between beta oscillations and mechanical impedance remain limited. Few studies have measured beta activity alongside co-contraction or limb mechanics, and the transition from stability to movement has yet to be examined explicitly. Consequently, it remains unclear whether beta directly reflects impedance, readiness to switch control regimes, or broader aspects of sensorimotor set. This thesis addresses these gaps by examining beta dynamics during tasks that require transitions between maintaining posture in unstable contexts to performing voluntary movement. By integrating neural, muscular, and behavioural measures, this work investigates how beta evolves across changes in impedance and how its persistence or release influences flexible motor control.

2.5. Robotic and Servomotor Manipulanda as Tools for Probing Mechanical Impedance

2.5.1. Introduction

Robotic and servomotor manipulanda provide powerful experimental tools for investigating the mechanical impedance of the human sensorimotor system under controlled conditions. By applying precisely defined torques and measuring the resulting kinematic, neural, and muscular responses, these systems enable systematic examination of impedance control and its contributing components. This section briefly reviews the use of robotic manipulanda for probing joint impedance in both healthy individuals and Parkinson's disease and summarises prior studies employing the same manipulandum designs as those used in this thesis.

2.5.2. Early History

Quantitative investigation of human joint impedance began in the 1980s and laid the foundations for later wrist-specific research. A seminal multi-joint study by Mussa-Ivaldi, Hogan, and Bizzi (1985) used a planar two-degree-of-freedom manipulandum to measure the endpoint stiffness of the human arm [216]. When the hand was displaced from an equilibrium posture, the arm generated predictable restoring forces that could be captured in a stiffness matrix. Graphically, these properties were represented as an ellipse centred on the hand. The size, shape, and orientation of this "stiffness ellipse" depended strongly on arm configuration, revealing that the arm's resistance to perturbation is anisotropic and posture-dependent, yet highly consistent within an individual [217].

This discovery - that the nervous system regulates a directional stiffness or impedance "field" - was pivotal. It aligned naturally with Hogan's impedance control framework (1985), which proposed that humans regulate mechanical impedance to ensure stability and task-appropriate behaviour [1]. Subsequent studies confirmed that endpoint stiffness is under voluntary control. Increasing co-contraction enlarges the stiffness ellipse, improving disturbance rejection in all directions [80], while later work demonstrated that participants tune the ellipse orientation to counter specific directional instabilities or to match task demands [80], [218]. These multi-joint investigations established the principle that the CNS actively modulates limb impedance, foreshadowing the widespread adoption of single-joint paradigms.

Single-joint impedance measurements followed a similar developmental trajectory. Early research focused on the ankle and elbow [19], [219], [220], and by the late 1980s attention had shifted to the wrist [58], [221], [222]. Gielen and Houk (1989) examined the "servo-like" properties of wrist control, modelling how stretch reflex pathways contribute to effective stiffness via long-loop feedback mechanisms [223]. Around the same time, Teräväinen et al. (1989) conducted one of the first objective assessments of wrist rigidity in Parkinson's disease using a torque motor [224]. By passively oscillating the hand and quantifying resisting torque in Newton-metres per degree, they observed that Parkinsonian rigidity increased at higher movement velocities. This finding challenged the classical clinical view of rigidity as velocity-independent, indicating a significant reflex contribution.

In healthy subjects, the interplay between reflexive and voluntary components of wrist impedance was further explored by De Serres and Milner (1991) [14] . Using a servomotor to impose small, rapid wrist displacements (3° and 10°) while participants maintained a steady posture against various loads, they showed that when confronting an unstable load, subjects markedly increased co-contraction of wrist flexors and extensors, thereby raising joint stiffness. Crucially, the phasic stretch reflex contributed little to this increased stiffness; the primary mechanism was elevated baseline muscle activation. This

demonstrated that, for moderate perturbations, impedance regulation is dominated by voluntary muscle tuning rather than reflex gain.

By the early 1990s, two core principles had therefore been established:

1. Humans can flexibly adjust joint impedance through muscle activation and co-contraction strategies.
2. Robotic and servomotor devices provide a precise means of quantifying these adjustments and the underlying reflex behaviour.

These principles set the stage for a proliferation of wrist-focused studies employing robotic manipulanda. Such devices now form essential tools for probing normal impedance regulation, exploring stability–movement transitions, and characterising pathological changes such as Parkinsonian rigidity.

2.5.3. Healthy Motor Control

Modern investigations of healthy wrist mechanics have made extensive use of single- and multi-degree-of-freedom robotic manipulanda to characterise joint impedance under controlled conditions. Although many studies isolate the primary axis of wrist flexion-extension (1-DOF), more recent work has adopted 2-DOF and 3-DOF devices capable of probing radial-ulnar deviation and forearm pronation–supination. These multi-DOF platforms allow researchers to map the directional structure of wrist impedance in a manner analogous to endpoint stiffness ellipses in the arm.

A consistent finding across these studies is that wrist impedance is highly anisotropic. Using wrist robots, Crisco et al. (2011) and Formica et al. (2012) demonstrated that stiffness is greatest along the anatomical axes of flexion-extension and radial-ulnar deviation, and lowest along the diagonal “dart thrower’s” motion path [8], [225]. This directional dependence suggests that even at a single joint, impedance emerges from a complex combination of passive tissue mechanics, joint geometry, and muscle-tendon coordination. Importantly, these anisotropic profiles are reproducible across participants, indicating a stable neuromechanical organisation of wrist impedance in healthy adults.

Robotic manipulanda have also enabled careful separation of passive and active impedance components. Studies using backdrivable wrist robots have quantified passive viscoelastic properties by displacing the relaxed wrist through small amplitudes and fitting viscoelastic models to the resulting torques. Passive stiffness estimates in healthy individuals typically fall in the range of 0.06–0.07 Nm/deg [8], with characteristic stiffness patterns that are consistent within subjects but vary modestly between them.

In contrast, active impedance depends strongly on task demands. Perturbation-based paradigms show that participants substantially increase co-contraction when stabilising against destabilising or unpredictable loads [14]. De Serres and Milner’s foundational observations have been extended by more recent work demonstrating that co-contraction increases sharply when interacting with mechanically unstable environments [226], tool dynamics [227], or noisy force fields [228]. For example, studies using handheld tools coupled to torque-controlled motors show that individuals rapidly increase wrist stiffness in anticipation of contact with rigid surfaces, highlighting the role of feedforward impedance control. Similarly, during interaction with unpredictable force perturbations, participants elevate active stiffness to reduce movement variance and enhance robustness.

Robotic studies consistently link impedance modulation to muscle activation patterns, particularly co-contraction of antagonist muscle pairs [14], [59], [229]. EMG recordings demonstrate that antagonist recruitment functions as a primary actuator of stiffness at the wrist, with reflex contributions playing a secondary, context-dependent role. Notably, voluntary co-contraction appears limited: maximum achievable wrist stiffness is only about 40–50% of what would be expected if flexors and extensors

exerted their maximal intrinsic stiffness [230]. This suggests that neuromuscular constraints and central control strategies prevent excessively rigid postures in healthy motor behaviour.

Overall, modern robotic studies have shown that wrist impedance in healthy individuals is highly tuneable, directionally structured, and regulated through a combination of reflex pathways, feedforward control, and flexible co-contraction strategies. These findings provide an essential baseline for interpreting the altered impedance regulation observed in neurological conditions such as Parkinson's disease, and they motivate the experimental paradigm developed in this thesis for studying stability–movement transitions.

2.5.4. Parkinson's Disease Research

Robotic and servomotor-driven manipulanda have been central to the quantitative study of Parkinson's disease (PD), particularly because rigidity is one of its defining motor symptoms and cannot be fully characterised through clinical examination alone. Early work in the 1980s and 1990s demonstrated the potential of motorised devices to move the wrist passively at controlled velocities and measure the resulting torques with far greater precision than manual assessment . A landmark contribution came from Teräväinen et al. (1989), who oscillated the wrist using a torque motor and introduced an objective rigidity score in physical units [224]. They found that PD patients produced significantly greater resistance torques than healthy controls, and that this rigidity increased with stretch velocity, implicating reflex hyper-excitability in its origin. Meara and Cody (1992) further probed the neuromuscular basis of rigidity [231]. They reported only a moderate relationship between background flexor EMG activity and clinical rigidity scores, suggesting that elevated tone alone could not fully explain rigidity. Their 1993 study showed that levodopa reduced both rigidity and long-latency stretch reflexes, indicating that altered transcortical reflex pathways contribute meaningfully to the phenomenon [232]. Around the same period, Caligiuri (1994) developed a portable, handheld device capable of generating an objective rigidity metric that correlated with clinical ratings [233]. This work demonstrated the feasibility of obtaining quantitative stiffness measures in typical clinical settings and underscored the moment-to-moment variability of rigidity, especially across medication cycles.

From the mid-2000s, research using servo-controlled manipulanda, particularly by Xia, Rymer, and colleagues, provided major mechanistic insights into PD rigidity [108], [234], [235]. These studies revealed that rigidity arises not only from exaggerated stretch reflexes but also from a pathological "shortening reaction", in which muscles abnormally activate when they shorten. Their work showed that these two mechanisms interact synergistically to elevate joint impedance. They also demonstrated that rigidity is direction-dependent: PD patients resisting imposed wrist movements exhibited greater torque during extension than flexion, a pattern absent in healthy controls. This asymmetry suggested that reflex hyper-resistance is more readily triggered in certain muscle groups, highlighting the nuanced and non-uniform nature of wrist rigidity. During the same period, robotic systems began to be used to quantify how behavioural and pharmacological interventions modulate rigidity. Powell et al. (2011) showed that contralateral voluntary movement markedly increased ipsilateral wrist rigidity, particularly in the OFF-medication state, and that dopaminergic therapy reduced both baseline rigidity and the exacerbating effect of activation [236]. Torque-controlled manipulanda have also been deployed to evaluate surgical interventions. Little et al. (2012) measured rigidity during deep brain stimulation (DBS) of the subthalamic nucleus and found that subtherapeutic low-frequency DBS increased rigidity, whereas high-frequency stimulation reduced it [169]. Studies by Rätsep and Asser (2011) similarly showed that effective DBS decreased the viscoelastic stiffness of wrist musculature, paralleling clinical improvements [237]. These findings reinforced the view that robotic measurements can serve as sensitive biomarker readouts for therapeutic effects.

Alongside rigidity, robotic manipulanda have also contributed to understanding bradykinesia, the cardinal PD symptom characterised by slowed movement, reduced movement amplitude, and impaired movement initiation. Whereas rigidity reflects elevated baseline impedance, bradykinesia reflects difficulty transitioning out of a stability-oriented, high-impedance control regime and into efficient

movement execution. Robotic reaching tasks, force-controlled paradigms, and repeated perturbation trials have consistently shown that individuals with PD exhibit delayed release of co-contraction, reduced scaling of muscle activation to task demands, and slower initiation of voluntary movement [238], [239]. These features manifest mechanically as prolonged reaction times, decreased peak velocities, longer movement durations, and impaired corrective responses, all of which can be captured with high temporal precision using servomotor systems. Importantly, several studies report that PD patients show excessive co-contraction even when movements are intended to be rapid or ballistic, suggesting a persistent reliance on high-impedance strategies that hinder fluid movement. These findings align with the broader perspective that PD impairs the neural mechanisms required for down-regulating impedance, engaging dynamic control, and updating motor commands efficiently.

Collectively, robotic manipulanda have provided a detailed biomechanical and neurophysiological characterisation of Parkinsonian motor impairment, extending beyond rigidity to capture the dynamics of bradykinesia and impaired movement initiation. These studies offer fine-grained insight into velocity dependence, directional asymmetries, reflex contributions, pathological coactivation patterns, and treatment-induced changes. Crucially, robotic tasks have revealed that PD patients struggle to down-regulate impedance and shift into a movement-oriented state, contributing simultaneously to rigidity and bradykinesia. These technologies thus offer a powerful means of probing the sensorimotor deficits underlying PD and provide a foundation for objective biomarkers for diagnosis. In this context, the robotic system developed for the present thesis contributes to a growing body of work that seeks to quantify these impairments with high precision, establish normative benchmarks in healthy individuals, and lay the groundwork for future diagnostic tools targeting the transitional dynamics of impedance control.

2.5.5. Hi5 and HRX-1 Haptic Robots

One of the aims of this project was to develop a robotic framework on which to explore the transitional dynamics of stability- and movement-orientation activity (**Aim 5**). To this end, production of a portable version of the Hi5 device was conducted. This manipulandum was used to establish the foundation of the experimental architecture as well as preliminary testing and development of the experimental protocol and analyses. Later, all formal experimental data reported in this thesis were collected using the HRX-1, a newer platform derived from the same design lineage but optimised for neuromechanical research and rehabilitation applications. The established literature on both devices provides useful context to understand their technical capabilities and the types of sensorimotor phenomena they have previously been used to probe.

The Hi5 robotic interface was introduced by Melendez-Calderon and colleagues in 2011 as a dual-wrist device for studying bimanual coordination and human–human interaction [240]. The original work established its core features, including high-bandwidth torque and position control. The Hi5 has primarily been utilised in studies examining human interaction under controlled coupling conditions, whether with human or robotic partners [241], [242], coordination of force output between dominant and non-dominant hands [243], and the rehabilitative assessment of tactile feedback [244]. In addition, the device has been used to investigate functional connectivity mapping in dystonia [245] and EMG co-activation under feedback manipulations in virtual reality [246]. Collectively, this literature demonstrates that the Hi5 is well suited for studying motor coordination, muscle co-contraction, and adaptation, making it an appropriate platform for impedance-based investigations.

The HRX-1 is an updated single-degree-of-freedom wrist manipulandum designed for neuromechanics research and rehabilitation. It extends the Hi5 by incorporating multiple control modes, a more compact form factor, improved control performance, and compatibility with real-time control architectures such as Simulink. Owing to its recent development, the HRX-1 has a limited publication history. Nevertheless, it has been validated for measuring muscle activation [247] and has been applied to studies of EMG co-activation during partnered visuo-haptic tasks [248], assistive robotic intervention combined with

electrical stimulation post-stroke [249], and virtual reality-supported training in individuals with functional neurological disorder [250]. Together, these studies indicate that the HRX-1 retains the high-fidelity torque control of the Hi5 while offering enhanced portability and usability. The device has been validated for measuring neuromechanical variables including EMG, torque responses, and coordination metrics, making it well suited for the high-resolution impedance characterisation undertaken in this thesis.

In summary, research using the Hi5 established a methodological foundation for investigating neural dynamics, muscle co-contraction, and adaptation in wrist motor control, while the HRX-1 extends this capability to a more robust and portable platform. The work presented in this thesis builds directly on this progression by using the HRX-1 to deliver controlled perturbations and to quantify impedance regulation and its neural correlates during stability–movement transitions.

2.5.6. Summary

Quantitative studies since the 1980s have established that humans actively regulate joint impedance in a directional, task-dependent manner. Early multi-joint work introduced the concept of stiffness fields, which was later translated to single-joint paradigms using robotic and servomotor devices to characterise wrist impedance with high precision. These studies showed that impedance is primarily modulated through voluntary muscle activation and co-contraction, with reflex contributions playing a secondary, context-dependent role.

In healthy individuals, wrist impedance is anisotropic and flexibly tuned to task demands, supporting stability in uncertain environments while remaining sufficiently low to permit efficient movement. In Parkinson's disease, robotic measurements have revealed pathological elevation and impaired regulation of impedance, driven by abnormal reflexes and muscle activation patterns. These abnormalities contribute not only to rigidity but also to bradykinesia, reflecting difficulty transitioning from stability-oriented to movement-oriented control.

The Hi5 and HRX-1 robotic manipulanda provide the technical foundation for investigating these mechanisms. Building on prior validation and applications, the present thesis uses the HRX-1 to quantify wrist impedance and, critically, the dynamics of transitions between postural stability and voluntary movement, offering a precise framework for studying both healthy motor control and Parkinsonian impairment.

2.6. Quantifying Mechanical Impedance in Healthy Individuals and Parkinson's Disease

2.6.1. Introduction

Mechanical impedance is a fundamental descriptor of how the sensorimotor system responds to external forces and imposed motion. In healthy individuals, impedance and its key component, stiffness, emerge from the interaction of muscle activation, reflex pathways and passive tissue properties, enabling stable, adaptable and goal-directed movement. Quantitative models of impedance and stiffness therefore provide a principled framework for investigating motor control that extends beyond observational or purely kinematic measures.

In Parkinson's disease (PD), characteristic motor impairments such as rigidity and reduced movement adaptability are closely associated with abnormal regulation of impedance and stiffness. Modelling these properties offers objective means to characterise disease-related changes, compare healthy and pathological control strategies, and assess the effects of therapeutic interventions. This section highlights several relevant models for quantifying mechanical impedance and stiffness in both healthy individuals and in Parkinson's disease.

2.6.2. Second-Order Impedance Model

Modelling mechanical impedance provides a principled way to interpret wrist behaviour under load and to separate the passive and active neuromechanical contributions to movement [3], [29], [34]. Although stiffness can be estimated with simple static ratios, a full description of wrist impedance requires capturing the dynamic relationship between torque and motion across time. This section expands the mathematical formulation of impedance.

The simplest and most widely used representation treats the joint as a linear, second-order rotational system:

$$F(t) = M\ddot{x}(t) + B\dot{x}(t) + Kx(t) \quad \textbf{(2.1)}$$

where
• $F(t)$is the applied torque (Nm),
• $x(t)$is the angular displacement (rad),
• $\dot{x}(t)$and $\ddot{x}(t)$are angular velocity and acceleration, respectively,
• $M$is rotational inertia (kg m2),
• $B$is damping (Nm s rad-1),
• $K$is stiffness (Nm rad-1).

This model treats the wrist as a rotational analogue of a mass-spring-damper system. It is usually linearised around a given posture to provide a local approximation of impedance.

In the frequency domain, taking the Laplace transform gives:

$$F(s) = (Ms^2 + Bs + K)X(s) \quad \textbf{(2.2)}$$

The mechanical impedance $Z(s)$is then defined as the ratio of torque to angular velocity:

$$Z(s) = \frac{F(s)}{\dot{X}(s)} = Ms + B + \frac{K}{s} \quad \textbf{(2.3)}$$

This decomposition clarifies how inertia, damping and stiffness contribute to mechanical impedance across frequencies. At high frequencies, impedance is dominated by inertial effects; at intermediate frequencies, damping is the principal contributor; and at low frequencies, stiffness predominates. Healthy individuals typically increase stiffness and damping when stabilising against unpredictable perturbations. In contrast, individuals with Parkinson's disease often exhibit elevated low-frequency impedance even during passive or voluntary movement, reflecting impaired modulation of active stiffness.

2.6.3. Parameter Identification

To estimate (M), (B), and (K), torque and high-precision kinematic data must be collected under controlled mechanical perturbations. Servomotor-driven manipulanda are commonly used to apply step, ramp-and-hold, broadband (chirp), PRBS, or stochastic torque inputs, thereby exciting the limb over a range of amplitudes and frequencies. Linear regression, least-squares fitting, or frequency-domain techniques such as coherence analysis can then be employed to identify impedance parameters.

In the time domain, mechanical impedance is typically modelled as a linear second-order relationship between joint torque and kinematics:

$$\tau(t) = Mx^{\cdot\cdot}(t) + Bx^{\cdot}(t) + Kx(t) \quad \textbf{(2.4)}$$

where $x(t)$, $\dot{x}(t)$, and $\ddot{x}(t)$denote joint position, velocity, and acceleration. This expression can be rewritten in regression form,

$$F(t) = X(t)\theta, X = [x^{\cdot\cdot}(t)\ \ x^{\cdot}(t)\ \ x(t)], \theta = [M\ \ B\ \ K]T \quad \textbf{(2.5)}$$

so that the parameter vector is recovered using ordinary least squares:

$$\theta = (X^T X)^{-1} X^T F \quad \textbf{(2.6)}$$

Mean-centring of kinematic and torque signals is commonly applied to define a local equilibrium point and isolate small-signal impedance about that operating state. Once estimated, the resulting parameters describe how inertia, damping, and stiffness shape impedance across frequencies: inertia dominates at high frequencies, damping at intermediate frequencies, and stiffness at low frequencies. In healthy individuals, estimated stiffness and damping increase systematically with antagonist co-contraction or environmental instability. In Parkinson's disease, both (K) and (B) are frequently elevated while (M) remains largely unchanged, consistent with impaired modulation of active stiffness rather than altered limb inertia.

2.6.4. Nonlinear Impedance Models

Although linear impedance models are widely used for identification and comparison, human joints exhibit clear nonlinear behaviour. Joint stiffness commonly increases with displacement, often referred to as quasi-stiffness, viscous effects may depend on movement velocity, and muscle activation introduces state-dependent modulation that cannot be fully represented by constant parameters. These nonlinearities become particularly evident at larger excursions or near the limits of the joint range of motion.

A simple and commonly adopted nonlinear extension introduces position-dependent stiffness, expressed as:

$$K(x) = K_0 + K_1 x + K_2 x^2 \tag{2.6}$$

so that:

$$F(t) = M\ddot{x}(t) + B\dot{x}(t) + (K_0 + K_1 x(t) + K_2 x^2(t))x(t) \tag{2.7}$$

This formulation allows stiffness to increase progressively with displacement, capturing the well-documented rise in resistance as the wrist approaches extreme postures. Such nonlinear models better reflect the physiological contributions of muscle length–tension properties and passive connective tissues. In Parkinson's disease, rigidity often appears exaggerated across the entire movement range rather than being confined to small perturbations around a neutral posture. As a result, nonlinear impedance formulations can provide a more accurate description of pathological stiffness and its abnormal modulation than linear models alone.

2.6.5. EMG-Driven Models

Mechanical impedance can also be modelled by explicitly linking joint stiffness to muscle activation. In such approaches, stiffness is expressed as the sum of a passive component and activation-dependent terms derived from electromyographic activity of antagonist muscles:

$$K(t) = K_{\text{passive}} + \alpha \cdot \text{EMG}_F(t) + \beta \cdot \text{EMG}_E(t) \tag{2.9}$$

where EMG_F and EMG_E denote filtered flexor and extensor EMG signals, and α and β quantify their respective contributions to stiffness. This formulation provides a direct physiological link between neural drive and mechanical impedance and naturally accounts for increases in stiffness arising from co-contraction.

More detailed muscle-based models extend this framework by incorporating force-length and force-velocity relationships:

$$F_m(t) = a(t) f_l(x) f_v(\dot{x}) + f_{\text{passive}}(x) \tag{2.10}$$

where muscle activation $a(t)$is obtained from processed EMG signals. These models capture how changes in muscle length, contraction velocity, and activation jointly shape force production and, in turn, joint impedance. Such formulations are particularly informative in Parkinson's disease, where elevated baseline activation, abnormal shortening reactions, and impaired reciprocal inhibition distort the normal relationship between EMG and mechanical impedance, leading to persistently increased and poorly modulated joint stiffness.

2.6.6. Mechanical Stiffness

Stiffness is the relationship between force applied and resultant displacement. When assessing joint mobilisation this relationship is best expression in terms of torsional stiffness:

$$K = \frac{M}{\theta} \tag{2.11}$$

where stiffness K(N·m/rad) is defined as the ratio of the applied joint moment M(N·m) to the angular displacement θ(rad). This formulation provides a direct mechanical interpretation of resistance to rotation and is well suited to the assessment of joint behaviour under controlled perturbations.

In individuals with Parkinson's disease, rigidity can be quantified objectively in terms of increased joint stiffness. Although clinicians commonly assess rigidity using ordinal clinical rating scales, such measures are subjective and lack sensitivity to subtle changes. Quantitative assessment of stiffness is therefore increasingly employed, using technologies such as servomotor-based systems [8], [14], [222], dynamometry [251], and vision-based motion analysis [252]. These approaches allow stiffness to be measured directly and reproducibly, supporting more precise characterisation of rigidity and its modulation across tasks and disease states.

2.6.7. Co-contraction Indices

Electromyographic (EMG) data can also be used to estimate stiffness by computing the degree of coactivation between antagonist muscles, presented as a co-contraction index (CCI) at each timestep. There are two commonly used formulas to compute CCI in EMG data:

$$CCI_1(t) = \frac{2 * EMG_L(t)}{EMG_L(t) + EMG_H(t)} [220] \tag{2.12}$$

$$CCI_2\,(t) = \frac{EMG_L(t)}{EMG_H(t)} \big(EMG_L(t) + EMG_H(t)\big) [253] \tag{2.13}$$

Where $EMG_L(t)$ is the less active muscle at timepoint (t) and $EMG_H(t)$ is the muscle with higher EMG activation at the same time point. CCI_1 computes the activity of the less active muscle as a ratio of the more active muscle returning a value between 0 and 1. CCI_2 scales the total activity to the ratio of activity between the two muscles, resulting in a value between 0 and $2 * EMG_L(t)$. With the knowledge that $EMG_L(t) \leq EMG_H(t)$, it is possible to reformulate CCI_2 to have a response range of 0-1, both for

drawing comparison between the two formulations and for clarity when interpreting CCI_2. Multiplication of the terms results in:

$$CCI_2\ (t) = \frac{EMG_L(t)^2}{EMG_H(t)} + EMG_L(t) \quad \textbf{(2.14)}$$

When $EMG_L(t) = EMG_H(t)$, $CCI_2\ (t) = 2 * EMG_H(t)$. As such, to ensure a response in the range of 0-1, there previous formulation can be divided by $2 * EMG_H(t)$, resulting in:

$$CCI_2\ (t) = \frac{EMG_L(t)^2 + (EMG_L(t) * EMG_H(t))}{2 * EMG_H(t)^2} \quad \textbf{(2.15)}$$

The response curves of CCI_1 and CCI_2 illustrates their divergence (**Figure 2.6**). While both now return values between 0-1, the inversion of the parabola results in a stronger response at lower values for CCI_1 while the response of CCI_2 is less sensitive at the lower range. Contrasting these two formulations has been performed in previous studies, showing CCI_1 to be correlated more closely to a measure of joint stiffness in post-stroke gait analysis [254]. However, it is unclear if this result is directly generalisable to other joints or clinical conditions.

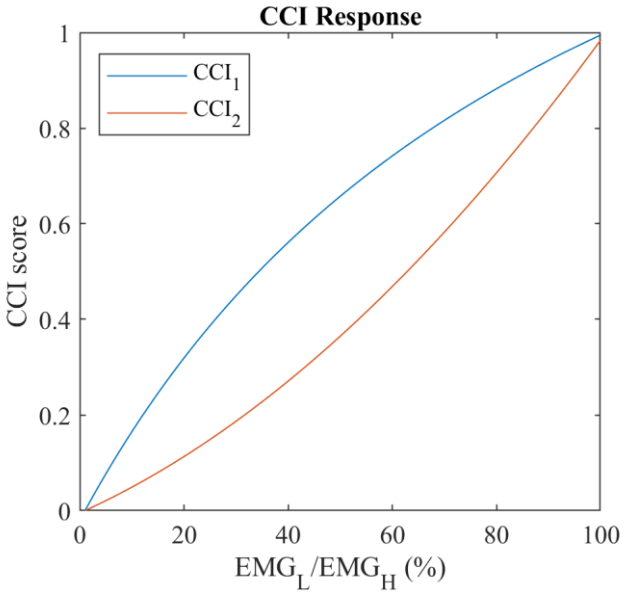

Figure 2.6. Response curves of each CCI formulation as EMG_L grows as a percentage of EMG_H

2.6.8. Objective Rigidity Measurement

Rigidity is a critical biomarker for diagnosing and monitoring the progression of PD [39], [255]. When compared with nonclinical populations, individuals with PD demonstrate elevated EMG activity both at rest [256] and during activity [257]. They also demonstrate significant delay in returning to baseline levels of activity after completing a movement, a feature absent in healthy individuals [256]. Individuals with PD have also shown an elevated shortening reaction during passive movement - a burst of EMG activity of the antagonist muscle during movement [258]. The presence of these features could be used

as the basis of diagnostic testing, subject to sufficient amplitude in the early or preclinical stages of disease progression.

When assessing within PD populations, rigidity is the cardinal motor symptom with the poorest reliability when assessed using the UPDRS [259]. This has resulted in numerous attempts to develop an objective rigidity measurement. The primary divide in the approaches developed is whether they are designed to integrate with current clinical testing practices or serve as an alternative to them.

Approaches that integrate with current clinical testing are designed operate alongside the assessments conducted by a clinician. These solutions utilise devices such as EMG [257], force sensors [251], inertial measurement units (IMU) [260] and even machine learning approaches applied to video recordings [252]. The advantage of such an approach is that it does not disrupt the established clinical protocol, and the quality of assessment is therefore directly comparable to the clinical scores provided. The disadvantage of these approaches is that the fundamental movements are still human-led so, although measured objectively, are subject to variability in the forces applied. The solution to this variability is to automate force application. This has been explored by studies deploying servomotor-based wrist manipulandum [127], [233], [255], [261] to produce smooth, repeatable torque profiles. Other designs have taken similar approaches using devices that sit within the user's palm [262] or as robotic glove [263]. These approaches have shown good coherence with clinical assessments but have failed to achieve widespread utilisation due to the requirement of specialised, often bulky equipment. However, they have been informative in understanding optimal strategies to detect rigidity in PD, showing that rigidity is most detectable in wrist movement speeds between 140-190°/s [224] and angles 60° - 90° [264].

2.6.9. Summary

In summary, mechanical impedance and stiffness models provide objective quantification of motor control in both healthy individuals and PD. Linear impedance formulations enable robust estimation of inertia, damping, and stiffness, while nonlinear and EMG-informed models capture physiological features such as displacement-dependent stiffness and abnormal muscle activation patterns. Direct stiffness estimation, combined with measures of muscular co-contraction, links endpoint impedance to underlying peripheral motor mechanisms, which can be integrated with neural indices such as beta-band power to enable a robust, multilayered analysis of the sensorimotor dynamics underlying impedance control. This framework underpins the experimental approach of this thesis, in which a robotic manipulandum is used to selectively challenge impedance regulation under controlled conditions, allowing temporally precise, objectively quantified, and context-specific assessment of the mechanisms governing stability–movement transitions. The insights gained through this experimental and analytical approach may also be leveraged to help inform the development of improved objective assessments of rigidity in Parkinson's disease.

2.7. Gaps in Knowledge

Transitions between stabilisation and voluntary movement are ubiquitous in natural behaviour, requiring the nervous system to rapidly reconfigure control strategies as it shifts from postural stabilisation to permitting movement. Despite their prevalence, existing work has largely focused on impedance responses either during sustained stabilisation or during movement execution in isolation, leaving the transitional period between these control states unexplored. In particular, little is known about how impedance is downregulated following externally imposed stability demands, or how short-term persistence of elevated impedance influences subsequent voluntary movement. It is the exploration of this uninvestigated aspect of motor control that underpins the present research. While the stability–movement transition is central to this thesis, related gaps in knowledge that operate alongside this primary gap are also addressed.

In healthy populations, impedance is typically treated as an instantaneous mechanical property rather than as a persistent control state that may persist across contexts. Consequently, insight into sustained or maladaptive impedance regulation has largely been inferred from pathological conditions, most notably Parkinson's disease (PD). While this clinical insight is valuable, PD rigidity provides only an indirect window onto healthy impedance control, inferred through its impairment. To better understand impedance control, it is therefore necessary to test these mechanisms directly in non-clinical populations. Exploration of context-specific and temporal aspects of impedance control represents an additional knowledge gap addressed by this thesis. Through a combination of multistage experimental trials and repeated-measures designs, this work examines impedance longitudinally in a manner largely absent from the current literature. This facilitates investigation of how impedance evolves across motor contexts and as a function of adaptation and learning, positioning impedance control in healthy motor behaviour as a dynamic phenomenon. This, in turn, provides a foundation for more targeted comparisons between healthy and clinically impaired impedance control.

While current approaches capture the mechanical expression of impedance, they provide limited insight into the neural processes governing how impedance is maintained, released, or reshaped across successive actions. As a result, it remains unclear how the nervous system negotiates the transition from a stabilised, high-impedance control state to a movement-permissive configuration, or whether residual impedance modulates the planning and execution of subsequent movement. This gap is particularly salient in clinical populations such as Parkinson's disease, where impaired neural regulation may lead to pathological persistence of stabilisation-related control, contributing to rigidity and difficulty initiating movement.

Together, these limitations represent both methodological and conceptual gaps in the literature. Although servomotor manipulanda provide the experimental control necessary to quantify impedance across control states, they have rarely been used to examine the temporal dynamics of impedance regulation specifically at stability–movement transitions or to link mechanical changes with underlying neural dynamics. Addressing these gaps is essential for integrating detailed impedance models with the flexible, context-dependent control observed in natural behaviour, and for improving understanding of how impaired impedance regulation contributes to disrupted transitions between stability and movement in clinical populations.

2.8. Literature Review Summary

This literature review synthesised research on impedance control to situate the present work within current understanding of both healthy impedance regulation and pathological rigidity. By outlining relevant neuroanatomical systems and sensorimotor dynamics, it provides a framework for interpreting the experimental results of this thesis in terms of both neural and mechanical function.

The review also highlights critical gaps in knowledge relating to healthy impedance control, particularly its temporal evolution, its transition across motor contexts, and the limited identification of clear neural correlates. Particular attention is given to beta-band sensorimotor oscillations and their role in motor planning, learning, and adaptation, as well as their alteration in PD. Post-movement beta rebound (PMBR) and corticomuscular coherence (CMC) are identified as key neural signatures of motor state change, guiding the investigations presented in this thesis. The review further summarises how servomotor manipulanda have been used to probe wrist impedance dynamics and outlines key mathematical models for objectively quantifying impedance, stiffness, and muscular co-contraction.

In closing, this review establishes both the conceptual and methodological foundation for the experimental work that follows, motivating the focus on stability–movement transitions and the combined mechanical and neural characterisation of impedance regulation.

III. Robotic Development

3.1. Introduction

The central investigation of the present work was to explore the sensorimotor dynamics of stability–movement transitions. To effectively explore these dynamics, a comprehensive robotic system that could effectively and precisely challenge the motor system to elevate impedance, visually cue the participant to appropriate action and integrate multiple high-precision data sources was required. No system that met these requirements was available at project onset. As such, a technical architecture capable of delivering the envisioned experimental paradigm needed to be developed.

The scope of required movement was constrained to flexion/extension (FE) of the wrist, defining the single degree of freedom that a robotic manipulandum was required to function in. To be effective, the manipulandum would need to be interacted with through a handle and comfortably support the participant's arm throughout the experiment. Making the device portable was also a central requirement as this would dramatically increase participant recruitment opportunities, especially when working with clinical populations.

In terms of function, the robot was required to provide real-time positional and force data while synchronising with EEG and EMG data streams. This necessitated extremely high precision as desynchronisation in a scale of tens of milliseconds could cause catastrophic failure of the analysis. This integration, particularly in real-time, was non-trivial and required extensive development to ensure the necessary precision.

Beyond passively recording, the system also needed to be able to effectively run the experiment. To do so, the system needed to provide responsive visual feedback in the context of the motor task, have the capability of providing scheduled perturbation of the handle at specific levels of torque and perform the meta-level operations of the experiment such as transitioning between tasks, performing calibrations and timestamping significant events (**Figure 3.1**).

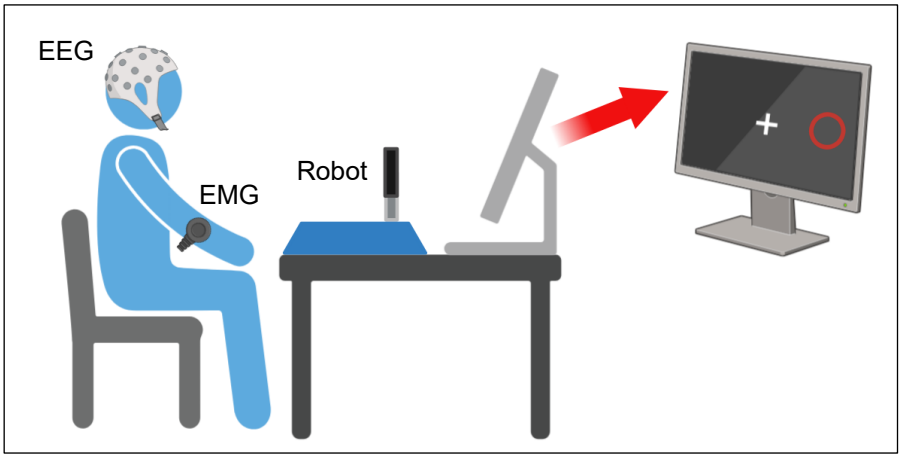

Figure 3.1. A simple visualisation of the experimental setup, highlighting the critical technical components that the participant would interact with.

These high-level requirements defined the scope of functionality necessary for an effective robotic solution but provided minimal definitive design specifications. To initiate the mechanical design process, consultation was sought with the Human Robotics Group at Imperial College London due to their expertise in haptic feedback experimentation. It was decided to develop a portable version of their non-portable Hi5 haptic feedback device [240] as this design provided much of the motor functionality

required. However, this was not a prepackaged solution. Not only did the design need to be made portable, but the more advanced functionality such as EEG integration and experimental management also needed to be developed.

With an outline of the design and an initial mechanical component list, development of the robotic system began. This was an iterative process involving recurrent design and testing phases. Throughout the process, the design of the robot evolved in conjunction with the software architecture and secondary devices utilised to provide necessary functionality. The guiding philosophy throughout the development process was to reduce the barriers to rapid system deployment, enhance portability and ease of use, while ensuring the system remained physically robust and produced high quality, precisely synchronised recordings.

3.2. System Requirements

When developing the portable Hi5 manipulandum, it became essential to formalise the full set of system requirements that would guide both the mechanical design and the broader software and integration architecture. Given the complexity of the intended application - which demanded precise neuromechanical interaction, reliable synchronisation with EEG and EMG systems, and seamless experimental control - a structured requirements specification was necessary to ensure that every critical element of the system was identified, justified, and verifiable.

The requirements table presented below consolidates these needs into a comprehensive framework covering functional, mechanical, data-synchronisation, software, integration, safety, usability, and development constraints (**Table 3.1**). Each requirement reflects either a direct operational necessity (such as the ability to deliver controlled torque perturbations), a constraint imposed by the experimental methodology (such as sub-20 ms timing alignment between data streams), or a practical consideration relating to portability, robustness, or ease of deployment. This requirements list guided the design and development process while providing a clear specification against which the performance of the system architecture could be evaluated.

Table 3.1. The system requirements table used to guide development of the portable Hi5 manipulandum.

Req. ID	Category	Requirement	Description / Notes	Priority
FR-01	Functional	Neuromotor challenge capability	System must apply controlled torque perturbations to elevate wrist stiffness.	High
FR-02	Functional	Real-time motion recording	Must capture wrist FE position, velocity, and force in real time.	High
FR-03	Functional	Visual feedback	Must deliver responsive visual cues synchronised to motor activity.	High
FR-04	Functional	Experimental workflow automation	Must manage tasks, transitions, calibrations, and event timestamping.	High
FR-05	Functional	Perturbation scheduling	Must apply programmable perturbations with user-defined parameters.	Medium
MR-01	Mechanical	Movement degree of freedom	Must permit wrist flexion/extension as the primary DOF.	High
MR-02	Mechanical	Ergonomic handle	Must include a comfortable handle for wrist FE interaction.	Medium
MR-03	Mechanical	Arm support	Must provide stable and adjustable forearm support.	Medium
MR-04	Mechanical	Portability	System must be portable for clinical deployment.	High
MR-05	Mechanical	Structural robustness	Must withstand repeated perturbations and maintain alignment.	High
DS-01	Data/Synch	High-precision synchronisation	Robot, EEG, and EMG must synchronise with < 20 ms drift.	High
DS-02	Data/Synch	Unified timestamping	All significant events must be timestamped across systems.	High
DS-03	Data/Synch	High-resolution sensing	Sensors must provide high-accuracy FE and force measurements.	High
SW-01	Software	Real-time control loop	Closed-loop motor control with low-latency response.	High

SW-02	Software	Data streaming	Continuous, high-speed streaming of motion/force data.	High
SW-03	Software	Visual cue system	Must display low-latency task feedback (target, cursor, cues).	Medium
SW-04	Software	Experiment control UI	User interface for task control, calibrations, start/stop functions.	Medium
IN-01	Integration	EEG/EMG trigger compatibility	Must integrate digital triggers for event alignment.	High
IN-02	Integration	Protocol compatibility	Must support standard communication protocols (TCP/UDP/serial).	Medium
SF-01	Safety	Mechanical limits	Range-of-motion and torque limits to protect participants.	High
SF-02	Safety	Emergency stop	Accessible to both operator and participant.	High
US-01	Usability	Quick setup	Calibration and setup must be rapid (< 10 minutes if possible).	Medium
US-02	Usability	Minimal training	Operators should require minimal training to run experiments.	Medium
DEV-01	Constraint	Iterative development	System must support rapid prototyping cycles.	Medium
DEV-02	Constraint	Prioritise portability and data quality	Design choices should favour portability and synchronisation accuracy.	High

3.3. Hi5 Configuration

This section provides an overview of the major design decisions underpinning the development of the initial robotic architecture and outlines how these decisions addressed the functional, mechanical and synchronisation requirements defined. This first-generation portable Hi5 system was developed within the scope of the present work and was used to collect preliminary data and run an initial test cohort.

The robotic interface was built around three key components: a Maxon RE-65 250 W DC motor, a HEDR-55L2-BY09 optical encoder, and a TRT-50 torque sensor. These components delivered the essential capability to record high-resolution wrist position and interaction forces (FR-02; DS-03) while also enabling controlled torque perturbations during the task (FR-01). All components were integrated into a custom acetal housing mounted on a central aluminium plate, providing the structural robustness required for repeated perturbation trials (MR-05).

A major constraint on the mechanical design emerged from the physical dimensions of the RE-65 motor. Its height (>130 mm) prevented conventional horizontal mounting on a tabletop, leading to a suspended configuration in which the motor housing extended over the table edge. To maintain correct alignment between the hand and the primary flexion–extension axis of the wrist (MR-01; MR-02), this arrangement required the addition of a 2:1 pulley-based transmission system linking the motor shaft to the handle. This transmission enabled the delivery of the torque profiles required by the experiment (FR-01) while preserving overall system portability (MR-04). The overall formfactor was developed to support this suspended-mount architecture, which significantly influenced the mechanical footprint of the design (**Figure 3.2**).

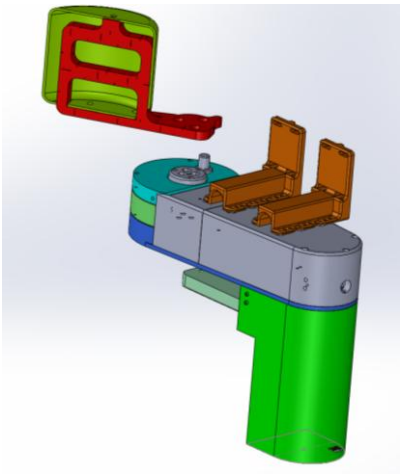

Figure 3.2. An early CAD assembly of the Hi5. The vertical green component is the motor housing. The robot sat on a table contacting the aluminium plate (dark blue), the motor housing hangs from the table's edge.

Experimental control, task visualisation, and data acquisition were handled through custom C++ software built using the Qt 5.10 framework and communicating with the EPOS2 motor controller via its native C API. This software infrastructure enabled centralised management of task execution (FR-04; SW-04), visual feedback (FR-03; SW-03), and high-throughput data capture (SW-02). The experimental sessions were defined using prefabricated JSON and CSV files that specified torque profiles, target locations, and event markers, ensuring consistency across participants and supporting rapid setup (US-01; US-02).

Integration of robotic data with EEG and EMG recordings required the system to support precise multimodal synchronisation. EEG and EMG data were collected at 300 Hz using a DSI-24 dry-electrode system with auxiliary EMG sensors, while torque and accelerometery were sampled at 512 Hz through a TMSi Porti amplifier. Both physiological streams were integrated with the robot via

LabStreamingLayer (LSL), meeting the requirement for standardised, compatible communication protocols (IN-02) and high-precision synchronisation across devices (IN-01; DS-01). Custom interfaces (dsi2lsl for the DSI system and OpenVibe for the TMSi amplifier) ensured seamless data flow into the main control software. Meanwhile, encoder position data were transmitted directly from the motor controller to maintain the low-latency kinematic reporting required for both visual feedback and motor control (SW-01; DS-03; FR-03).

To meet the stringent synchronisation requirement of maintaining <20 ms drift across all recorded data (DS-01), the software architecture was implemented using lockless programming principles. Each incoming data stream was assigned to its own dedicated thread, accessed exclusively via atomic operations, and timestamp-corrected using LSL's clock-synchronisation algorithms. This architecture consistently produced timing errors well below the required threshold and supported reliable motor recruitment within 0.1 Nm of the target torque on >99% of trials, fulfilling the needs of real-time, closed-loop motor control (SW-01; FR-01) and precise kinematic measurement (FR-02). However, while effective, the architecture deployed required the integration of multiple hardware devices and several software packages (**Figure 3.3**), providing numerous potential points of failure and increasing the overall complexity of system maintenance and troubleshooting.

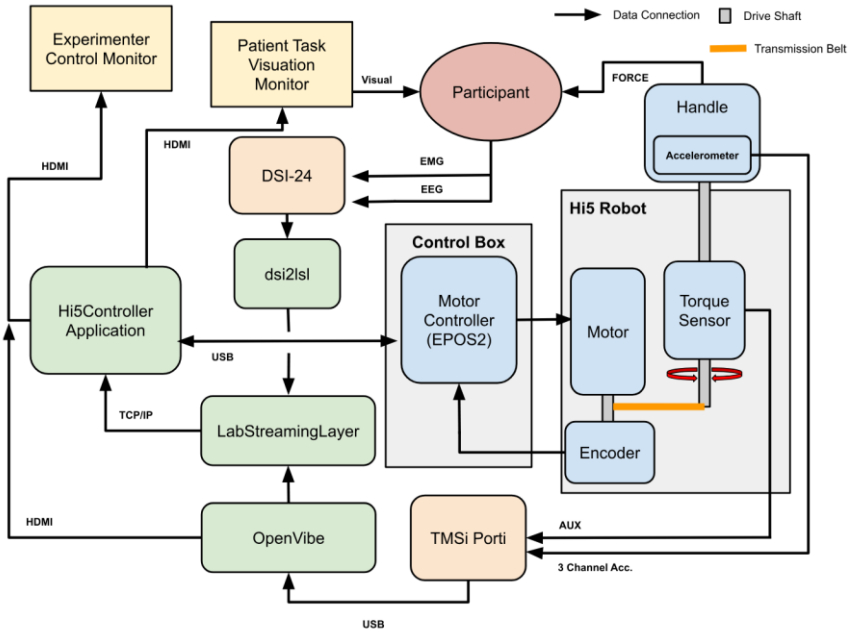

Figure 3.3. Control architecture and informational flow of the system built around the portable Hi5.

Despite overall strong system performance, several limitations emerged in practice. The suspended motor configuration caused occasional displacement of the device during higher-torque interactions. Although the system was secured using spring-loaded toggle clamps (**Figure 3.4**), the asymmetric weight distribution made it difficult to prevent small shifts during use. These movements, while usually minor, had the potential to introduce noise into the recorded data (DS-03) and could disrupt participant comfort (SF-01).

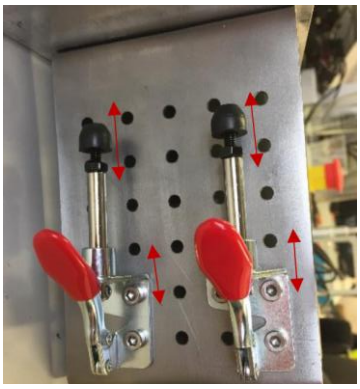

Figure 3.4. The spring-loaded toggle clamps used to secure the Hi5. While moderately effective, the overbalancing cause by the suspended motor was difficult to fully compensate for.

A more substantial limitation arose from the belt-based transmission. The need to manually tension the polyurethane belt using an adjustable tensioner introduced minor asymmetries in torque and positional measurements, particularly if the belt required re-tensioning between participants (**Figure 3.5**). Although presumed small, these effects could not be precisely quantified and represented a potential source of measurement variability (DS-03; FR-02). More critically, belt slippage occasionally occurred during use. In extreme cases, slippage caused the physical handle position to become misaligned with the displayed cursor position, preventing participants from completing the task correctly. This error affected three of fourteen participants in the test cohort, resulting in the exclusion of impacted trials and demonstrating a significant reliability constraint inconsistent with the required robustness of task execution (FR-03; FR-04; SF-01).

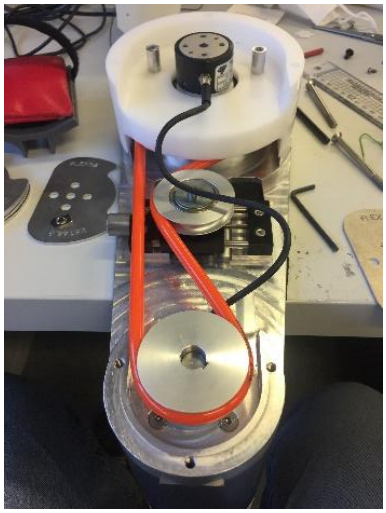

Figure 3.5. The transmission system with polyurethane belt and tensioner pulley. Tension is achieved by turning the push screws, drawing the tensioner pulley across the belt.

Overall, the initial portable Hi5 system successfully met the primary functional and synchronisation requirements of the project, demonstrating that high-precision control, multimodal integration, and automated experimentation could be achieved within a portable robotic platform (MR-04; FR-01-04; DS-01, **Figure 3.6**). However, the mechanical challenges introduced by the suspended motor design and belt transmission system combined with the overall system complexity highlighted critical areas for refinement in subsequent development, guiding improvements in mechanical stability, transmission reliability, and long-term usability (DEV-01; DEV-02).

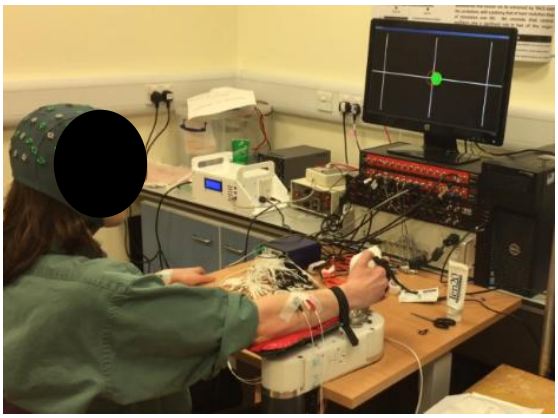

Figure 3.6. Photograph of the Hi5 being tested. n.b. The EEG cap pictured is a fitted cap system designed to work with the TMSi Porti and is not the DSI-24 used in the final deployment.

3.4. HRX-1 Configuration

This section details the configuration used when operating the HRX-1 portable haptics robot and outlines how its updated supporting architecture met the system requirements while addressing the limitations of the Hi5 configuration. The HRX-1 served as the primary experimental configuration throughout the present work and was acquired through a spinout company of the Human Robotics Group – HumanRobotix Ltd. The HRX-1 is an upgraded version of the experimental portable Hi5 device that was being developed as part of the present work. Throughout the development of the Hi5, the design and deployment challenges were reported back to the Human Robotics Group, providing feedback to assist in the design the HRX-1. The transition to this upgraded device aligned with the need for improved robustness and simplified operation identified in the requirements table (DEV-02; US-01; MR-05).

The most substantial improvement introduced by the HRX-1 was the replacement of the bulky Maxon RE-65 250 W motor with the significantly more compact Maxon EC 90 Flat 600 W motor. The EC 90 Flat, with a height of only 30 mm, could be mounted directly beneath the handle on a tabletop without elevating the user's arm. This addressed several critical requirements. First, it eliminated the belt-based transmission system needed in the Hi5, resolving issues of belt tension variability, torque asymmetry, and occasional belt slippage that previously affected measurement consistency (DS-03; FR-02) and, in severe cases, disrupted task execution (FR-03; FR-04; SF-01). Second, the compact motor corrected the poor weight distribution of the Hi5, preventing the device from shifting during torque application and thereby improving mechanical stability (MR-05) and safety (SF-01). Finally, this more integrated mechanical layout greatly enhanced portability and simplified setup (MR-04; US-01), addressing a central design requirement for deployment in clinical environments.

The HRX-1 also introduced improvements in system integration and software architecture. The EPOS2 motor controller used in the Hi5 was replaced with the EPOS4, which could interface directly with the torque sensor. This removed the need for the external TMSi Porti amplifier, thereby reducing the number of hardware components required to operate the system and eliminating a known point of potential failure - changes directly aligned with the requirements for a more streamlined integration architecture (IN-02; DEV-02) and improved portability (MR-04). Because the Porti was no longer required, EEG acquisition could be streamlined by operating the DSI-24 system independently and synchronising it with the robot through a hardware trigger box. Although this optical trigger was binary and required event classification to be reconstructed during offline processing, it provided reliable alignment within approximately 3.3 ms, comfortably satisfying the system's synchronisation requirements (DS-01; DS-02) while significantly simplifying the data architecture (IN-01; SW-02).

The transition to the HRX-1 was accompanied by a substantial reconfiguration of the software environment (**Figure 3.7**). Whereas the Hi5 relied on a custom C++/Qt codebase, the HRX-1 was driven through MATLAB. This shift reduced the complexity of maintenance and made the system far more accessible to researchers without extensive C++ experience, directly addressing usability and maintainability requirements (US-02; DEV-02). MATLAB's native handling of data structures allowed experimental recordings to be saved directly into efficient object formats, avoiding the file-writing overhead associated with large CSV or text files and therefore supporting smoother experimental operation (SW-02). Integration with the Psychtoolbox software package introduced an additional benefit: task visualisation could now be synchronised precisely with the screen refresh cycle, ensuring tightly coupled alignment between robot commands and visual cues (FR-03; SW-03; DS-02) and reducing the code required to implement this functionality (DEV-02).

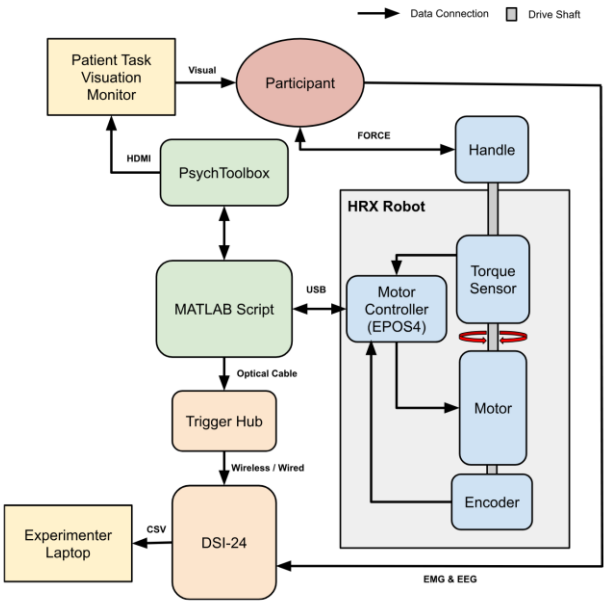

Figure 3.7. Control architecture and informational flow of the experimental system built around the HRX-1.

Despite these substantial advances, several limitations accompanied the HRX-1. Most notably, the updated system did not include a dedicated accelerometer. Although velocity and acceleration could be estimated from positional data, this introduced the risk of noise amplification and removed a useful redundancy present in the Hi5, affecting the precision of certain kinematic measurements (DS-03). A more consequential limitation arose from the use of mex files in the MATLAB EPOS4 API: because mex files cannot be safely multithreaded, the multistream, lockless architecture previously implemented in C++ was no longer possible. As a result, robot polling, control updates, and visual stimulus presentation had to occur within the same loop, constraining the sampling rate to 60 Hz to remain aligned with the monitor refresh rate. Although still sufficient for the planned experiments, this represented a substantial reduction from the 512 Hz sampling rate achieved with the Hi5 (SW-01; DS-03) and therefore constituted the principal performance trade-off introduced by the new system.

Overall, the transition from the Hi5 to the HRX-1 resolved the most significant mechanical and integration-related limitations of the original system, namely those concerning stability, torque transmission, portability, and architectural complexity, while better fulfilling a wide range of system requirements (MR-04; MR-05; FR-01–04; IN-01–02; DS-01–02; US-01). At the same time, the adoption of MATLAB introduced new constraints related to sampling rate and the absence of dedicated accelerometery (**Table 3.2**). Nonetheless, the HRX-1 configuration provided a more stable, reliable, and practical platform for large-scale data collection and better aligned with the core functional and operational requirements of the present work.

Table 3.2. Comparison of the Hi5 and HRX-1 system architectures.

Feature / Requirement Area	Hi5 (Initial System)	HRX-1 (Updated System)
Motor	Maxon RE-65, 250 W; tall, required suspended mounting	Maxon EC 90 Flat, 600 W; compact 30 mm height; tabletop mounting
Transmission	Belt and pulley system; tension-dependent; occasional slippage (DS-03)	Direct drive; no belt; eliminates slippage and asymmetry (FR-02)
Mechanical Stability	Susceptible to shifting due to overhanging motor (MR-05)	Stable footprint with improved weight distribution (SF-01)

Torque Sensor Integration	Required external TMSi Porti (IN-02)	Direct EPOS4 integration; Porti removed (IN-02; MR-04)
Controller	EPOS2 in external control box	EPOS4 embedded in robot; enhanced portability (MR-04)
EEG/EMG Synchronisation	LSL-based multisource setup (DS-01)	Hardware trigger; ~3.3 ms alignment; simpler (DS-01; IN-01)
Software Environment	Custom multithreaded C++/Qt (SW-01)	MATLAB with Psychtoolbox; simpler and more accessible (US-02)
Data Storage	CSV/TXT; higher overhead (SW-02)	MATLAB objects; low overhead (SW-02)
Sampling Rate	Up to 512 Hz (DS-03)	60 Hz loop-bound operation (SW-01; DS-03)
Accelerometer	Dedicated 3-axis sensor (DS-03)	Removed; derived acceleration only
Primary Strengths	High temporal resolution; flexible architecture	Mechanical robustness; stability; simplified integration
Primary Limitations	Instability; belt slippage; complex architecture	Lower sampling rate; no dedicated accelerometer

3.5. Summary

The development of the portable Hi5 system and its subsequent replacement with the HRX-1 represented an iterative, requirement-driven refinement of the experimental platform necessary to support robust data collection (**Aim 5**). The Hi5 served as a critical proof of concept, demonstrating that precise torque perturbations, high-resolution kinematic sensing, and sub-10 ms multimodal synchronisation were achievable within a portable robotic system. However, its deployment revealed several limitations. Mechanical issues arising from the large RE-65 motor, suspended mounting geometry, and belt transmission introduced instability, torque inconsistencies, and occasional failures that compromised measurement fidelity and operational reliability.

The HRX-1 addressed these shortcomings through targeted design improvements. Adoption of the compact EC 90 Flat motor eliminated the transmission system, corrected weight distribution, and substantially improved mechanical stability and safety. Integrating the EPOS4 controller directly into the robot removed external hardware dependencies and simplified system architecture, reducing setup complexity and improving portability. In parallel, the transition to MATLAB and Psychtoolbox streamlined software maintenance and enhanced synchronisation between robotic control and visual feedback, aligning the platform more closely with the system requirements.

Although these changes introduced new constraints, most notably a reduced sampling rate and the removal of the dedicated accelerometer, the HRX-1 provided a markedly more reliable and operationally robust platform for large-scale data collection. Overall, the transition from Hi5 to HRX-1 reflects a clear empirical design trajectory in which observed limitations directly informed successive architectural decisions, resulting in a system capable of supporting the experimental aims of this thesis with high reliability and precision.

IV. Sensorimotor Modulation of the Stability–Movement Transition in Healthy Motor Control

4.1. Introduction

To examine how elevated limb impedance influences subsequent voluntary movement, an experimental paradigm was required that reliably induced sustained impedance prior to movement initiation. Previous work indicates that increases in mechanical impedance via muscle co-contraction are primarily recruited to counteract instability in the motor environment [81]. Accordingly, participants were challenged to maintain postural stability under externally imposed mechanical disturbances.

A one-degree-of-freedom robotic manipulandum constrained motion to the wrist flexion–extension plane. Participants were first required to stabilise the handle at a neutral position while destabilising force perturbations were applied to elicit elevated impedance through muscle co-contraction. These stabilisation phases were followed by a cue to initiate voluntary flexion or extension, enabling assessment of how an impedance-dominated motor state influenced subsequent movement execution.

Although predictably timed perturbations have been reported to be insufficient to induce sustained increases in impedance [82], [83], the present study systematically manipulated perturbation amplitude and temporal predictability to directly test this assumption. This design enabled identification of which features of mechanical instability most effectively modulate tonic impedance, how these dynamics shape subsequent voluntary movement, and how both evolve across repeated task blocks.

Beyond peripheral motor control, the task was designed to evaluate the role of beta-band (13–30 Hz) sensorimotor dynamics in resolving impedance-related trade-offs. While beta-band activity is well characterised in relation to maintenance of the current motor set and its suppression during movement initiation, its role in mediating conflicts between stability-oriented and movement-oriented motor goals has not been directly tested. The present work therefore tested the hypothesis that elevated beta-band oscillations encode maintenance of the current motor state as a proxy for stability [150], by imposing competing demands between postural stabilisation and movement initiation. The stabilisation-movement transition implemented here provides a novel and direct framework for interrogating these dynamics as participants must remain prepared to resist perturbations while simultaneously preparing to initiate voluntary movement.

In summary, this experimental framework was designed to probe how the sensorimotor system negotiates the transition between stability and movement under conditions of heightened impedance. By systematically manipulating mechanical instability and examining its effects on both neuromechanical control and sensorimotor beta-band dynamics, the present work provides a unified approach to studying how the nervous system balances competing demands for stability and flexibility. This paradigm therefore offers a principled means of linking impedance regulation, voluntary motor execution, and beta-band activity within a single task, enabling direct tests of how stability-oriented control strategies shape subsequent movement behaviour and underlying neural dynamics. More broadly, this work establishes a mechanistic framework for interpreting Parkinsonian motor impairments in terms of maladaptive stability–movement trade-offs, while also providing potential design principles for neurorobotic systems and rehabilitation strategies aimed at restoring flexible, context-appropriate impedance regulation during voluntary movement.

4.2. Methods

4.2.1. Apparatus

All data presented within this section was collected utilising the **HRX-1 configuration**.

Participants engaged with the device through a rubber-coated bicycle-style handle grip while the device supported their arm from wrist to elbow (**Figure 4.1**). Participants were secured through Velcro straps at the wrist and forearm to limit compensatory movement from the elbow during assessment. Participants were orientated facing a computer monitor and their chair height adjusted to ensure comfortable position with a shoulder abduction of ~ 40° and shoulder flexion ~ 20°.

EMG electrodes were placed on the muscle body of the flexor carpi ulnaris and extensor digitorum communis as antagonist muscles that make major contributions to wrist flexion and extension respectively [265]. EEG was fitted using an adjustable 24-electrode cap, aligned under the guidelines set by the manufacturer to conform to the International 10-20 system.

Figure 4.1. The HRX-1 configuration in use during the main motor protocol. The handle is currently off-target resulting in a red target circle and visible position crosshair.

After initial setup and orientation, task instructions were delivered on the computer monitor using simple visual cues and brief keyword prompts. The primary visual display used throughout the protocol consisted of two elements: a white crosshair indicating the handle's current position, and a target circle (**Figure 4.2**). The target circle appeared in one of three fixed screen locations: left, right, or centre. The centre position corresponded to the midpoint of the handle's arc at the neutral position, while the left and right positions were set to 50% of the participant's maximum range of motion (ROM). Transitions between target locations were instantaneous, occurring within a single frame without animation.

The target circle was shown as a red outline when the crosshair was not aligned with the target location, and it switched to a filled green circle when the participant reached the target, at which point the green fill obscured the crosshair. A trial was considered on-target when the angular difference between the target and handle positions was less than 3°.

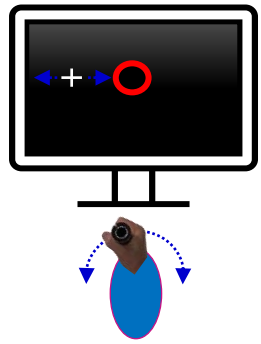

Figure 4.2. A simple visualisation of the key components of the protocol. Movement of the device's handle produced corresponding directional movement of the crosshair on the screen.

4.2.2. Participants

Healthy participants were recruited via college wide invitation. All participants were able to understand and complete the task without assistance, had no history of motor-impairment or significant injury to their dominant hand and had normal or normal-corrected vision. Each gave informed consent prior to participation. This study was approved by the Imperial College Research Ethics Committee (ICREC) and performed in accordance with the Declaration of Helsinki.

Two initial cohorts of fourteen participants were collected, with each cohort assigned to a different experimental condition group. One cohort examined the influence of temporal predictability on impedance modulation, while the second cohort assessed the effects of perturbation amplitude. Details of these experimental conditions are provided in the **Main Task Design** section of this document. Following preliminary analyses, the temporal predictability cohort showed the strongest effects. To improve statistical power and the robustness of the findings, ten additional participants were recruited for this cohort. The results presented do not distinguish between the initial and subsequent recruitment; all analyses reflect the full participant set for each experimental condition. The demographic information of each cohort is presented in **Table 4.1**.

Table 4.1. Demographic breakdown of both cohorts of healthy participants.

Cohort	Count	Age - Mean (SD)	Age - Median (IQR)	Sex (M/F)	Dominant Hand (R/L)
Perturbation Amplitude	14	26.2(6.51)	24 (22.00 - 30.25)	8/6	11/3
Temporal Predictability	24	25.7(5.51)	24 (22.00 - 29.00)	12/12	22/2

4.2.3. Main Task Design

The rationale behind the main task design was to create conflicting motor incentives between stability-oriented demands and movement-oriented goals. This was achieved by first presenting participants with a postural stabilisation phase in which they were required to maintain posture while the robot delivered mechanical perturbations. Following this phase, they were cued without warning to initiate a voluntary reaching movement.

To enable valid comparisons within and between cohorts, all aspects of task dynamics were kept consistent except for the specific experimental feature under investigation. Each task began with a 3 s grace period, followed by a 14.5 s stabilisation phase containing eight 0.5 s step perturbations. Perturbation directions were balanced, with four flexion-directed and four extension-directed perturbations in every trial. The onset of the first perturbation was aligned with the start of the

stabilisation window, and the final perturbation ended exactly at the window's conclusion, ensuring consistent temporal structure across trials. During the stabilisation phase, the target circle remained in the central position.

To introduce movement-oriented demands, participants were cued 2 s after the stabilisation phase to perform a voluntary flexion or extension movement. The cue was provided by shifting the target circle to the left or right screen position. Participants were given a 6 s window to complete the movement, which included a mandatory 1 s hold on the target. This hold phase ensured that participants genuinely reached and stabilised at the target rather than just passing the handle through it (**Figure 4.3**).

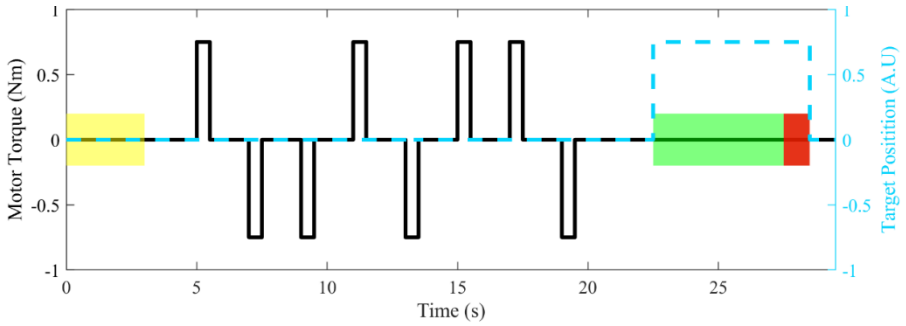

Figure 4.3. Illustration of applied motor torque and target visual position during a trial. The yellow region indicates the 3 s grace period preceding each trial. The green/red region denotes the movement success window: green marks the 5 s interval in which successful movement completion can occur, while red indicates insufficient remaining time for stabilisation. If stabilisation is not achieved, the trial is deemed failed 6 s after the voluntary movement cue.

The experimental conditions of temporal predictability and perturbation amplitude were examined within the described framework. During the postural stabilisation phase, perturbation dynamics were modified while all key structural features of the task were preserved. For the amplitude cohort, perturbations were delivered at uniform intervals, with each perturbation beginning 1.5 s after the end of the previous one. Within a given trial, the perturbation amplitude was constant and set to either a high-amplitude level (1 Nm) or a low-amplitude level (0.5 Nm).

For the temporal predictability cohort, perturbation amplitude was fixed at 0.75 Nm, but the timing of perturbations was manipulated. In the predictable condition perturbations followed the same uniform 1.5 s interval used in the amplitude cohort. In the uncertain condition the intervals between perturbations varied randomly between 0.5 s and 3 s. As before, the first perturbation coincided with the onset of the stabilisation window, and the final perturbation ended exactly at the window's termination, ensuring consistent alignment with the overall task structure. An overview of the key perturbation dynamics is presented in **Table 4.2**.

Table 4.2. Summary of the defining features of each cohort's perturbation scheduling.

Condition	Amplitude (Nm)	Count	Timing
Perturbation Amplitude	0.5 / 1.0	8	1.5
Perturbation Predictability	0.75	8	1.5 / 0.5 - 3

Participants were naive to their experimental cohort, the dynamics of the stabilisation phase and the direction of the upcoming movement cue. Successful performance under these competing demands

required the adoption of control strategies that were simultaneously robust to external disturbances and adaptable to unexpected changes in task requirements.

Task blocks consisted of an initial 3 s visual countdown followed by sixteen trials. There was a 2 s gap between the completion of the preceding trial and onset of the subsequent trial. Within each block, the experimental condition remained consistent (i.e. all low-amplitude or all high-amplitude trials). However, the direction of the cued voluntary movement in each trial was pseudo-randomly assigned to ensure an equal number of voluntary flexion and extension movements (eight of each). Across trials within a block, perturbation directions were kept constant, but the perturbation direction was randomised between blocks.

The rationale for this design choice was that maintaining consistent perturbation directions within a block allowed participants to establish stable control strategies specific to the current task dynamics, while randomising these directions between blocks prevented long-term adaptation to a single perturbation pattern. This approach ensured that measured impedance responses reflected the intended experimental manipulations rather than habituation to a fixed perturbation profile.

4.2.4. Voluntary Movement Onset Detection and Trial Validation

The timestamps associated with the cueing and termination of voluntary movements were readily identifiable in the recorded data through a combination of timed event markers and a Boolean flag indicating whether the participant was on-target. In contrast, movement onset was not explicitly defined and therefore had to be determined during post-processing.

Movement onset was identified using a threshold-based algorithm applied to velocity signals. Baseline windows of 1 s preceding the visual cue were used to characterise baseline dynamics, as these periods were largely free from significant movement. Velocity amplitudes were computed as the absolute values of the respective signals.

The mean and standard deviation of velocity during the baseline period were calculated, and a threshold of three standard deviations above the mean was used to detect movement onset. Velocity was required to exceed this threshold continuously for 50 ms in the correct direction, providing robustness against transient fluctuations and minor corrective movements. A minimum latency threshold of 100 ms was imposed to reflect a biologically plausible response to the visual cue. Trials in which movement onset was detected earlier than this threshold were excluded, as the movement was not initiated in response to the visual cue (**Figure 4.4**). Trials in which movement onset was detected more than 1 s after the cue were also excluded, as such delays were indicative of insufficient engagement with the task.

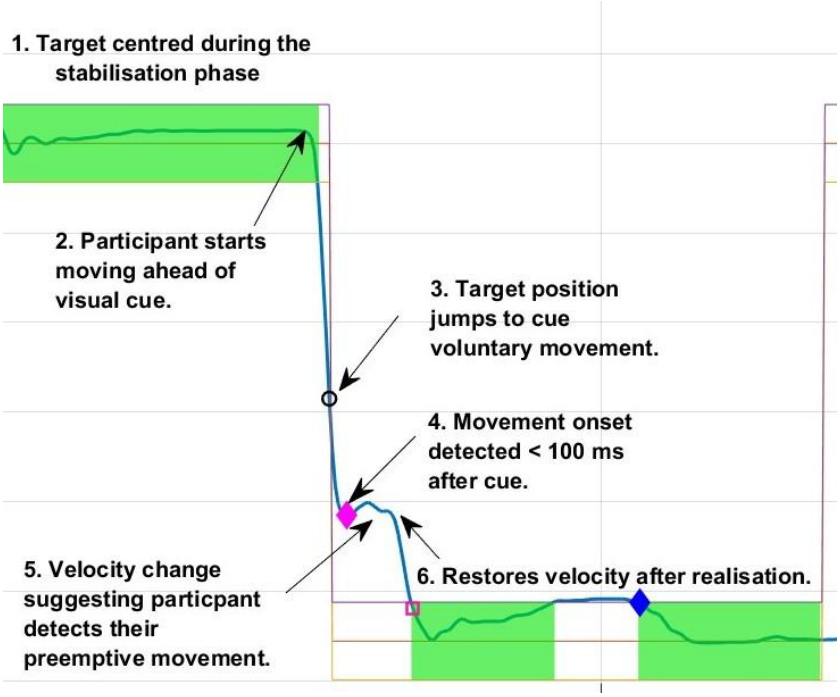

Figure 4.4. A visualisation from the movement detection algorithm showing a trial discarded due to early movement onset. Handle position is indicated by the blue trace, on-target bounds fall within the purple and yellow lines and currently being on-target is indicated by the green shaded areas. In this example, the participant initiates movement prior to the visual cue moving, resulting in a detection of movement onset < 100 ms causing the trial to be discarded. The magenta diamond is the detected movement onset, the red box is the first on-target timestep following the movement cue and the blue diamond is the first timestep of being stabilised on-target for 1 s.

The detection and validation procedures ensured the integrity of the task data by retaining only trials that met predefined compliance criteria. Trial retention remained high following these exclusions, with 98.22% of trials retained in the temporal predictability cohort and 97.64% in the perturbation amplitude cohort. Moreover, trial losses were minimal and sparsely distributed, with an average of 0.26 ± 0.63 trials lost per block in the temporal predictability cohort and 0.33 ± 0.78 lost per block for the perturbation amplitude cohort (**Table 4.3**).

Table 4.3. Breakdown of trial retention (including baseline blocks) after movement onset detection and movement validation.

Cohort	Total Trials	Early Movement	Late Movement	Lost Trials	Percentage Retention
Predictability	4550	59 (1.29%)	22 (0.48%)	81 (1.78%)	98.2%
Amplitude	2664	56 (2.12%)	4 (0.15%)	60 (2.26%)	97.64%

4.2.5. Supporting Blocks in the Experimental Protocol

In addition to the primary task blocks that constituted the core of the experimental protocol, several supplementary block types were included in the paradigm. An overview of these blocks is provided below and how they were structured with the paradigm is found in the **Experimental Session Overview**.

Range Calibration Blocks: To establish a comfortable range of movement (ROM) for each participant, the experimental protocol began with a brief calibration phase. Participants were instructed to oscillate the handle to the maximum comfortable limits of flexion and extension for a total of 10 s. The maximal displacement of the handle relative to the neutral position was then used to scale all subsequent

movement ranges, ensuring that the experimental parameters were individually tailored. Although selecting a predefined ROM based on existing literature was a feasible alternative, this bespoke approach was chosen in anticipation of future applications of the protocol to clinical populations, where levels of impairment may necessitate more precise and adaptive calibration. Implementing this bespoke scaling ensured that all participants, regardless of their natural movement capacity, engaged with movement ranges that were appropriately scaled, safe and achievable.

Baseline Blocks: To account for individual differences in baseline performance, the experimental protocol incorporated baseline blocks at specific intervals. These blocks were used both to correct for participant-specific variability and to assess any evolving effects of the protocol over time. Baseline blocks consisted of ten voluntary reaching movements that followed the same movement dynamics as those used in the **Main Task Design**: targets were positioned at 50% of each participant's range of motion, and participants were required to maintain stabilisation on the target for 1 s within a 6 s movement window. The sequence of reaches was psuedorandomly ordered and balanced, containing five flexion and five extension movements. Each movement cue was presented 2 s after the completion of the previous trial.

Passive Assessment Blocks: These blocks formed the basis of a supplementary analysis of impedance control, specifically stiffness regulation, in response to steady external manipulation of the wrist. Their distribution mirrored that of the main task blocks, with each baseline and task block followed by a corresponding passive assessment block. Full methodological details and analyses are presented in **Passive Wrist Stiffness in Healthy Motor Control Following Stability–Movement Transitions and at Baseline in Parkinson's Disease**. The description provided here is included for completeness and to situate the assessment blocks within the broader structure of the experimental protocol.

4.2.6. Experimental Session Overview

Following initial orientation and familiarisation with the experimental setup, participants completed a range calibration block to establish the movement scaling used for all subsequent tasks. They were then trained on both the main task and the passive assessment task to familiarise them with the protocol. Once participants confirmed their understanding, the main experimental session commenced.

Each session followed a balanced crossover design. The session was divided into two halves, with each half dedicated to one experimental condition (high- vs. low-amplitude perturbations; predictable vs. uncertain perturbation scheduling). Participants completed one condition, took a short break of 2-5 minutes, and then completed the second condition. They were not informed of the differences between the two phases.

Each conditional half began with baseline task and passive assessment blocks, followed by five paired main task and passive assessment blocks. Each main task block contained sixteen trials. Before the baseline block of the second conditional half, a second passive range assessment block was included. Although the results from this block were recorded for later analysis, they were not used to rescale any tasks, ensuring that all task parameters remained consistent across both conditions. After completing the second condition, participants performed a final baseline block (**Figure 4.5**). Within each cohort, the order of condition presentation was counterbalanced across participants to ensure an even distribution of condition A versus condition B starts.

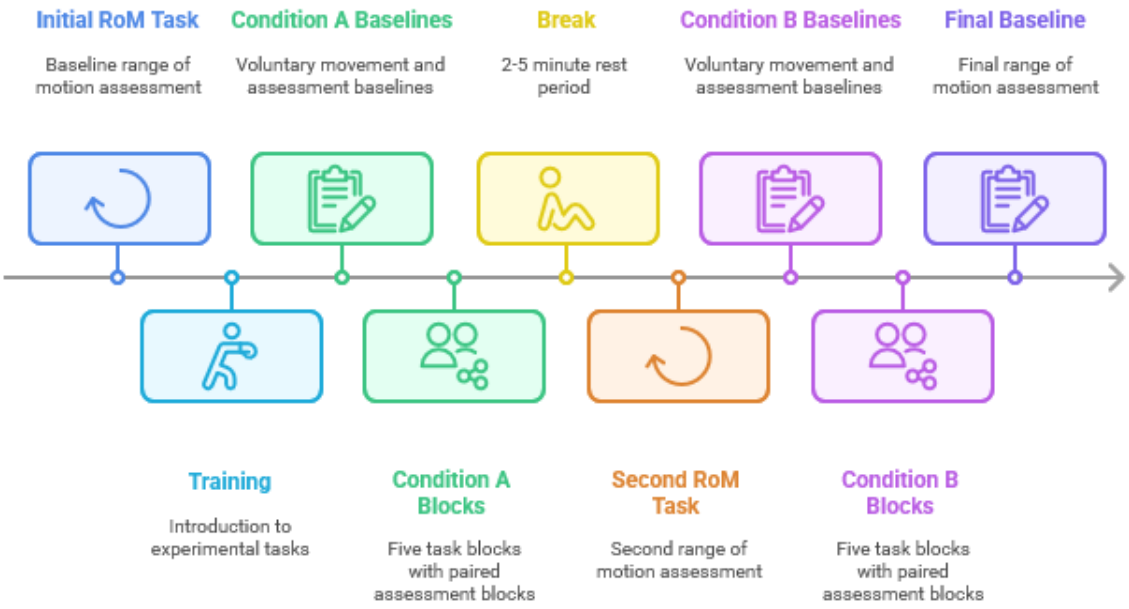

Figure 4.5. Flowchart detailing the different tasks and stages of the experimental protocol.

4.2.7. EMG Processing

EEG and EMG was recorded using a 24-channel DSI-24 system (Wearable Sensing Inc.) with auxiliary bipolar EMG sensors at 300 Hz. EEG and EMG channels were separated to be processed independently.

EMG data were processed offline in MATLAB using a custom pipeline designed to clean raw bipolar recordings, extract a linear envelope and generate a normalised amplitude measure. All processing was performed for the ulnaris and digitorum channels independently.

Missing samples were treated as gaps and linearly interpolated over time using sample indices as the independent variable; the first and last valid values were extended to the edges where needed. To remove any constant offset, the mean of the signal was subtracted from the entire time series, yielding a zero-mean signal.

To isolate the physiological EMG bandwidth, the signal was band-pass filtered using a 4th-order Butterworth filter implemented in zero-phase form. A range of 20-130 Hz was applied to attenuate movement artefacts and very low-frequency drift, as well as high-frequency noise outside the typical EMG spectrum.

Residual power-line contamination was removed using a series of IIR notch filters at 50 Hz and 100 Hz (**Equation 4.1**). A quality factor Q = 35 was assumed. For each harmonic h, a 2nd-order notch filter was designed with normalised centre frequency and bandwidth determined by Q. Each notch was applied in zero-phase.

$$w_0 = \frac{h \cdot 50}{fs/2}, \tag{4.1}$$

To reduce occasional sharp artefacts or spikes that are not physiologically plausible, a Hampel filter was applied. A sliding window length of 100 ms was used. Within each window, samples classified as outliers relative to local statistics were replaced with robust estimates. The signal was then rectified by taking the absolute value of each sample.

A linear envelope was extracted from the rectified signal using a 4th-order Butterworth low-pass filter at 6 Hz. The resulting envelope was then clipped at zero to prevent small negative values due to numerical filtering artefacts.

To allow comparison across muscles, the envelope was normalised by an estimate of its maximum amplitude and scaled to the 95th percentile. Scaling to the 95th percentile provided robustness against any residual erroneous activities spikes while providing strong 0-1 scaling for most of the data.

EMG was primarily assessed through the calculation of co-contraction indices. Two common formulas - CCI_1 [220] and CCI_2 [253] - were explored. The specification of each formula can be found in the **Co-contraction Indices** section of the literature review. Based on the response characteristics of each formulation, CCI_1 exhibits a steeper increase at low values of antagonist activation, whereas CCI_2 is deliberately less sensitive in this region due to its nonlinear scaling (**Figure 2.6**). In healthy individuals, co-contraction during voluntary movement or postural control is typically low and finely modulated. The formulation with higher gain at low activation levels - CCI_1 was therefore better suited to capturing subtle, task-dependent changes in antagonist activity that were likely to contribute to physiological modulation of joint impedance.

4.2.8. Mechanical Impedance

Mechanical impedance was estimated from the segments of kinematic and torque data recorded during active perturbation. Angular position, velocity, and acceleration were measured at the handle, together with the interaction torque. Angular kinematics were converted from degrees to radians prior to analysis. For each perturbation, a fixed 0.5s analysis window corresponding to the active perturbation interval was selected. Samples containing non-finite values were discarded. Estimates of mechanical impedance were produced using least-squares estimates to regress a second-order impedance model:

$$F(t) = M\ddot{x}(t) + B\dot{x}(t) + Kx(t) \quad \textbf{(4.2)}$$

A scalar impedance estimate was then obtained as the magnitude of the frequency-domain impedance evaluated at a reference frequency:

$$(f_0 = 1 \text{ Hz}): \hat{Z} = \left| (K - I\omega_0^2) + j(B\omega_0) \right| \quad \textbf{(4.3)}$$

Where $\omega_0 = 2\pi f_0$ is the angular frequency corresponding to the reference frequency $f_0 = 1$Hz. The reference frequency ($f_0 = 1$ Hz) was selected to approximate the dominant low-frequency content of the 0.5 s step perturbations, yielding a scalar impedance estimate representative of the quasi-static response to steady external torques. Impedance is reported in units of $N \cdot m \cdot rad^{-1}$. The full specification of the model can be found in the **Second-Order Impedance Model** section of the literature review and an explanation of how the regression is performed is detailed in the **Parameter Identification** section found immediately after.

4.2.9. EEG Preprocessing, Post Movement Beta Rebound and Beta Corticomuscular Coherence

EEG and EMG was recorded using a 24-channel DSI-24 system (Wearable Sensing Inc.) with auxiliary bipolar EMG sensors at 300 Hz. EEG and EMG channels were separated to be processed independently.

EEG data preprocessing was performed in EEGLAB (2024.2.0). EEG data were restricted to the DSI-24 scalp channels. Mastoids (A1/A2) were retained only for initial referencing and were removed before artifact correction. Channel labels were mapped to the modern 10–05 system when necessary. Before re-referencing or artifact correction, narrow zero-phase notch filters were applied at 50 and 100 Hz to reduce global line-noise contamination while preserving physiological oscillations. Data were high-pass filtered at 1 Hz to improve ICA stability.

Artifact reduction proceeded in a repair-focused manner without removing time segments. Channels were automatically evaluated for signal quality using several criteria: channels exhibiting flatlining for longer than 5 s were flagged as bad; channels whose correlation with the robust estimate of the remaining data fell below 0.8 were considered poorly coupled to the scalp field and removed; and channels dominated by excessive line noise, defined as line-noise power exceeding clean data estimates by more than 8 standard deviations, were rejected. Transient high-amplitude artifacts were addressed using an adaptive burst correction procedure with a burst threshold of 15 standard deviations relative to the data distribution. Importantly, this procedure was configured to repair contaminated segments rather than excise time windows, ensuring that the continuous temporal structure of the recording was preserved. All scalp channels removed during this stage were logged for later interpolation.

Following automated cleaning, the data were re-referenced to the common average and subjected to independent component analysis (ICA). To avoid rank deficiency and overfitting, the effective data rank was estimated from the covariance structure, and the decomposition was constrained to this rank. Independent components were then automatically classified into neural and non-neural categories. Components were rejected if their estimated probability exceeded class-specific thresholds for non-neural sources: ≥75% for muscle activity, ≥85% for ocular activity, and ≥90% for cardiac, line-noise, channel-noise, or unclassified (“other”) components, while no lower bound was imposed on the probability of neural components. All components meeting these rejection criteria were removed, and the cleaned EEG signal was reconstructed from the remaining components. Summary metrics, including the number of components before and after rejection and the dominant artifact classes among rejected components, were retained for quality control.

After ICA-based artifact removal, any scalp channels previously excluded during automated cleaning were restored via spherical interpolation using the original sensor geometry. The data were then re-referenced again to the common average to ensure consistency after interpolation. A final low-pass filter at 100 Hz was applied to remove residual high-frequency noise and standardise the analysed bandwidth.

A scalp-only current source density (CSD) transformation using a spherical spline surface Laplacian, excluding mastoids was applied. This transformation yielded reference-free estimates of local radial current flow and reduced the influence of broadly distributed volume-conducted activity. For quality assurance, power spectral density summaries were generated over sensorimotor electrodes (C3 and C4) to visually compare raw, cleaned, and CSD-transformed data (**Figure 4.6**), and key preprocessing metrics were exported for downstream inspection.

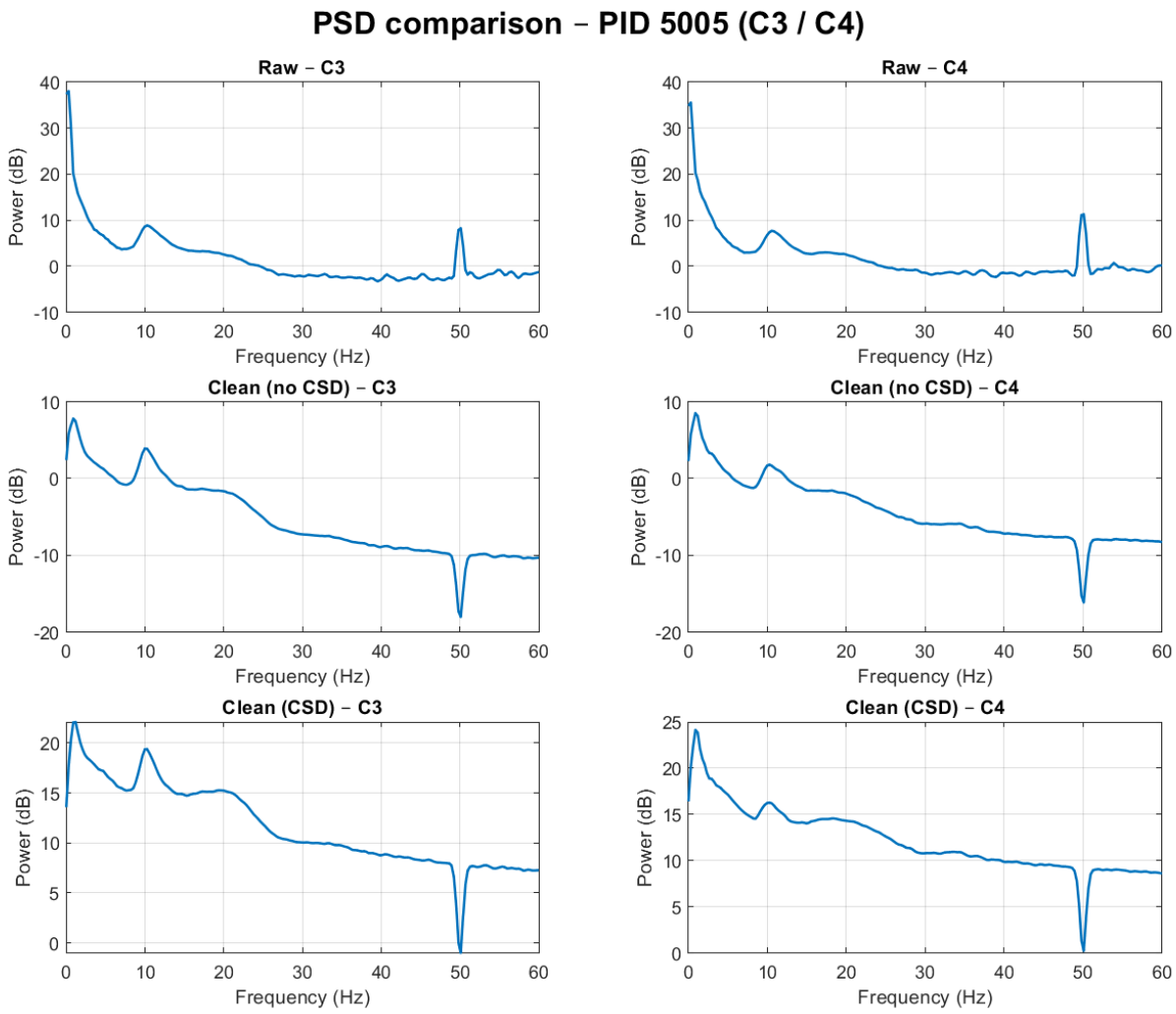

Figure 4.6. Sample power spectral density (PSD) plots illustrating successive stages of the EEG preprocessing pipeline. Spectra are shown for electrodes C3 and C4, selected to represent contralateral and ipsilateral motor cortex, respectively. For each channel, PSDs are displayed for the raw data, the cleaned average-referenced data (no CSD), and the cleaned data after application of the scalp-only CSD transform. The progression demonstrates attenuation of line noise and broadband artifacts following automated cleaning and ICA-based component rejection, as well as the expected reduction in low-frequency spatially diffuse power after CSD, reflecting increased spatial specificity of sensorimotor activity.

Beta-band power was quantified from the cleaned continuous EEG in a single target sensorimotor electrode selected a priori based on the moving hand (C3 for right-hand movements; C4 for left-hand movements). The continuous channel time series (μV) was transformed into a continuous estimate of beta-band power using a Morlet wavelet decomposition spanning 13–30 Hz. Specifically, the signal was convolved with a family of complex Morlet wavelets whose centre frequencies were linearly spaced across the beta range (25 frequencies between 13 and 30 Hz). To balance temporal and spectral resolution across the band, the number of wavelet cycles increased with frequency (linearly from 6 cycles at the low end of the band to 10 cycles at the high end). For each centre frequency, the analytic wavelet output was obtained and instantaneous power was computed as the squared amplitude of the complex coefficient. Power estimates were then averaged across all beta frequencies at each time point, yielding a single continuous beta power trace (μV^2) matched in length to the original recording. To reduce high-frequency jitter in the power envelope, the continuous power series was smoothed using a short sliding median window (100 ms).

For normalisation and subsequent statistical extraction, power was converted to decibels (dB) as $10\log_{10}(\text{power} + \epsilon)$, where ϵ was a small constant to avoid taking the logarithm of zero. Trial-wise beta-power time courses were then constructed by extracting segments from the continuous beta power trace time-locked to movement termination events. Only trials whose full analysis window lay within the recorded data were retained. Each trial segment spanned −1 to +1 s relative to movement termination, with termination aligned to 0 s. Within each trial segment, baseline correction was applied in dB units by subtracting a baseline level from a pre-trial window of 3 s in which the participant was at rest. Each trial's beta-power time course was smoothed using a third-order Savitsky–Golay filter with a 100 ms moving window to attenuate transient, burst-like fluctuations and improve the stability of the power signals. Signals were then filtered based on the trial criteria outlined in **Voluntary Movement Onset Detection and Trial Validation** section before being averaged over each movement direction. Extraction of post-movement beta rebound (PMBR) was then performed by detecting the maximum power in the 0.1 s–1 s following movement termination. This window ensured that the PMBR extracted was temporally separated from peri-movement beta desynchronization and reflected the sustained PMBR rather than transient termination-related fluctuations. The 1 s range was shorter than some traditional PMBR extractions but was necessitated by the scheduling of experimental events; however, it was still large enough to capture the peak rebound response in most trials while preventing contamination from subsequent task-related events. A 50 ms average was taken around the maximum power to control for local volatility at the peak and to provide a more robust estimate of PMBR amplitude. Averaging prior to peak detection was selected to improve the signal-to-noise ratio of this time-locked modulation and to reduce the upward bias that can arise when maxima are selected from noisy single-trial traces. Traces were inspected visually at both the individual-trial level and as block-averaged responses, and the effects of extracting PMBR from single-trial peak detection versus from averaged traces were directly compared. Noise driven by small, transient fluctuations was prominent in individual trials, whereas averaged traces consistently revealed robust movement-related beta dynamics in the majority of cases (**Figure 4.7**), supporting the use of averaged, smoothed power estimates for reliable quantification of PMBR in this paradigm. PMBR was converted from dB to percentage change to provide a more intuitive and physiologically interpretable measure of beta modulation relative to baseline. Percentage units also facilitated comparison across participants and conditions with differing baseline power and yield clearer group-level statistics and visualisations.

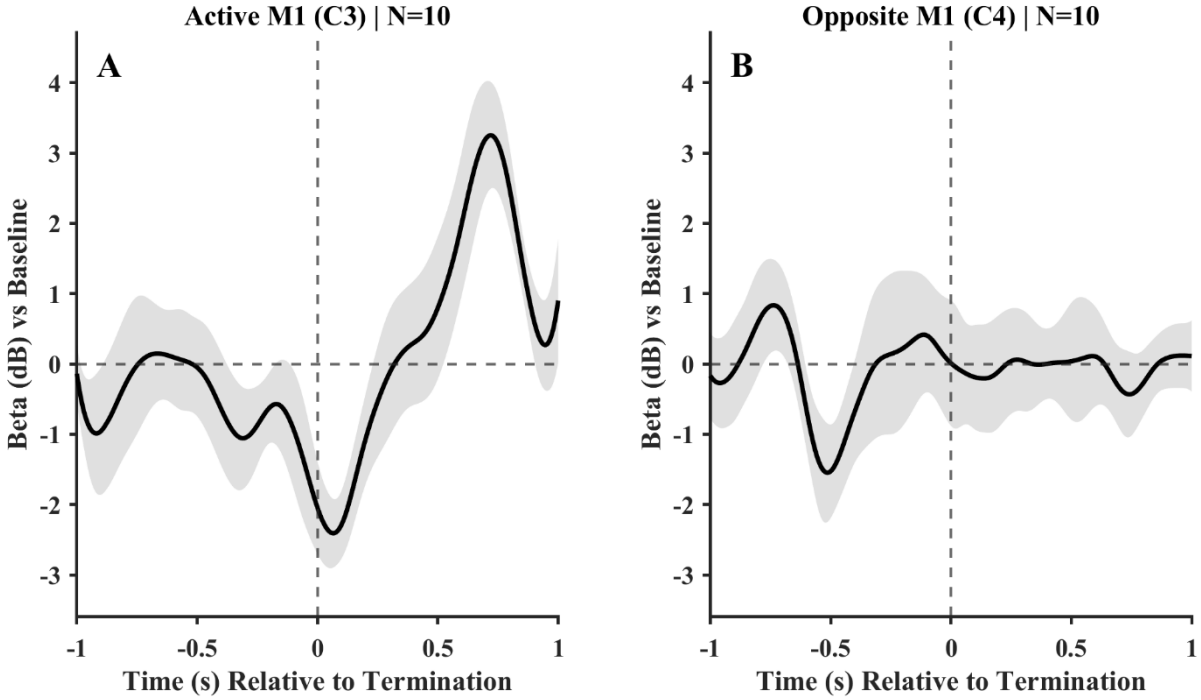

Figure 4.7. Block-averaged beta-band power (dB relative to baseline) from a baseline block in a representative right-handed participant. Time is shown relative to movement termination (0 s; vertical dashed line). Panel A shows activity over the active primary motor cortex (C3), contralateral to the moving hand, and panel B shows activity over the ipsilateral motor cortex (C4). The solid black line denotes the mean across blocks (N = 10), and the shaded region indicates variability across blocks (±SEM). The horizontal dashed line marks baseline (0 dB). The contralateral M1 exhibits a clear movement related beta decrease followed by a pronounced post-movement beta rebound, whereas the ipsilateral M1 does not show clear movement-related modulation.

In addition to purely neural measures of beta activity, it was necessary to quantify the degree of coordination between cortical and muscular activity at key phases of the experiment. Beta corticomuscular coherence (β-CMC) was computed in line with the methodology outlined in [10] using phase-locking value (PLV) [266]. Phase locking values (PLV) were computed as a complementary measure of corticomuscular coupling that is more robust to short data segments than coherence. Analysis windows over the duration of the postural stabilisation phase and each voluntary movement were defined. For each trial and analysis window, the contralateral sensorimotor EEG signal and the corresponding EMG signal were first aligned in time, truncated to equal length, and cleared of non-finite samples. Segments shorter than 250 ms or containing fewer than six beta cycles at the lower band edge (13 Hz) were excluded. Both signals were mean-centred and band-pass filtered in the beta range (13–30 Hz). The analytic representations were then obtained using the Hilbert transform, and instantaneous phase time series were extracted for EEG and EMG. PLV was calculated as the amplitude of the mean complex phase difference across time:

$$PLV = | \langle ej(\phi EEG - \phi EMG) \rangle | \quad \textbf{(4.3)}$$

where ϕ_{EEG} and ϕ_{EMG} are the instantaneous phases of the EEG and EMG signals, respectively, and $e^{j(\cdot)}$ maps the phase difference onto the unit circle in the complex plane. The resulting PLV ranges from 0 (no consistent phase relationship) to 1 (perfect phase locking). PLV was computed separately for each trial and window, and block-level summaries were obtained by averaging valid per-trial PLV values, with the number of contributing trials retained for quality control.

4.2.10. Single-Outcome Statistical Analysis

Analyses were conducted at the block level to account for inter-trial variability and to yield more interpretable and robust statistics. Where possible, block-level values were baseline-corrected relative to the corresponding baseline block to control for inter-participant variability and to ensure that observed dynamics reflected changes across the experimental protocol rather than absolute magnitude. Direct baseline subtraction was used rather than percentage change to avoid introducing scale-dependent variance and to maintain interpretability in the original measurement units.

Data were analysed using mixed-effects models to examine how outcome measures evolved over repeated task blocks under simultaneous estimation of population-level effects (fixed effects) and while accounting for the non-independence of repeated observations within participants (random effects). These models accommodated the experiment's hierarchical data structure, allowed for precise modelling of interacting fixed and random effects, and were robust to any data imbalanced or dropout.

For the primary analysis, each outcome measure was modelled individually. When applicable, individual trial values were averaged by movement direction to produce mean flexion and mean extension values for each block. For outcome measures in which directionality was not applicable, trials were averaged across all movements within each block. Two linear mixed-effects models were fitted. In the first model, task block number was centred within each condition; in the second, block number was treated as a continuous variable across the entire session. In both models, block number was centred such that effects reflected changes across blocks rather than relative to the initial block. These complementary modelling approaches enabled assessment of changes occurring within conditions as well as cumulative effects across the session.

In addition to task block number, fixed effects were included for experimental condition, movement direction, and condition order (i.e., whether a condition was performed first or second). The inclusion of condition order, in conjunction with overall session block number, allowed differentiation between ordering effects specific to the period in which task blocks were completed and gradual drift across the session. For the within-condition model, a binary indicator identifying the first block of each condition was included to assess whether initial task blocks exhibited dynamics distinct from subsequent blocks. The global model additionally included a binary indicator for the first task block of the second condition to assess potential switching effects between conditions. Interaction terms were included where relevant to assess how effects changed in combination, specifically over task block count and in relation to each experimental condition.

Random intercepts and random slopes for block were specified for each participant, allowing individual differences in both the expected outcome at the reference block (centred block index = 0) and block-related change, as well as their covariance. Although outcome measures were baseline-corrected, participant-specific random intercepts were retained to account for residual between-participant differences, measurement error in baseline estimates, and within-participant dependence across repeated observations. Because analyses were conducted on block-averaged and baseline-corrected reaction times, which were approximately symmetric, data were modelled using Gaussian mixed-effects models with an identity link to preserve additive interpretation in the original units.

Overall significance of fixed effects and their interactions was obtained directly from the mixed-effects models; however, planned linear contrasts were used to address condition- and direction-specific hypotheses. Primary analyses tested whether outcome measures deviated from baseline for the initial task block and overall, within each condition-direction combination. For the initial deviation test, the model-predicted mean for each condition-direction combination was evaluated at the first task block and tested against zero using linear contrasts of the fixed effects. For the overall deviation test, the predicted mean was evaluated at the centred block, corresponding to the average task block, and similarly tested against zero. Linear contrasts of block-related slopes were used to assess learning effects. Inclusion of an indicator for the initial task block and its interactions with condition and movement direction enabled testing of whether initial block deviations differed from those in subsequent

blocks. Additional contrasts assessed between-condition differences in overall level and rate of change within each movement direction. All tests were two-sided and conducted using Wald tests on fixed-effect contrasts. Results obtained from Wald tests and directly from the mixed-effects models are reported as effect sizes (β), 95% confidence intervals, and p-values (p).

Additional supplementary analyses of the initial task blocks were conducted using nonparametric methods. When no baseline was available, participant-level comparisons between conditions were performed using Wilcoxon signed-rank (WSR) tests on paired values to assess whether conditions differed significantly in the measured outcome. When baselines were available, outcomes from the initial task block were first compared with the corresponding baseline using WSR tests to determine whether a significant deviation was present. The resulting change-from-baseline values were then compared between conditions using WSR tests to assess whether baseline-adjusted effects differed across conditions. These supplementary analyses were intended to provide a simplified assessment of effects in the initial task blocks, where effects were expected to be most pronounced. Results from the Wilcoxon signed-rank tests are reported as rank-biserial correlation coefficients (r), reflecting the consistency of the paired differences; z-scores (z), indicating the degree of deviation from the null distribution; and p-values (p), representing statistical significance.

4.2.11. Correlation-Based Statistical Analysis

To examine relationships between outcome measures while accounting for the experimental design and repeated-measures structure, relational linear mixed-effects models were fitted with one measure as the outcome and another as the predictor. To dissociate stable between-participant differences from transient within-participant covariation, the predictor was decomposed into a participant-specific mean within each condition and a within-participant deviation component per block. The participant means reflected coupling at the level of stable individual differences, whereas effects associated with the deviation component reflected momentary within-participant covariation between measures.

Models were fitted at the block level using Gaussian linear mixed-effects models with an identity link. Fixed effects included task condition, movement direction, centred block index, and all relevant interactions with predictor components; secondary outcome-specific covariates, such as first block indicators, were omitted to avoid overspecification. When available, baseline values were included to control for inherent participant differences. Random intercepts and block slopes were specified for each participant, consistent with the individual outcome models, to account for individual differences in baseline level and adaptation rate.

Inference focused on planned contrasts testing condition- and direction-specific coupling. Simple slopes for the mean and deviation components were evaluated within each condition–direction combination, with additional contrasts testing differences in coupling between conditions within each movement direction. Aggregate between- and within-participant coupling was also summarised using slopes evaluated at the reference levels of effects-coded factors. All tests used two-sided Wald tests, with effects reported as β, 95% confidence intervals, and p-values.

4.3. Postural Stabilisation Phase Motor and Behavioural Dynamics

4.3.1. Introduction

The postural stabilisation phase of the experimental protocol was designed to challenge participants' ability to maintain wrist position in the presence of environmental instability induced through mechanical perturbations. The aim was to establish a clear stability-oriented motor context that encouraged the sensorimotor system to generate an elevated and sustained level of impedance to counteract the induced environmental instability. In addition, the effects of altered perturbation dynamics, defined by force amplitude and temporal predictability, were examined across two cohorts to evaluate the sensitivity of sensorimotor adaptation along these two dimensions.

Although the primary focus of this thesis is the carryover effects of these postural challenges on subsequent voluntary movement, contextualisation of the impedance dynamics observed during voluntary movement required quantification of the impedance expressed during the stabilisation phase. The impact of the perturbations was therefore quantified across three principal domains.

First, the applied torque and the resulting kinematic data were used to regress a second-order impedance model, allowing direct quantification of mechanical impedance in response to the applied perturbations.

Second, behavioural responses to perturbation were assessed by measuring both the angular displacement induced by each perturbation and the time required for participants to return the handle to the neutral position following a perturbation, thereby restoring posture.

Finally, the motor activity underlying these mechanical and behavioural responses was evaluated by quantifying co-contraction of the antagonist muscles involved in wrist flexion and extension. Unlike the mechanical and behavioural measures described above, co-contraction could be assessed relative to levels established during the baseline blocks. This allowed a more targeted evaluation of how participants modulated the degree of co-contraction in response to the stabilisation challenges, rather than simply quantifying its absolute level.

The measurements obtained during the postural stabilisation phase were analysed primarily as a function of perturbation condition and task block count. This approach facilitated evaluation of the effects of altered perturbation dynamics on active impedance modulation, as well as examination of how this modulation changed with repeated exposure.

4.3.2. Mechanical Impedance in Response to Perturbation

Mechanical impedance was estimated for each applied perturbation using a linear, time-domain, second-order impedance model. Impedance estimates were then averaged by direction at the trial level, after which a block-level average was computed for each direction.

When assessing the impact of temporal predictability, impedance was consistently higher in the predictable condition compared with the uncertain condition ($\beta = 0.04$, 95% CI = [0.01, 0.06], $p = .008$). This effect was particularly prominent in response to perturbations in the extension direction ($\beta = 0.05$, 95% CI = [0.02, 0.08], $p = .003$) but was evident only as a trend in the flexion direction ($\beta = 0.03$, 95% CI = [-1.25×10^{-3}, 0.06], $p = .060$, **Figure 4.8**). No condition- or direction-linked adaptation in impedance levels across repeated task blocks reached statistical significance ($p \geq .112$). However, there was a steady increase in impedance across task blocks over the course of the experimental session ($\beta = 0.02$, 95% CI = [0.01, 0.03], $p = .003$). No other significant effects were observed within the mixed-effects models. Secondary non-parametric analyses of impedance differences within the

initial task blocks revealed no significant differences between conditions for either movement direction ($p \geq .145$).

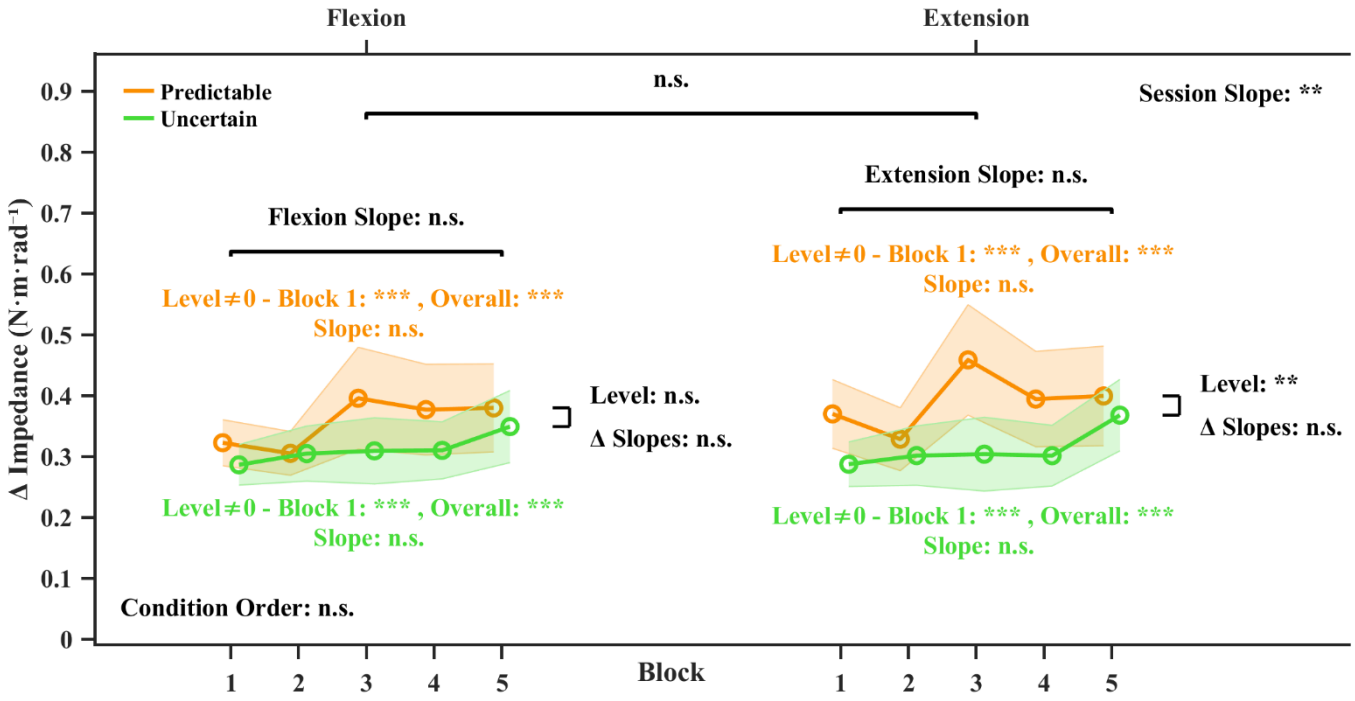

Figure 4.8. Mean impedance (N·m·rad⁻¹) across experimental blocks for flexion (left) and extension (right) under temporally predictable (orange) and uncertain (green) perturbation conditions. Circles denote block-wise means and shaded regions represent variability (±SEM). For each condition-direction combination, impedance was tested for statistical divergence from zero (Level ≠ 0) at the initial task block and the combination overall. Level effects indicate overall differences in impedance amplitude, whereas Slope effects indicate linear trends across repeated blocks. Significance codes: * p < 0.05, ** p < 0.01, *** p < 0.001; n.s., not significant.

Alteration of perturbation amplitude did not induce a significant change in the observed impedance ($\beta = 0.01$, 95% CI = [−0.04, 0.07], $p = .588$). However, movement direction had a significant effect ($\beta = -0.03$, 95% CI = [−0.05, −0.01], $p = .012$), which was primarily attributable to the 0.5 Nm condition ($\beta = -0.05$, 95% CI = [−0.09, −0.02], $p = .002$, **Figure 4.9**). Impedance levels remained stable across repeated exposures, with no significant effect of additional task blocks within either condition or across the overall experimental session ($p \geq .133$), and no evidence of adaptation modulated by movement direction or perturbation amplitude ($p \geq .444$). Non-parametric analyses of the initial task blocks similarly revealed no significant differences for either movement direction ($p \geq .221$).

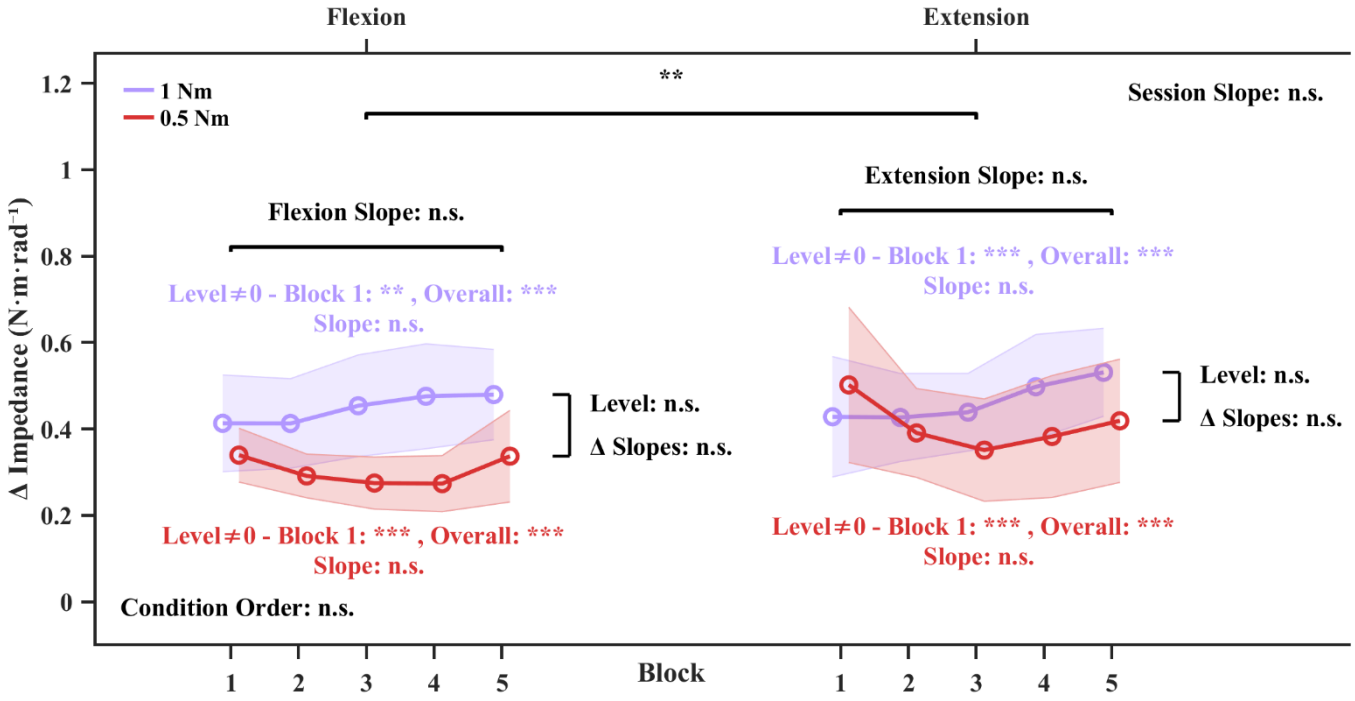

Figure 4.9. Mean impedance (N·m·rad⁻¹) across experimental blocks for flexion (left) and extension (right) under high-amplitude (purple) and low-amplitude (red) perturbation conditions. Full plot description - Figure 4.8.

Across both cohorts, perturbation-induced impedance was robust, rapidly established, and stable across repeated task blocks. This temporal stability argues against gradual error-driven optimisation and instead suggests that participants quickly selected an impedance level appropriate to task demands and maintained it. Manipulating perturbation amplitude produced no systematic change in impedance. In contrast, reduced temporal predictability led to a significant decrease in impedance. This effect was not confined to initial task blocks but emerged across the session, indicating a sustained change in control strategy rather than a transient bias. Directional differences were observed, with generally lower impedance in flexion than extension, though their magnitude and statistical robustness varied across models and conditions. Importantly, these directional effects did not account for the primary experimental findings: neither predictability nor amplitude effects depended strongly on movement direction.

Overall, impedance during postural maintenance was stable over time and directionally biased, but only changes in temporal predictability - not perturbation amplitude - reliably modulated its level. These results indicate that impedance regulation reflects sensitivity to task uncertainty rather than scaling with mechanical perturbation magnitude.

4.3.3. Peak Angular Displacement

Peak angular displacement was measured in response to each applied perturbation. Following perturbation onset, the maximum angular deviation of the handle relative to the neutral position was calculated, providing a robust measure of the behavioural impact of each perturbation. The underlying assumption was that sufficiently increased impedance would reduce the amplitude of displacement elicited by perturbations of consistent amplitude.

Participants were not instructed to adopt a specific control strategy and were only required to maintain the manipulandum handle at the neutral position. Consequently, they were free to optimise their own strategies and to determine whether minimising immediate displacement was the most effective or energetically efficient approach. Displacement measures were first averaged by perturbation direction

within trials and subsequently averaged across task blocks. This yielded direction-specific estimates for each task block, enabling examination of how perturbations applied in flexion and extension were differentially controlled. As perturbations were absent during baseline blocks, peak displacement was evaluated in absolute terms rather than relative to baseline.

Peak angular displacement exhibited robust non-zero offsets across both movement directions and conditions, indicating consistent perturbation-induced displacement throughout task exposure (**Figure 4.10**). Mixed-effects analyses revealed a significant main effect of direction, with larger peak displacements observed in extension than in flexion (β = 3.26, 95% CI = [2.45, 4.06], p < .001). Across directions, there was evidence of a higher overall displacement in the predictable condition compared with the uncertain condition. The main effect of condition reached significance (β = 2.07, 95% CI = [0.06, 4.07], p = .043), indicating larger average peak displacements under predictable dynamics. This effect was direction-dependent. When examined separately, a significant between-condition difference was observed in extension (β = 2.55, 95% CI = [0.54, 4.56], p = .013), whereas the corresponding difference in flexion was not significant (β = 1.59, 95% CI = [−0.42, 3.60], p = .122).

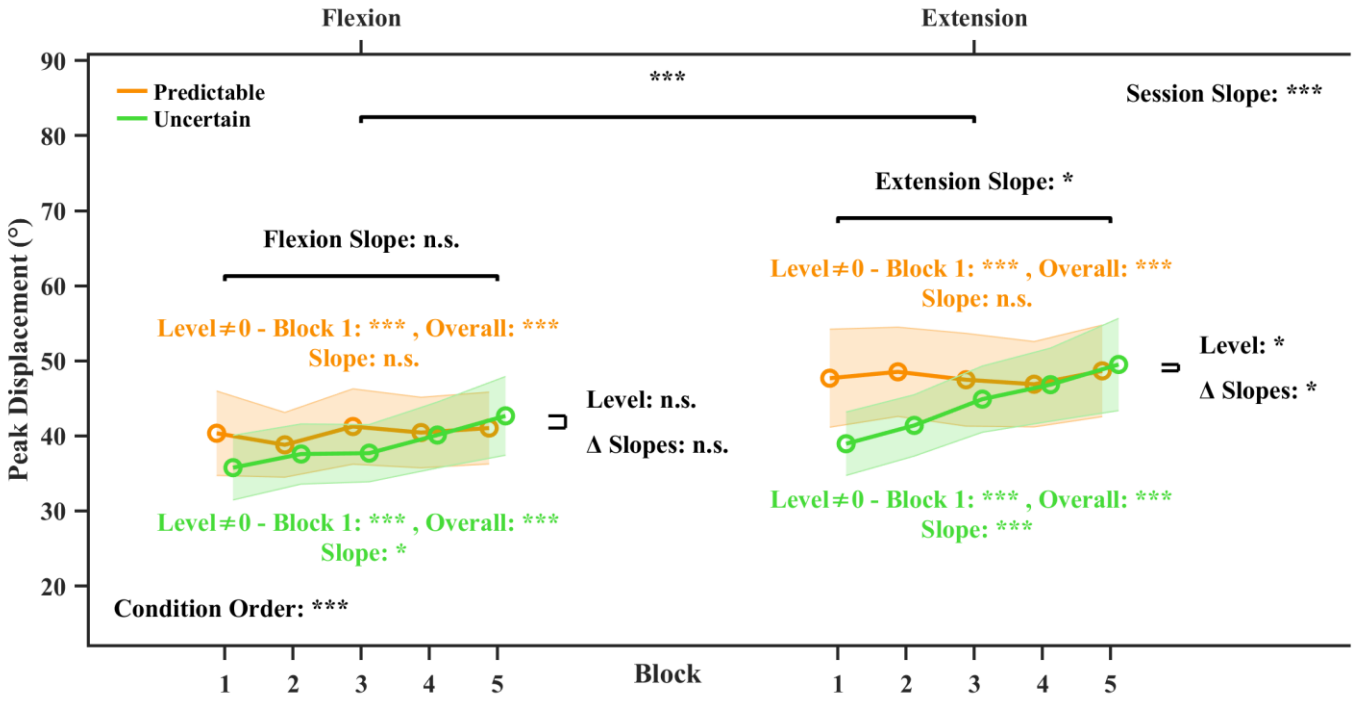

Figure 4.10. Peak angular displacement (°) induced by perturbation averaged across experimental blocks for flexion (left) and extension (right) under temporally predictable (orange) and uncertain (green) perturbation conditions. Full plot description - Figure 4.8.

In addition to differences in overall displacement magnitude, the predictable and uncertain conditions showed clear divergence in their evolution across repeated task blocks. For both flexion and extension perturbations, there was no significant change in displacement across blocks in the predictable condition (p ≥ .584). In contrast, the uncertain condition exhibited a steady increase in peak angular displacement over task blocks for both extension (β = 2.71, 95% CI = [1.20, 4.22], p < .001) and flexion (β = 1.69, 95% CI = [0.18, 3.20], p = .028).

Peak angular displacement was also strongly influenced by task order. Completing a condition second was associated with increased displacement (β = 2.92, 95% CI = [−3.99, −1.85], p < .001), alongside a steady increase in displacement across task blocks over the session (β = 1.62, 95% CI = [0.78, 2.46], p < .001). Although no significant effect of being the first task block was detected overall or within either condition (p ≥ .558), a marked increase in displacement was observed for the first block of the second condition (β = 2.34, 95% CI = [0.87, 3.81], p = .002). This effect was not sensitive to the specific condition presented (p = .494).

Supplementary analysis of the first task blocks in isolation was consistent with the condition-dependent dynamics observed in the primary analysis, with a statistically significant increase in angular displacement under predictably timed perturbations compared with the uncertain condition for extension (p = .030, z = 2.17, r = 0.44, **Figure 4.11B**), but not for flexion (p = .199, z = 1.29, r = 0.26, **Figure 4.11A**).

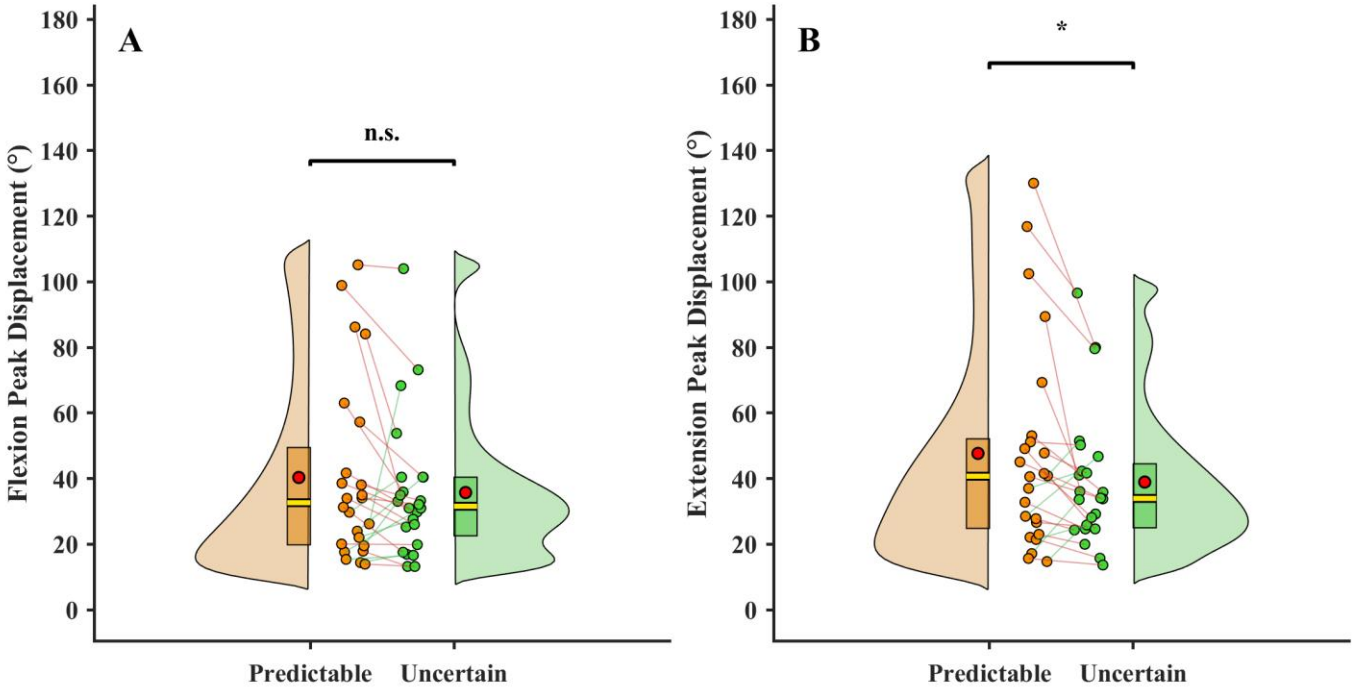

Figure 4.11. Distribution of peak angular perturbation-induced displacement during initial task blocks for (A) flexion and (B) extension under temporally predictable (orange) and uncertain (green) perturbation conditions. Half-violin plots illustrate the distribution of individual participant values. Overlaid dots represent individual observations, with lines connecting paired measurements across conditions. Red circles indicate condition means and yellow horizontal lines indicate medians. Brackets denote statistical comparisons between conditions. Significance codes: * p < 0.05, ** p < 0.01, *** p < 0.001; n.s., not significant.

In the perturbation amplitude cohort, peak displacement was reliably greater than zero for both movement directions across conditions, both in the initial task block (p ≤ .001) and across task blocks (p ≤ .001, **Figure 4.12**). Across directions, peak displacement was significantly larger in the 1 Nm condition than in the 0.5 Nm condition (β = 9.32, 95% CI = [6.36, 12.28], p ≤ .001). Direction-specific analyses were consistent with this overall effect, demonstrating clear separation between amplitude conditions for both flexion and extension perturbations (p ≤ .001). There was no significant change in peak displacement across task blocks at any level of analysis (p ≥ .486). Despite this consistency across perturbation directions, a significant main effect of direction was observed, with flexion perturbations producing a small but reliable increase in displacement relative to extension (β = 3.13, 95% CI = [1.62, 4.64], p < .001).

Unlike the predictability cohort, there was no significant effect of the order in which conditions were completed (β = 1.24, 95% CI = [−0.59, 3.07], p = .185). In addition, there was a trend towards increasing peak displacement across task blocks over the session (β = 1.41, 95% CI = [−0.10, 2.92], p = .066), and this effect was significantly modulated by perturbation amplitude (β = −1.10, 95% CI = [−2.14, −0.06], p = .039).

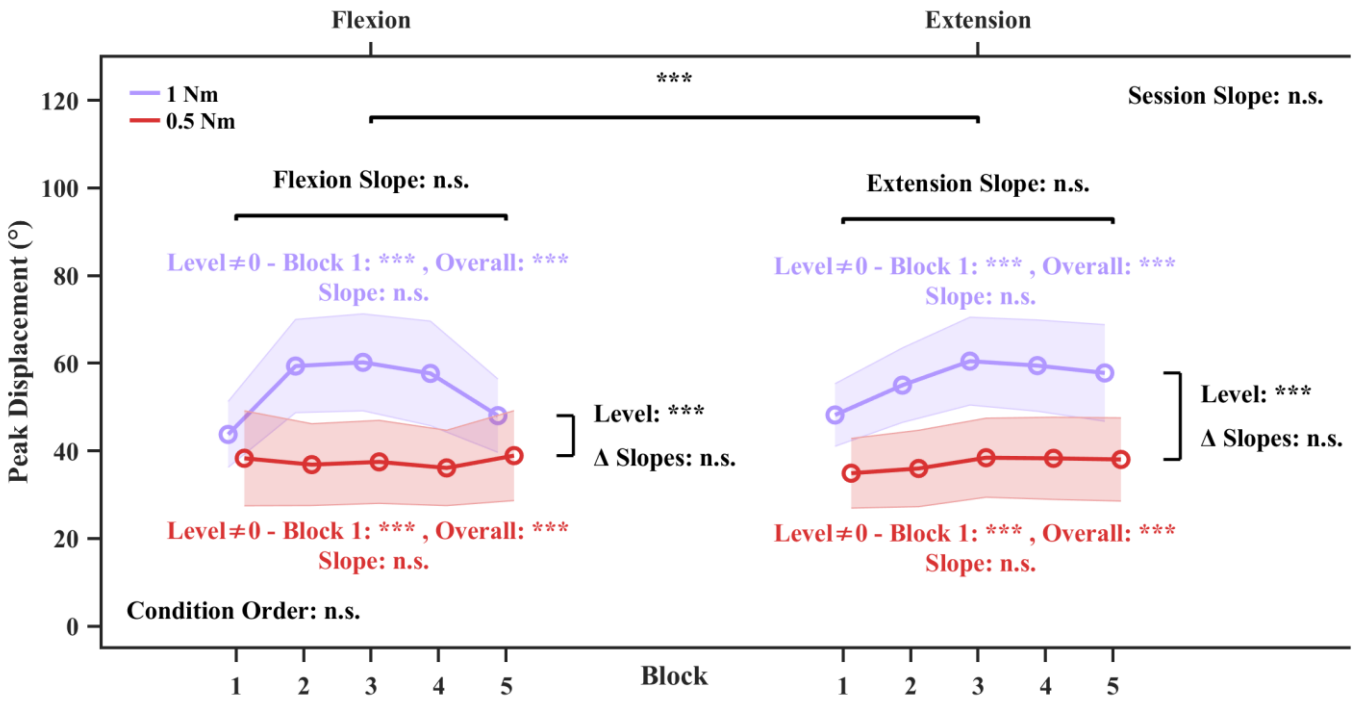

Figure 4.12. Peak angular displacement (°) induced by perturbation across experimental blocks for flexion (left) and extension (right) under high-amplitude (purple) and low-amplitude (red) perturbation conditions. Full plot description - Figure 4.8.

Supplementary analysis of the initial task blocks demonstrated greater peak displacement for the high amplitude (1 Nm) condition compared with the low-amplitude (0.5 Nm) condition in both flexion ($p = .012$, $z = 2.51$, $r = 0.72$, **Figure 4.13A**) and extension ($p = .008$, $z = 2.67$, $r = 0.71$, **Figure 4.13B**).

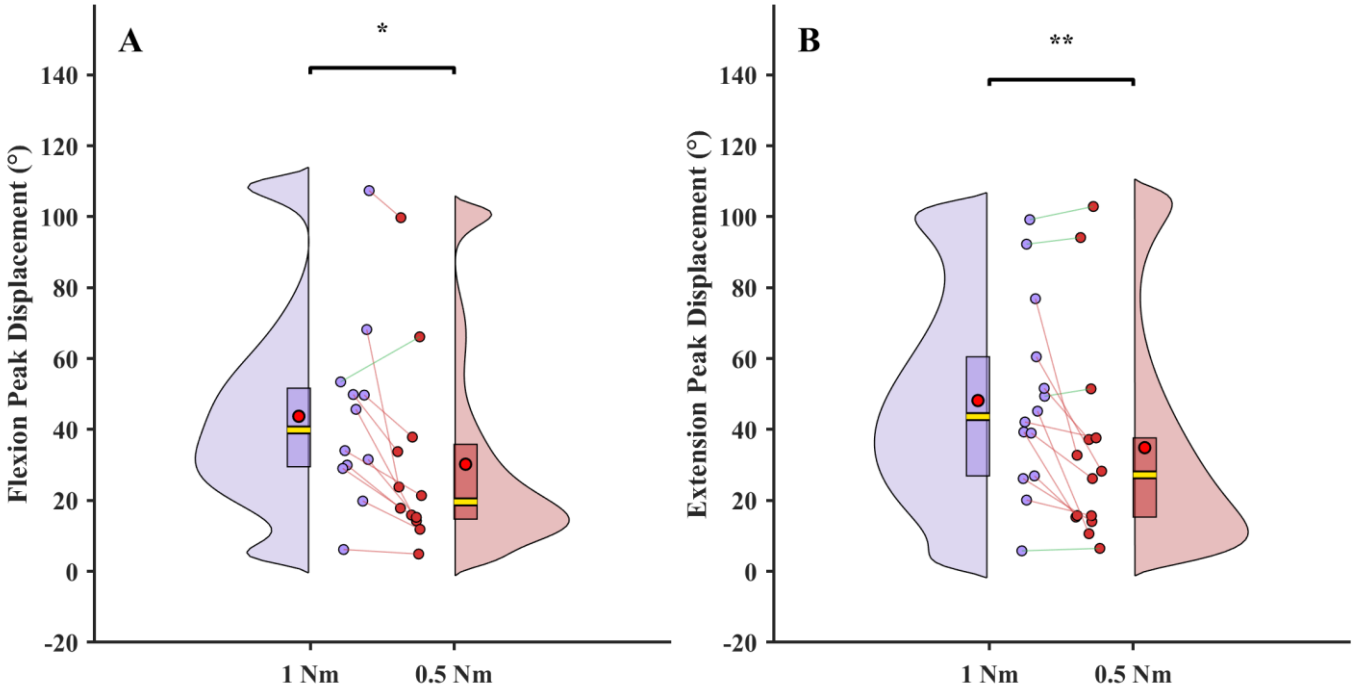

Figure 4.13. Distribution of peak angular perturbation-induced displacement (°) during initial task blocks for (A) flexion and (B) extension under high-amplitude (purple) and low-amplitude (red) perturbation conditions. Full plot description - Figure 4.11.

Across both cohorts, peak displacement showed a reliable non-zero offset from the first task block, indicating consistent perturbation-induced displacement. The factors shaping this offset differed between cohorts.

In the temporal predictability cohort, peak displacement was larger under predictable than uncertain dynamics, particularly in extension. This difference was present from the first block. Under temporal uncertainty, displacement in extension increased across blocks, suggesting an initially conservative strategy that relaxed with experience. Effects were weaker in flexion.

In the perturbation amplitude cohort, peak displacement scaled with perturbation magnitude. Larger perturbations produced greater displacement from the first block onward across directions. Displacement did not change systematically across blocks, indicating no learning effect.

Overall, perturbation amplitude set the scale of displacement in a time-invariant manner, while temporal predictability modulated displacement adaptively. Directional asymmetries were present but did not account for the primary effects.

4.3.4. Post-Perturbation Stabilisation Time

Post-perturbation stabilisation time was calculated from perturbation onset to the time point at which participants restored the handle position to neutral for at least 0.5 s. This window was selected because it was shorter than the minimum inter-perturbation interval of 0.75 s in the uncertain condition of the temporal predictability cohort, while remaining sufficiently long to indicate complete movement termination. If a participant failed to stabilise the handle following a perturbation, the corresponding interval was excluded from the analysis. Stabilisation times were averaged by direction at the trial level and subsequently used to compute a block-level average for each direction.

Stabilisation times were reliably greater than zero for all directions and conditions in the predictability cohort for both the initial task blocks and condition averages ($p \leq .001$, **Figure 4.14**). There was no evidence of an overall condition difference in stabilisation time ($\beta = 0.01$, 95% CI = [−0.01, 0.02], $p = .480$). This lack of significance was consistent across both movement directions ($p \geq .252$). There was also no significant evidence of adaptation across repeated task blocks, either overall or within each movement direction ($p \geq .381$).

Despite the absence of robust within-condition adaptation, the rate of change differed between conditions for extension movements. Specifically, extension perturbations exhibited a significantly less positive slope in the predictable condition than in the uncertain condition ($\beta = -0.01$, 95% CI = [-0.01, -1.23×10^{-3}], $p = .019$). No corresponding difference in slopes was observed for flexion ($p = .254$).

Analyses revealed no overall effects of movement direction ($p = .512$), initial condition ($p = .189$), carryover effects of condition order ($p = .146$), or switching between conditions ($p = .359$) on stabilisation time. However, there was evidence that session-wide block count interacted with condition ($\beta = -4.68 \times 10^{-3}$, 95% CI = [-0.01, -8.06×10^{-4}], $p = .018$), suggesting that condition may have modulated the trajectory stabilisation times modestly with over the session. A non-parametric comparison of the first task blocks yielded a non-significant result for flexion ($p = .317$, $z = 1.00$, $r = 0.20$) and a robust trend towards increased stabilisation time in the predictable condition during extension ($p = .059$, $z = 1.89$, $r = 0.38$).

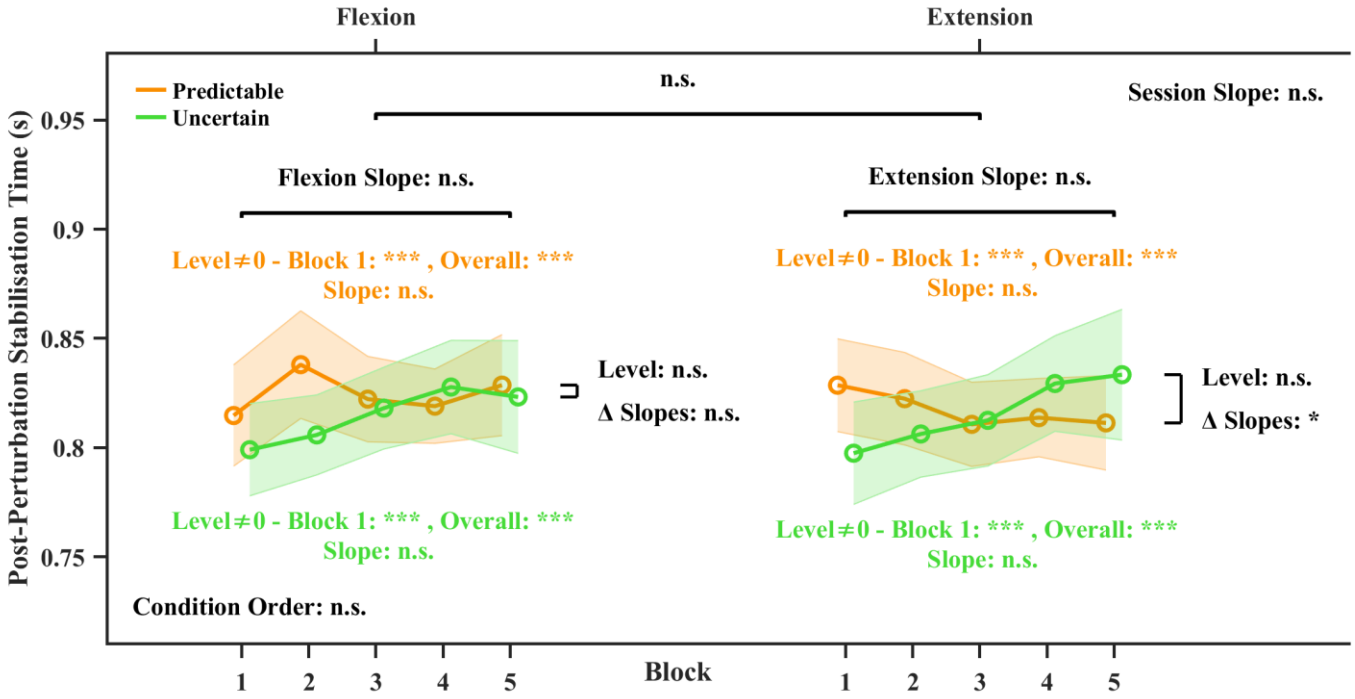

Figure 4.14. Post-perturbation stabilisation time (s) following perturbation across experimental blocks for flexion (left) and extension (right) under temporally predictable (orange) and uncertain (green) perturbation conditions. Full plot description - Figure 4.8.

Within the perturbation amplitude cohort, stabilisation time was reliably greater than zero for both the first task block and the overall level across both conditions and directions ($p \leq .001$, **Figure 4.15**). Across directions, perturbation amplitude exerted a robust effect on stabilisation time, with longer stabilisation times observed for 1 Nm compared with 0.5 Nm ($\beta = 0.04$, 95% CI = [0.02, 0.05], $p < .001$). This effect was highly consistent across both movement directions (flexion: $\beta = 0.04$, $p < .001$; extension: $\beta = 0.04$, $p < .001$). No reliable main effect of movement direction was observed ($p = .668$), indicating comparable stabilisation times in flexion and extension after accounting for perturbation amplitude and task block.

There was limited evidence for systematic adaptation across task blocks. The overall effect of block count did not reach statistical significance ($p = .178$), and block-within-direction effects were non-significant for flexion ($p = .530$) and marginal for extension ($p = .055$). Similarly, condition-specific slopes across blocks were generally small; however, the targeted estimates indicated a significant negative slope in flexion for the high-amplitude (1 Nm) condition ($\beta = -0.01$, 95% CI = [-0.02, -1.18×10^{-3}], $p = .030$), whereas all other slopes were non-significant. Critically, there was no evidence that adaptation differed between perturbation amplitudes. The difference in change across blocks between conditions was non-significant overall ($p = .432$) and within each movement direction ($p \geq .243$).

Analyses indicated a significant effect of the order in which conditions were completed, with shorter post-perturbation stabilisation times observed in whichever condition was performed second ($\beta = -0.02$, 95% CI = [-0.03, -4.48×10^{-3}], $p = .010$). There was no significant effect of the specific condition order, switching between conditions, or overall task block count ($p \geq .603$).

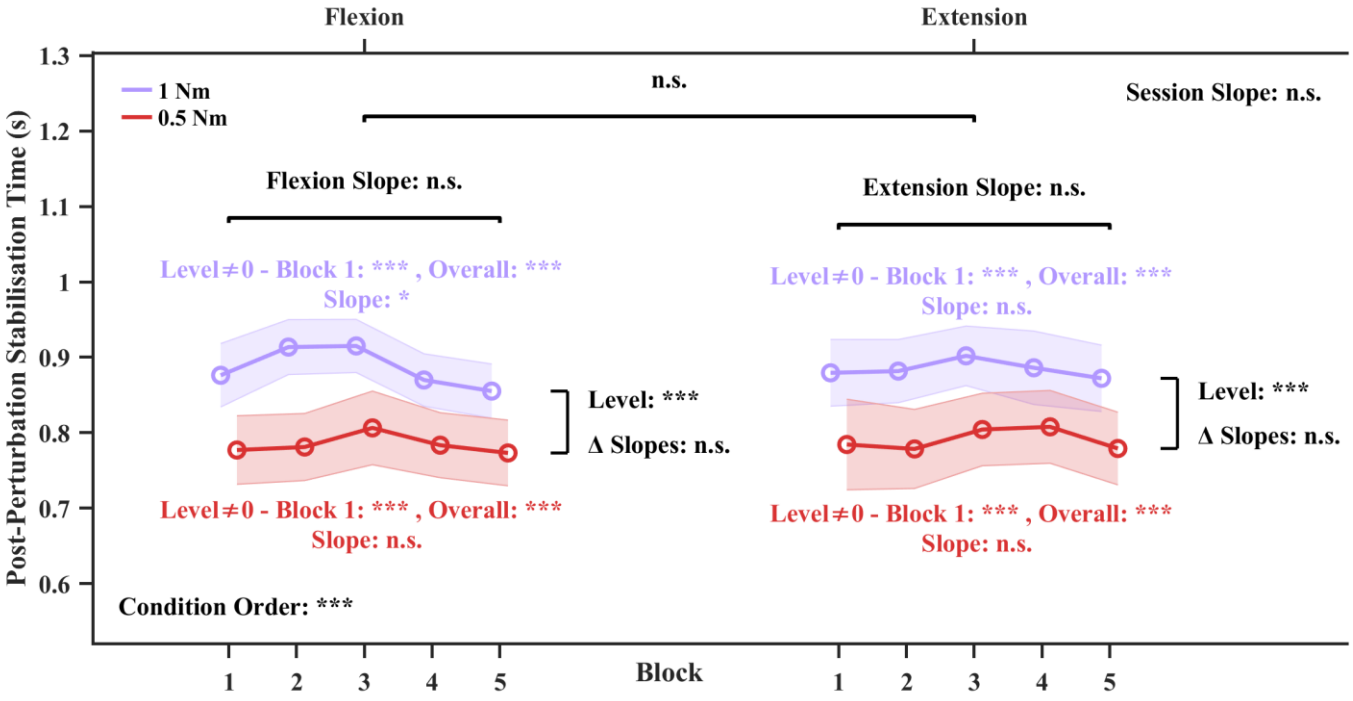

Figure 4.15. Post-perturbation stabilisation time (s) following perturbation across experimental blocks for flexion (left) and extension (right) under high-amplitude (purple) and low-amplitude (red) perturbation conditions. Full plot description - Figure 4.8.

Consistent with the model-based findings, nonparametric comparisons at the first task block showed longer stabilisation times in the high-amplitude (1 Nm) condition relative to the low-amplitude (0.5 Nm) condition for both flexion ($p = .005$, $z = 2.79$, $r = 0.75$, **Figure 4.16A**) and extension ($p = .016$, $z = 2.42$, $r = 0.65$, **Figure 4.16B**).

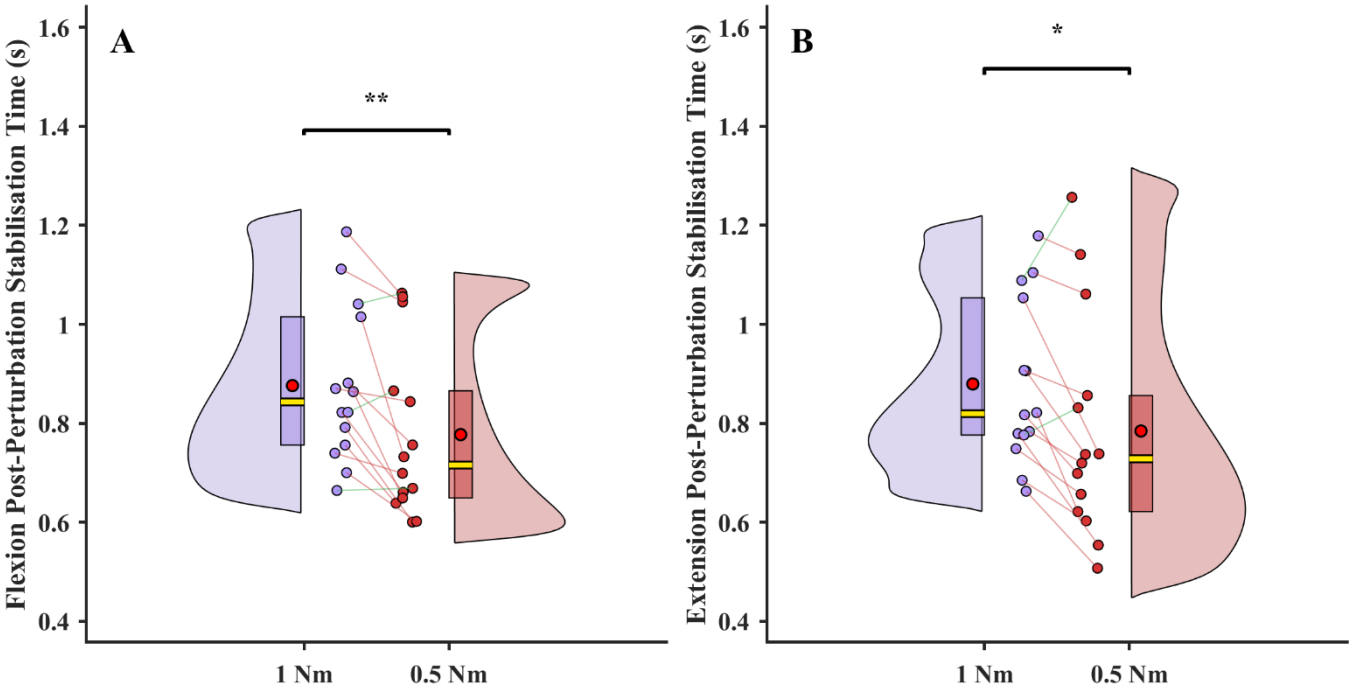

Figure 4.16. Distribution of post-perturbation stabilisation times (s) during initial task blocks for (A) flexion and (B) extension under high-amplitude (purple) and low-amplitude (red) perturbation conditions. Full plot description - Figure 4.11.

Post-perturbation stabilisation time showed a clear amplitude-dependent offset, with longer times for 1 Nm than 0.5 Nm perturbations from the first block onward. This effect persisted across the session, with minimal change across blocks and no difference in learning rate between amplitudes. In the temporal predictability cohort, stabilisation time was largely invariant, with no overall effects of predictability or direction and little adaptation. However, a small, direction-specific reduction across blocks was observed in extension under predictable timing. Overall, stabilisation time was primarily determined by perturbation amplitude and general task familiarity, with only weak modulation by predictability or direction.

4.3.5. Relationship Between Peak Angular Displacement and Post-Perturbation Stabilisation Time

Peak angular displacement was a strong and consistent predictor of post-perturbation stabilisation time, with clear contributions from both between-participant and within-participant components. At the between-participant level, larger average peak displacement ranges were associated with longer stabilisation times ($\beta = 2.08 \times 10^{-3}$, 95% CI = [$1.41 \times 10^{-3}$, 2.76×10^{-3}], $p < .001$, **Figure 4.17**). This relationship was robust across movement directions and predictability conditions. Simple-slope analyses revealed significant positive associations in both flexion and extension, under both temporally predictable and uncertain perturbations ($p \leq .001$), indicating that participants who generally experienced larger perturbation-induced displacements required more time to re-stabilise. This relationship was stable across task blocks ($\beta = 2.12 \times 10^{-5}$, 95% CI = [$-1.21 \times 10^{-4}$, 1.63×10^{-4}], $p = .770$).

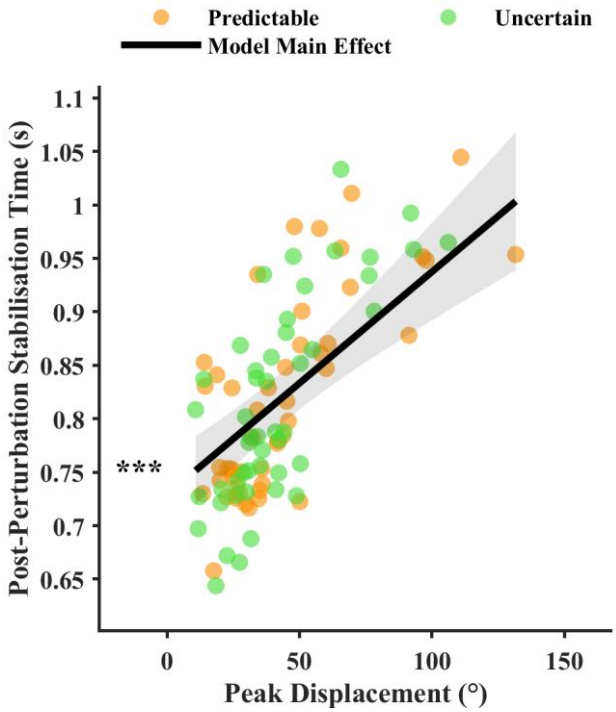

Figure 4.17. Relationship between peak joint displacement (°) and post-perturbation stabilisation time (s). Participant-level mean values are shown for the temporally predictable (orange) and uncertain (green) task blocks. The solid black line represents the model-estimated main effect across conditions, with the shaded band indicating the 95% confidence interval. The asterisk denotes the significance of the overall model effect. Significance codes: * p < 0.05, ** p < 0.01, *** p < 0.001; n.s., not significant.

Temporal predictability modulated this relationship asymmetrically. There was a statistically significant alteration in the relationship between mean peak angular displacement and mean post-perturbation stabilisation time dependent on predictability condition ($\beta = -5.07 \times 10^{-4}$, 95% CI = [$-7.08 \times 10^{-4}$, -3.06

× 10^{-4}], p < .001). Temporal uncertainty strengthened the relationship between the peak angular displacement induced by perturbation and the time taken to restore posture. This relationship was consistent across both flexion (**Figure 4.18A**) and extension perturbations (**Figure 4.18B**), was highly significant in both directions (p ≤ .001), and of similar amplitude (flexion: β = 9.79 × 10^{-4}; extension: β = 1.05 × 10^{-3}).

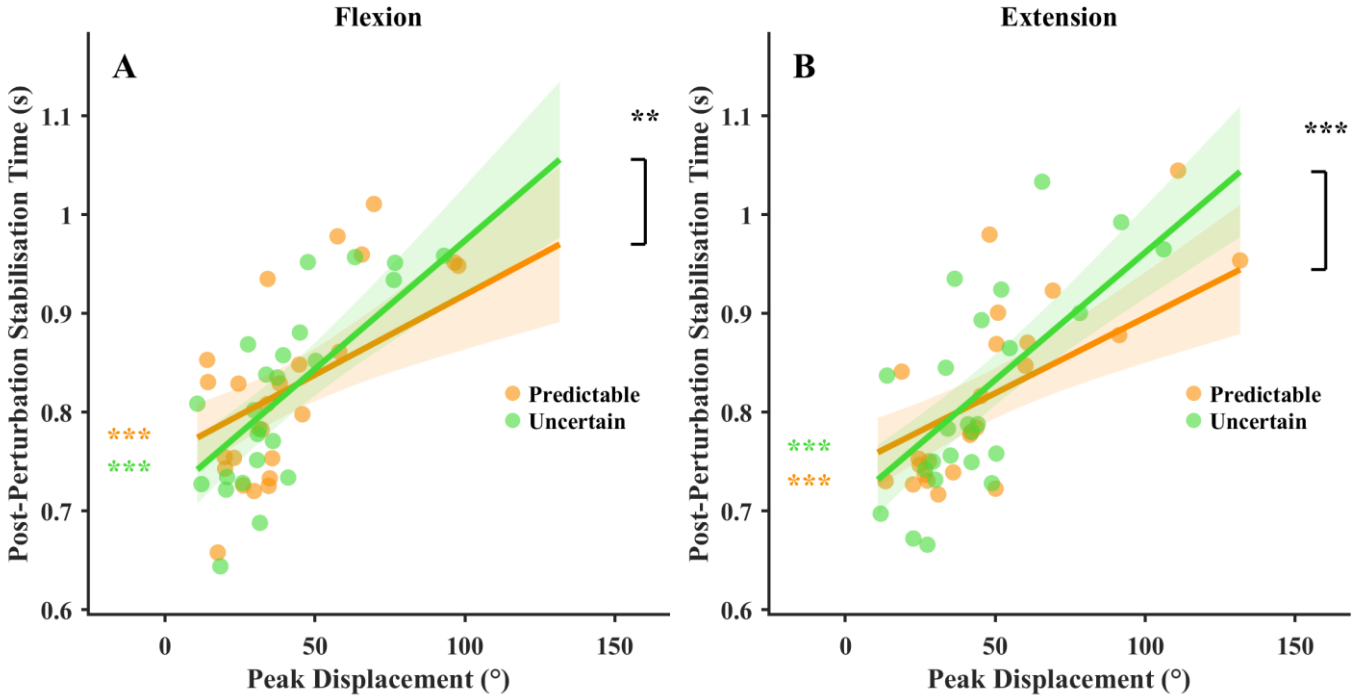

Figure 4.18. Between-participant relationship between mean peak angular displacement (°) and post-perturbation stabilisation time (s) for (A) flexion and (B) extension. Each point represents an individual participant's mean level for a given condition (predictable, orange; uncertain, green). Solid lines depict condition-specific model fits, with shaded bands indicating the corresponding 95% confidence intervals. Asterisks adjacent to the axes denote the statistical significance of the respective model fits, while brackets indicate comparisons between fits. Scatter points reflect raw between-participant means and do not account for additional model coefficients, which may result in a visual mismatch between the fitted lines and the distribution of points. Significance codes: * p < 0.05, ** p < 0.01, *** p < 0.001; n.s., not significant.

Within participants, block-to-block increases in peak offset range were also strongly associated with longer stabilisation times (β = 3.89 × 10^{-3}, 95% CI = [3.33 × 10^{-3}, 4.45 × 10^{-3}], p < .001). This effect was present for both movement directions and both task conditions. Predictable and uncertain conditions each showed significant positive slopes in flexion and extension (p ≤ .001), demonstrating a block-to-block coupling between perturbation displacement and stabilisation times. Unlike at the between-participant level, correlations at the within-participant level were only modulated by condition during extension movements, resulting in a non-significant interaction between task condition and within-participant changes in peak angular displacement (β = −6.35 × 10^{-4}, 95% CI = [−1.37 × 10^{-3}, 9.54 × 10^{-5}], p = .088). For extension movements, the correlation between within-participant changes in peak angular displacement and post-perturbation stabilisation time was significantly stronger (β = 2.82 × 10^{-3}, 95% CI = [1.06 × 10^{-3}, 4.59 × 10^{-3}], p = .002, **Figure 4.19B**), while failing to reach significance for flexion (p = .777, **Figure 4.19A**).

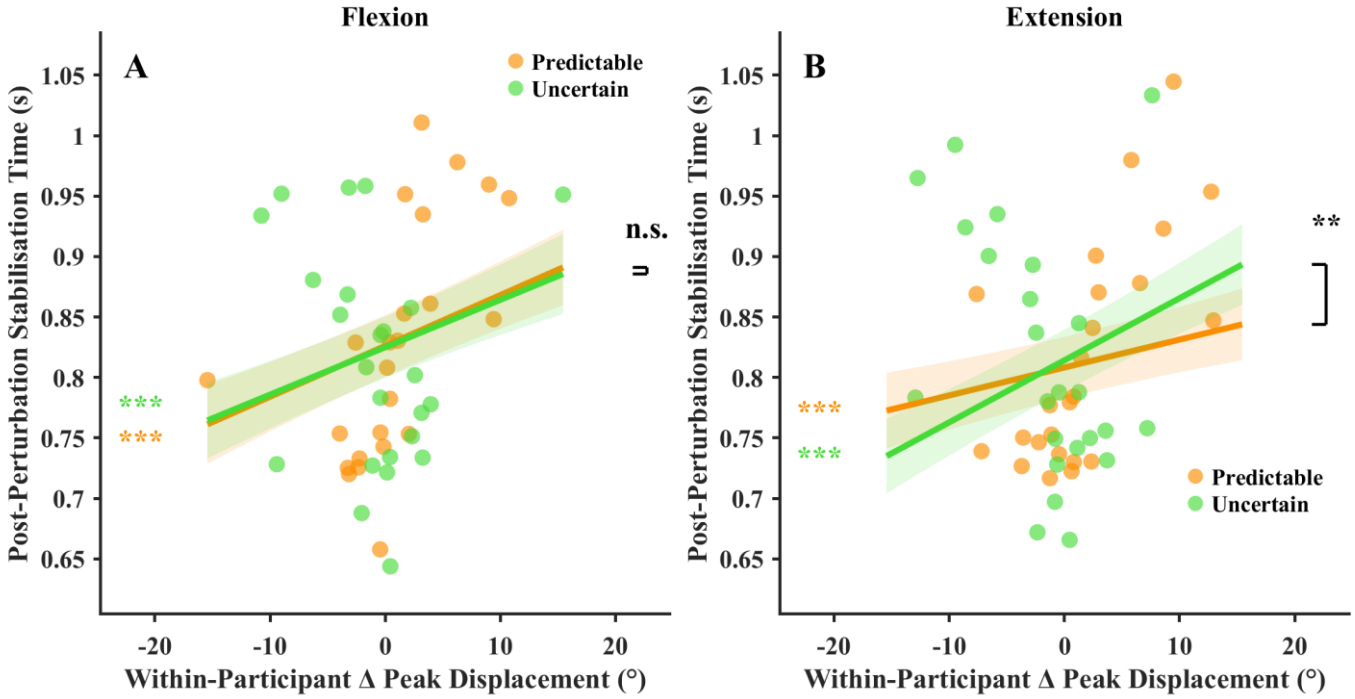

Figure 4.19. Within-participant relationship between changes in peak joint displacement (Δ peak displacement, °) and post-perturbation stabilisation time (s) for (A) flexion and (B) extension. Each point represents an individual participant's deviation from their own mean for a given condition (predictable, orange; uncertain, green). Full plot description - Figure 4.18.

In the perturbation amplitude cohort, peak offset range showed a strong, highly consistent relationship with the outcome across both between-participant and within-participant levels, indicating that larger perturbation amplitudes reliably translated into larger behavioural consequences.

At the between-participant level, individuals with larger average peak offset ranges exhibited significantly larger responses ($\beta = 3.69 \times 10^{-3}$, 95% CI = [$2.79 \times 10^{-3}$, 4.59×10^{-3}], $p < .001$, **Figure 4.20**). This effect was robust across movement directions and perturbation amplitudes. Simple-slope analyses confirmed positive effects for both flexion and extension at 1 Nm and 0.5 Nm ($p \leq .001$). However, the strength of this relationship was systematically reduced at the higher perturbation amplitude, as reflected by a reduction in the predictive power of peak angular offset under the high-amplitude condition ($\beta = -7.54 \times 10^{-4}$, 95% CI = [$-9.31 \times 10^{-4}$, -5.77×10^{-4}], $p < .001$). This was consistent across both movement directions with each showing reduced correlation between peak angular displacement and post-perturbation stabilisation time in the high-amplitude condition ($p \leq .001$). The strength of the relationship between peak angular displacement and stabilisation time diminished over task blocks ($\beta = -1.56 \times 10^{-4}$, 95% CI = [$-3.07 \times 10^{-4}$, -5.35×10^{-6}], $p = .042$).

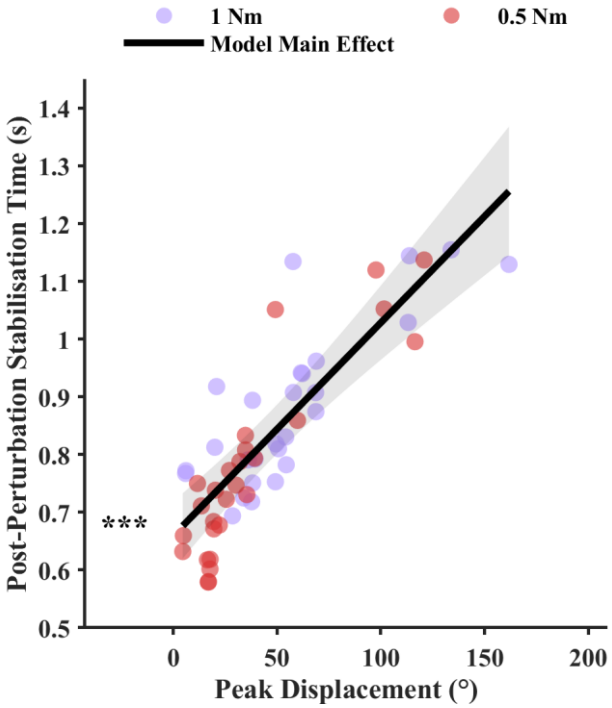

Figure 4.20. Relationship between peak joint displacement (°) and post-perturbation stabilisation time (s). Participant-level mean values are shown for the high-amplitude (purple) and low-amplitude (red) perturbation task blocks. Full plot description - Figure 4.17.

Within participants, block-to-block fluctuations in peak offset range were also strongly predictive ($\beta = 3.56 \times 10^{-3}$, 95% CI = [$2.84 \times 10^{-3}$, 4.28×10^{-3}], $p < .001$). Simple-slope analyses revealed significant positive effects in both movement directions and at both force amplitudes ($p \leq .006$). The within-participant correlations were not influenced by perturbation amplitude ($\beta = 3.69 \times 10^{-4}$, 95% CI = [$-5.41 \times 10^{-4}$, 1.28×10^{-3}], $p = .425$) and remained stable over task blocks ($\beta = -3.11 \times 10^{-4}$, 95% CI = [$-8.00 \times 10^{-4}$, 1.77×10^{-4}], $p = .211$).

Peak offset range emerged as a key determinant of post-perturbation stabilisation demands. Across both cohorts, larger displacements were reliably associated with longer stabilisation times, indicating that recovery dynamics scale with the spatial magnitude of deviation. This relationship was present both between participants and within participants across task blocks.

Between participants, larger average displacements predicted longer stabilisation times across directions. This scaling was amplified when perturbations were temporally unpredictable. Within participants, block-to-block increases in peak offset were similarly linked to longer stabilisation times, with particularly strong effects in extension under temporal uncertainty. These within-participant effects were often larger than between-participant effects. In the perturbation amplitude cohort, the displacement–stabilisation relationship weakened at higher amplitudes and over blocks, suggesting saturation or adaptation with experience. In contrast, within-participant coupling remained robust and insensitive to amplitude or practice.

Overall, peak offset range is a strong predictor of stabilisation dynamics, reflecting both stable individual differences and block-level variability, with distinct modulation by temporal predictability and perturbation amplitude.

4.3.6. Relationship Between Impedance and Behavioural Responses to Perturbation

Within the temporal predictability cohort, impedance showed a clear dissociation between between- and within-participant effects. At the between-participant level, higher mean impedance strongly predicted smaller peak angular displacements ($\beta = -46.94$, 95% CI = [−67.50, −26.37], $p < .001$). This relationship was stable across predictability condition, movement direction, task block, and higher-order interactions ($p \geq .331$), indicating a trait-like protective effect of impedance on displacement. In contrast, within-participant fluctuations in impedance were not associated with concurrent changes in displacement ($\beta = -5.72$, 95% CI = [−13.75, 2.32], $p = .163$).

A complementary pattern emerged for stabilisation time. Within participants, higher-than-usual impedance was associated with faster stabilisation ($\beta = -0.07$, 95% CI = [−0.12, −0.03], $p = .002$), most evident in flexion under predictable timing ($\beta = -0.10$, 95% CI = [−0.18, −0.03], $p = .009$). This relationship did not differ reliably between predictability conditions ($p = .831$). Between-participant differences in impedance were unrelated to stabilisation time overall ($p = .549$).

Stabilisation time showed little sensitivity to condition or direction (both $p \geq .085$) but improved more across blocks in the predictable condition ($\beta = -5.29 \times 10^{-3}$, 95% CI = [$-8.98 \times 10^{-3}$, -1.60×10^{-3}], $p = .005$). A modest direction-specific between-participant effect was observed, with higher mean impedance predicting longer stabilisation times in flexion than extension ($\beta = 0.03$, 95% CI = [6.54×10^{-3}, 0.05], $p = .010$).

In the perturbation amplitude cohort, impedance was not associated with peak angular displacement at either the between-participant ($p = .385$) or within-participant level ($p = .752$), indicating no systematic effect on displacement. Between-participant impedance was also unrelated to overall stabilisation time ($p = .900$). Within participants, higher impedance showed only a weak, non-significant tendency toward faster stabilisation ($\beta = -0.04$, 95% CI = [−0.08, 2.90×10^{-3}], $p = .068$).

Despite the absence of a main effect, between-participant impedance showed strong context dependence. Mean impedance interacted with perturbation amplitude ($\beta = -0.04$, 95% CI = [−0.06, −0.01], $p < .001$), indicating different impedance–stabilisation relationships at 1 Nm and 0.5 Nm. In flexion, mean impedance was unrelated to stabilisation time at 1 Nm ($p = .992$) but tended to predict longer stabilisation at 0.5 Nm, with a significant difference in slopes between amplitudes ($\beta = 0.08$, 95% CI = [7.78×10^{-3}, 0.15], $p = .029$, **Figure 4.21A**). A similar torque-dependent divergence was observed in extension ($\beta = 0.07$, 95% CI = [0.02, 0.11], $p = .005$, **Figure 4.21B**), despite non-significant simple slopes within each condition.

Direction further modulated between-participant impedance effects, with higher mean impedance more strongly associated with longer stabilisation times in flexion than extension ($\beta = 0.03$, 95% CI = [4.08×10^{-3}, 0.06], $p = .025$). No higher-order interactions involving mean impedance were reliable. In contrast, within-participant impedance showed no contextual modulation, with no significant interactions with perturbation amplitude, direction, or their combination ($p \geq .120$).

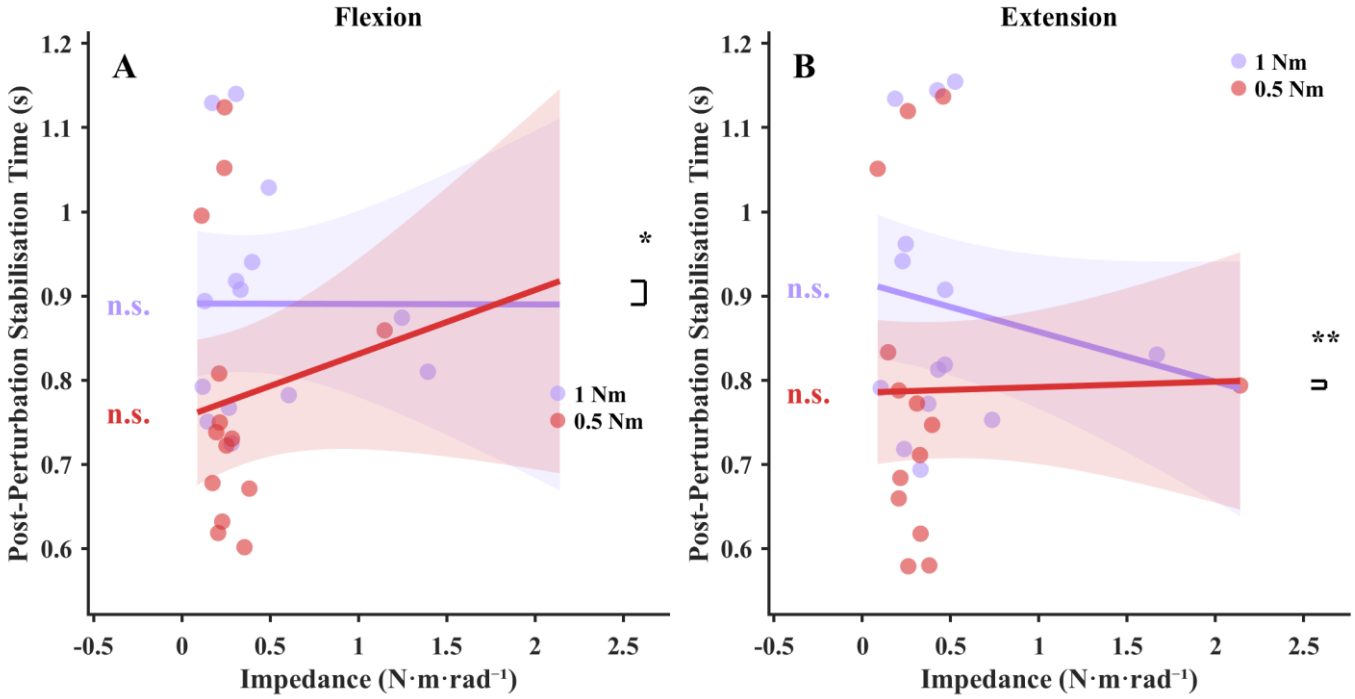

Figure 4.21. Between-participant relationship between Impedance (N·m·rad⁻¹) and post-perturbation stabilisation time (s) for (A) flexion and (B) extension. Each point represents an individual participant's mean level for a given condition (high-amplitude, purple; low-amplitude, red). Full plot description - Figure 4.18.

Across cohorts, a consistent dissociation emerged between the functional roles of trait-like (between-participant) and state-dependent (within-participant) impedance, but the expression of this dissociation depended strongly on task structure. In the temporal predictability cohort (n = 24), between-participant impedance robustly constrained peak displacement, while within-participant impedance regulation selectively supported faster stabilisation under predictable flexion perturbations, indicating a clear division between structural protection and online control. In contrast, the perturbation amplitude cohort (n = 14) showed no reliable impedance–displacement coupling and only weak, context-fragmented effects on stabilisation time, with between-participant impedance influencing performance only through higher-order interactions with torque amplitude and direction.

The absence of coherent effects in the amplitude cohort likely reflects both reduced statistical power and increased mechanical heterogeneity. The smaller sample size limited sensitivity to detect moderate between-participant effects, while varying perturbation amplitude altered task demands in a way that may have reduced the utility of impedance as a global stabilisation strategy. Under these conditions, impedance effects emerged only in specific mechanical contexts, rather than as stable or generalisable relationships.

4.3.7. Stabilisation Through Antagonist Muscle Co-Contraction

Co-contraction indices were computed at each time step during the dynamic stabilisation phase and then averaged across the entire window to estimate the level of muscular activity employed to counteract the induced instability. Averaging yielded a single value per trial that captured the overall level of motor activity throughout the phase, encompassing both active modulation by participants and transient fluctuations induced directly by the perturbations. As perturbation dynamics were identical across conditions except for the parameter under investigation, collapsing each trial in this manner preserved direct comparability between conditions. For each task block, the grand mean co-contraction index was calculated and baseline co-contraction was subtracted. This approach provided a

quantification of how co-contraction index levels were modulated during the dynamic stabilisation phase relative to each participant's inherent level at rest.

When examining the role of temporal uncertainty in modulating co-contraction index (CCI), mixed-effects modelling indicated that the level of co-contraction induced was generally a stable characteristic of the condition presented (**Figure 4.22B**). Overall stabilisation phase CCI modulation was significantly lower in the predictable condition than in the uncertain condition (β = −0.03, 95% CI = [−0.06, −0.01], p = .018). There was no meaningful change in CCI modulation across blocks for either condition or for the cohort (p ≥ .544).

Despite this clear difference in the effect size between conditions, both conditions exhibited highly significant CCI modulation relative to baseline when averaged across blocks (p ≤ .001) and within the initial block of each condition (p ≤ .001). Furthermore, modulation in the initial block did not differ significantly from the block-averaged modulation for either condition (p ≥ .693), providing further evidence that the effects of the stabilisation phase were immediate and remained stable over time.

A supplementary analysis comparing baseline with the initial task block supported this interpretation, with both conditions producing a clear increase in CCI (p ≤ .002, **Figure 4.22A**). This simplified analysis suggested that the difference in CCI modulation between conditions in the initial block approached, but did not reach, statistical significance (p = .110, z = −1.60, r = −0.33), although the limited scope of this analysis may have reduced statistical power. The order of condition presentation and the total number of task blocks completed during the session had no meaningful effect on the degree of CCI modulation observed (p ≥ .465).

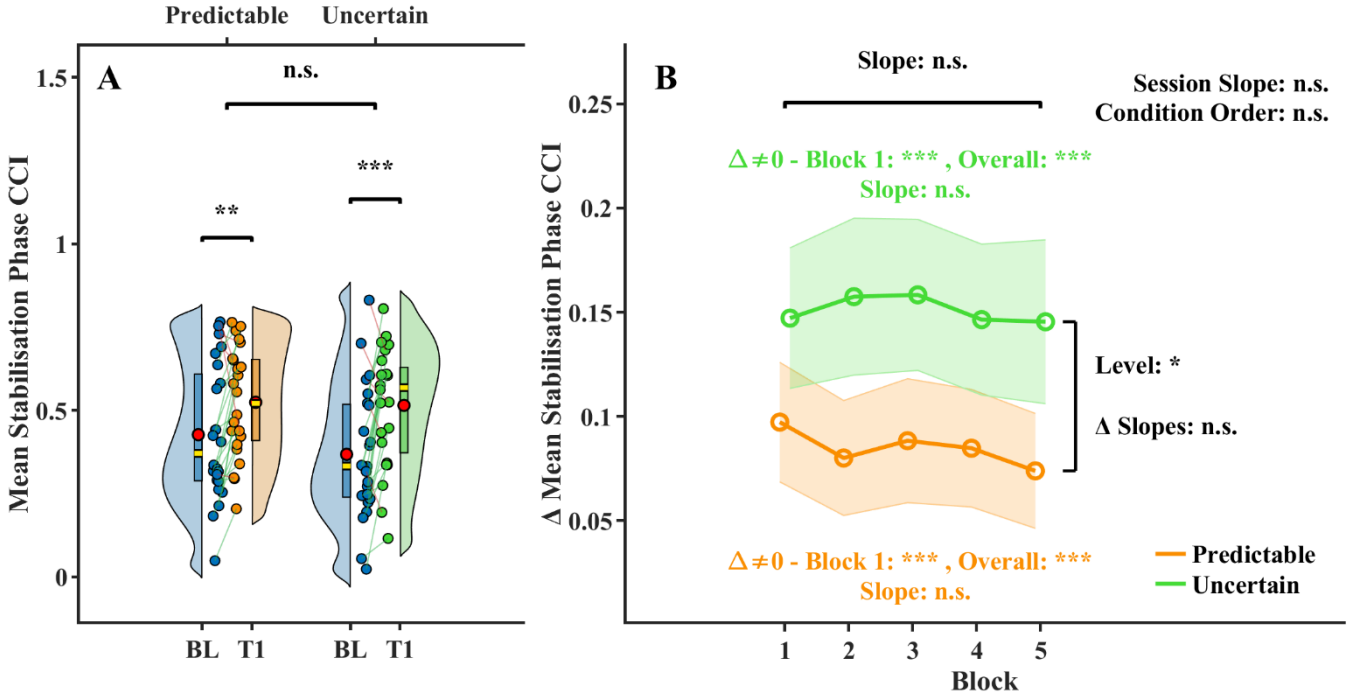

Figure 4.22. (A) Mean stabilisation phase CCI at baseline (BL) and initial task block (T1) for temporally predictable (orange) and uncertain (green) conditions. Scatter points are individual participants. IQR displayed by box internal to each violin with mean indicated by the red circle and median by the yellow line. (B) Change from baseline CCI across task blocks divided by condition with (±SEM): predictable (orange), uncertain (green). Significance codes: * p < 0.05, ** p < 0.01, *** p < 0.001; n.s., not significant.

The dynamics observed when examining the impact of perturbation amplitude were less pronounced than those associated with temporal uncertainty. Neither condition exhibited reliable CCI modulation in the initial task blocks or when averaged across conditions (p ≥ .157, **Figure 4.23B**). In addition, variation in perturbation amplitude had no significant effect on CCI modulation (p = .586). These

findings were supported by a supplementary analysis of the initial task blocks (**Figure 4.23A**). No significant change from baseline was observed for the 0.5 Nm perturbation condition ($p = .272$, $z = -1.10$, $r = -0.29$), whereas a trend was evident for the 1 Nm perturbation condition ($p = .074$, $z = -1.79$, $r = -0.48$). This pattern suggested that increased perturbation amplitude may influence CCI modulation, at least during the initial task block. However, the difference between the two amplitude conditions in this initial comparison was also non-significant ($p = .510$, $z = 0.66$, $r = 0.18$).

No systematic trends were observed across blocks within conditions or across the session ($p \geq .586$). However, the order in which conditions were presented significantly influenced CCI modulation. The second condition completed was associated with a small but statistically significant increase in CCI modulation compared with the first condition ($\beta = 0.02$, 95% CI = [0.00103, 0.04], $p = .038$). This effect was not sensitive to the specific condition presented and did not reflect a significant change specifically associated with the transition point between conditions ($p \geq .529$).

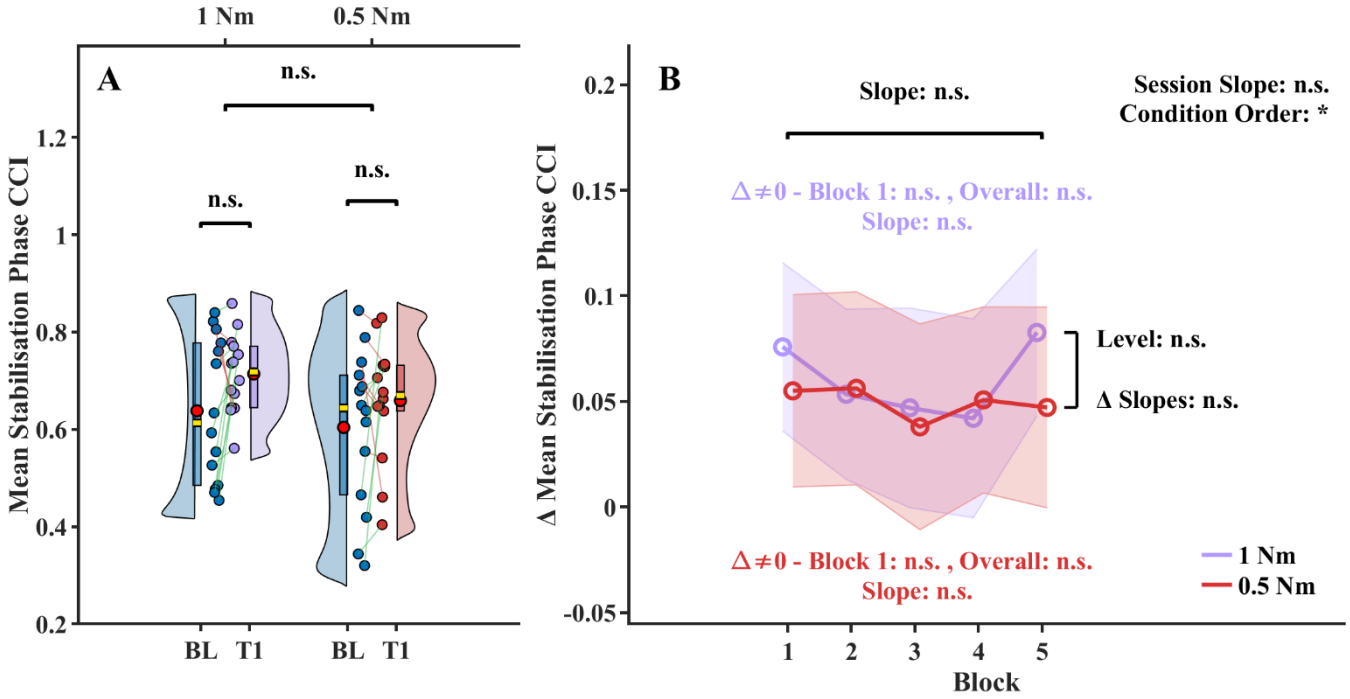

Figure 4.23. (A) Mean stabilisation phase CCI at baseline (BL) and initial task block (T1) for high-amplitude and low-amplitude perturbation conditions. Full plot description - Figure 4.22.

Stabilisation phase co-contraction was modulated by temporal predictability but not by perturbation amplitude. In the predictability manipulation, CCI increased from baseline to task in both conditions, indicating a general shift toward greater stabilisation under perturbation. Critically, CCI was consistently higher under temporal uncertainty, with this elevation present from initial exposure and maintained across blocks. There were no differences in block-wise change or learning rate, indicating that uncertainty altered the co-contraction set-point rather than its evolution over time.

In contrast, varying perturbation amplitude (0.5 vs. 1 Nm) had no reliable effect on stabilisation phase CCI. There were no differences in baseline-to-task change, overall co-contraction level, or block-wise trends, and stabilisation remained low and stable across amplitudes. This absence of amplitude effects suggests that co-contraction is not scaled to mechanical load within the tested range. Overall, stabilisation phase co-contraction reflects a context-sensitive control strategy driven by temporal uncertainty rather than perturbation strength. Once engaged, stabilisation levels are rapidly established and remain stable across repeated exposure, supporting a role for predictive structure rather than force scaling in shaping stabilising motor responses.

4.3.8. Co-Contraction and Its Contribution to Impedance Regulation and Behavioural Responses to Perturbations

Across outcome measures and task structures, co-contraction showed a systematic dissociation between trait-like (between-participant) and state-dependent (within-participant) contributions, with its functional role varying across experimental cohort.

For mechanical impedance, co-contraction did not account for stable inter-individual differences in either cohort. In the predictability cohort, mean co-contraction was unrelated to impedance ($p = .227$), and this null effect was not modulated by predictability or learning ($p \geq .449$). Within participants, increases in co-contraction were associated with modest reductions in impedance ($\beta = -0.38$, 95% CI = [−0.63, −0.12], $p = .004$), an effect that was weakly direction-dependent and most evident during extension. In the perturbation amplitude cohort, impedance varied strongly with perturbation amplitude but showed little systematic relationship with co-contraction at either the between-participant ($\beta = 0.95$, 95% CI = [−0.79, 2.69], $p = .284$) or within-participant level ($\beta = -0.06$, 95% CI = [−0.72, 0.59], $p = .851$), indicating that perturbation-induced impedance largely unfolded independently of global co-contraction.

In contrast, peak angular displacement showed a clearer coupling to co-contraction. In the predictability cohort, stable differences in co-contraction did not predict peak angular displacement ($\beta = -27.48$, 95% CI = [−83.30, 28.34], $p = .334$), but within-participant increases in co-contraction robustly reduced displacement amplitude ($\beta = -59.80$, 95% CI = [−77.56, −42.04], $p < .001$), with no modulation by predictability, direction, or task block ($p \geq .462$, **Figure 4.24**). This pattern indicates a strongly state-dependent role of co-contraction in limiting displacement under predictable timing. By contrast, in the perturbation amplitude cohort, peak offset was dominated by trait-like effects: higher mean co-contraction predicted substantially smaller peak offsets ($\beta = -397.32$, 95% CI = [−575.44, −219.20], $p < .001$), particularly during flexion ($\beta = -204.38$, 95% CI = [−227.11, −181.64], $p < .001$), with little contribution from within-participant fluctuations ($\beta = -34.53$, 95% CI = [−95.16, 26.10], $p = .263$).

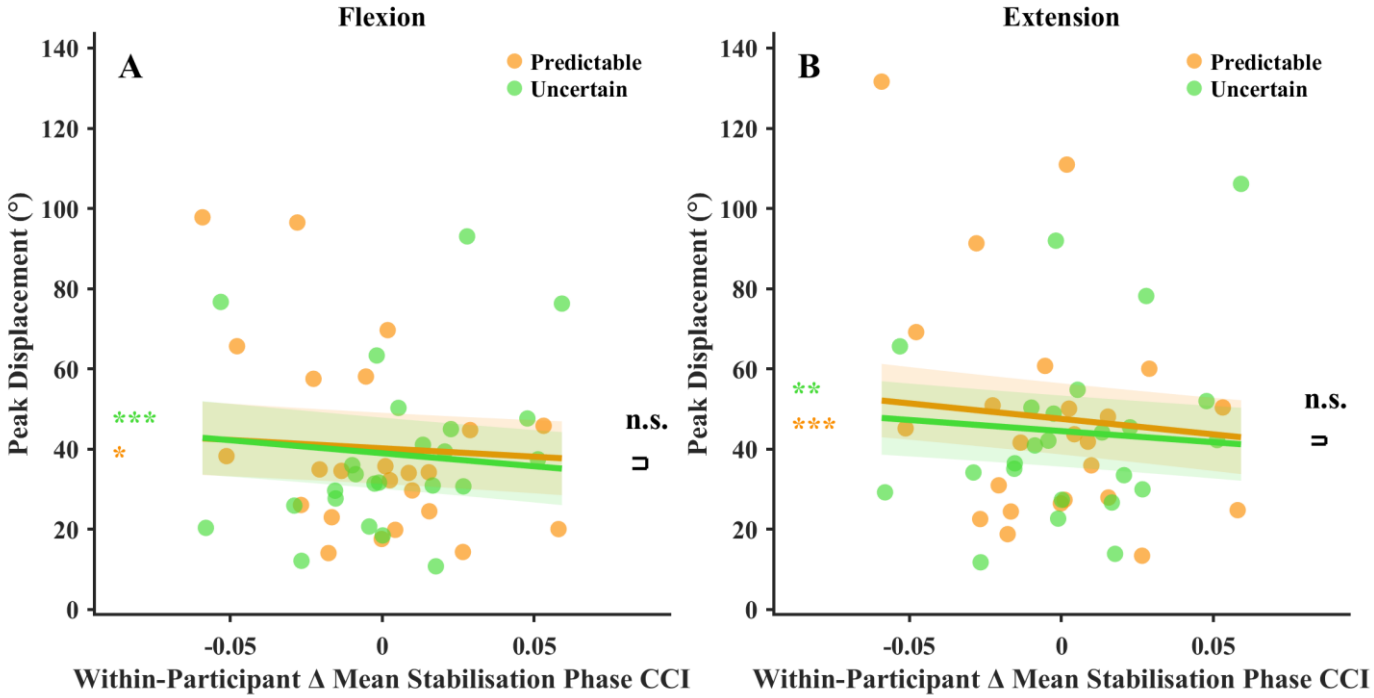

Figure 4.24. Within-participant relationship between changes in stabilisation phase co-contraction (Δ CCI) and peak angular displacement (°) for (A) flexion and (B) extension. Each point represents an individual participant's deviation from their own mean for a given condition (predictable, orange; uncertain, green). Full plot description - Figure 4.18.

A parallel dissociation emerged for post-perturbation stabilisation time. In the temporal predictability cohort, average co-contraction was unrelated to stabilisation speed ($p = .467$), whereas within-participant increases in co-contraction reliably accelerated recovery ($\beta = -0.28$, 95% CI = [−0.38, −0.17], $p < .001$). This state-dependent effect strengthened across blocks ($\beta = -0.13$, 95% CI = [−0.20, −0.06], $p < .001$) and was most pronounced during flexion and during extension under uncertainty. In contrast, when perturbation amplitude varied, stabilisation time depended on both timescales: participants with higher average co-contraction stabilised faster overall ($\beta = -1.04$, 95% CI = [−1.63, −0.45], $p < .001$, **Figure 4.25**), and block-to-block increases in co-contraction further reduced stabilisation time ($\beta = -0.30$, 95% CI = [−0.47, −0.13], $p < .001$), particularly during high-amplitude extension perturbations.

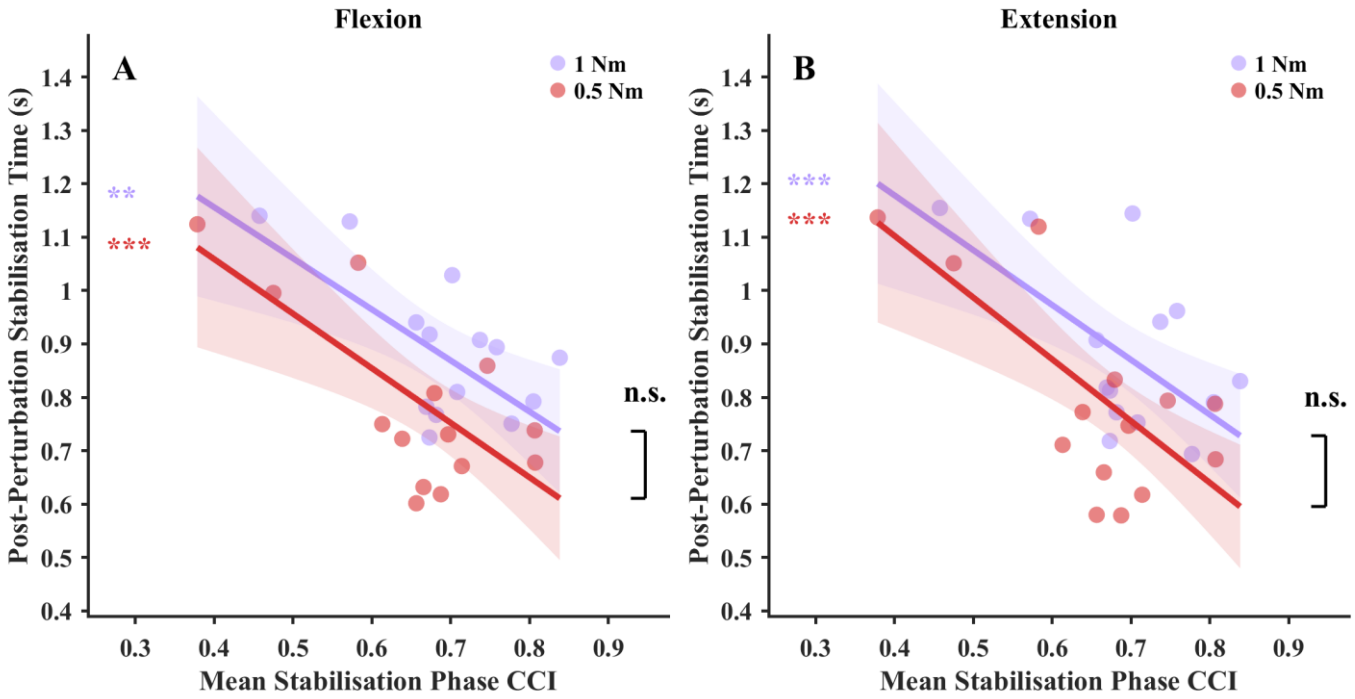

Figure 4.25. Between-participant relationship between mean stabilisation phase co-contraction (CCI) and post-perturbation stabilisation time (s) for (A) flexion and (B) extension. Each point represents an individual participant's mean level for a given condition (high-amplitude (1 Nm), purple; low-amplitude (0.5 Nm), red). Full plot description - Figure 4.18.

Taken together, these findings indicate that co-contraction does not serve as a general determinant of mechanical impedance but plays outcome- and context-dependent roles in shaping perturbation responses. Under predictable timing, co-contraction functions primarily as a flexible, online control strategy that limits displacement and speeds recovery on a block-by-block basis. When mechanical demands vary in amplitude, co-contraction additionally operates as a tonic, trait-like strategy that constrains peak mechanical deviation and supports faster stabilisation. This shift underscores that the functional contribution of co-contraction is contingent on task structure and mechanical regime, rather than reflecting a unitary control mechanism.

4.3.9. Summary

This chapter examined how humans regulate mechanical impedance in response to externally applied mechanical perturbations, and how these outcomes are shaped by temporal predictability, perturbation amplitude and movement direction. Across all analyses, a consistent picture emerges in which stable biomechanical properties and flexible block-to-block control mechanisms play distinct and dissociable roles.

At the level of mechanical impedance, temporal predictability exerted a modest but systematic influence. Temporally predictable perturbations were associated with elevated impedance relative to temporally uncertain perturbations, an effect that reached statistical significance in extension and was present as a trend in flexion (**Figure 4.8**). Importantly, this difference was not evident in the very first task block, indicating that predictability-related modulation of impedance emerged with exposure rather than reflecting an immediate anticipatory setting. Across blocks within conditions, there was no clear evidence for learning or adaptation specific to temporal predictability; instead, impedance showed only a small global increase over the course of the experiment. Perturbation amplitude did not significantly modulate impedance, whereas movement direction exerted a strong and consistent influence, with substantially higher impedance in extension than flexion, particularly at lower amplitudes (**Figure 4.9**). These findings indicate that impedance is shaped primarily by intrinsic biomechanical and directional factors, with predictability exerting a secondary, experience-dependent modulation.

In contrast, peak angular displacement was highly sensitive to task structure and perturbation characteristics. All perturbations reliably produced measurable displacement across cohorts, directions, and conditions, confirming the effectiveness of the experimental manipulations (**Figure 4.10**, **Figure 4.12**). In the predictability cohort, displacement was larger in extension than flexion and was greater for the temporally predictable than uncertain condition, an effect driven primarily by extension movements. Notably, predictable perturbations showed no evidence of adaptation across repeated blocks, whereas uncertain perturbations led to progressively larger displacements over time, particularly in extension. This divergence suggests that uncertainty disrupts the maintenance of displacement-limiting strategies rather than just promoting conservative control. In the amplitude cohort, displacement scaled strongly with perturbation amplitude, with 1 Nm perturbations producing larger displacements than 0.5 Nm, again most clearly in extension. Unlike the predictability cohort, there were no systematic block-wise trends or ordering effects, indicating stable control once amplitude was established. Across both cohorts, non-parametric analyses of initial task blocks were consistent with the mixed-effects results, reinforcing the robustness of these findings (**Figure 4.11**, **Figure 4.13**).

Post-perturbation stabilisation time showed a markedly different sensitivity profile. In the predictability cohort, stabilisation time was largely unaffected by condition, direction, or block, with only subtle differences emerging in the rate of change across blocks for extension movements (**Figure 4.14**). Predictable perturbation displacement remained stable over time, whereas uncertain perturbations were associated with gradually increasing stabilisation times. This pattern suggests a mild cumulative cost of uncertainty rather than adaptive improvement. In the perturbation amplitude cohort, stabilisation time was strongly determined by amplitude condition, with 1 Nm perturbations consistently requiring longer recovery than 0.5 Nm, irrespective of direction (**Figure 4.15**). There was no evidence of learning across blocks, but a clear session-order effect emerged, with faster stabilisation in whichever condition was completed second, indicating general task familiarisation rather than condition-specific adaptation. Again, non-parametric analyses of initial blocks corroborated these results (**Figure 4.16**).

Integrating these outcome measures with the mixed-effects analyses of impedance-behaviour relationships and co-contraction, a coherent functional dissociation becomes apparent. Peak displacement is primarily constrained by stable, between-participant properties, such as mean impedance and, under higher mechanical demand, average co-contraction. By contrast, post-perturbation stabilisation time is more strongly influenced by within-participant, block-to-block modulation, particularly changes in impedance and co-contraction that accelerate recovery without necessarily limiting initial movement. Co-contraction emerged as a flexible, context-dependent control mechanism - momentary increases consistently reduced displacement and stabilisation time, while stable individual differences in co-contraction only became behaviourally relevant when perturbation amplitude increased (**Figure 4.25**).

Overall, these findings demonstrate that sensorimotor responses to perturbations are governed by multiple interacting control layers. Direction-specific biomechanics set a strong baseline for impedance and displacement, temporal predictability subtly biases impedance regulation with experience, and perturbation amplitude scales both displacement and recovery demands. Superimposed on these

factors, rapid modulation of impedance and co-contraction supports efficient recovery, whereas stable individual differences primarily shape how much the limb moves in the first place. Together, the results argue against a single, unitary control strategy and instead support a multi-timescale framework, in which impedance and muscle activation are deployed differently to manage movement amplitude and post-perturbation stability.

4.4. Voluntary Movement Motor and Behavioural Dynamics

4.4.1. Introduction

Following completion of the postural stabilisation phase, participants were cued to initiate voluntary movement through a change in the position of the visual target. Participants were naïve to the direction of the forthcoming voluntary movement and were not informed about the structure or timing of the postural stabilisation phase. This design required spontaneous modification of the prevailing motor context, shifting from one that demanded stability in the presence of environmental instability to one that required rapid and precise voluntary movement.

This requirement for spontaneous voluntary movement, tightly coupled to the preceding stabilisation demands, implicitly linked the dynamics of the voluntary movement to the impedance dynamics established during the postural stabilisation phase. To evaluate how these dynamics shaped subsequent movement, key outcome measures associated with movement quality, namely accuracy, reaction time and movement duration, were assessed relative to baseline voluntary movements performed prior to exposure to stabilisation challenges. In addition, the motor dynamics of voluntary movement were assessed through analysis of co-contraction, evaluating whether voluntary movements performed after the stabilisation demands exhibited different levels of antagonist muscle activity compared with baseline. Finally, these performance measures and motor dynamics were correlated with the degree of co-contraction expressed during the stabilisation phase to determine the strength of the coupling between stabilisation-related motor control and subsequent voluntary movement dynamics.

Overall, this exploration facilitated a precise examination of the behavioural and motor control dynamics fundamental to the investigation of stability–movement transitions that define the novelty of this thesis. Taken together, the analyses establish a coherent framework for interpreting how context-dependent stabilisation strategies influence subsequent voluntary action. This motor framework, in combination with the cortical results presented in the next chapter, provides a novel model of the sensorimotor dynamics underpinning impedance trade-offs across evolving motor contexts.

4.4.2. Movement Accuracy

When cued to initiate voluntary movement, participants were instructed to move to the target as quickly and accurately as possible and to maintain the on-target position for 1 s. The inclusion of this brief hold ensured that movements reached complete termination rather than just passing through the target. In addition, the hold period enabled clear differentiation between clean, accurate movements and less stable attempts that required corrective adjustments. Movement accuracy was assessed by identifying trials in which the movement was completed in a single, direct action. Specifically, accurate movements were defined as those in which the initial time point of being on target coincided with the onset of the final on-target hold period. This approach allowed a robust assessment of endpoint accuracy despite the limited range of the movements performed.

Within the temporal predictability cohort, the dominant effect across all analyses was movement direction. Accuracy changes were reliably more negative during flexion than extension, indicating a greater reduction from baseline accuracy for flexion movements ($\beta = -8.01$, 95% CI = [−10.39, −5.62], $p < .001$, **Figure 4.26**). There was no evidence that temporal predictability modulated this directional asymmetry, as the interaction between condition and direction was not significant ($p = .822$).

Within each condition, changes in accuracy did not evolve systematically across task blocks. There was no main effect of block within condition ($p = .888$) and no evidence of differential learning rates between predictable and uncertain conditions ($p = .631$). Rate-of-change contrasts computed

separately within each movement direction likewise revealed no reliable differences between conditions ($p \geq .526$). Cell-wise slope estimates further confirmed the absence of meaningful within-condition learning effects across all condition and direction combinations ($p \geq .392$).

In contrast to the absence of learning effects, substantial initial offsets from baseline accuracy were observed, particularly for flexion movements. At the first task block within a condition, predictable flexion trials showed a significant reduction in accuracy relative to baseline ($\beta = -16.77$, 95% CI = [−30.45, −3.09], $p = .016$), whereas the corresponding effect in the uncertain condition did not reach significance ($p = .169$). When evaluated across all task blocks, both predictable and uncertain flexion movements remained significantly below baseline ($p \leq .049$). No reliable deviations from baseline were observed for extension movements at either the initial task block or across blocks ($p \geq .519$).

Session-level factors did not account for these effects. There was no evidence of overall task-order drift ($p = .873$), no switch cost ($p = .694$), and no interaction between condition and either order or switch terms ($p \geq .377$). The condition completed second showed a trend towards reduced accuracy ($\beta = -5.31$, 95% CI = [−10.71, 0.08], $p = .053$), although this effect did not interact with condition ($p = .823$).

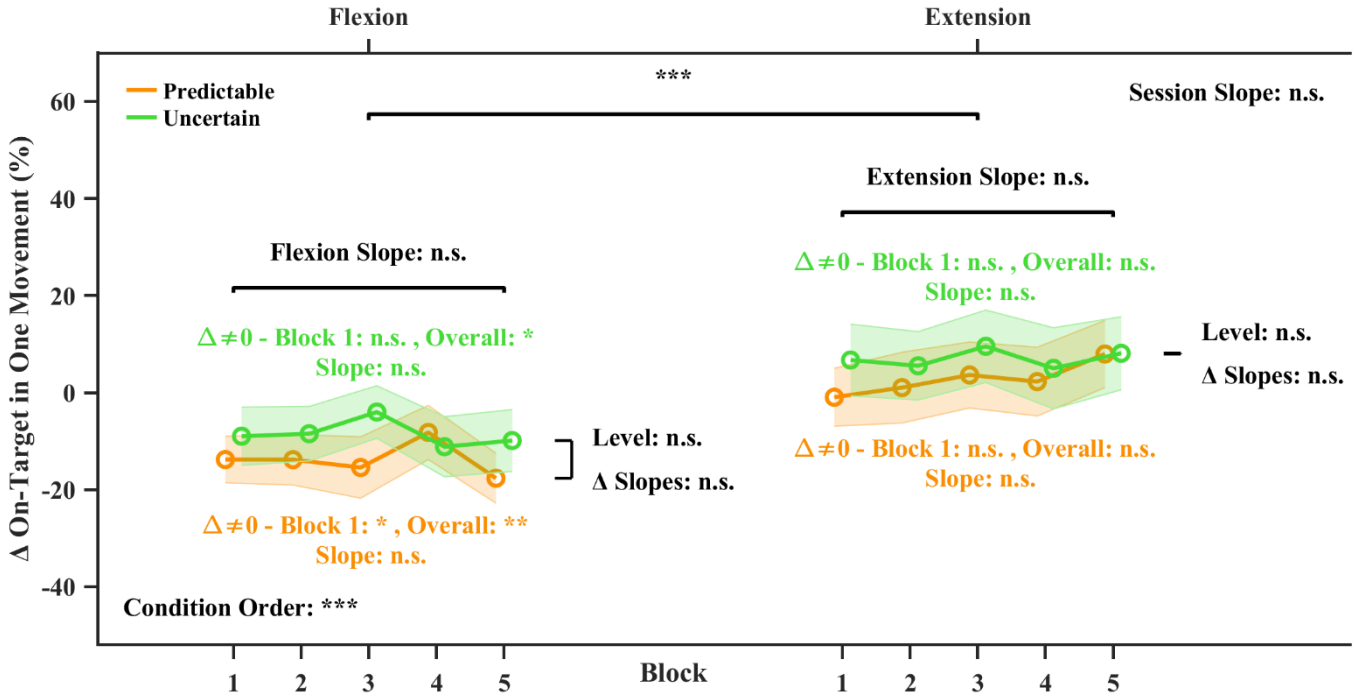

Figure 4.26. Change from baseline accuracy (%) across experimental blocks for flexion (left) and extension (right) following temporally predictable (orange) and uncertain (green) perturbation conditions. Circles denote block-wise means and shaded regions represent variability (±SEM). For each condition-direction combination, change in accuracy was tested for statistical divergence from baseline (Δ ≠ 0) at the initial task block and the combination overall. Level effects indicate overall differences in impedance amplitude, whereas Slope effects indicate linear trends across repeated blocks. Significance codes: * p < 0.05, ** p < 0.01, *** p < 0.001; n.s., not significant.

Non-parametric analyses of the initial task block corroborated the findings of the mixed-effects models. In flexion, accuracy decreased relative to baseline in the predictable condition ($p = .009$, $z = 2.60$, $r = 0.60$), whereas no reliable change was observed in the uncertain condition ($p = .102$). Importantly, the between-condition comparison of baseline-corrected change scores was not significant ($p = .715$). In extension, neither condition differed from baseline ($p \geq .360$), and there was no between-condition difference ($p = .484$). A complementary paired analysis likewise showed no significant baseline-to–block 1 change in either condition (predictable: $p = .082$; uncertain: $p = .932$) and no difference between conditions ($p = .617$).

In contrast to the temporal predictability cohort, there was no reliable overall effect of movement direction in the perturbation amplitude cohort. Accuracy changes did not differ between flexion and extension (p = .655, **Figure 4.27**). There was likewise no main effect of condition, indicating that average accuracy changes did not differ between the 1 Nm and 0.5 Nm conditions (p = .625).

Within conditions, there was no evidence for systematic learning or drift across blocks. The main effect of task block within condition was not significant (p = .883), and slopes did not differ between conditions (p = .965). Rate-of-change contrasts computed separately within each movement direction also showed no reliable condition differences (p ≥ .728). Slope estimates confirmed the absence of meaningful within-condition changes over time across all condition and direction combinations (p ≥ .627). At the initial task block, there was no clear evidence for robust deviations from baseline accuracy. Cell-wise tests at the first block showed that neither amplitude condition differed significantly from baseline in either flexion or extension (p ≥ .637). Similarly, overall accuracy did not differ from baseline for any condition and direction combination (p ≥ .273), indicating that accuracy remained broadly stable across the session.

Although most session-level covariates were not influential, a switch-related effect was observed. Accuracy was reduced in the first block following a condition switch (β = −5.31, 95% CI = [−10.48, −0.15], p = .044), indicating a transient cost associated with transitioning between amplitude conditions. No overall task-order drift was evident (p = .444), and there was no main effect of whether a condition was completed first (p = .217).

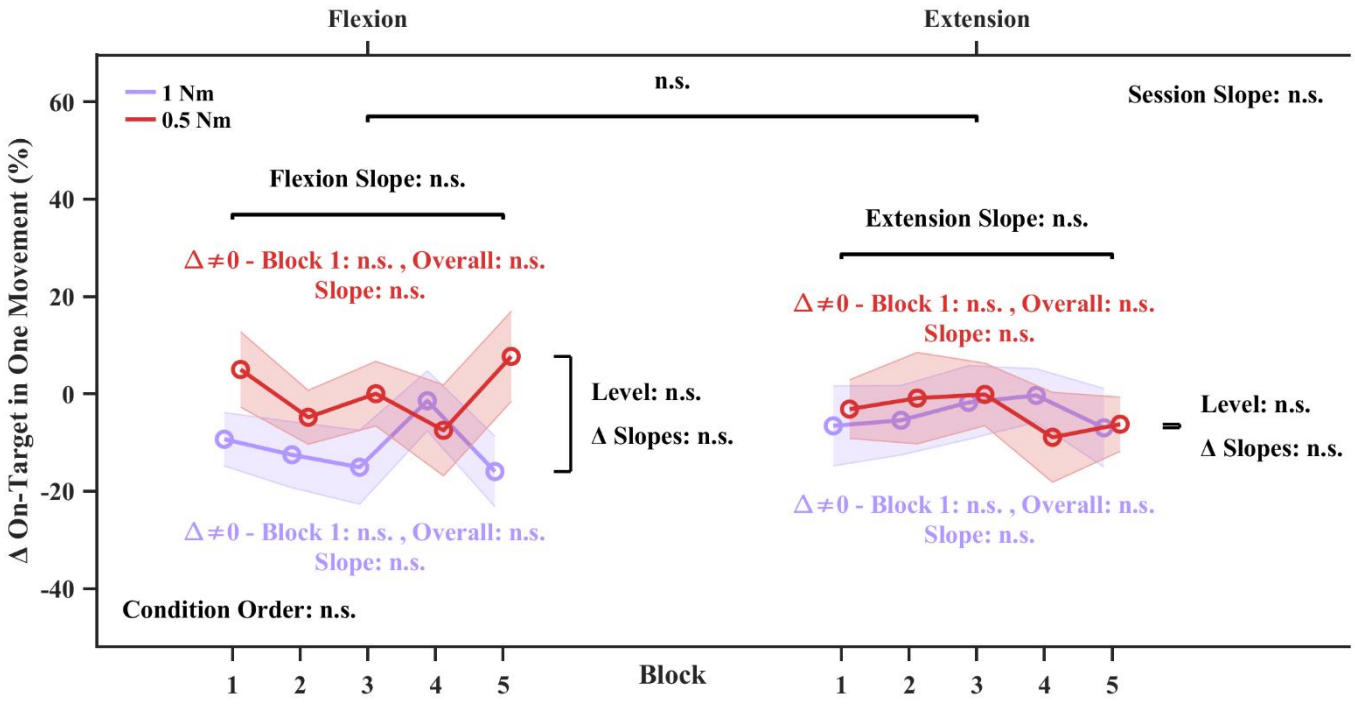

Figure 4.27. Change from baseline accuracy (%) across experimental blocks for flexion (left) and extension (right) following high-amplitude (purple) and low-amplitude (red) perturbation conditions. Full plot description - Figure 4.26.

However, a condition-dependent directional modulation emerged in the interaction terms. Specifically, the interaction between condition and movement direction reached significance (β = −2.58, 95% CI = [−5.12, −0.04], p = .046), and this effect was further qualified by a strong three-way interaction with condition order (β = 6.78, 95% CI = [4.24, 9.32], p < .001). Together, these interactions indicate that directional differences in accuracy depended on both preceding perturbation amplitude and whether the condition was performed first or second, rather than reflecting a stable, direction-specific effect.

Non-parametric analyses of the initial task block were consistent with the model-based results. In flexion, neither the 1 Nm nor the 0.5 Nm condition differed significantly from baseline (1 Nm: $p = .093$, 0.5 Nm: $p = .624$), and the between-condition comparison of baseline-corrected change scores was not significant ($p = .142$). In extension, no within-condition differences from baseline were observed ($p \geq .509$), and there was no between-condition difference ($p = .730$). Paired violin analyses similarly showed no significant baseline-to–block 1 changes within either torque condition (1 Nm: $p = .286$; 0.5 Nm: $p = .975$) and no difference between conditions ($p = .330$).

Across both cohorts, change-from-baseline accuracy during voluntary movement was not reliably modulated by condition and showed no evidence of within-condition learning. In both datasets, block-wise slopes were near zero and did not differ between conditions, indicating that accuracy did not systematically improve or degrade with exposure.

The cohorts diverged in the role of movement direction. In the predictability cohort, accuracy showed a robust and stable directional asymmetry, with substantially larger reductions from baseline during flexion than extension that were present from the first block and persisted across the session. This effect was independent of condition and was confirmed by both model-based and nonparametric analyses. In contrast, the amplitude cohort showed no overall directional effect, with flexion and extension exhibiting comparable changes from baseline.

Initial-block effects were likewise cohort-specific. The predictability cohort exhibited clear early accuracy costs in flexion, particularly in the predictable condition, although these did not translate into reliable between-condition differences. The amplitude cohort showed no consistent deviations from baseline at initial exposure in either direction or condition. Session-level structure played a limited role overall. Neither cohort showed evidence of global task-order drift or condition-dependent learning, but the perturbation amplitude cohort exhibited a transient switch cost following condition changes, along with higher-order interactions involving direction and period that did not reflect stable condition effects.

Taken together, the results indicate that direction-specific control demands, rather than temporal predictability or perturbation amplitude, dominated accuracy changes when present, whereas in their absence accuracy remained largely stable. Across cohorts, condition manipulations did not produce reliable or sustained effects on voluntary movement accuracy.

4.4.3. Reaction Time

Reaction time was calculated as the interval between presentation of the visual movement cue and movement initiation, following the methodology outlined in **Voluntary Movement Onset Detection and Trial Validation**. Under this approach, no distinction was made between cognitive processing time and the initiation of overt movement. Accordingly, the reaction time measure encapsulates the full duration required for the sensorimotor system to respond to a novel movement imperative.

Within the temporal predictability cohort, reaction time (RT) exhibited a clear and robust pattern of early slowing relative to baseline, accompanied by modest but consistent effects of condition and movement direction, and little evidence of learning across task blocks. Across the experimental session, RTs were reliably longer in the uncertain condition than in the predictable condition ($\beta = -0.01$, 95% CI = [-0.02, -4.58×10^{-3}], $p = .002$, **Figure 4.28**). This effect did not depend on movement direction, indicating generally faster responses following predictable stabilisation challenges. In addition, RTs were slightly but significantly longer during flexion than extension. Although small in amplitude, this effect was consistent ($\beta = 3.80 \times 10^{-3}$, 95% CI = [$7.88 \times 10^{-4}$, 0.01], $p = .014$). There was no evidence that temporal predictability differentially modulated flexion relative to extension, as the condition-by-direction interaction was negligible ($p \geq .980$).

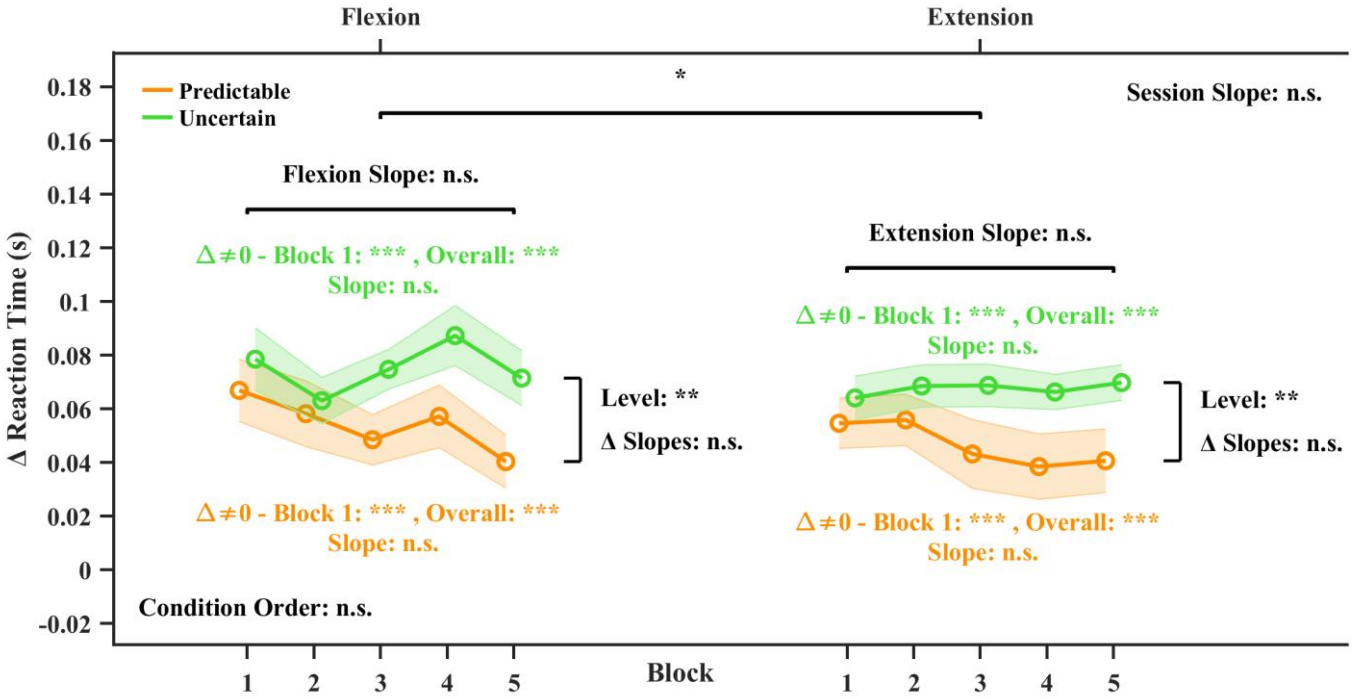

Figure 4.28. Change from baseline reaction time (s) across experimental blocks for flexion (left) and extension (right) following temporally predictable (orange) and uncertain (green) perturbation conditions. Full plot description - Figure 4.26.

From the initial task block, RTs increased sharply relative to baseline across all conditions and movement directions. Cell-wise estimates at the first block revealed large and highly reliable increases in reaction time for both predictable and uncertain conditions in flexion and extension ($p \leq .001$). These effects persisted across subsequent task blocks, indicating that reaction times remained elevated above baseline throughout the session. Non-parametric analyses of the initial block confirmed these findings, with robust baseline-to–block increases observed in both conditions and directions ($p \leq .001$, (**Figure 4.29**). Importantly, although reaction times increased markedly from baseline, the amplitude of this initial slowing did not differ between conditions, as between-condition comparisons of baseline-corrected change scores were not significant for either movement direction ($p \geq .265$).

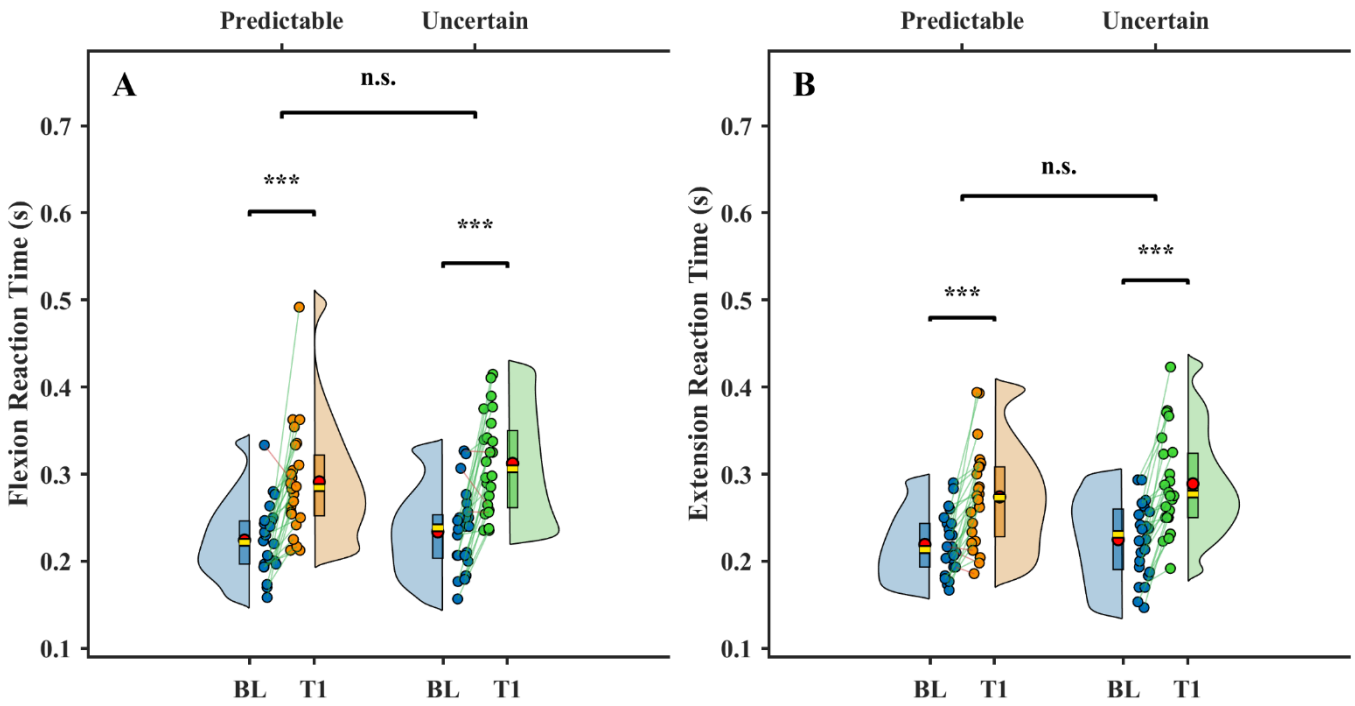

Figure 4.29. Contrasts in reaction time (s) between baseline blocks and initial task blocks for (A) flexion and (B) extension after temporally predictable (orange) and uncertain (green) perturbation conditions. BL = baseline, T1 = initial task block. Half-violin plots illustrate the distribution of individual participant values. Overlaid dots represent individual observations, with lines connecting paired measurements. Red circles indicate condition means and yellow horizontal lines indicate medians. Brackets denote statistical comparisons between associated BL and T1 groups, with an additional contrast between BL-T1 pairings. Significance codes: * p < 0.05, ** p < 0.01, *** p < 0.001; n.s., not significant.

Despite the pronounced initial offset, there was no evidence of systematic learning or recovery across task blocks. RT did not change reliably as a function of block within condition ($p = .505$). Block-wise slopes also did not differ significantly between predictable and uncertain conditions, although a robust trend suggested divergent trajectories across task blocks ($\beta = -3.36 \times 10^{-3}$, 95% CI = [$-0.01$, 7.36×10^{-5}], $p = .055$). Direction-specific rates of change were likewise non-significant ($p \geq .513$), and cell-wise slope estimates showed no reliable decreases in reaction time over time ($p \geq .110$). Taken together, these results indicate that the early increase in RT was sustained rather than progressively diminishing with repeated exposure.

Session-level structure contributed minimally. There was no overall effect of completing a condition first ($p = .675$), no global task-order drift ($p = .259$), and no switch-related cost ($p = .820$). One exception was a modest interaction between condition and task order ($\beta = -3.58 \times 10^{-3}$, 95% CI = [$-0.01$, -1.04×10^{-3}], $p = .006$), suggesting slightly greater RT reductions over the session in the predictable condition, though this did not manifest as a clear block-wise learning effect.

For the perturbation amplitude cohort, RT again showed a strong initial increase relative to baseline, but the structure of the effects differed from the predictability cohort, with clearer contributions from movement direction and session-level factors and little influence of perturbation amplitude.

Across the session, RTs were consistently longer during flexion than extension, indicating slower response initiation for flexion movements regardless of prior perturbation amplitude ($\beta = 0.01$, 95% CI = [3.30×10^{-3}, 0.01], $p < .001$, **Figure 4.30**). In contrast, there was no main effect of perturbation amplitude on RT, with comparable response times in the 1 Nm and 0.5 Nm conditions ($p = .328$). The condition-by-direction interaction was also not significant ($p \geq .169$), indicating that perturbation amplitude did not differentially affect RTs in flexion versus extension.

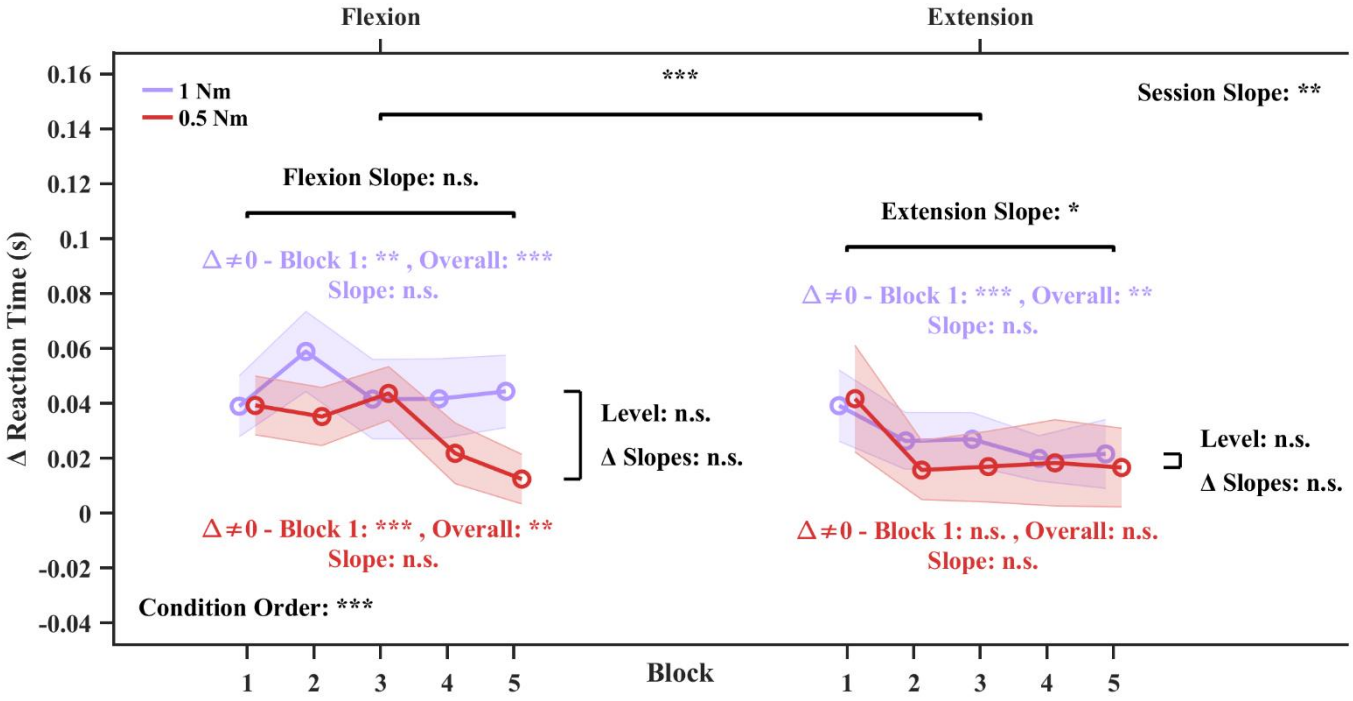

Figure 4.30. Change from reaction time (s) across experimental blocks for flexion (left) and extension (right) following high-amplitude (purple) and low-amplitude (red) perturbation conditions. Full plot description - Figure 4.26.

For the initial task block, RTs increased markedly relative to baseline across conditions and movement directions. Cell-wise analyses showed significant first-block increases in RT for flexion in both amplitude conditions ($p \leq .002$) and for extension in the 1 Nm condition ($\beta = 0.04$, 95% CI = [0.02, 0.07], $p < .001$), with a weaker, non-significant effect for extension at 0.5 Nm ($p = .207$). These elevations persisted across subsequent task blocks, with RTs remaining significantly above baseline in flexion for both conditions and in extension for the 1 Nm condition ($p \leq .008$).

Non-parametric analyses of the initial task block confirmed these results, revealing significant baseline to initial task block increases in RT in flexion for both torque levels ($p \leq .009$, **Figure 4.31A**) and in extension for the 1 Nm condition ($p = .006$, **Figure 4.31B**). Importantly, between-condition comparisons of baseline-corrected change scores were not significant for either movement direction ($p \geq .778$), indicating that perturbation amplitude did not influence the amplitude of the initial slowing in RT.

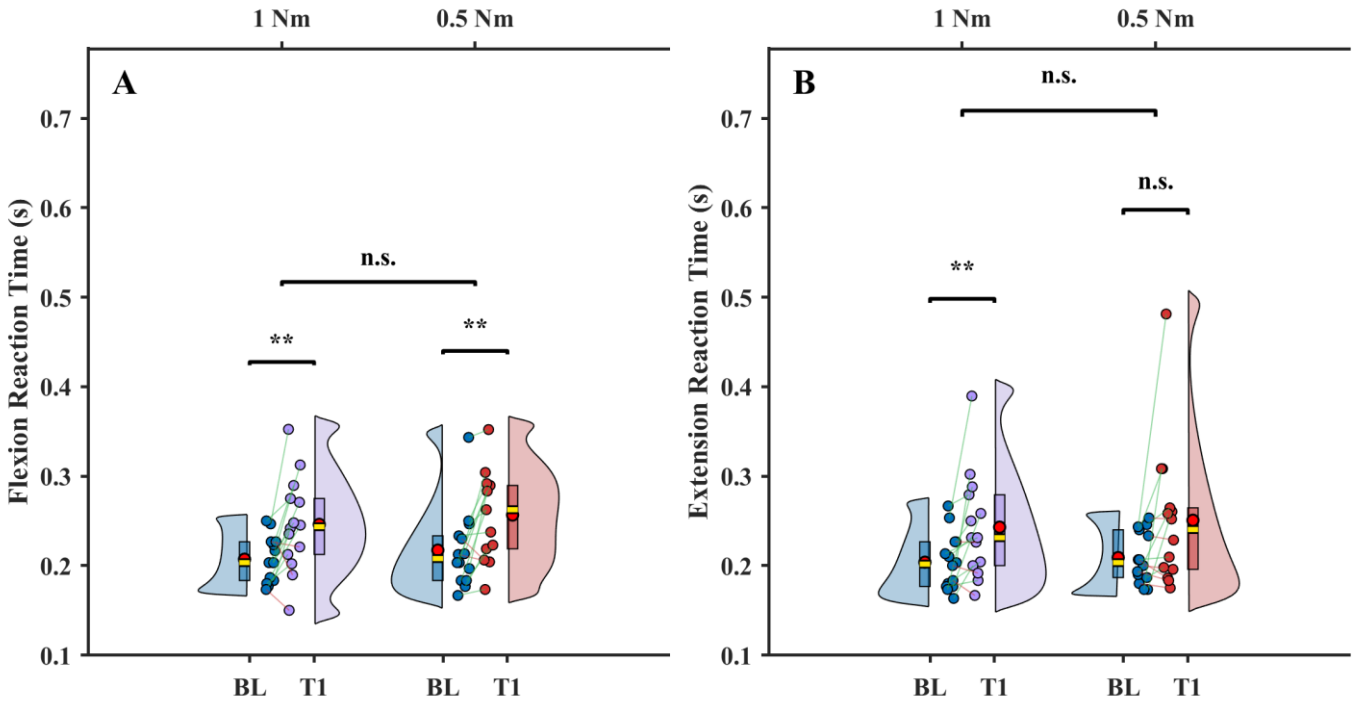

Figure 4.31. Contrasts in reaction time (s) between baseline blocks and initial task blocks for (A) flexion and (B) extension after high-amplitude (purple) and low-amplitude (red) perturbation conditions. Full plot description - Figure 4.29.

Unlike the predictability cohort, there was evidence of a modest reduction in RT across task blocks that was independent of condition when perturbation amplitude was altered. Within condition, a small but significant negative effect of block was observed ($\beta = -4.02 \times 10^{-3}$, 95% CI = [−0.01, -4.69×10^{-4}], p = .027). At the global level, RT similarly decreased with the total number of task blocks completed ($\beta = -4.20 \times 10^{-3}$, 95% CI = [−0.01, -1.02×10^{-3}], p = .010), indicating gradual speeding with practice. However, this recovery did not differ between torque conditions (p = .877) or between flexion and extension (p = .740), and condition-specific rates of change within each movement direction were non-significant (p ≥ .446).

Session structure further modulated RT. RTs were longer when a condition was performed second ($\beta = 0.01$, 95% CI = [4.72×10^{-3}, 0.01], p < .001), and flexion-specific slowing was accentuated during the second period ($\beta = 0.01$, 95% CI = [3.08×10^{-4}, 0.01], p = .041). A significant interaction between condition, movement direction, and task order ($\beta = -4.43 \times 10^{-3}$, 95% CI = [−0.01, -9.91×10^{-4}], p = .012) indicated that flexion-related slowing depended jointly on perturbation amplitude and session order, rather than reflecting a stable effect of perturbation amplitude alone.

Across cohorts, RT showed a highly consistent task-onset cost, with marked increases relative to baseline appearing in the very first block and persisting throughout the session. This initial RT elevation was large, reliable, and present across conditions and movement directions. Nonparametric analyses confirmed that the magnitude of this change did not differ between experimental conditions. This indicates that the dominant RT effect reflected engagement with the task context itself rather than predictability or torque amplitude.

Beyond this shared onset effect, the cohorts diverged in how RT was structured by direction and practice. In the temporal predictability cohort, RT differences were largely static offsets: responses were consistently faster in the predictable condition than in the uncertain condition and slightly slower during flexion than extension, but there was no meaningful reduction in RT across blocks, indicating little evidence for learning or recovery once the initial slowing had occurred. Temporal predictability influenced overall response speed but did not alter how RT evolved with experience.

In contrast, the perturbation amplitude cohort showed no reliable condition effect on RT, but exhibited a robust and consistent directional asymmetry, with flexion movements eliciting longer RTs than extension. Importantly, this cohort also showed gradual RT shortening with practice, reflected in both block-within-condition and global task-order effects, indicating partial recovery from the initial slowing over the course of the session. These practice effects were direction- and condition-independent.

Taken together, the cross-cohort pattern indicates that RT during voluntary movement is dominated by a large, nonspecific task-onset cost, while secondary structure depends on cohort-specific factors. Temporal predictability modulated overall RT, whereas directional control demands and practice-related speeding were more prominent in the perturbation amplitude cohort. Across both cohorts, experimental condition manipulations did not systematically alter RT learning rates, suggesting that RT primarily reflects global engagement and directional control demands rather than adaptation to predictable versus stronger perturbations.

4.4.4. Movement Duration

Movement duration was quantified as the interval between movement initiation and the first time point at which participants successfully maintained the on-target position for the required 1 s hold. As such, movement duration reflected the total time required to accurately complete the voluntary movement, inclusive of any time necessary to perform corrective adjustments. In this way, the duration encapsulated both the initial transport phase of the movement and any subsequent refinement required to achieve a stable and accurate endpoint.

For the predictability cohort, change-from-baseline movement duration exhibited a clear pattern of early, condition-independent slowing, with little evidence of sustained learning or directional modulation across task blocks. Movement duration did not differ reliably between flexion and extension, nor did it depend on condition ($p \geq .389$, **Figure 4.32**). Likewise, there was no evidence that movement duration changed systematically across blocks within a condition ($p = .601$), or that block-wise slopes differed between predictable and uncertain conditions ($p = .838$). Rate-of-change contrasts within flexion and extension were similarly non-significant ($p \geq .401$), indicating an absence of condition-dependent learning effects.

Despite the absence of sustained effects, robust initial increases in movement duration relative to baseline were evident. At the first task block, the predictable condition showed significant slowing in both flexion ($\beta = 0.18$, 95% CI = [0.05, 0.32], $p = .008$) and extension ($\beta = 0.26$, 95% CI = [0.13, 0.40], $p < .001$). In contrast, the initial task blocks in the uncertain condition did not elicit comparable increases in movement duration for either flexion or extension ($p \geq .217$). When evaluated across task blocks, movement duration remained significantly elevated above baseline in the predictable condition for both movement directions ($p \leq .010$), whereas effects in the uncertain condition did not reach statistical significance ($p \geq .090$).

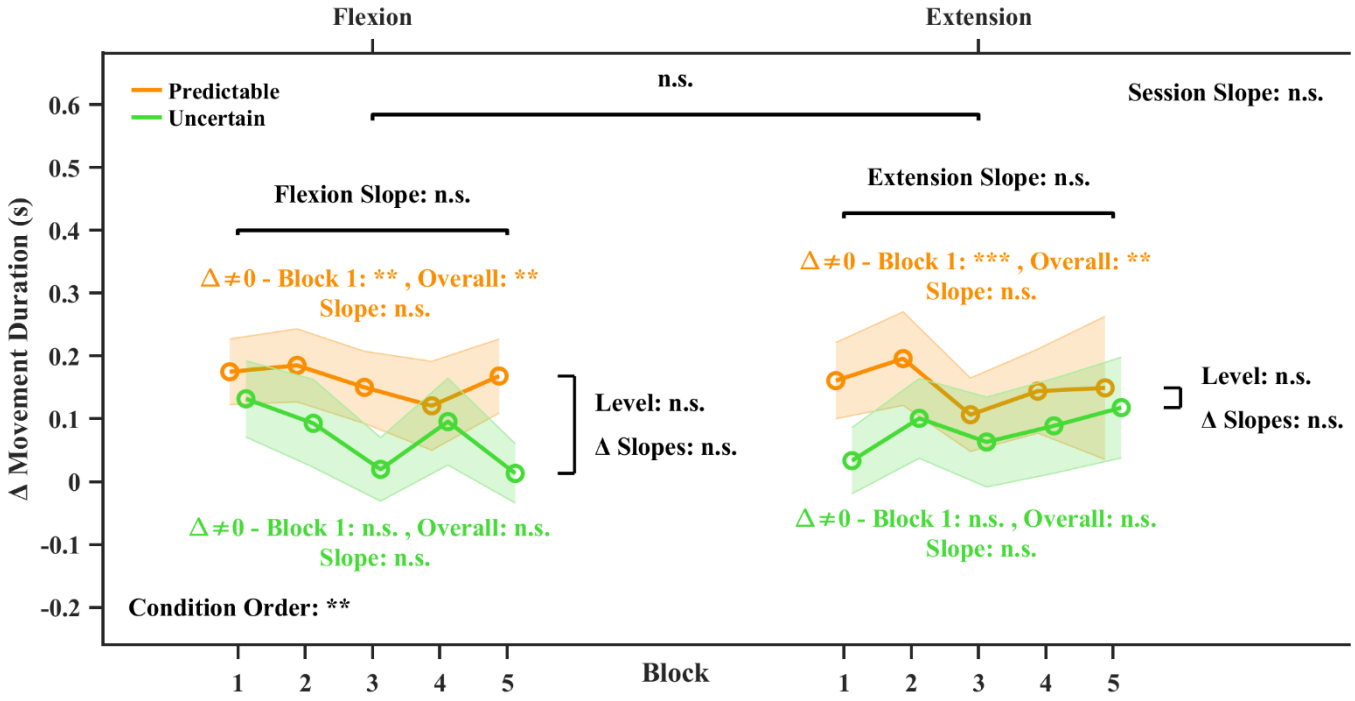

Figure 4.32. Change from baseline movement duration (s) across experimental blocks for flexion (left) and extension (right) following temporally predictable (orange) and uncertain (green) perturbation conditions. Full plot description - Figure 4.26.

Nonparametric analyses of the initial task block corroborated these findings for the predictable condition. Relative to baseline, movement duration increased reliably in predictable trials for both flexion ($p = .004$, $z = -2.91$, $r = -0.59$, **Figure 4.33A**) and extension ($p = .037$, $z = -2.09$, $r = -0.43$, **Figure 4.33B**). In the uncertain condition, a significant increase was observed in flexion that was not detected in the full model ($p = .043$, $z = -2.03$, $r = -0.41$), whereas extension remained non-significant ($p = .391$). Importantly, between-condition comparisons of baseline-corrected change scores were not significant for either movement direction (flexion: $p = .775$; extension: $p = .170$), indicating that predictability did not modulate the amplitude of the initial slowing in movement duration.

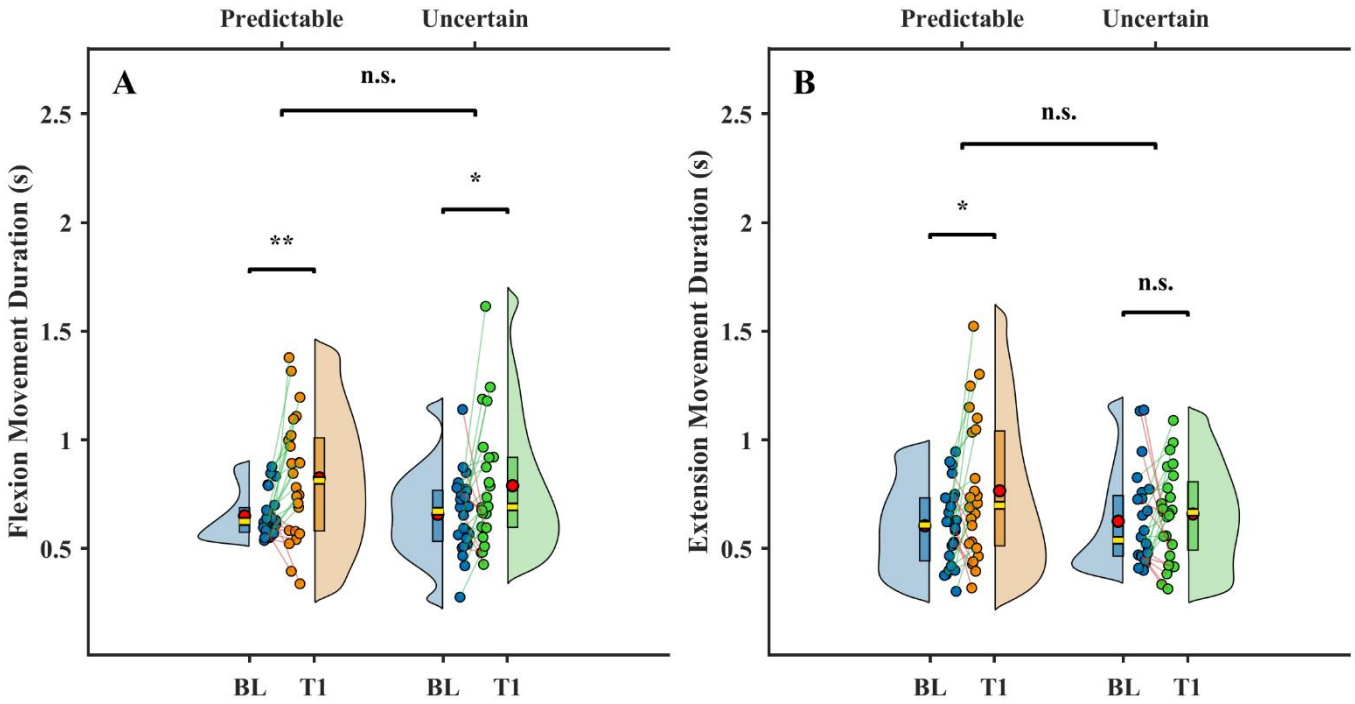

Figure 4.33. Contrasts in movement duration (s) between baseline blocks and initial task blocks for (A) flexion and (B) extension after temporally predictable (orange) and uncertain (green) perturbation conditions. Full plot description - Figure 4.29.

Session-level factors played a minor role in shaping movement duration. There was no evidence of global task-order drift ($p = .438$), no main effect of period in the global model ($p = .527$), and no switch-related effect on movement duration ($p = .575$). A small interaction between condition and switch status emerged in the global model ($\beta = 0.05$, 95% CI = [4.74×10^{-3}, 0.10], $p = .032$); however, this effect was not reflected in consistent block-wise or direction-specific patterns.

For the perturbation amplitude cohort, change-from-baseline movement duration remained largely stable across conditions, directions, and blocks, with no evidence for sustained learning or condition-dependent modulation. Movement duration did not differ reliably between flexion and extension, although a weak trend toward shorter durations in flexion was observed ($\beta = -0.02$, 95% CI = [−0.05, 0.002], $p = .071$, **Figure 4.34**). There was no main effect of torque condition ($p = .147$), no overall period effect ($p = .190$), and no evidence of overall session drift ($p = .176$). Switch-related effects were modest and did not reach significance in the global model ($p = .087$).

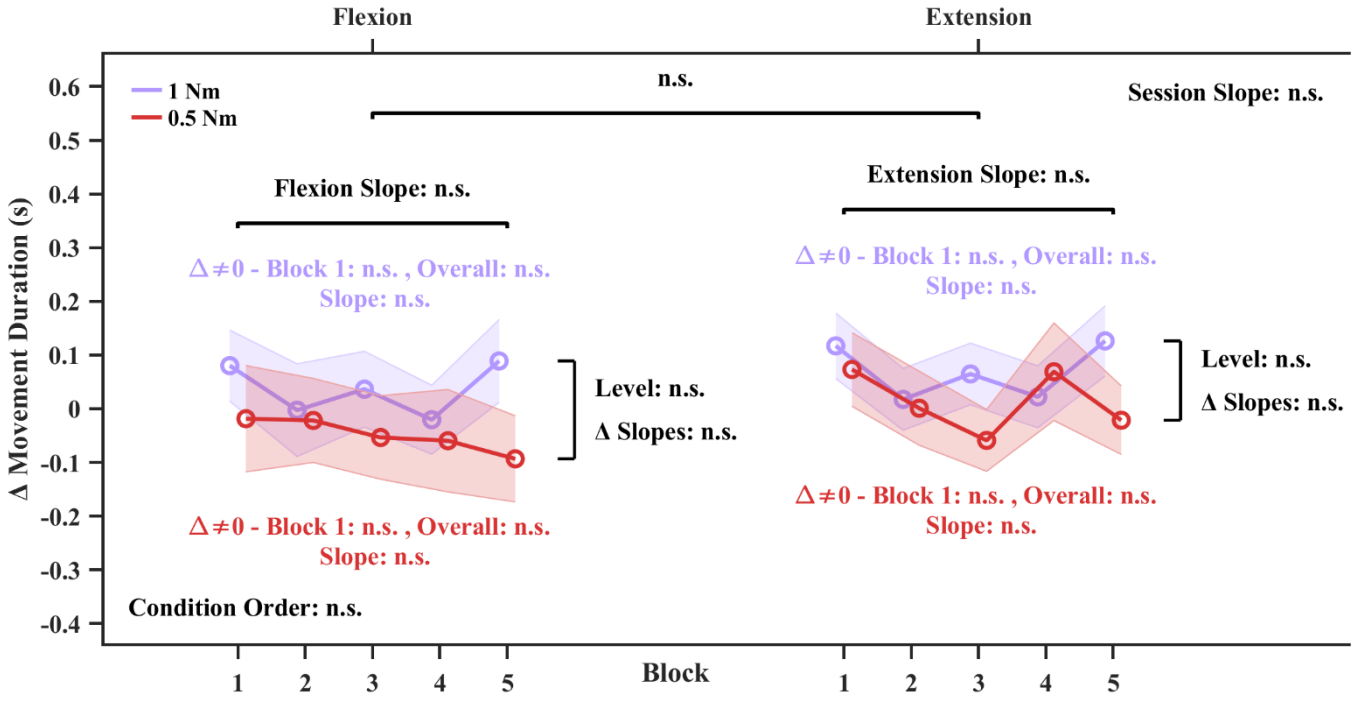

Figure 4.34. Change from baseline movement duration (s) across experimental blocks for flexion (left) and extension (right) following high-amplitude (purple) and low-amplitude (red) perturbation conditions. Full plot description - Figure 4.26.

There were systematic changes in movement duration across blocks within condition ($p = .618$), no condition-block interaction ($p = .270$), and no rate-of-change differences between conditions within either flexion or extension (flexion: $p = .345$; extension: $p = .390$). Cell-wise slope estimates confirmed the absence of meaningful learning effects across all condition-direction combinations ($p \geq .319$).

Unlike the predictability cohort, there was no reliable initial slowing relative to baseline. Cell-wise tests showed that movement duration at the first task block did not differ significantly from baseline in either torque condition or movement direction ($p \geq .402$). Estimates over task blocks were likewise nonsignificant across all cells ($p \geq .236$), indicating stable execution timing throughout the session. One consistent session-structure effect emerged in the within-condition model. Movements were shorter on the very first block within a condition ($\beta = -0.10$, 95% CI = [−0.17, −0.03], $p = .003$) and longer on the first block following a condition switch ($\beta = 0.13$, 95% CI = [0.03, 0.22], $p = .008$). These effects indicate transient adjustments associated with task structure rather than learning or stable condition-related differences. Higher-order interactions involving direction, condition, and period reached significance, most notably a condition-direction-order interaction ($\beta = -0.04$, 95% CI = [-0.06, -0.01], $p = .008$). However, these interactions were not accompanied by consistent simple effects at the block or cell level and therefore do not reflect stable differences in movement duration between torque conditions.

Nonparametric analyses of the initial block were consistent with the model-based findings. No within-condition baseline differences were observed in flexion (1 Nm: $p = .363$; 0.5 Nm: $p = .975$) or extension (1 Nm: $p = .064$; 0.5 Nm: $p = .300$), and between-condition comparisons of baseline-corrected changes were nonsignificant in both directions (flexion: $p = .730$; extension: $p = .551$).

Across cohorts, movement duration showed a consistent pattern of minimal sensitivity to experimental manipulations and no evidence of learning across blocks, with cohort-specific differences confined to transient, early-session effects.

In the temporal predictability cohort, movement duration increased reliably relative to baseline at task onset, producing a clear initial slowing that was evident in both flexion and extension and most pronounced in the predictable condition. These increases were present from the first block and persisted at the session reference point but did not evolve across blocks and did not differ reliably

between conditions or movement directions. Nonparametric analyses confirmed these early duration increases, while mixed-effects models showed no sustained condition-, direction-, or block-dependent modulation.

In contrast, the perturbation amplitude cohort showed no reliable change in movement duration from baseline at either initial exposure or across the session. Movement duration remained stable across torque conditions, directions, and blocks, with no evidence of systematic learning or condition effects. Instead, the only consistent influences were transient structure-related effects, with shorter movements on the very first block within a condition and longer movements immediately following condition switches.

Taken together, these findings indicate that movement duration is largely robust to temporal predictability and torque amplitude manipulations and does not exhibit gradual adaptation with practice. When present, changes in movement duration appear as early, nonspecific adjustments to task engagement or brief responses to condition transitions, rather than sustained, condition-dependent changes in voluntary movement execution.

4.4.5. Do Delayed Reaction Times and Longer Movement Durations Reflect a Combined Slowed Moment State?

This analysis tested whether RT covaried with subsequent movement duration, separating stable between-participant differences from within-participant block-to-block fluctuations, to evaluate whether delayed initiation and prolonged execution reflect a unified slowed motor state.

In the temporal predictability cohort, movement duration was strongly predicted by baseline duration ($\beta = 0.36$, 95% CI = [0.21, 0.51], $p < .001$), indicating stable individual timing characteristics. At the between-participant level, average RT was not reliably related to movement duration ($p = .145$), and this null relationship was consistent across predictability, movement direction, and block ($p \geq .630$). Simple-slope analyses confirmed that participants with generally slower RTs did not systematically execute longer movements in any condition ($p \geq .690$).

In contrast, within-participant fluctuations in RT showed a robust state-dependent coupling with movement duration. Block-to-block increases in RT predicted longer movement durations ($\beta = 1.16$, 95% CI = [0.54, 1.79], $p < .001$). This effect was direction dependent, being stronger during extension than flexion ($\beta = -0.65$, 95% CI = [−1.27, −0.03], $p = .039$). Simple slopes showed reliable coupling during extension in both predictable ($\beta = 1.25$, 95% CI = [0.04, 2.46], $p = .043$) and uncertain conditions ($\beta = 2.38$, 95% CI = [1.01, 3.74], $p < .001$), with no corresponding effects in flexion. These results indicate a tight, state-dependent linkage between preparation and execution timing that was largely insensitive to temporal predictability.

In the perturbation amplitude cohort, baseline movement duration again strongly predicted movement duration ($\beta = 0.36$, 95% CI = [0.21, 0.51], $p < .001$). However, neither between-participant nor within-participant RT showed a reliable main effect (Between: $p = .680$, Within: $p = .907$). Thus, unlike the predictability cohort, there was no evidence for a general state-dependent coupling between RT and movement duration. Instead, RT effects in the amplitude cohort were context specific. A significant interaction between perturbation amplitude, movement direction, and mean RT ($\beta = 0.62$, 95% CI = [0.10, 1.15], $p = .020$) indicated that stable RT differences predicted movement duration only under particular mechanical conditions. In flexion, higher mean RT tended to predict longer durations at 1 Nm ($\beta = 0.88$, 95% CI = [-0.36, 2.12], $p = .164$) but shorter durations at 0.5 Nm ($\beta = -1.11$, 5% CI [-2.42, 0.21], $p = .099$), with a reliable divergence between torque levels ($\beta = -1.99$, 95% CI = [−3.38, −0.59], $p = .005$). No corresponding effects were observed in extension, and within-participant RT showed no contextual modulation ($p \geq .283$).

In summary, the relationship between RT and movement duration depended strongly on task structure. In the temporal predictability cohort, delayed RTs and prolonged movement duration covaried dynamically within individuals, consistent with a transient slowed motor state linking preparation and execution. When perturbation amplitude was varied, this state-dependent coupling disappeared, and RT influenced movement duration only through context-specific trait differences.

4.4.6. Co-Contraction During Movement

For the temporal predictability cohort, change-from-baseline co-contraction during movement showed a selective dependence on movement direction and predictability, with little evidence for learning across blocks and no consistent global session effects.

Across the cohort, co-contraction was lower during flexion than extension (β = −0.01, 95% CI = [−0.02, -4.75×10^{-3}], p = .002, **Figure 4.35**). However, this directional asymmetry was strongly modulated by predictability. Although no significant difference was observed between flexion movements following the uncertain and predictable stabilisation conditions (p = .461), a significant condition-dependent modulation of co-contraction was evident for extension movements (β = −0.02, 95% CI = [−0.05, -6.48×10^{-4}], p = .044). Overall, only extension movements following uncertainty demonstrated a significant deviation from baseline co-contraction levels. This increase was significant in the initial task block (β = 0.05, 95% CI = [1.75×10^{-4}, 0.11], p = .049) but fell marginally short of conventional significance when assessed across all task blocks (β = 0.04, 95% CI = [-7.20×10^{-4}, 0.08], p = .054).

Despite these directional effects, neither any condition-by-direction combination nor the overall effect showed significant change across task blocks (p ≥ .545), resulting in nonsignificant differences between slopes (p ≥ .91). Session-level factors did not contribute meaningfully. There were no effects of condition order, total block count, or conditional switch effects (p ≥ .480), and no evidence that these factors interacted with condition or direction in a way that explained the observed effects.

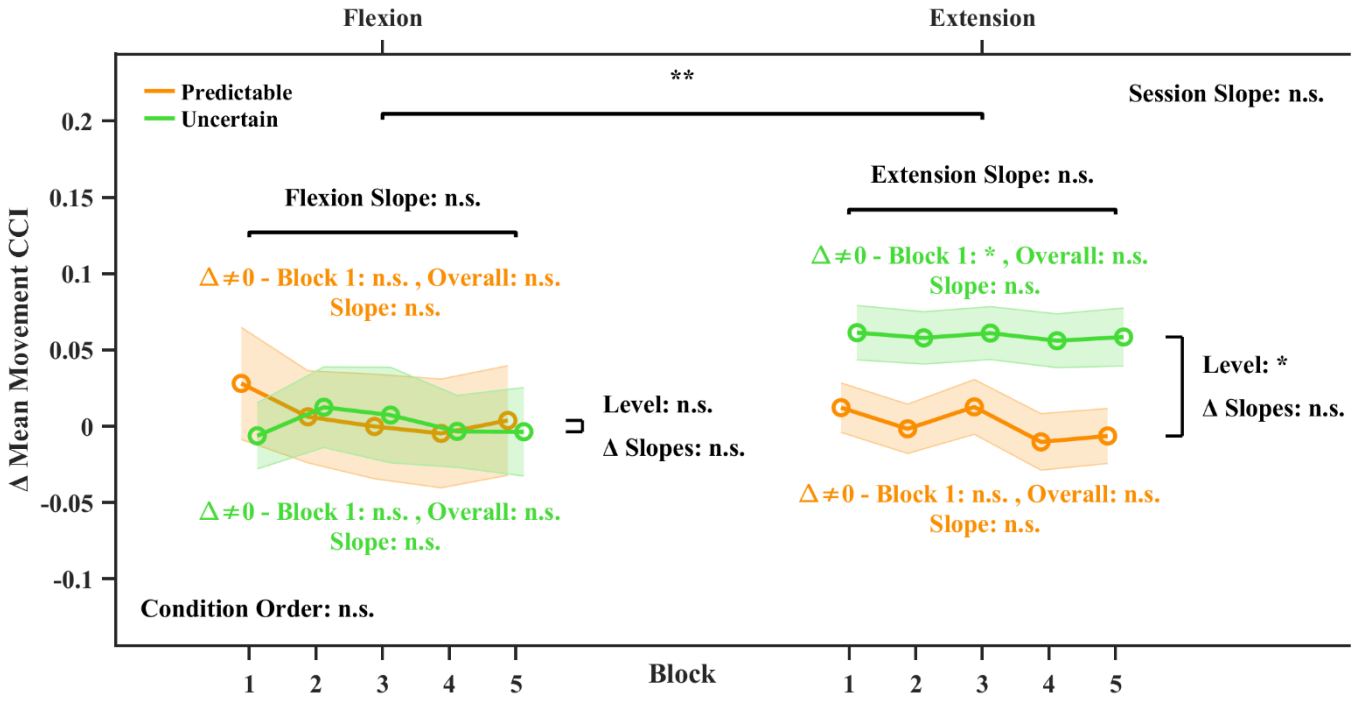

Figure 4.35. Change from baseline co-contraction (CCI) across experimental blocks for flexion (left) and extension (right) following temporally predictable (orange) and uncertain (green) perturbation conditions. Full plot description - Figure 4.26.

Nonparametric analyses of the initial block broadly supported the observations made in the mixed models. No baseline differences were observed in flexion for either condition ($p \geq .59$, **Figure 4.36A**). In extension, co-contraction increased relative to baseline in the uncertain condition ($p = .005$, $z = 2.83$, $r = 0.58$, **Figure 4.36B**) and showed a trend in the predictable condition ($p = .059$). Importantly, the between-condition comparison of baseline-corrected change scores in extension was significant ($p = .037$, $z = 2.09$, $r = 0.43$), indicating greater early co-contraction increases under uncertain dynamics.

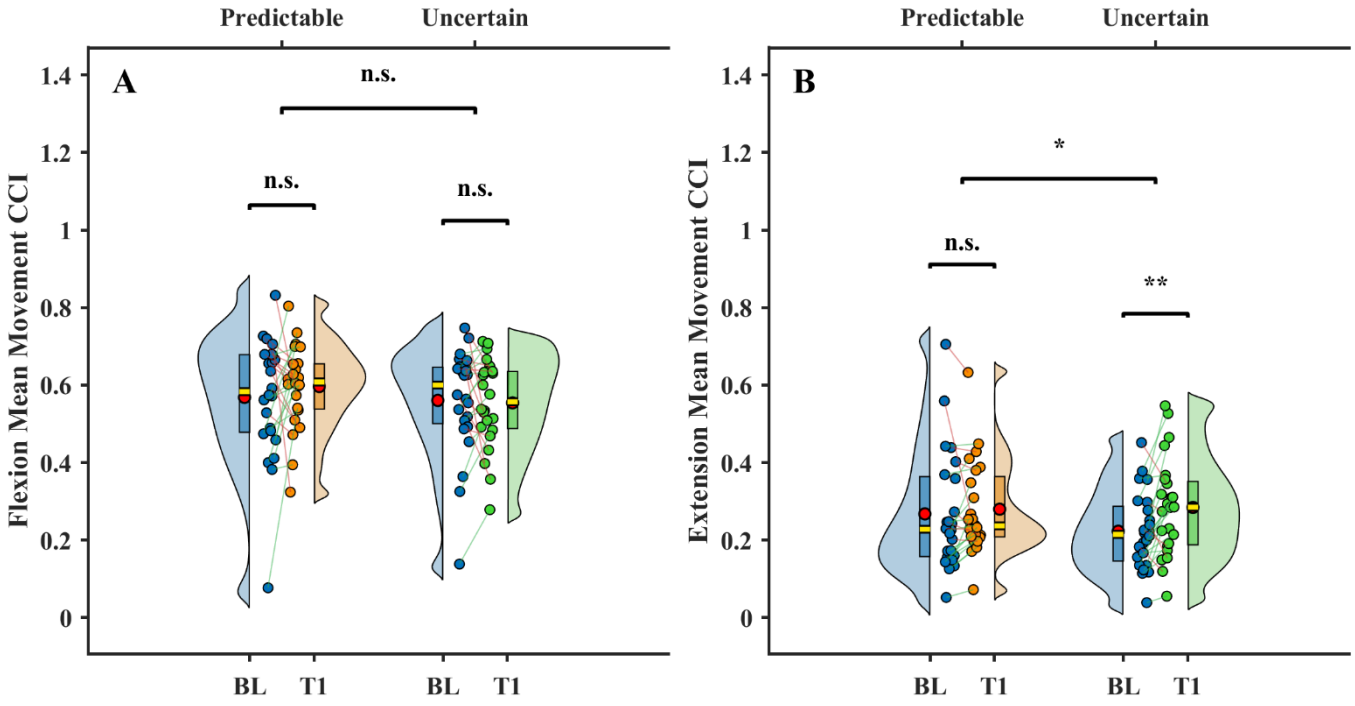

Figure 4.36. Contrasts in movement co-contraction (CCI) between baseline blocks and initial task blocks for (A) flexion and (B) extension after temporally predictable (orange) and uncertain (green) perturbation conditions. Full plot description - Figure 4.29.

For the perturbation amplitude cohort, change-from-baseline co-contraction during movement was dominated by a strong and consistent directional effect, with additional evidence for modest practice-related reductions and minimal influence of perturbation amplitude. Across the session, co-contraction was substantially lower during flexion than extension, irrespective of stabilisation phase condition. This effect was large and highly reliable ($\beta = -0.04$, 95% CI = [−0.04, −0.03], $p < .001$, **Figure 4.37**). Only flexion movements showed significant deviations in co-contraction relative to baseline, with reductions that were significant for both conditions at the initial task block and when assessed across all task blocks ($p \leq .012$). Unlike the predictability cohort, this directional asymmetry was not strongly modulated by condition, although a moderate trend suggested direction-dependent condition effects ($\beta = -0.01$, 95% CI = [-0.02, 2.88×10^{-4}], $p = .058$). In addition, there was no overall effect of perturbation amplitude on the movement co-contraction index ($p = .349$).

Movement co-contraction did not show systematic adaptation across repeated task blocks ($p = .129$) and exhibited no significant differences in the rate of change between condition-specific slopes for either movement direction ($p \geq .215$). Despite this lack of significant divergence, there was a significant reduction in CCI for flexion movements following the high amplitude condition over repeated task blocks ($\beta = -0.02$, 95% CI = [-0.03, -1.54×10^{-3}], $p = .031$), suggesting modest adaptation under higher torque demands.

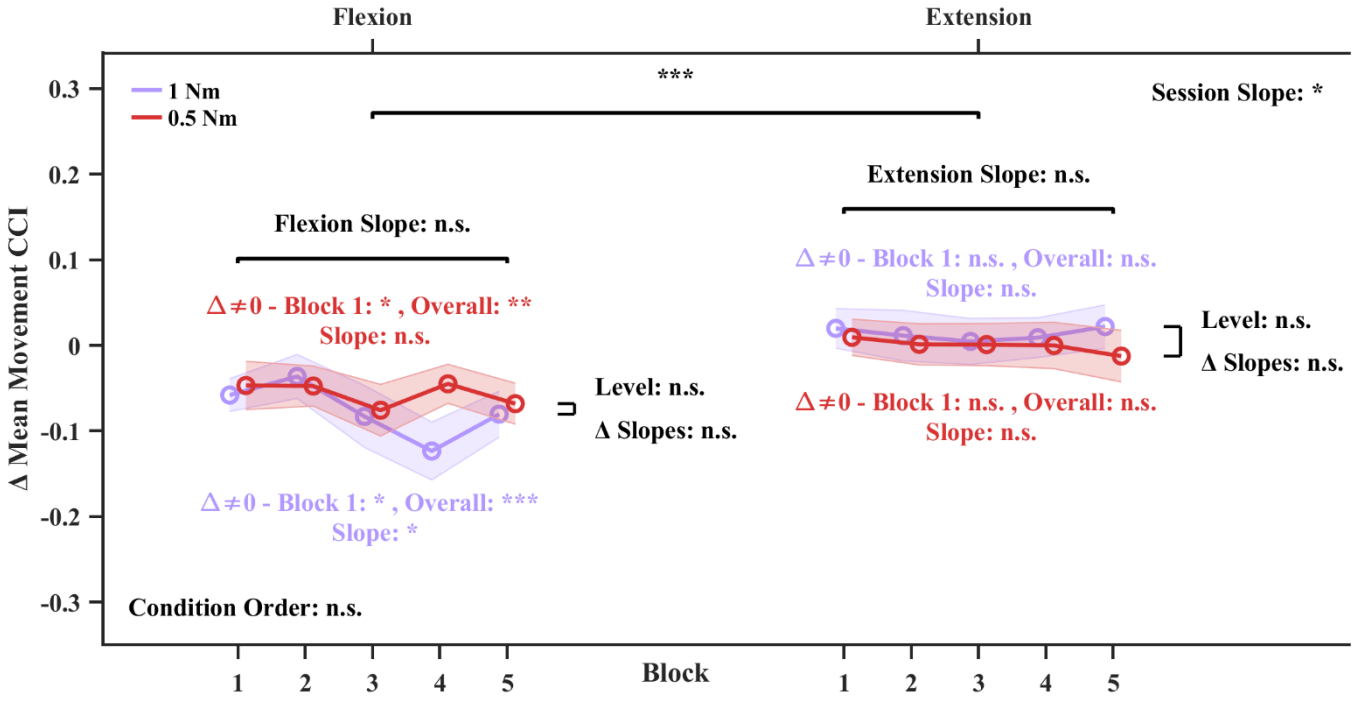

Figure 4.37. Change from baseline co-contraction (CCI) across experimental blocks for flexion (left) and extension (right) following high-amplitude (red) and low-amplitude (purple) perturbation conditions. Full plot description - Figure 4.26.

Session-structure effects were minor. Effects of condition order were weak, and no reliable switch-related costs were observed ($p \geq .082$). Higher-order interactions involving condition, movement direction, and period approached statistical significance in several cases ($p \geq .058$) but were not accompanied by consistent or interpretable simple effects. When evaluated across the session, the co-contraction index gradually decreased over repeated task blocks ($\beta = -0.01$, 95% CI = [-0.02, -2.96×10^{-4}], $p = .042$), suggesting an overall increase in task familiarity and a reduction in motor impairment.

Nonparametric analyses of the initial task block were broadly consistent with the model-based results. In flexion, co-contraction increased relative to baseline in the 1 Nm condition ($p = .022$, $z = 2.29$, $r = 0.61$, **Figure 4.38A**), whereas no reliable change was observed in the 0.5 Nm condition ($p = .198$). In extension, neither condition differed from baseline ($p \geq .551$, **Figure 4.38B**), and there were no between-condition differences in baseline-corrected change scores for either direction ($p \geq .683$).

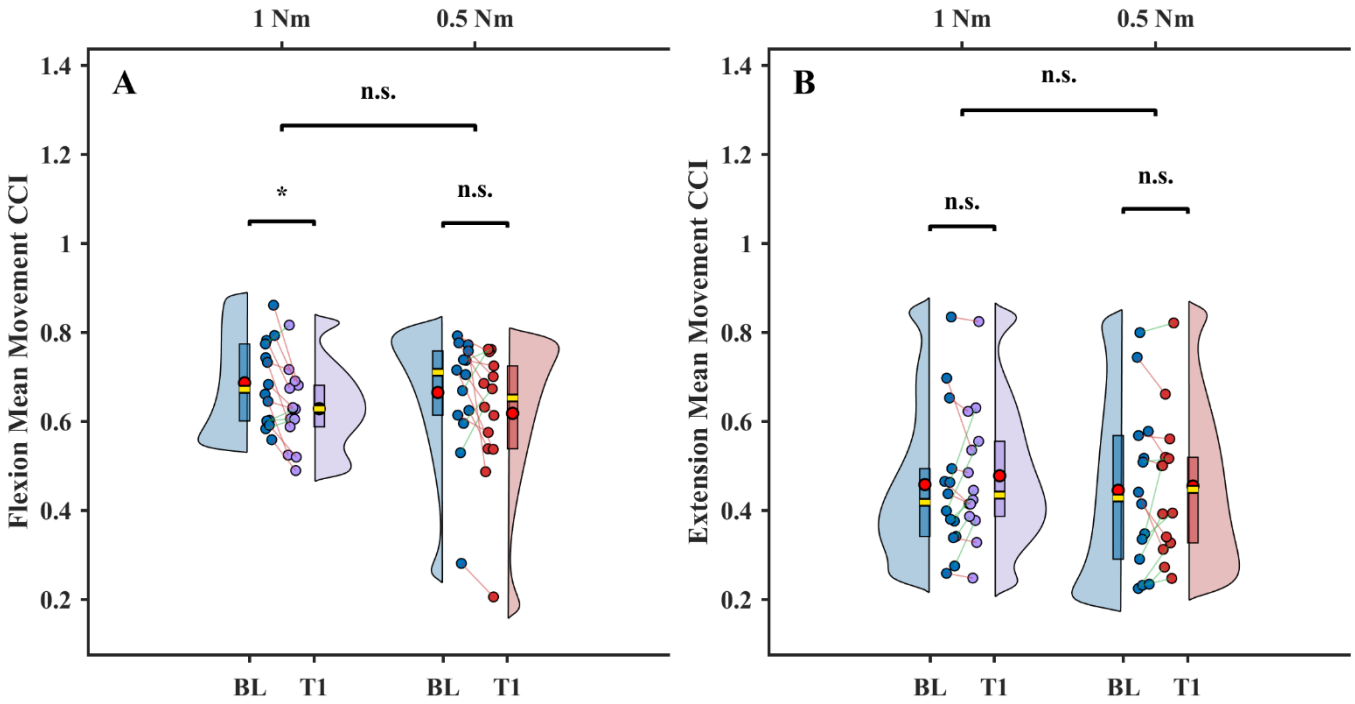

Figure 4.38. Contrasts in movement co-contraction (CCI) between baseline blocks and initial task blocks for (A) flexion and (B) extension after high-amplitude (purple) and low-amplitude (red) perturbation conditions. Full plot description - Figure 4.29.

Across cohorts, voluntary co-contraction was dominated by movement direction, with consistently lower coactivation during flexion than extension. This directional asymmetry was robust across sessions, indicating a stable biomechanical or control-related difference rather than an effect of experimental manipulation.

Cohorts differed in how task context modulated this pattern. In the temporal predictability cohort, the flexion-related reduction in co-contraction was strongly shaped by predictability: uncertainty accentuated the flexion–extension contrast and selectively increased early co-contraction during extension, consistent with transient stiffening under uncertain dynamics. These effects emerged early and showed no evidence of learning across blocks. In contrast, the perturbation amplitude cohort exhibited a more uniform pattern that was largely insensitive to torque level. Flexion-related reductions were present from the outset, with only small practice-related decreases in co-contraction over time, particularly under higher torque.

Overall, co-contraction during voluntary movement reflected stable, direction-specific control strategies. Task uncertainty modulated early stiffness regulation, while practice produced only minor reductions in coactivation. Neither predictability nor torque amplitude drove sustained adaptation, indicating that co-contraction was governed primarily by baseline control demands rather than experimental context.

4.4.7. Does Stabilisation Phase Co-Contraction Persist into Voluntary Movement?

This analysis tested whether co-contraction during the postural stabilisation phase predicted co-contraction during the subsequent voluntary movement, indicating a carryover of motor state across task phases, while accounting for task condition, movement direction, task block, and baseline movement-phase co-contraction.

In the temporal predictability cohort, baseline movement phase co-contraction was a strong predictor of subsequent co-contraction ($\beta = 0.37$, 95% CI = [0.31, 0.43], $p < .001$), indicating stable individual activation patterns across phases. At the between-participant level, higher average stabilisation phase

co-contraction predicted higher average movement phase co-contraction (β = 0.20, 95% CI = [0.09, 0.32], p < .001). This relationship was strongly direction dependent, being present during extension but not flexion (β = −0.17, 95% CI = [−0.21, −0.13], p < .001). Simple slopes confirmed robust associations during extension under both predictable (β = 0.32, 95% = CI [0.18, 0.45], p < .001) and uncertain conditions (β = 0.43, 95% CI = [0.30, 0.57], p < .001, **Figure 4.39B**).

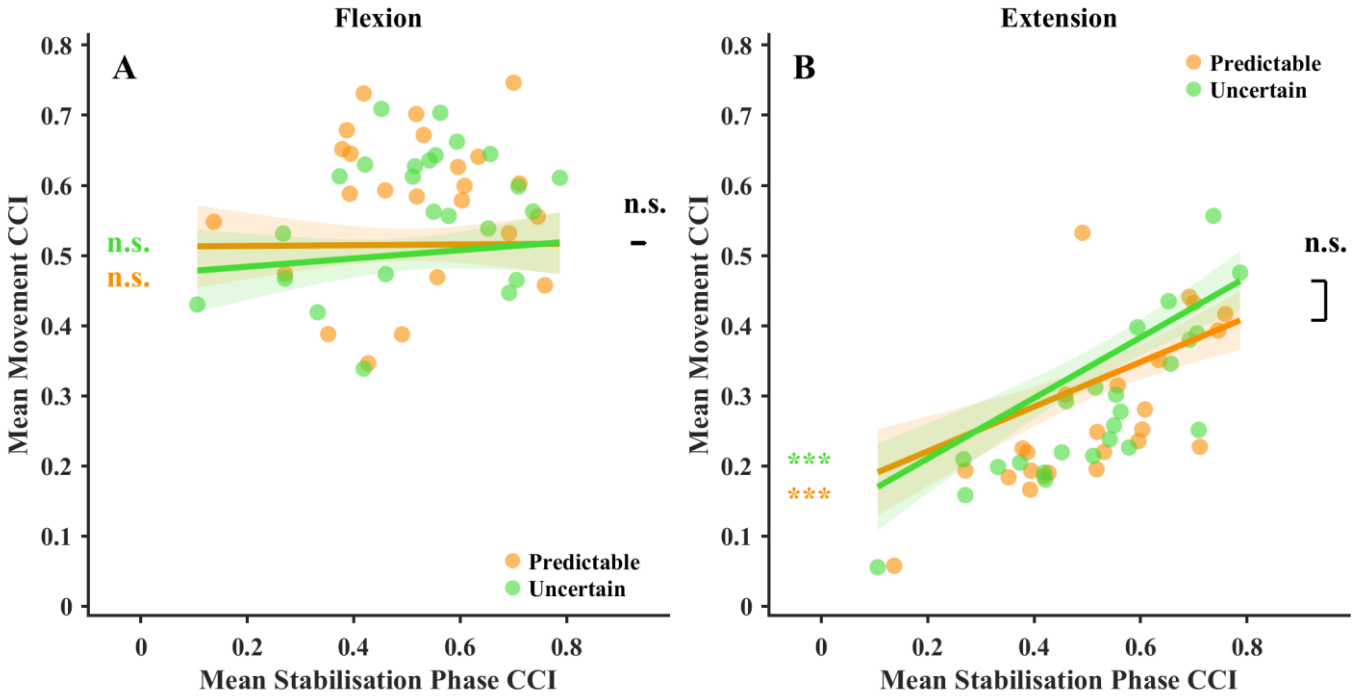

Figure 4.39. Between-participant relationship between stabilisation phase co-contraction (CCI) and voluntary movement co-contraction (CCI) for (A) flexion and (B) extension. Each point represents an individual participant's mean level for a given condition (predictable, orange; uncertain, green). Solid lines depict condition-specific model fits, with shaded bands indicating the corresponding 95% confidence intervals. Asterisks adjacent to the axes denote the statistical significance of the respective model fits, while brackets indicate comparisons between fits. Scatter points reflect raw between-participant means and do not account for additional model coefficients, which may result in a visual mismatch between the fitted lines and the distribution of points. Significance codes: * p < 0.05, ** p < 0.01, *** p < 0.001; n.s., not significant.

Within participants, block-to-block increases in stabilisation phase co-contraction strongly predicted increases in movement-phase co-contraction (β = 0.50, 95% CI = [0.36, 0.63], p < .001). This carryover was robust during extension in both predictable (β = 0.64, 95% CI = [0.35, 0.93], p < .001) and uncertain conditions (β = 0.58, 95% CI = [0.26, 0.79], p < .001). During flexion, the effect was present only under temporal uncertainty (β = 0.53, 95% CI = [0.32, 0.85], p < .001).

In the perturbation amplitude cohort, baseline movement phase co-contraction was again the dominant predictor (β = 0.70, 95% CI = [0.63, 0.76], p < .001, **Figure 4.40**). Between participants, average stabilisation phase co-contraction robustly predicted movement phase co-contraction (β = 0.40, 95% CI = [0.21, 0.59], p < .001), with a weaker association during flexion than extension (β = −0.09, 95% CI = [−0.17, −0.005], p = .036). Simple slopes were significant across all amplitude–direction combinations, strongest during extension at both 1 Nm (β = 0.50, 95% CI = [0.27, 0.74], p < .001) and 0.5 Nm (β = 0.47, 95% CI = [0.24, 0.70], p < .001). Within participants, block-to-block increases in stabilisation phase co-contraction reliably predicted movement phase co-contraction across both amplitudes and directions (β = 0.55, 95% CI = [0.34, 0.76], p < .001), with no reliable amplitude-dependent differences.

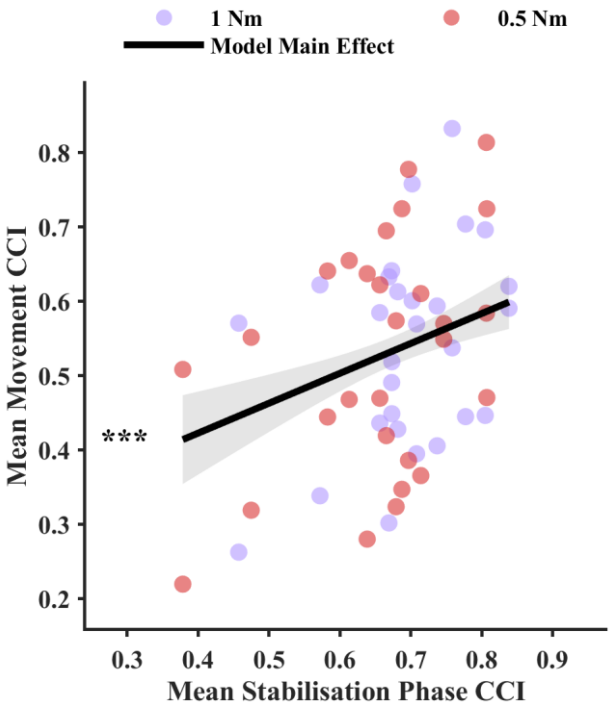

Figure 4.40. Relationship between stabilisation phase co-contraction (CCI) and movement phase co-contraction (CCI). Participant-level mean values are shown for the high-amplitude (purple) and low-amplitude (red) task blocks. The solid black line represents the model-estimated main effect across conditions, with the shaded band indicating the 95% confidence interval. The asterisk denotes the significance of the overall model effect. Significance codes: * p < 0.05, ** p < 0.01, *** p < 0.001; n.s., not significant.

Across cohorts, a consistent pattern emerged: co-contraction during the stabilisation phase strongly and reliably carried over into voluntary movement. This continuity was evident both in stable individual differences and in block-to-block fluctuations across both the temporal predictability and perturbation amplitude cohorts. This relationship was modestly modulated by movement direction. There was no evidence for a reset of co-contraction between task phases. Instead, co-contraction appears to reflect a persistent control state that bridged reactive and voluntary motor behaviour.

4.4.8. Does Stabilisation Phase Co-Contraction Drive Voluntary Movement Impairment?

This analysis tested whether co-contraction during the perturbation phase predicted subsequent voluntary RT and movement duration, while accounting for task condition, movement direction, task block, and baseline performance.

In the temporal predictability cohort, stabilisation phase co-contraction showed a selective relationship with voluntary RT. Between participants, average co-contraction did not reliably predict RT ($p = .296$), although predictability moderated this relationship: higher average co-contraction was associated with shorter RTs in the temporally predictable relative to the temporally uncertain condition ($\beta = -0.03$, 95% CI = [−0.05, −0.01], $p = .001$). Within participants, block-to-block increases in co-contraction predicted faster reactions ($\beta = -0.09$, 95% CI = [−0.16, −0.02], $p = .010$), an effect most evident during flexion in the predictable condition ($\beta = -0.21$, 95% CI = [−0.37, −0.06], $p = .007$, **Figure 4.41A**). The coupling between RT and co-contraction also decreased across task blocks in the temporally predictable condition but not under the uncertain condition ($\beta = -3.30 \times 10^{-3}$, 95% CI = [$-5.58 \times 10^{-3}$, -1.03×10^{-3}], $p = .004$). Together, these findings indicate that transient increases in co-contraction were associated with enhanced readiness for voluntary action, particularly when perturbations were temporally predictable.

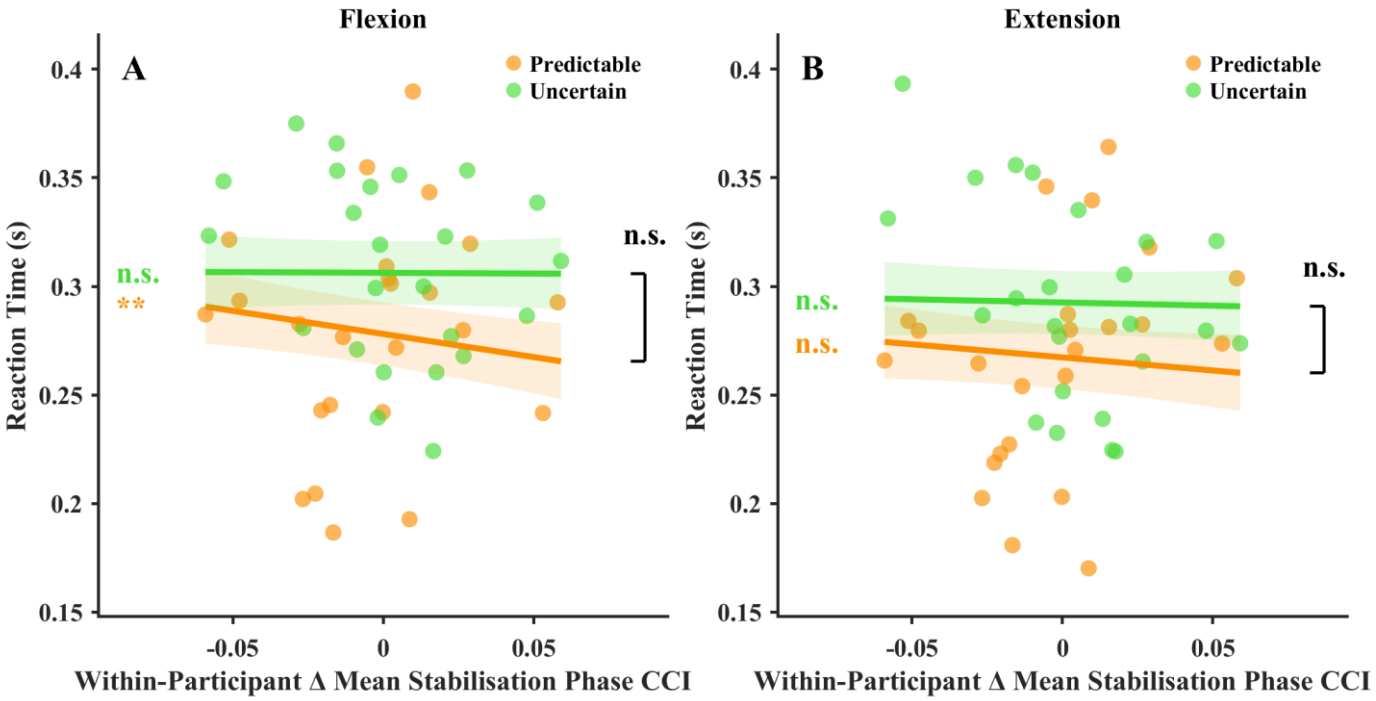

Figure 4.41. Within-participant relationship between stabilisation phase co-contraction (Δ CCI) and voluntary movement reaction time (s) for (A) flexion and (B) extension. Full plot description - Figure 4.39.

For voluntary movement duration in the same cohort, baseline timing strongly predicted subsequent duration (β = 0.37, 95% CI = [0.22, 0.52], p < .001). Average stabilisation phase co-contraction did not predict movement duration (p = .944), although direction and predictability condition modulated this relationship: higher co-contraction was associated with longer durations during flexion relative to extension (β = 0.15, 95% CI = [0.01, 0.28] , p = .033), an effect amplified in the predictable condition (β = 0.21, 95% CI = [0.07, 0.35], p = .003). Within participants, co-contraction showed little systematic influence, with one context-specific effect whereby greater co-contraction predicted shorter durations during extension following temporal uncertainty (β = −1.19, 95% CI = [−2.11, −0.26], p = .012). Overall, movement duration was only weakly and contextually related to co-contraction.

In the perturbation amplitude cohort, voluntary RT and movement duration were largely independent of stabilisation phase co-contraction. RT was dominated by baseline response speed (β = 0.20, 95% CI = [0.03, 0.37], p = .025), with no reliable between- or within-participant effects of co-contraction (p ≥ .187). Similarly, movement duration was strongly predicted by baseline timing (β = 0.29, 95% CI = [0.15, 0.43], p < .001) , but not by co-contraction at either the between-participant or within-participant level (p ≥ .456). No consistent modulation by perturbation amplitude was observed.

In summary, stabilisation phase co-contraction influenced subsequent voluntary behaviour primarily in the temporal predictability cohort, where transient increases were associated with faster reactions and, in limited contexts, shorter movements. When perturbation amplitude was manipulated, voluntary RT and movement duration were largely insensitive to co-contraction and instead reflected stable timing characteristics and movement direction. These findings suggest that co-contraction carries forward into voluntary motor preparation chiefly under predictable temporal structure, with little impact on voluntary timing when mechanical demands vary in amplitude.

4.4.9. Summary

This chapter examined how alterations in temporal predictability and perturbation amplitude stabilisation challenges shaped subsequent voluntary movement, focusing on accuracy, reaction time, movement duration, and muscle co-contraction. Across measures, the dominant pattern was one of immediate, stable effects rather than gradual adaptation. Movement direction consistently exerted a strong influence alongside temporal predictability or perturbation amplitude manipulation, and most condition effects appeared as baseline offsets or transient early responses rather than learning across task blocks.

Voluntary movement accuracy showed little sensitivity to either experimental manipulation and no evidence of within-condition learning. In the temporal predictability cohort, accuracy was consistently reduced during flexion relative to extension, with deficits present from the first block and persisting throughout the session, independent of predictability condition (**Figure 4.26**). In contrast, the perturbation amplitude cohort showed no reliable directional asymmetry or stable accuracy changes across conditions (**Figure 4.27**). These findings indicate that when accuracy costs occur, they are driven by direction-specific control demands rather than temporal structure or mechanical load, with limited scope for adaptation in the constrained task.

Reaction time was dominated in both cohorts by a large, nonspecific task-onset cost, with marked slowing relative to baseline appearing at the first task block and persisting across the session (**Figure 4.28**, **Figure 4.30**). Beyond this shared effect, cohort-specific structure emerged. In the temporal predictability cohort, RTs were consistently faster under predictable than uncertain dynamics and slightly slower during flexion than extension. In the perturbation amplitude cohort, RT was insensitive to amplitude condition but showed a robust flexion-related slowing and a gradual speeding with practice indicating partial recovery from the initial task-onset cost.

Movement duration was the most stable measure. In the predictability cohort, durations increased at the initial task block, particularly under predictable dynamics (**Figure 4.33**), but showed no systematic change across blocks and no reliable differences between conditions or directions (**Figure 4.32**). In the perturbation amplitude cohort, movement duration remained close to baseline throughout the session (**Figure 4.34**), with only brief adjustments linked to condition entry or switching. Across cohorts, movement duration showed no evidence of sustained adaptation, suggesting tight regulation of movement completion despite changes in preparatory demands.

Co-contraction during voluntary movement revealed the clearest and most consistent structure. Across both cohorts, co-contraction was reliably lower during flexion than extension, indicating a stable, direction-specific control strategy. In the temporal predictability cohort, this asymmetry was modulated by task context, with temporal uncertainty selectively increasing co-contraction during extension, particularly at initial exposure (**Figure 4.35**). These effects emerged early and showed no learning across blocks. In the perturbation amplitude cohort, co-contraction patterns were largely insensitive to amplitude condition, with only modest practice-related reductions over time, especially under high-amplitude perturbations (**Figure 4.37**). Overall, co-contraction reflected baseline control demands more than experimental manipulation.

A key finding was the strong carryover of co-contraction from the perturbation phase into subsequent voluntary movement. In both cohorts, stabilisation phase co-contraction robustly predicted movement-phase co-contraction at both the level of stable individual differences and between block deviations, with stronger effects during extension (**Figure 4.39**, **Figure 4.40**). This continuity indicates that muscle activation does not reset between reactive and voluntary phases but reflects a persistent motor control state spanning the stability–movement transition. The influence of this persistent state on voluntary performance depended on task structure. In the predictability cohort, increases in stabilisation phase co-contraction were associated with faster RTs, particularly under predictable dynamics (**Figure 4.41**), suggesting enhanced readiness for action. This coupling weakened with repeated exposure, indicating reduced reliance on stiffness-based preparation. Effects on movement duration were weak and context

dependent. In contrast, in the amplitude cohort, reaction time and movement duration were largely independent of co-contraction, instead reflecting stable individual timing and movement direction.

Together, these findings suggest that voluntary behaviour following postural perturbation is governed primarily by task engagement and movement direction, with preceding stabilisation dynamics exerting secondary, selective influences. Co-contraction emerges as a central organising variable, reflecting a persistent control state that bridges reactive and voluntary behaviour. Temporal predictability shapes how this state interacts with motor preparation, whereas changes in perturbation amplitude do not produce comparable effects. Rather than gradual adaptation, voluntary movement appears to rely on stable, direction-specific control strategies established early and maintained across experience.

4.5. Cortical Beta Activity

4.5.1. Introduction

Cortical beta-band activity (13–30 Hz) is a dominant feature of sensorimotor processing during tasks that require postural maintenance [10], [153], force regulation [154], and resistance to external perturbation [155]. Rather than supporting movement generation, beta activity is consistently associated with stabilisation of the current motor state [150], promoting precise control of muscle activation and limb impedance. Elevated beta power and beta-band corticomuscular coupling are most prominent during steady contractions and postural tasks and are suppressed when the motor system transitions toward movement initiation [214]. This pattern has led to the interpretation of beta activity as a neural signature of stability-oriented control, reflecting an emphasis on maintaining sensorimotor predictions, regulating impedance, and resisting change. Within this framework, beta dynamics are well suited to mediate trade-offs between competing motor goals, such as the need to remain mechanically stable while preparing to move.

In the context of the present work, cortical beta activity is therefore positioned as a candidate mechanism underpinning impedance control around stability–movement transitions. By embedding movement initiation within a task that requires sustained stabilisation under mechanical instability, the paradigm directly probes how beta-band dynamics evolve when stability-oriented control must be relinquished in favour of movement. This enables assessment of whether elevated beta activity persists under heightened impedance demands, how it is modulated by perturbation structure, and how its suppression relates to the release of impedance and initiation of voluntary action. As such, beta activity is treated not merely as a correlate of movement suppression, but as an active component of the neural control architecture governing stability–movement transitions.

4.5.2. Beta Power During Stabilisation and Movement

Mean beta power was examined during the postural stabilisation phase and subsequent voluntary movement. Across both cohorts, no reliable effects were observed, indicating that this measure did not capture beta-band dynamics associated with the impedance-related processes under investigation.

In the temporal predictability cohort, beta power during stabilisation did not differ from baseline for any condition or movement direction ($p \geq .105$), did not change across task blocks at any level ($p \geq .172$), and did not differ between predictable and uncertain timing ($p = .660$). Beta power during voluntary movement likewise showed no significant deviation from baseline or modulation by condition, direction, or block ($p \geq .115$).

A similar pattern was observed in the perturbation amplitude cohort. Beta power during stabilisation showed no significant change from baseline ($p \geq .188$), no systematic change across blocks ($p \geq .563$), and no difference between perturbation amplitudes ($p = .640$). No significant beta power effects were detected during voluntary movement in this cohort either ($p \geq .234$).

In summary, mean beta power did not significantly deviate from baseline levels and was stable across conditions, task phases, and repeated exposure. These null effects suggest that either beta-band activity is not strongly engaged by the stabilisation and impedance processes probed here, or that relevant neural dynamics occur at a finer temporal, spectral, or spatial scale not captured by phase-averaged beta power.

4.5.3. Beta Corticomuscular Coherence During Stabilisation

Beta corticomuscular coherence (β-CMC) reflects the continuous cortical involvement needed to stabilise and regulate muscle output. Strong β-CMC is associated with postural control and joint stabilisation, where the nervous system prioritises precise regulation of impedance over movement initiation. By modulating beta-band coupling, the motor cortex can tune limb impedance to resist perturbations, support accurate force control, and maintain stable interactions with the environment. During the stabilisation phase, beta corticomuscular coherence showed a large, immediate reduction from baseline that was highly consistent across cohorts and task conditions, with no evidence for learning or adaptation.

In the temporal predictability cohort, nonparametric analyses revealed a pronounced disruption of β-CMC from baseline to the first task block in both the temporally predictable and uncertain conditions ($p \leq .001$, **Figure 4.42A**), with no difference in the amplitude of baseline-corrected change between conditions ($p = .361$). Linear mixed-effects models converged on the same conclusion: β-CMC was strongly reduced relative to baseline at both the first task block and across each condition ($p \leq .001$, **Figure 4.42B**). There was no evidence of change across blocks per condition ($p \geq .906$), no block main effect ($p = .955$), and no condition-by-block interaction ($p = .879$). A small condition effect showing that the reduction of β-CMC was greater in the temporally predictable condition compared to the uncertain condition was observed ($\beta = -3.77 \times 10^{-3}$, 95% CI = $[-1.00 \times 10^{-2}, -4.54 \times 10^{-5}]$, $p = .047$).

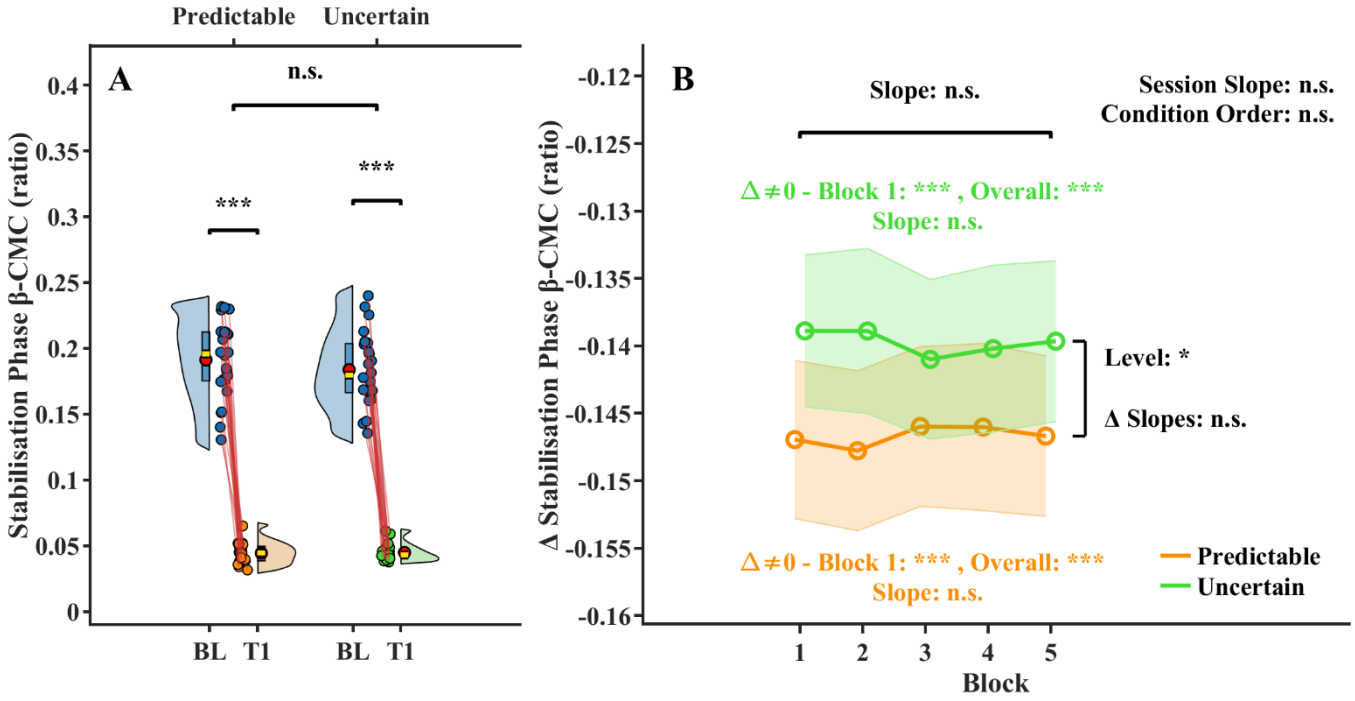

Figure 4.42. (A) Mean stabilisation phase β-CMC at baseline (BL) and initial task block (T1) for temporally predictable and uncertain conditions. Scatter points are individual participants. IQR displayed by box internal to each violin with mean indicated by the red circle and median by the yellow line. (B) Change from baseline β-CMC across task blocks divided by condition with (±SEM): predictable (orange), uncertain (green). Significance codes: * p < 0.05, ** p < 0.01, *** p < 0.001; n.s., not significant.

An almost identical pattern was observed in the amplitude cohort. β-CMC dropped sharply from baseline to the first stabilisation block at both 1 Nm and 0.5 Nm ($p \leq .001$, **Figure 4.43A**), with no difference in baseline-corrected change between amplitude conditions ($p = .975$). Model-based analyses again showed large and equivalent reductions at both the first block and overall ($p \leq .001$,

Figure 4.43B), no evidence of block-wise change ($p \geq .759$), no block main effect ($p = .803$), and no condition-by-block interaction ($p = .856$). Perturbation amplitude did not influence overall β-CMC levels during stabilisation ($p \geq .861$). Session-level effects were limited to a condition order effect, with lower β-CMC in the second condition irrespective of amplitude condition ($p < .001$).

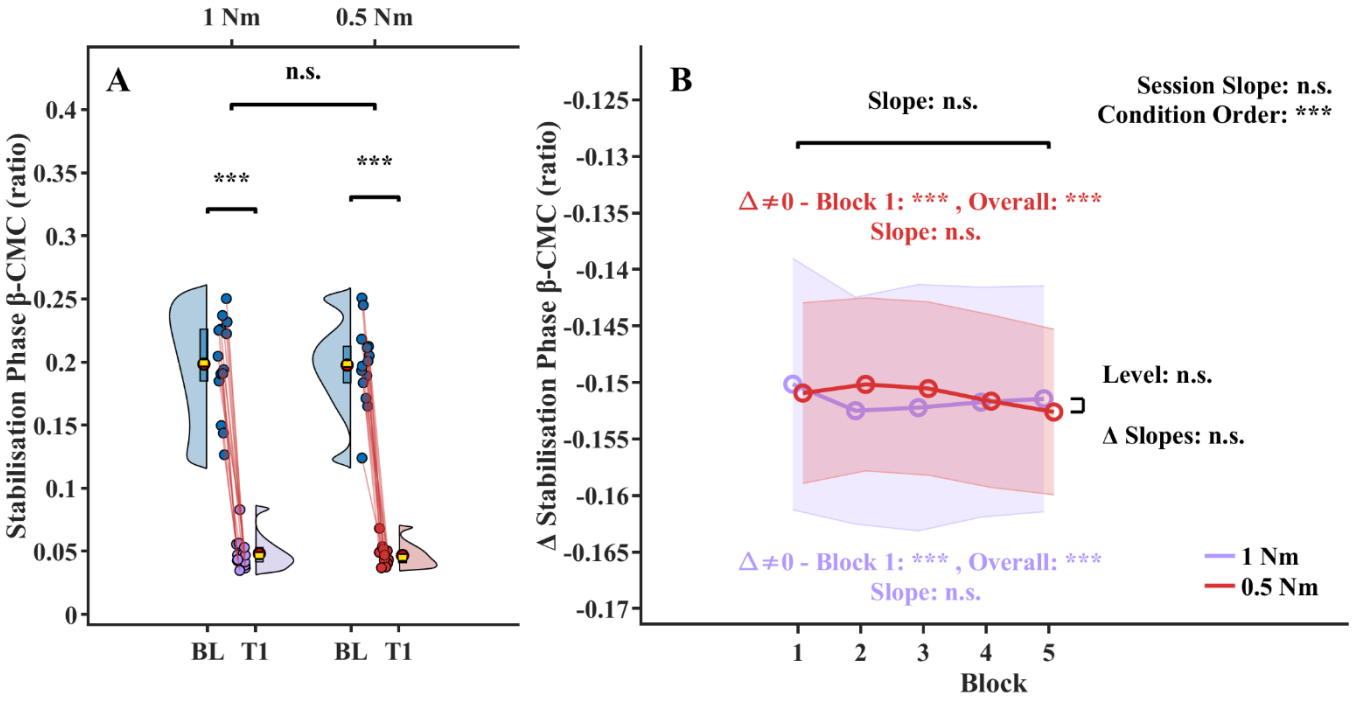

Figure 4.43. (A) Mean stabilisation phase β-CMC at baseline (BL) and initial task block (T1) for high-amplitude (1 Nm) and low-amplitude (0.5 Nm) conditions. Full plot description - Figure 4.42.

Across cohorts, the stabilisation phase was characterised by a robust and sustained reduction in β-CMC relative to baseline level. While this reduction emerged immediately and remained stable across blocks, a consistent and statistically significant difference was observed between temporal conditions: under temporally uncertain perturbations, the reduction in β-CMC was reliably smaller than in the temporally predictable condition. This effect was stable across perturbation amplitude, indicating that although β-band corticospinal coupling during stabilisation reflects a common impedance-dominated control state, it remains selectively sensitive to temporal uncertainty in the task environment rather than being fully invariant to higher-level task structure.

4.5.4. Does Beta Corticomuscular Coherence Correlate with Co-Contraction During Stabilisation?

This analysis examined the relationship between β-CMC during the stabilisation phase and co-contraction (CCI), focusing on between-participant mean levels and within-participant trial-to-trial fluctuations, collapsed across movement direction.

In the predictability cohort, mean stabilisation phase CCI was not associated with β-CMC ($p = .567$), and this null relationship was consistent across predictable and uncertain conditions ($p = .798$). Simple-slope analyses confirmed no between-participant association in either condition ($p \geq .533$). In contrast, within-participant increases in CCI were robustly associated with higher β-CMC ($\beta = 0.025$, 95% CI = [0.01, 0.04], $p < .001$). This effect was most evident under temporal uncertainty ($\beta = 0.03$, 95% CI = [8.05×10^{-3}, 0.05] $p = .007$), with a weaker, non-significant trend in the predictable condition ($\beta = 0.02$,

95% CI = [−2.75e × 10^{-3}, 0.04], p = .083), although the interaction with condition was not reliable (p = .640). These results indicate that β-CMC tracked transient increases in stabilising co-contraction rather than stable individual differences.

In the amplitude cohort, mean CCI was again unrelated to β-CMC (p = .334), despite a significant interaction with perturbation amplitude (p < .001). Condition-specific slopes remained weak and non-significant, indicating that this interaction reflected relative shifts between amplitudes rather than a meaningful predictive role of mean CCI. Within participants, changes in CCI were not associated with β-CMC at the model level (p = .174). However, simple-slope analyses revealed a selective effect at higher load: during 1 Nm perturbations, increases in CCI predicted higher β-CMC (β = 0.04, 95% CI [6.26 × 10^{-3}, 0.07] p = .020, **Figure 4.44**).

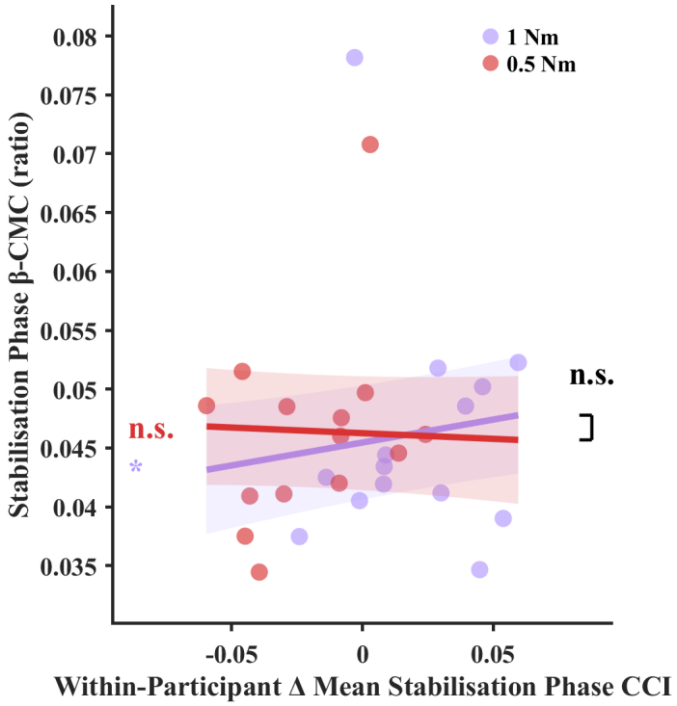

Figure 4.44. Relationship between within-participant changes in stabilisation phase co-contraction (CCI) and stabilisation phase levels of beta corticomuscular coherence (β-CMC). High perturbation amplitude (1 Nm) fit and per-participant centroids shown in purple, low-amplitude (0.5 Nm) equivalents shown in red. Individual datapoints show the mean deviation from each participant's average for illustrative purposes and do not account for additional model coefficients, which may result in a visual mismatch between the fitted lines and the distribution of points. Significance codes: * p < 0.05, ** p < 0.01, *** p < 0.001; n.s., not significant.

Across cohorts, a consistent dissociation emerged between trait-like and state-dependent effects. Mean levels of co-contraction did not predict β-CMC, indicating that corticomuscular coupling does not reflect stable individual differences in stabilisation strategy. Instead, β-CMC primarily tracked transient increases in co-contraction within individuals. Under temporal uncertainty, this coupling was robust and general, whereas under amplitude manipulation it emerged only at higher mechanical load. Together, these findings suggest that β-CMC reflects dynamic engagement of stabilising control rather than tonic stiffness, with its sensitivity shaped by whether uncertainty is temporal or mechanical in nature.

4.5.5. Beta-band Corticomuscular Coherence During Movement

During voluntary movement, β-CMC showed no consistent change from baseline and little evidence of learning across blocks in either cohort. Instead, corticomuscular coupling was weakly but systematically shaped by interactions between task context and movement direction.

In the temporal predictability cohort, nonparametric analyses of the first voluntary movement block revealed no significant deviations from baseline in either condition or direction ($p \geq .178$). Linear mixed-effects models likewise showed no block-wise change within flexion or extension and no condition-dependent learning rates ($p \geq .211$, **Figure 4.45**), indicating stable β-CMC expression across the session. Despite this absence of adaptation, overall β-CMC amplitude differed by condition and direction. Collapsing across blocks, β-CMC was elevated in the uncertain condition ($\beta = 0.02$, 95% CI = [0.01, 0.03], $p < .001$) but not in the predictable condition ($p = .142$). This effect was direction-specific: β-CMC was higher in the uncertain than predictable condition during extension ($\beta = 0.03$, 95% CI = [0.01, 0.04], $p = .006$), with no difference in flexion ($p = .998$). Consistent with this pattern, a robust condition-by-direction interaction was observed ($\beta = -0.02$, 95% CI = [−0.02, −0.01], $p < .001$), indicating that temporal predictability selectively modulated extension-related β-CMC rather than producing a global shift in coupling.

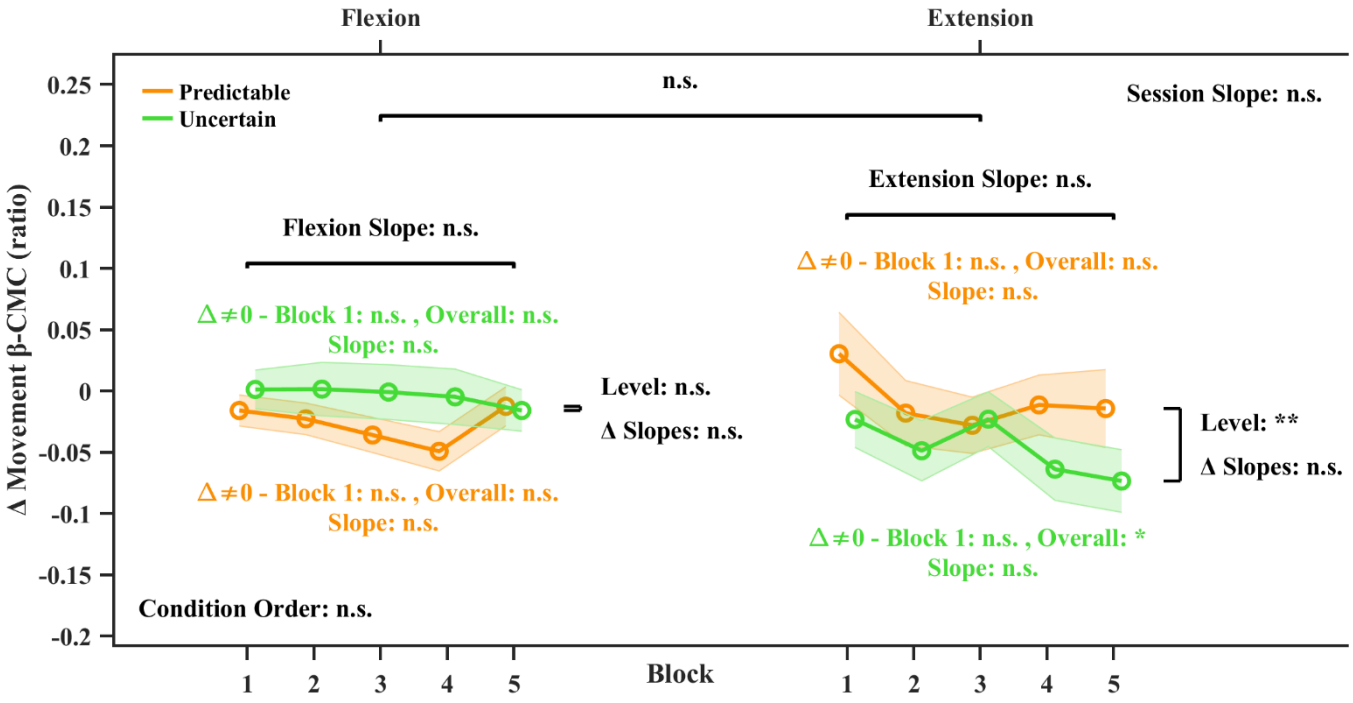

Figure 4.45. Change from baseline β-CMC (ratio) across experimental blocks for flexion (left) and extension (right) following temporally predictable (orange) and uncertain (green) perturbation conditions. Circles denote block-wise means and shaded regions represent variability (±SEM). For each condition-direction combination, change in β-CMC was tested for statistical divergence from baseline (Δ ≠ 0) at the initial task block and the combination overall. Level effects indicate overall differences in β-CMC amplitude, whereas Slope effects indicate linear trends across repeated blocks. Significance codes: * p < 0.05, ** p < 0.01, *** p < 0.001; n.s., not significant.

A similar overall pattern was observed in the perturbation amplitude cohort. Initial voluntary blocks showed no reliable baseline-related changes in β-CMC for either torque condition or direction ($p \geq .552$). Mixed-effects models provided little evidence for learning across blocks within either direction or condition ($p \geq .198$, **Figure 4.46**). Instead, torque amplitude modulated β-CMC in a direction-specific manner. When collapsing across blocks, β-CMC was higher than baseline in the 1 Nm condition ($\beta = 0.03$, 95% CI = [0.01, 0.04], $p = .002$) but not in the 0.5 Nm condition ($p = .285$). Averaged across each

condition, this difference was evident during extension (β = −0.04, 95% CI = [-0.06, -0.01], p = .014), with not in flexion (p = .899). Both within-session and global models confirmed a significant condition-by-direction interaction (p ≤ .005), indicating that perturbation amplitude altered the directional profile of β-CMC during movement rather than its overall level.

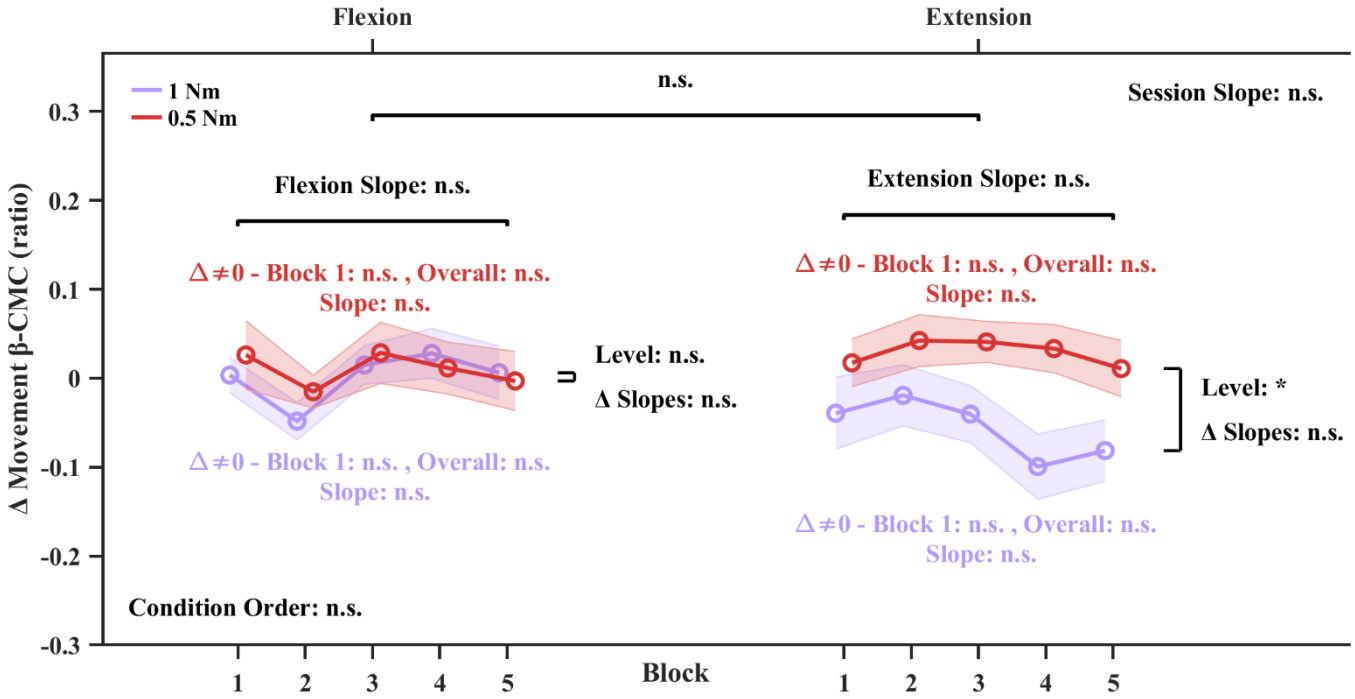

Figure 4.46. Change from baseline β-CMC (ratio) across experimental blocks for flexion (left) and extension (right) following high-amplitude (purple) and low-amplitude (red) perturbation conditions. Full plot description - Figure 4.45.

Across cohorts, β-CMC during voluntary movement was therefore not characterised by baseline shifts or progressive adaptation with practice. Instead, corticospinal coupling was modestly and selectively shaped by task context in a direction-dependent manner, with temporal predictability and perturbation amplitude influencing extension-related β-CMC. These findings suggest that β-CMC during voluntary movement reflects stable, context-specific control strategies rather than learning-related changes.

4.5.6. Does Stabilisation Phase Beta Corticomuscular Coherence Carryover into Movement?

Across both cohorts, the relationship between stabilisation phase β-CMC and subsequent movement β-CMC was characterised by a clear dominance of between-participant effects and a strong dependence on movement direction, with only weak and context-specific modulation by task structure.

In the temporal predictability cohort, average stabilisation β-CMC reliably predicted movement β-CMC (β = 2.18, 95% CI = [0.03, 4.32], p = .047), whereas within-participant variability did not (p = .362). The mean β-CMC carryover was highly asymmetric with a strong directional differences (β = -2.19, 95% CI = [-3.58, -0.81], p = .002) showing that the stabilisation-movement linkage was expressed almost exclusively during extension (**Figure 4.47B**). Simple slope analysis confirmed robust positive associations in extension under both predictable (β = 3.64, 95% CI = [0.59, 6.69], p = .019) and uncertain conditions (β = 5.09, 95% CI = [1.89, 8.30], p = .002), with no corresponding effects in flexion (p ≥ .797). Importantly, temporal predictability did not modulate this relationship (p = .439), indicating that the carryover reflected a stable individual property rather than a strategic response to uncertainty.

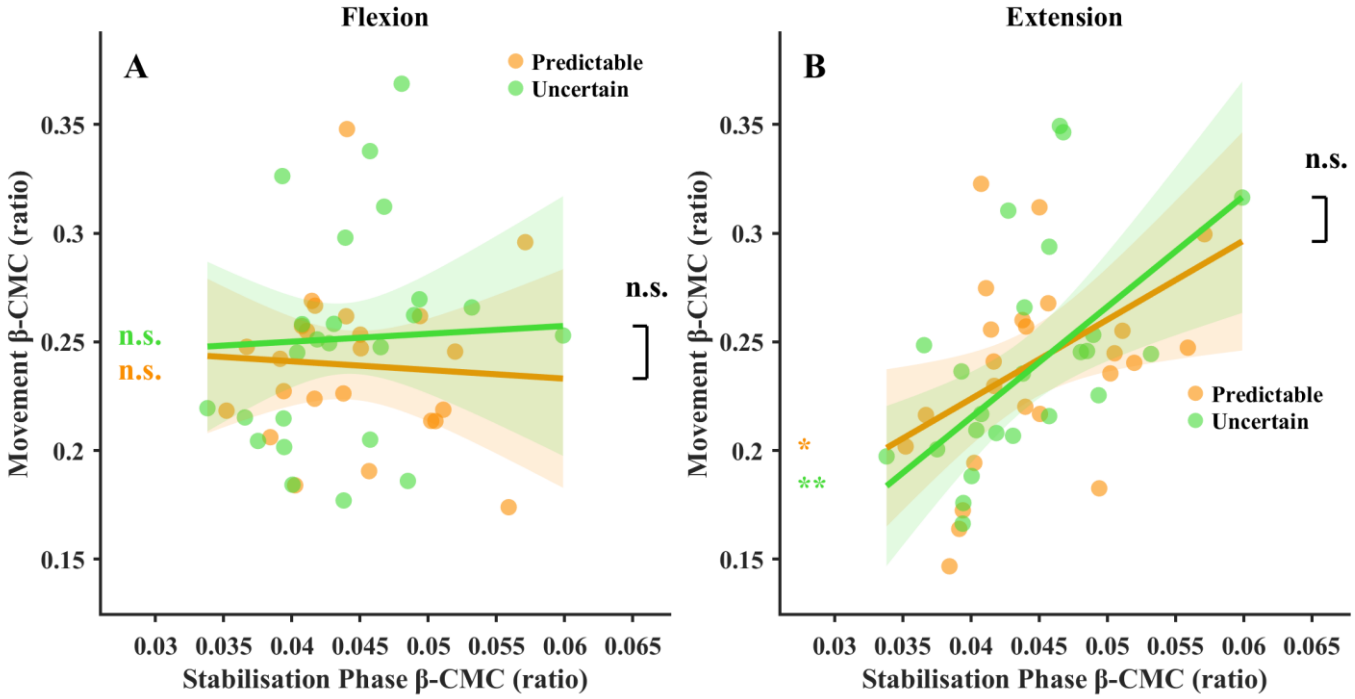

Figure 4.47. Between-participant relationship between stabilisation phase beta corticomuscular coherence (β-CMC) and voluntary movement beta corticomuscular coherence (β-CMC) for (A) flexion and (B) extension. Each point represents an individual participant's mean level for a given condition (predictable, orange; uncertain, green). Solid lines depict condition-specific model fits, with shaded bands indicating the corresponding 95% confidence intervals. Asterisks adjacent to the axes denote the statistical significance of the respective model fits, while brackets indicate comparisons between fits. Scatter points reflect raw between-participant means and do not account for additional model coefficients, which may result in a visual mismatch between the fitted lines and the distribution of points. Significance codes: * p < 0.05, ** p < 0.01, *** p < 0.001; n.s., not significant.

The amplitude cohort exhibited a similar but less robust pattern. Neither the between-participant nor within-participant effects of mean β-CMC reached conventional significance (between-participant: β = 1.38, 95% CI = [−0.06, 2.83], p = .060; within-participant: β = 1.70, 95% CI = [−0.10, 3.50], p = .064), potentially reflecting reduced statistical power due to the smaller sample size in this cohort. As in the temporal predictability cohort, direction critically modulated the effect: a significant interaction between movement direction and mean β-CMC (β = −1.14 , 95% CI = [−2.14, −0.13], p = .026) indicated that any carryover was again restricted to extension. Simple-slope analyses confirmed a positive effect of mean β-CMC during extension at the lower load (β = 3.31, 95% CI = [1.10, 5.51], p = .003, **Figure 4.48A**), with no reliable effects observed in flexion (p ≥ .766, **Figure 4.48B**). The within-participant slope for the low-amplitude condition approached significance (β = 3.19, 95% CI = [−0.57, 6.95], p = .096), whereas all other condition- and direction-specific within-participant associations were weak and non-significant (p ≥ .251).

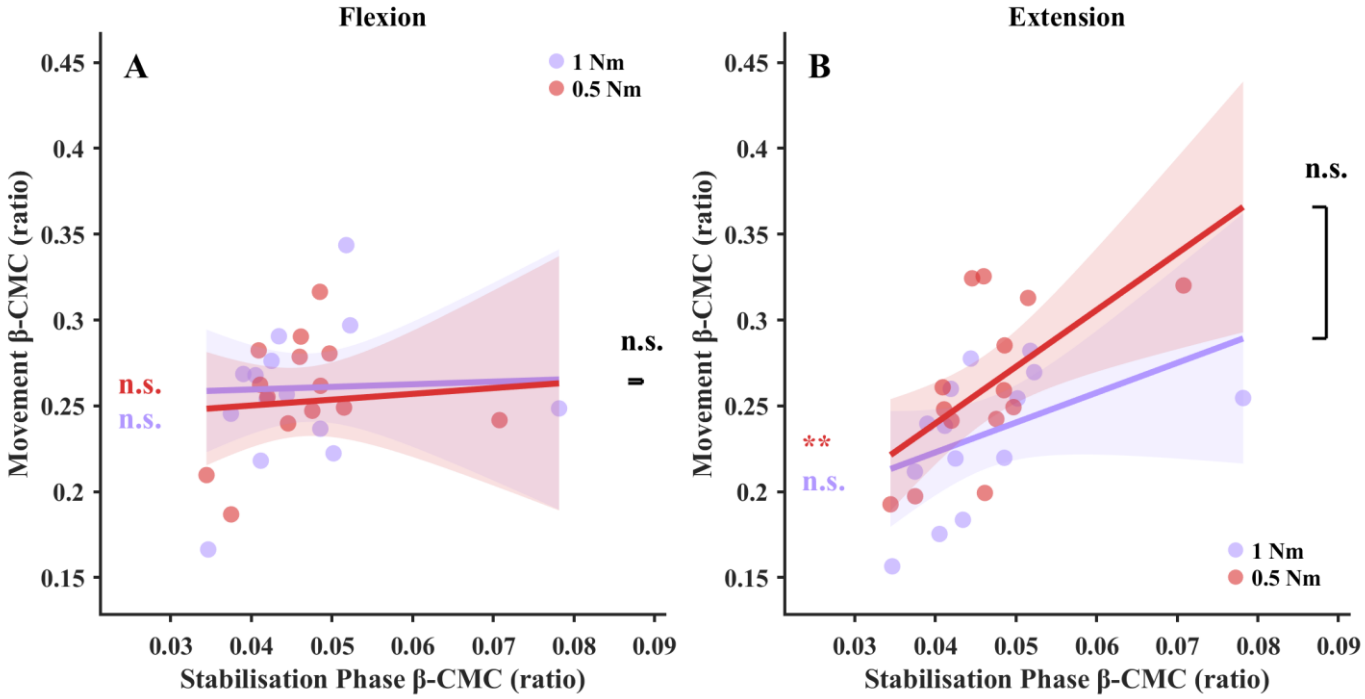

Figure 4.48. Between-participant relationship between stabilisation phase beta corticomuscular coherence (β-CMC) and voluntary movement beta corticomuscular coherence (β-CMC) for (A) flexion and (B) extension. Full plot description Figure 4.47.

Across cohorts, the relationship between stabilisation and movement β-CMC was driven primarily by stable between-participant differences and was strongly direction dependent, with minimal modulation by task structure. In the temporal predictability cohort, higher stabilisation β-CMC reliably predicted higher movement β-CMC during extension only, independent of temporal uncertainty, indicating a trait-like carryover rather than a strategic response. The amplitude cohort showed a similar but weaker pattern, again confined to extension and most evident at low load, likely reflecting reduced power. Together, these results suggest that stabilisation-related β-CMC establishes a persistent, direction-specific control state that shapes subsequent movement execution.

4.5.7. Do Levels of Movement Beta Corticomuscular Coherence Impact Voluntary Movement Dynamics?

Across both experimental cohorts, there were no significant main effects relating to interactions between movement-related β-CMC and reaction times (RTs). This was not the case, however, for the relationship between movement β-CMC and movement duration.

β-CMC showed a robust relationship with overall movement duration that was modulated by task condition and movement direction. Critically, stronger β-CMC was associated with shorter movement durations both between-participants ($\beta = -3.63$, 95% CI = [−4.81, −2.46], $p < .001$) and within-participants across blocks ($\beta = -0.94$, 95% CI = [−1.31, −0.57], $p < .001$). The between-participant relationship was further modulated by condition ($\beta = -1.05$, 95% CI = [−1.71, −0.38], $p = .002$) and direction ($\beta = 1.02$, 95% CI = [0.25, 1.78], $p = .009$), indicating stronger negative coherence–duration coupling under predictable dynamics and during extension movements.

Direction- and condition-specific slope analyses confirmed this pattern. At the between-participant level, higher β-CMC predicted shorter movements for both conditions and directions, with particularly steep associations during extension under predictable dynamics ($\beta = -5.85$, 95% CI = [−7.51, −4.18], $p < .001$, **Figure 4.49B**) and a significant slope divergence between predictable and uncertain conditions ($\beta = 2.40$, 95% CI = [0.49, 4.30], $p = .014$). Flexion movements showed similarly negative slopes in

both conditions (p ≤ .047), with a nonsignificant divergence (p = .060, **Figure 4.49A**). Within-participant analyses also revealed negative coherence-duration relationships across conditions, reaching significance in flexion for both predictable (β = −1.24, 95% CI = [−2.11, −0.37], p = .006) and uncertain dynamics (β = −0.87, 95% CI = [−1.60, −0.14], p = .020), and in extension under uncertain dynamics (β = −1.10, 95% CI = [−1.77, −0.43], p = .001), with no reliable slope divergences (p ≥ .234).

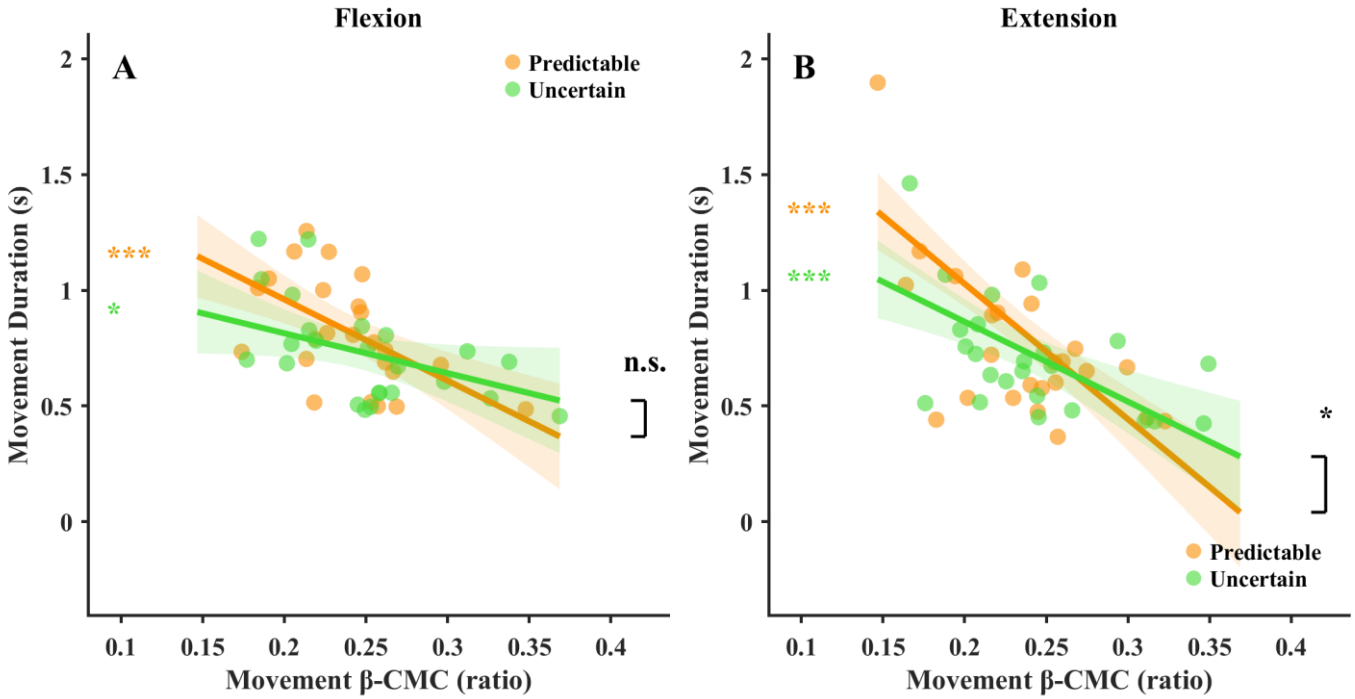

Figure 4.49. Between-participant relationship between movement beta corticomuscular coherence (β-CMC) and voluntary movement duration (s) for (A) flexion and (B) extension. Full plot description Figure 4.47.

In the perturbation amplitude cohort, movement β-CMC was again robustly related to overall movement duration; however, unlike the temporal predictability cohort, this relationship was not modulated by perturbation amplitude or movement direction at the model level (**Figure 4.50**). Critically, higher β-CMC was associated with shorter movement durations both between-participants (β = −1.91, 95% CI = [−2.92, −0.89], p < .001) and within-participants across trials (β = −1.03, 95% CI = [−1.44, −0.61], p < .001), indicating a stable negative coherence-duration relationship that was not influenced by perturbation amplitude.

Direction- and condition-specific slope analyses were consistent with this pattern. At the between-participant level, higher β-CMC predicted shorter movements across both perturbation levels and directions, with significant negative slopes for flexion at 1 Nm (β = −2.18, 95% CI = [−4.16, −0.20], p = .031) and 0.5 Nm (β = −2.39, 95% CI = [−4.43, −0.34], p = .022), and for extension at 1 Nm (β = −1.64, 95% CI = [−3.19, −0.09], p = .038). No slope divergences between amplitude conditions were detected (p ≥ .824). Within participants, negative coherence-duration relationships were also evident, reaching significance for flexion at 1 Nm (β = −1.42, 95% CI = [−2.35, −0.48], p = .003) and for extension at 0.5 Nm (β = −1.41, 95% CI = [−2.18, −0.64], p < .001), with no reliable divergences between perturbation amplitudes (p ≥ .184). Overall, these findings indicate that while stronger beta β-CMC consistently predicts shorter movement durations, this relationship is largely invariant to perturbation amplitude and movement direction.

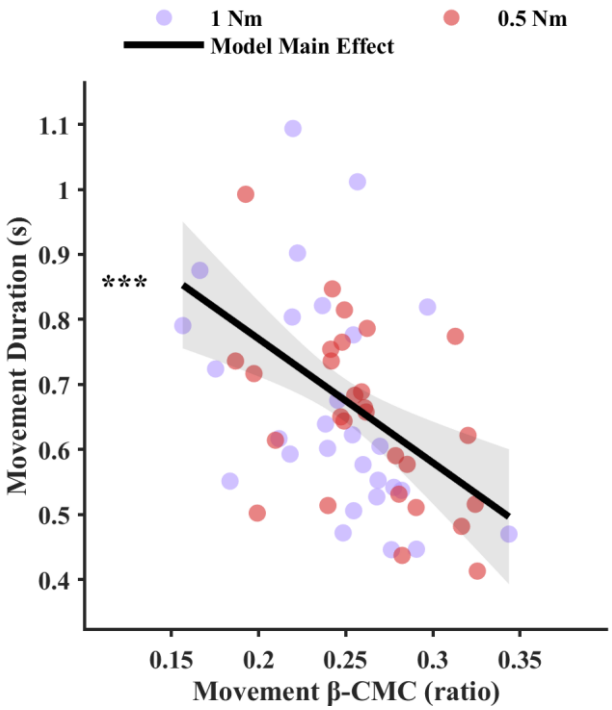

Figure 4.50. Between-participant relationship between movement beta corticomuscular coherence (β-CMC) and voluntary movement duration (s) across movement directions. Full plot description Figure 4.47.

Across both cohorts, movement-related β-CMC showed a robust and consistent negative relationship with overall movement duration, such that higher coherence was associated with faster, more temporally efficient movements. This effect was evident both between-participants and within-participants across task blocks, indicating that β-CMC captures stable individual differences in motor execution as well as transient fluctuations in performance. In both cohorts, baseline coherence strongly predicted task coherence, supporting the interpretation that individual beta coupling strength reflects a trait-like characteristic that carries over into task performance.

Despite this shared core relationship, the way β-CMC interacted with task context differed across cohorts. In the temporal predictability cohort, coherence-duration coupling was clearly modulated by task demands and movement direction: predictable dynamics strengthened the negative association between coherence and movement duration, particularly during extension movements, and produced significant slope divergences between predictable and uncertain conditions. This pattern suggests that β-CMC is sensitive to the availability of temporal structure in the task, with stronger coherence potentially reflecting more effective engagement of corticospinal control when upcoming dynamics can be anticipated. In contrast, in the perturbation amplitude cohort, coherence-duration relationships were largely invariant to perturbation amplitude and movement direction, with no reliable condition-level modulation or slope divergence. Together, these findings indicate that β-CMC primarily indexes movement efficiency, but that its functional role is selectively shaped by higher-order task structure rather than by changes in perturbation amplitude alone.

4.5.8. Does Stabilisation Phase Beta Corticomuscular Coherence Predict Voluntary Movement Dynamics?

In the temporal predictability cohort, stabilisation phase β-CMC robustly predicted reaction time (RT) at both the between- and within-participant levels. At the between-participant level, higher average stabilisation phase β-CMC was associated with faster RTs (β = −3.16, 95% CI = [−5.26, −1.06], p = .003). This relationship was significantly moderated by predictability, with a stronger negative association in predictable trials (β = −1.39, 95% CI = [−1.99, −0.79], p < .001). Follow-up slope analyses confirmed robust negative slopes under the predictable condition for both flexion and extension (p ≤ .001), whereas corresponding slopes under uncertainty were not significant (p ≥ .097). Slope divergence between predictable and uncertain conditions was significant for both movement directions (p ≤ .004, **Figure 4.51**).

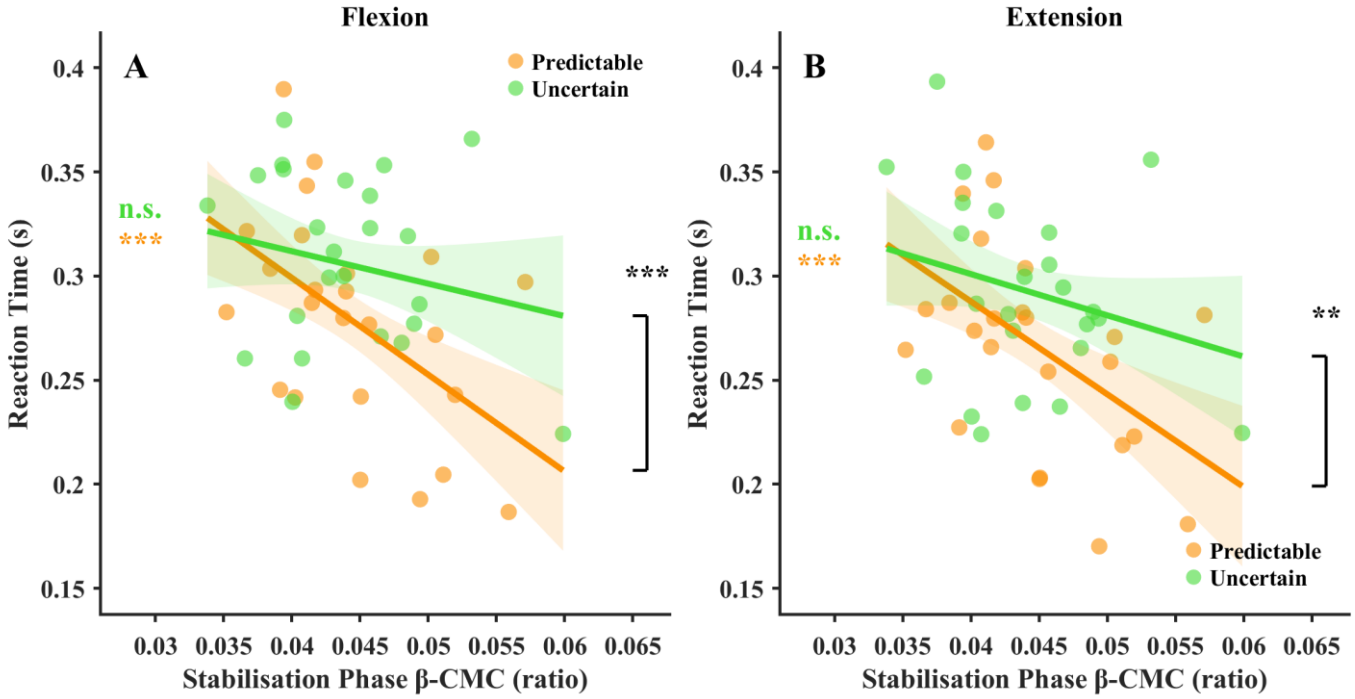

Figure 4.51. Between-participant relationship between stabilisation phase beta corticomuscular coherence (β-CMC) and voluntary movement reaction time (s) for (A) flexion and (B) extension. Full plot description Figure 4.47.

At the within-participant level, block-to-block increases in stabilisation phase β-CMC were also associated with faster RTs, as indicated by a significant negative main effect (β = −0.89, 95% CI = [−1.52, −0.25], p = .006). This effect did not significantly vary with predictability condition (p = .268). Direction-specific analyses showed limited evidence for condition-dependent modulation, with only the predictable-extension slope reaching significance (p = .021); all other slopes and slope divergences were not significant (p ≥ .134).

In contrast, the perturbation amplitude cohort showed no consistent evidence that stabilisation phase β-CMC predicted RT. At the between-participant level, the main effect was not significant (p = .593), although it interacted with amplitude condition (β = −0.47, 95% CI = [−0.84, −0.10], p = .014). Despite this interaction, follow-up slope analyses revealed no significant relationships within individual perturbation amplitude or direction conditions (p ≥ .357), except for a significant slope divergence for extension between load levels (p = .007). At the within-participant level, neither the main effect for within-participant change nor its interaction with amplitude condition was significant (p ≥ .487), and all direction-specific slopes and divergences were non-significant (p ≥ .187).

For movement duration in the temporal predictability cohort, there was limited evidence for a systematic association with stabilisation phase β-CMC. At the between-participant level, the main effect of mean β-CMC was not significant (p = .180); however, it interacted with movement direction (β = 5.75, 95% CI = [1.65, 9.86], p = .006). Follow-up analyses indicated that under extension in the predictable condition, higher average β-CMC was associated with shorter movement durations (β = −19.95, 95% CI = [−36.78, −3.11], p = .020), whereas the corresponding slope under uncertainty was not significant (p = .149). No reliable relationships were observed for flexion (p ≥ .442), and slope divergence between conditions was not significant for either direction (p ≥ .202). At the within-participant level, neither the main within-participant effect nor any interactions reached significance (p ≥ .292), and all direction- and condition-specific slopes were non-significant (p ≥ .129).

In the perturbation amplitude cohort, stabilisation phase β-CMC showed a modest but selective between-participant association with movement duration. Higher average β-CMC was associated with shorter movement durations, as indicated by a significant mean β-CMC main effect (β = −4.84, 95% CI = [−9.62, −0.05], p = .048). This effect did not reliably vary as a function of perturbation amplitude or movement direction at the interaction level (p ≥ .075). Follow-up slope analyses revealed that the negative association was evident under the high-amplitude condition (1 Nm) for both flexion and extension (p ≤ .046), whereas slopes under the low-amplitude condition were not significant (p ≥ .125, **Figure 4.52**). Slope divergence between perturbation conditions was not significant for either direction (p ≥ .097). At the within-participant level, there was no evidence that block-to-block fluctuations in stabilisation phase β-CMC predicted movement duration, with neither the main within-participant effect nor any interactions reaching significance (p ≥ .347).

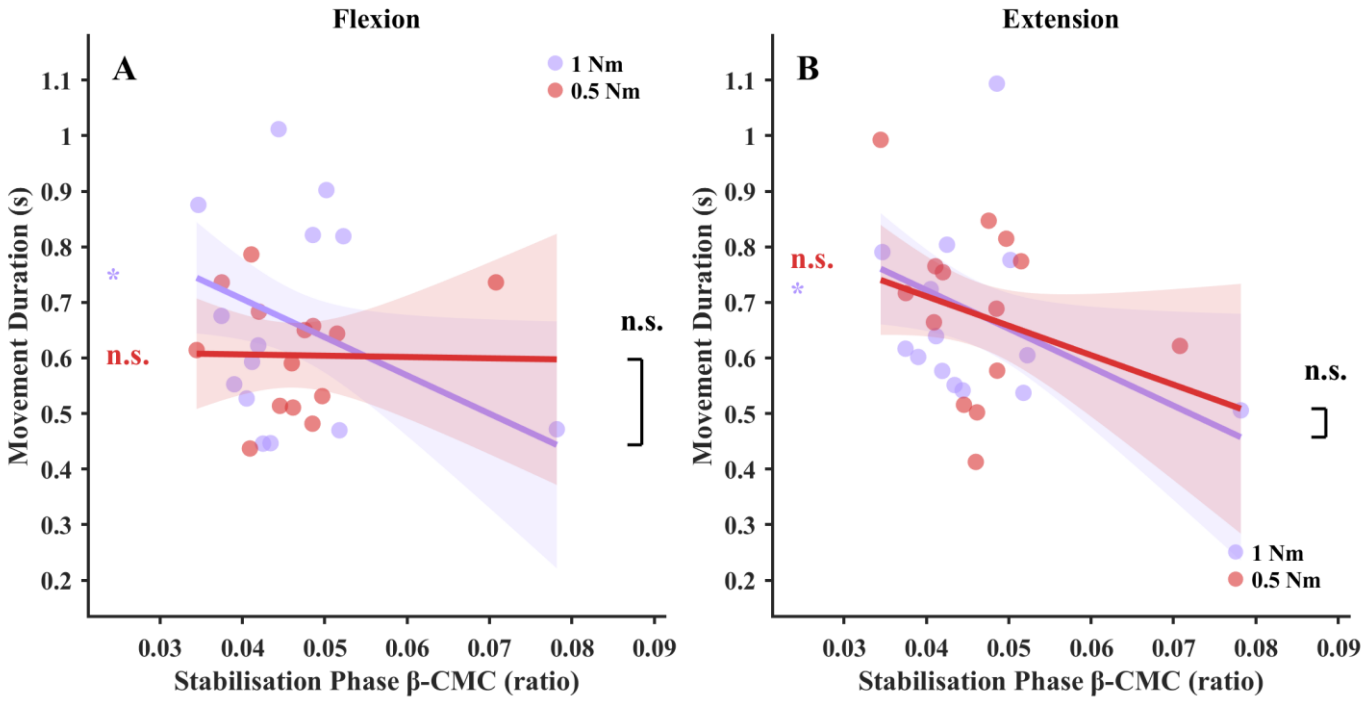

Figure 4.52. Between-participant relationship between stabilisation phase beta corticomuscular coherence (β-CMC) and voluntary movement reaction time (s) for (A) flexion and (B) extension. Full plot description Figure 4.47.

Across cohorts, stabilisation phase β-CMC was more consistently related to behaviour at the between-participant than within-participant level, suggesting it primarily reflects stable individual differences rather than trial-to-trial control processes. In the temporal predictability cohort, higher average β-CMC was associated with faster RTs, particularly under predictable conditions, indicating that stronger corticospinal coupling during stabilisation may support more efficient movement initiation when upcoming demands can be anticipated. The absence of comparable effects under uncertainty implies that the behavioural relevance of β-CMC is gated by task predictability.

Within-participant effects were weak and largely invariant across conditions, providing little evidence that momentary fluctuations in β-CMC drive block-to-block variability in performance. In the perturbation magnitude cohort, reaction time showed no reliable association with β-CMC, pointing to limited generalisability of initiation-related effects and sensitivity to task or sample characteristics.

Associations with movement duration were modest and context dependent. In the temporal predictability cohort, higher β-CMC predicted shorter movement durations only for extension movements under predictable conditions, whereas in the perturbation magnitude cohort this relationship emerged primarily under higher load. Together, these findings suggest that stabilisation phase β-CMC indexes a trait-like efficiency of sensorimotor integration whose behavioural impact becomes evident only under task conditions that emphasise anticipation or mechanical demand.

4.5.9. Post Movement Beta Rebound

Post-movement beta rebound (PMBR) was calculated within the 1 s following movement termination. Movement-related beta decreases were also examined but showed no consistent or significant effects in amplitude or timing and are therefore not reported. PMBR timing measures were likewise nonsignificant; accordingly, analyses focused exclusively on PMBR amplitude.

The temporal predictability cohort showed a clear and robust modulation of PMBR by task condition that was strongly shaped by movement direction, with no evidence for systematic learning across blocks. At the initial task block, nonparametric analyses revealed significant baseline-to-task decreases in PMBR under uncertain dynamics for both flexion ($p = .025$, $z = -2.24$, $r = -0.50$, **Figure 4.53A**) and extension ($p = .007$, $z = -2.67$, $r = -0.65$, **Figure 4.53B**), whereas movements following the temporally predictable condition only showed significant decrease in extension, and to a lesser extent than following the uncertain condition ($p = .030$, $z = -2.17$, $r = -0.48$, **Figure 4.53B**). Although several elevated baseline values were present in the uncertain condition, the use of a median-based Wilcoxon signed-rank test and the similarity of distribution medians suggest that the observed baseline-to-task effects are not driven by these extreme values. Despite these within-condition effects, changes from baseline did not differ significantly between conditions at the first block ($p \geq .272$), indicating that early PMBR increases were condition-specific but not statistically separable initially.

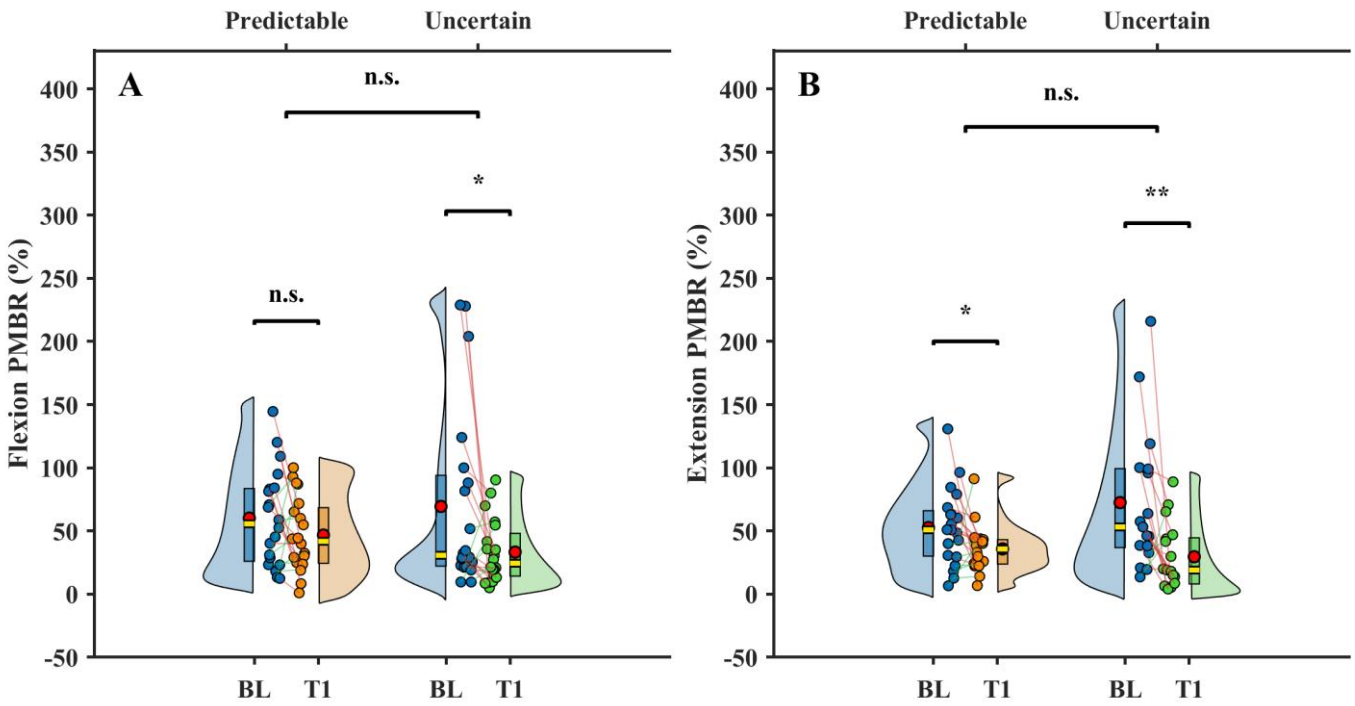

Figure 4.53. Contrasts in PMBR (%) between baseline blocks and initial task blocks for (A) flexion and (B) extension after temporally predictable (orange) and uncertain (green) perturbation conditions. BL = baseline, T1 = initial task block. Half-violin plots illustrate the distribution of individual participant values. Overlaid dots represent individual observations, with lines connecting paired measurements. Red circles indicate condition means and yellow horizontal lines indicate medians. Brackets denote statistical comparisons between associated BL and T1 groups, with an additional contrast between BL-T1 pairings. Significance codes: * p < 0.05, ** p < 0.01, *** p < 0.001; n.s., not significant.

Although the difference between conditions was not initially significant in supplementary nonparametric tests, mixed-effects modelling demonstrated that separation between conditions was substantially more robust across the session. The overall condition effect indicated that PMBR was significantly suppressed following the temporally uncertain condition relative to the predictable condition (β = −11.83, 95% CI = [−22.00, −1.67], p = .023). This effect was particularly pronounced during extension voluntary movements (β = −19.11, 95% CI = [−33.45, −4.77], p = .009, **Figure 4.54**) but was nonsignificant during flexion movements (p = .380). Despite these changes in the significance of condition effects, no impact of task block was detected at either the model level (p = .520) or the individual condition–direction level (p ≥ .222). Differences by movement direction did not reach significance but showed a robust trend, with PMBR being more strongly reduced following exposure to temporally uncertain stabilisation challenges (β = −5.12, 95% CI = [−10.73, 0.49], p = .074). Condition order exerted a strong main effect (β = 22.26, 95% CI = [15.22, 29.30], p < .001), which was significantly modulated by condition (β = −12.08, 95% CI = [−23.00, −1.16], p = .030).

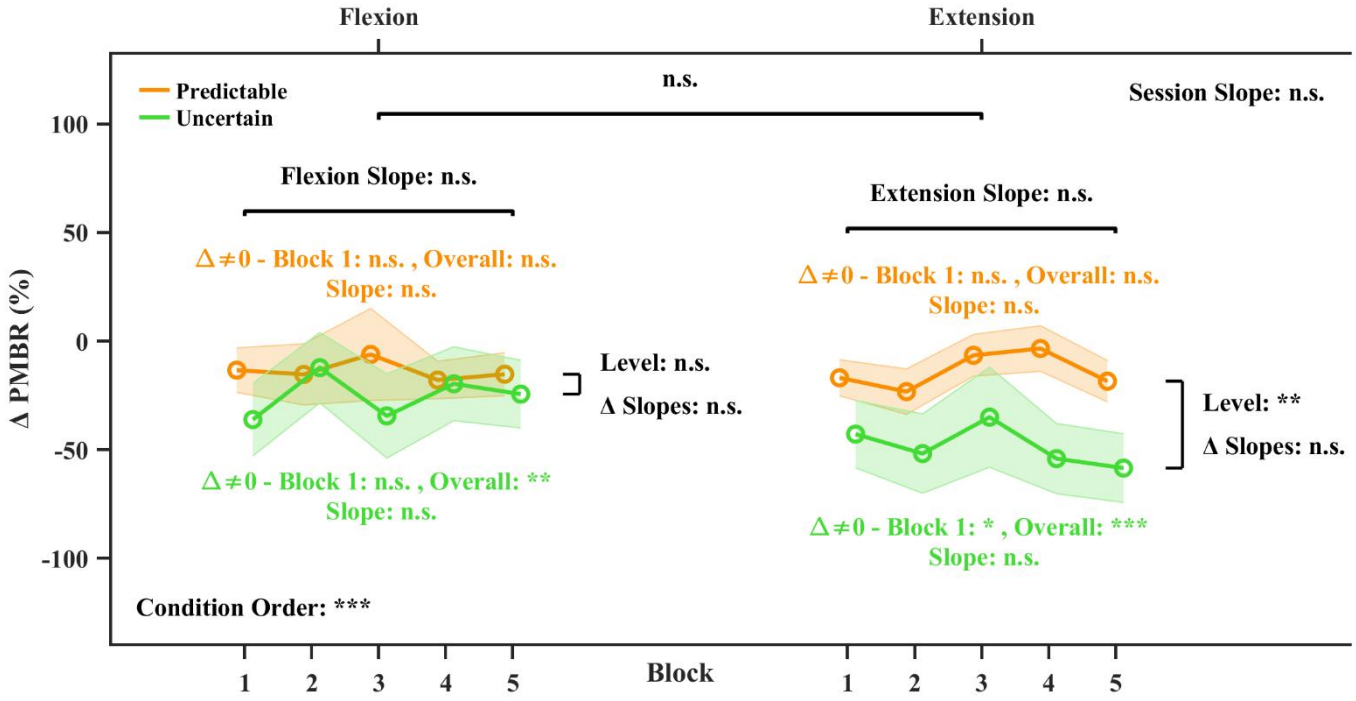

Figure 4.54. Change from baseline PMBR (%) across experimental blocks for flexion (left) and extension (right) following temporally predictable (orange) and uncertain (green) perturbation conditions. Full plot description - Figure 4.45.

Within the perturbation amplitude cohort, PMBR differed reliably by movement direction but not by condition ($p = .107$) or task block ($p = .415$). Flexion movements were associated with substantially less reduction in PMBR amplitude overall ($\beta = 21.26$, 95% CI = [12.91, 29.61], $p < .001$, **Figure 4.55**), an effect that was also evident within each condition individually ($p \leq .001$). No evidence of adaptation in PMBR amplitude was detected at any level ($p \geq .914$), resulting in nonsignificant condition contrasts ($p \geq .526$) and no differences in the rate of change across conditions ($p \geq .352$). No consistent or significant global effects were observed for condition order, switching effects, or task block count across the session ($p \geq .144$).

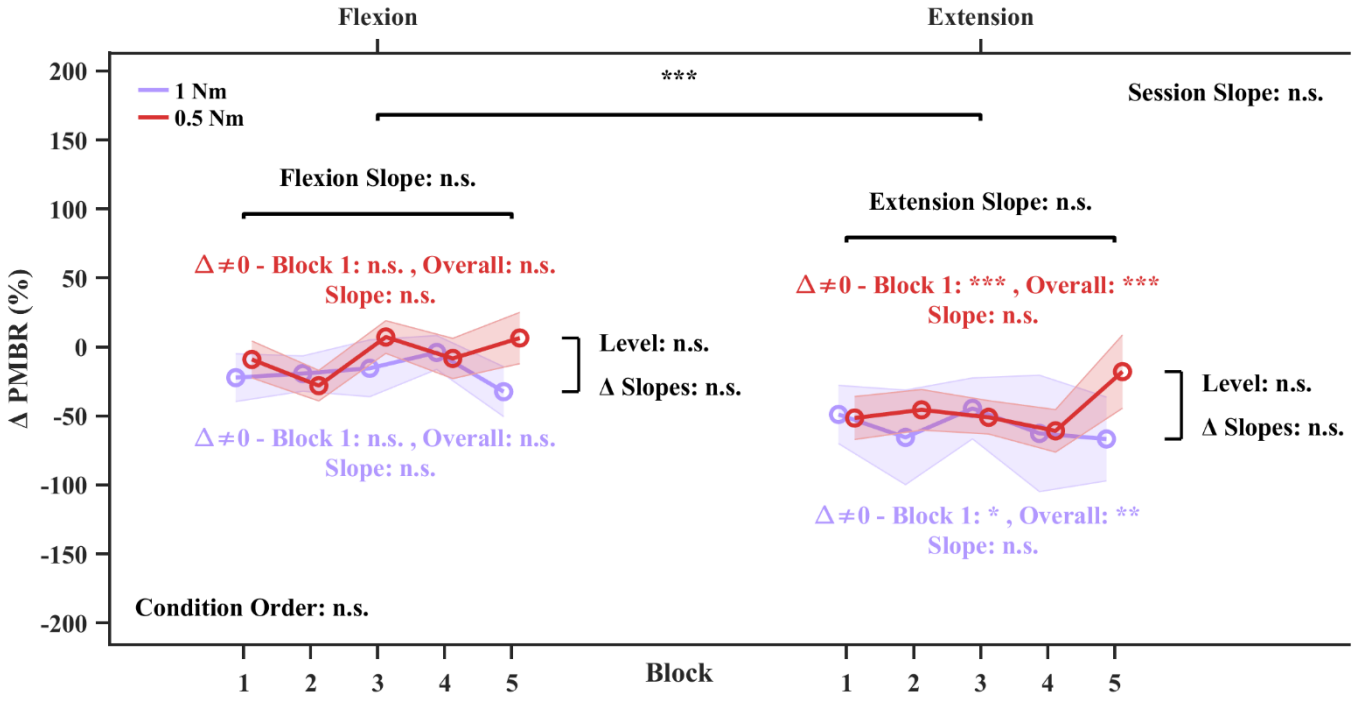

Figure 4.55. Change from baseline PMBR (%) across experimental blocks for flexion (left) and extension (right) following high-amplitude (purple) and low-amplitude (red) perturbation conditions. Full plot description - Figure 4.45.

As an additional qualitative analysis, grand-average PMBR plots were generated across all valid trials and participants, separated by condition (**Figure 4.56**). Across both cohorts, the grand-average time courses exhibited a consistent, stereotyped PMBR response: activity decreased below baseline during movement execution, reached a pronounced negative trough near movement termination, and was followed by a robust post-movement rebound peaking several hundred milliseconds after termination. In the perturbation-amplitude cohort, the low-amplitude (0.5 Nm) and high-amplitude (1 Nm) traces overlapped closely across the full time course, with only minor amplitude differences, indicating broadly similar PMBR dynamics across perturbation amplitudes. In the temporal predictability cohort, predictable and uncertain conditions showed the same overall temporal profile; however, the predictable condition displayed a visibly larger post-movement rebound, whereas the uncertain condition appeared more attenuated and prolonged. Overall, these qualitative dynamics closely mirror those observed in the main analyses and further validate the analytical approach, demonstrating that PMBR responses are temporally consistent and condition-modulated in amplitude while occurring well within the 1 s post-termination analysis window.

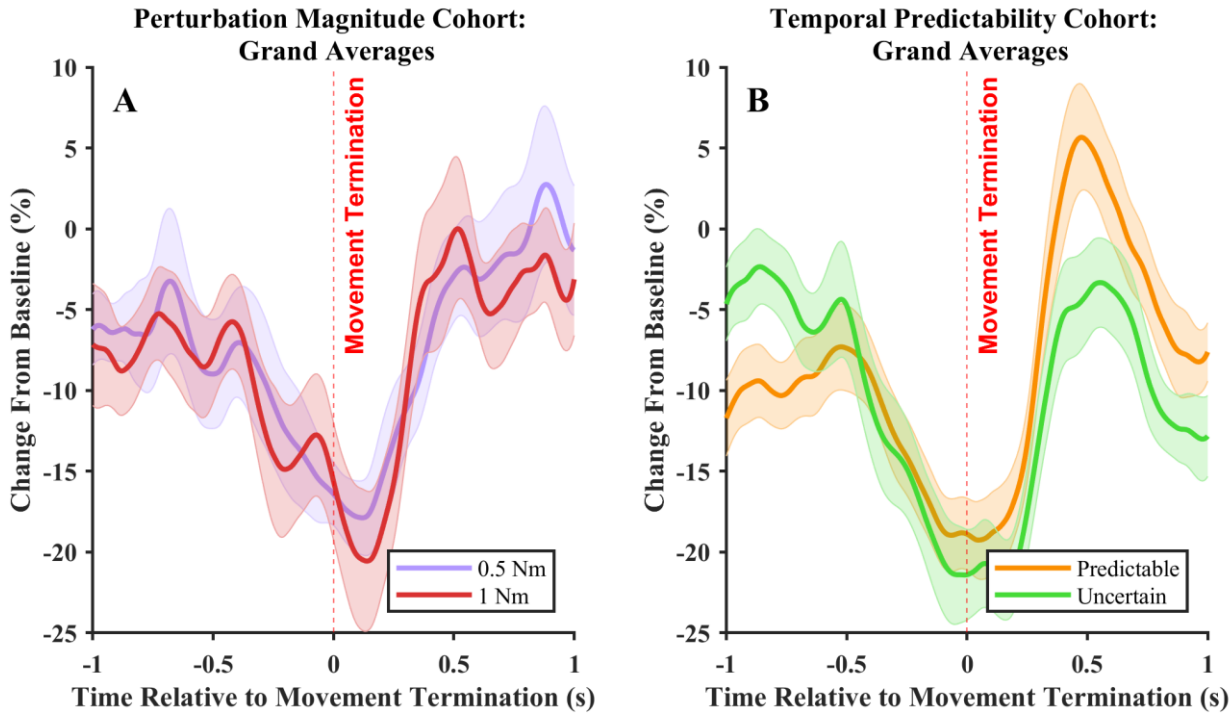

Figure 4.56. Cohort-wide grand average plots of the beta power around movement termination for the (A) perturbation amplitude cohort and (B) the temporal predictability cohort.

Across both cohorts, PMBR provided a robust and temporally well-defined marker of post-movement cortical processing, whereas movement-related beta decreases and PMBR timing measures did not show reliable effects. Focusing on PMBR amplitude within the 1 s post-termination window therefore captured the dominant and behaviourally relevant beta-band modulation. In the temporal predictability cohort, PMBR was strongly shaped by task context and movement direction: preceding temporally uncertain dynamics consistently suppressed PMBR relative to predictable dynamics, with the effect most pronounced during extension movements. While early nonparametric comparisons revealed condition-specific baseline-to-task changes that were not yet separable between conditions, mixed-effects modelling demonstrated that this separation emerged robustly across the session, indicating a stable contextual modulation rather than short-lived or block-specific effects. Notably, the absence of learning- or block-related effects suggests that PMBR primarily reflected ongoing task demands and sensorimotor uncertainty rather than gradual adaptation.

In contrast, the perturbation amplitude cohort showed no evidence that PMBR amplitude scaled with perturbation amplitude condition, despite clear directional modulation. Flexion movements were consistently associated with less PMBR reduction than extension across both torque levels, and neither practice nor rate-of-change effects were observed. Together with the qualitative grand-average waveforms, these results suggest that PMBR is more sensitive to the task structure and temporal predictability of sensorimotor demands than to perturbation amplitude directly. The close correspondence between qualitative and quantitative findings further supports the validity of the analytical approach and confirms that PMBR dynamics are stable, directionally tuned, and selectively modulated by task context within a well-contained post-movement temporal window.

4.5.10. Does Post Movement Beta Rebound Amplitude Reflect Voluntary Movement Dynamics?

While robust condition-based modulation of PMBR amplitude was present in each experimental cohort, it was necessary to assess whether these amplitudes encoded aspects of the preceding voluntary movement dynamics in terms of reaction time (RT) and overall movement duration.

In the temporal predictability cohort, mean RT showed a negative, trend-level association with PMBR, such that participants with slower average RTs tended to exhibit reduced PMBR amplitude (β = −100.77, 95% CI = [−220.76, 19.22], p = .099). This relationship was not modulated by predictability, movement direction, or block progression (p ≥ .204), and simple slopes were consistently negative but non-significant across contexts and directions (p ≥ .074).

Within-participant RT variability showed no overall association with PMBR amplitude (β = 38.98, 95% CI = [−62.74, 140.70], p = .452), nor reliable modulation by predictability, direction, or block (p ≥ .097). However, planned slope analyses revealed a selective effect: during flexion movements in the predictable condition, slower-than-usual RTs were associated with larger PMBR amplitude (β = 235.18, 95% CI = [24.28, 446.08], p = .029, **Figure 4.57A**). This coupling was absent under temporal uncertainty (p = .878), with no significant slope divergence between conditions (p = .118), and no within-participant RT–PMBR relationships were observed for extension movements (p ≥ .542, **Figure 4.57B**).

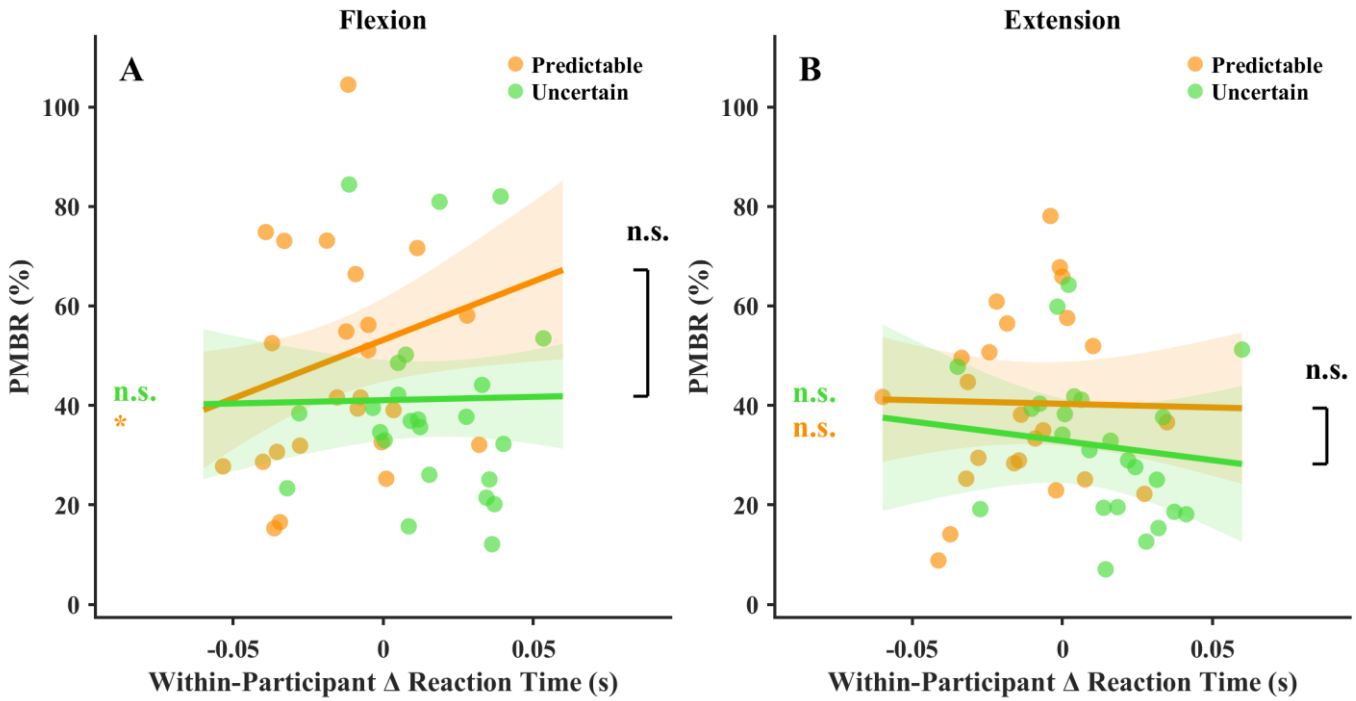

Figure 4.57. Within-participant relationship between change in voluntary movement reaction time (s) and PMBR amplitude (%) for (A) flexion and (B) extension. Full plot description Figure 4.47.

In the perturbation amplitude cohort, neither mean RT nor within-participant RT variability was associated with PMBR amplitude. The between-participant RT effect (β = −85.55, 95% CI = [−285.92, 114.82], p = .401) and within-participant RT effect (β = 56.08, 95% CI = [−150.63, 262.79], p = .593) were non-significant, and neither was modulated by perturbation amplitude, movement direction, or block progression (p ≥ .185). Simple-slope analyses similarly showed no reliable RT–PMBR relationships across perturbation amplitudes or directions (p ≥ .108), indicating an absence of both trait-like and state-dependent RT effects in this cohort.

Movement duration was likewise decomposed into between- and within-participant components. In the temporal predictability cohort, neither mean movement duration nor within-participant duration variability showed a main effect on PMBR amplitude (between-participant: β = 13.29, 95% CI = [−9.69, 36.27], p = .256; within-participant: β = 9.69, 95% CI = [−5.70, 25.07], p = .217), and these null effects were not modulated by predictability, direction, or block (p ≥ .117). Consistent with this, between-participant slopes were non-significant across contexts and directions (p ≥ .168). As with RT, a selective within-participant effect emerged: during predictable flexion movements, longer-than-usual movement durations were associated with larger PMBR amplitude (β = 39.12, 95% CI = [4.78, 73.47], p = .026, **Figure 4.58A**). This effect was absent under temporal uncertainty (p = .936), with no significant slope divergence (p = .112), and no effects were observed for extension movements (p ≥ .697, **Figure 4.58B**).

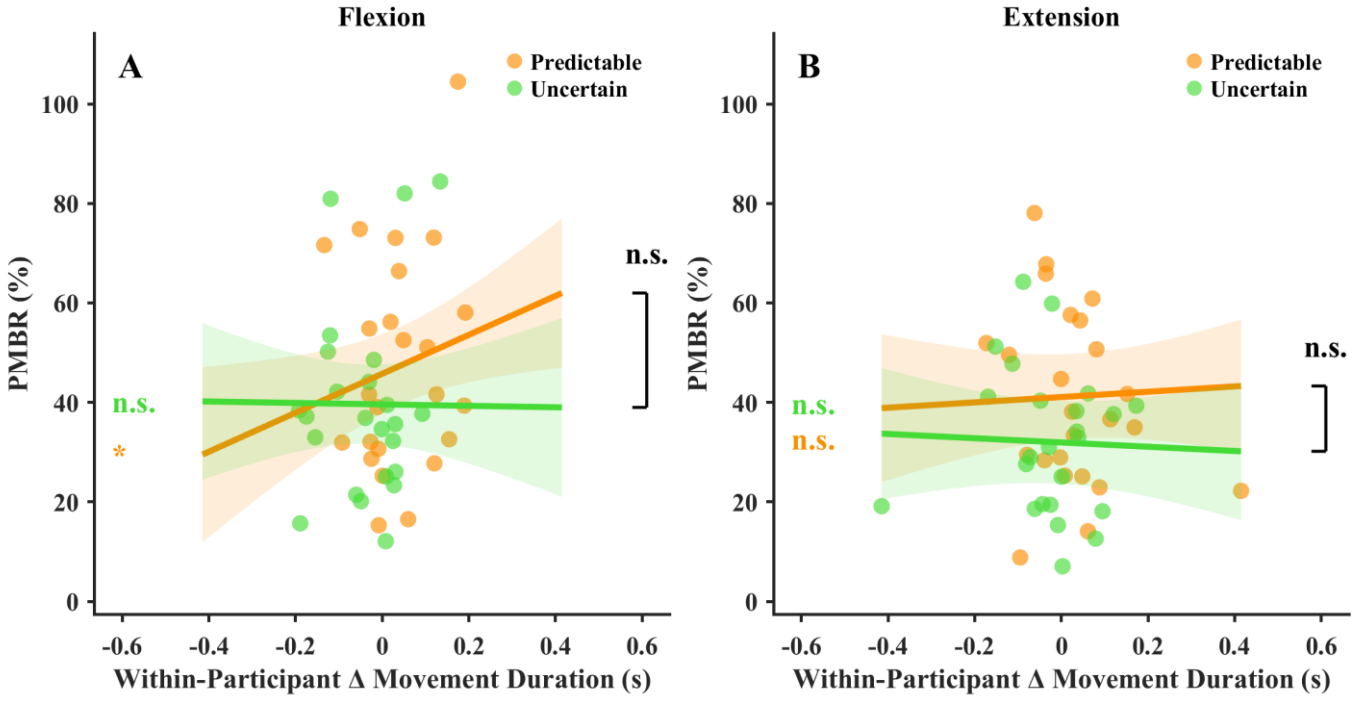

Figure 4.58. Within-participant relationship between change in voluntary movement duration (s) and PMBR amplitude (%) for (A) flexion and (B) extension. Full plot description Figure 4.47.

In the perturbation amplitude cohort, movement duration showed no relationship with PMBR amplitude at either the between- or within-participant level. The between-participant effect (β = −0.46, 95% CI = [−52.57, 51.64], p = .986) and within-participant effect (β = 4.09, 95% CI = [−19.87, 28.05], p = .737) were effectively null, with no modulation by perturbation amplitude, movement direction, or block (p ≥ .085). Simple-slope analyses confirmed the absence of movement duration effects across all conditions and directions (p ≥ .277), with no evidence for slope divergence (p ≥ .322).

Across both cohorts, PMBR amplitude showed limited and highly context-dependent relationships with voluntary movement dynamics. Between participants, neither RT nor movement duration reliably predicted PMBR, with only weak, non-significant trends observed in the temporal predictability cohort and no evidence of such effects when perturbation amplitude was manipulated. This suggests that stable individual differences in movement speed are not a dominant determinant of PMBR expression.

In contrast, selective within-participant effects emerged under conditions of high temporal predictability. Block-to-block increases in RT and movement duration were associated with larger PMBR amplitude during predictable flexion movements, an effect that was absent under temporal uncertainty and did not generalize to extension movements. The restriction of these effects to predictable contexts suggests that PMBR is sensitive to state-dependent variations in motor engagement or evaluative processing when stabilisation challenges can be reliably anticipated, rather than reflecting movement

kinematics. The absence of comparable effects in the perturbation amplitude cohort further indicates that PMBR–behaviour coupling depends more on temporal structure than on perturbation intensity. Overall, these findings support an interpretation of PMBR as reflecting post-movement state updating that is selectively engaged when task timing is predictable, rather than a general consequence of movement execution dynamics.

4.5.11. Summary

Across this section, beta-band activity was treated as a stability-oriented control signal that supports impedance regulation and resists state changes, making it a plausible mechanism for managing stability–movement transitions. Consistent with this framing, stabilisation elicited a large, immediate suppression of β-CMC from baseline that was highly stable across blocks and showed little evidence of adaptation (**Figure 4.42**, **Figure 4.43**). Despite this robustness, β-CMC was not fully invariant to task structure: temporally uncertain perturbations reliably produced less suppression than predictable perturbations, while perturbation amplitude had minimal influence on overall stabilisation β-CMC. Relationships with co-contraction further indicated that β-CMC primarily reflected state-dependent engagement of stabilising control rather than tonic stiffness: mean CCI did not predict mean β-CMC, but within-participant increases in CCI tended to coincide with higher β-CMC, most consistently under temporal uncertainty and, for amplitude manipulations, mainly at higher load (**Figure 4.44**).

During voluntary movement, β-CMC showed no consistent baseline shift during the initial task block and little learning across blocks, but it was modestly shaped by context in a direction-dependent way, with effects most evident during extension (**Figure 4.45**, **Figure 4.46**). Stabilisation-to-movement carryover was dominated by between-participant differences and was again strongly extension-specific (**Figure 4.47**, **Figure 4.48**), suggesting a persistent, direction-tuned coupling profile that individuals bring into both phases rather than a purely strategic, condition-dependent adjustment. Behaviourally, movement β-CMC showed a robust negative relationship with movement duration across cohorts - higher coupling predicted shorter movements both between and within participants, supporting the idea that β-CMC indexes movement efficiency. In contrast, stabilisation phase β-CMC predicted faster RTs mainly in the temporal predictability cohort, with the strongest effects under predictable dynamics (**Figure 4.51**), implying that any initiation benefit is gated by temporal structure and does not generalise straightforwardly to amplitude manipulations.

PMBR provided a clear post-movement marker whose amplitude (but not timing) was strongly modulated by temporal uncertainty - suppressed following uncertain perturbation dynamics, especially for extension (**Figure 4.54**) - while showing little sensitivity to perturbation amplitude aside from directional differences (**Figure 4.55**). PMBR- behaviour relationships were largely null at the between-participant level and only selectively present within participants under predictable flexion (**Figure 4.57**), suggesting PMBR reflects context-dependent post-movement updating rather than movement timing.

Across all explored dynamics, two organising principles emerge. First, beta-band coupling contains a substantial trait-like component (baseline predicting task β-CMC; stabilisation-to-movement carryover; stronger between- than within-participant effects), implying stable individual differences in beta-mediated sensorimotor integration. Second, temporal predictability repeatedly shaped beta dynamics and their behavioural relevance more than perturbation amplitude, modulating stabilisation β-CMC suppression, gating links to RT, strengthening coherence–duration coupling, and suppressing PMBR under uncertainty. Overall, beta-band measures appear tuned not only to impedance dynamics but also to the predictability of prior sensorimotor events: β-CMC most consistently indexed efficient corticospinal engagement and state regulation when stabilisation structure was predictable, whereas PMBR reflected uncertainty-sensitive post-movement state updating rather than the simple encoding of movement dynamics.

4.6. Discussion

4.6.1. Introduction

Within this section, the key results are integrated and contextualised within the theoretical framework established at the outset of this thesis. The principal findings are interpreted in relation to existing literature, providing a coherent account of how the observed behavioural, muscular, and neural dynamics relate to current models of sensorimotor control. This section therefore synthesises the complex results presented to address the central question of the thesis: how the sensorimotor system regulates impedance during transitions between postural stability and voluntary movement.

4.6.2. Impedance is Successfully Elevated During the Postural Stabilisation Task

A foundational requirement of this thesis was to establish that the postural stabilisation task reliably induced a stability-oriented control state characterised by elevated mechanical impedance. This requirement directly addressed **Aim 1A** and **Research Question 1**, as demonstrating a robust and sustained impedance increase was a necessary precondition for examining whether such a control state persists into, or interferes with, subsequent voluntary movement. Across cohorts, the present findings provide evidence that participants consistently elevated mechanical impedance during postural stabilisation, confirming impedance regulation as a core component of the control strategy engaged in response to externally imposed instability.

Critically, observed impedance levels in response to perturbation exceeded those attributable to passive joint mechanics alone [8], [9], indicating active modulation of limb dynamics rather than reliance on intrinsic musculoskeletal properties. This finding aligns with a substantial body of work demonstrating that humans increase impedance through sensorimotor control processes such as altered muscle activation patterns, reflex gains, and intermuscular coordination when confronted with unstable or unpredictable environments [14], [17], [31], [34], [82]. The present results extend this literature by showing that such impedance elevation is not only present but robustly expressed across repeated task exposure and varied perturbation structures.

Notably, impedance elevation emerged from the first task block and remained largely stable across the session, providing little evidence for gradual, error-driven optimisation. Instead, participants appeared to rapidly adopt an impedance set-point appropriate to the stabilisation demands of the task. This pattern is inconsistent with views that conceptualise impedance as a slowly tuned mechanical parameter [4], [82], [267] and instead supports frameworks that describe impedance modulation as an anticipatory, context-dependent control policy [1], [268]. Within these frameworks, impedance is deployed proactively based on task demands and environmental structure, rather than incrementally adjusted through trial-by-trial error correction.

The functional relevance of this impedance elevation was clearly reflected in behavioural outcomes. Higher impedance was associated with reduced peak angular displacement and faster post-perturbation stabilisation, confirming that impedance regulation contributed meaningfully to mechanical stability. Importantly, however, the expression of these relationships depended on task structure, revealing distinct functional roles for impedance across contexts. In the temporal predictability cohort, between-participant differences in impedance strongly constrained peak displacement, suggesting that impedance operated as a trait-like protective factor that limited the mechanical consequences of perturbation onset. At the same time, within-participant fluctuations in impedance selectively supported faster stabilisation, particularly when perturbation timing was predictable. This dissociation supports a functional distinction whereby relatively stable impedance levels shape resistance to perturbation, while state-dependent modulation contributes to efficient post-perturbation recovery dynamics.

A contrasting pattern was observed in the perturbation amplitude cohort. Although impedance was robustly elevated, it showed no reliable association with peak angular displacement or stabilisation time, with only a weak, non-significant tendency toward faster stabilisation within participants. Instead, between-participant impedance effects were strongly context dependent, interacting with perturbation amplitude and direction such that higher impedance tended to predict longer stabilisation for the low-amplitude condition but showed no relationship at high-amplitude. No comparable modulation was observed within-participants. The small sample size in this cohort likely reduced sensitivity to detect the more systematic impedance–behaviour relationships seen within the temporal predictability cohort. Nevertheless, the overall trend suggests that at higher perturbation amplitudes, where displacement was significantly increased, the imposed forces may have exceeded the range over which impedance can be effectively employed as a stabilisation strategy. Under these conditions, behavioural outcomes were dominated by the perturbation mechanics, rendering impedance a less reliable contributor to stability.

Analysis of muscle co-contraction provided important mechanistic context for the observed impedance effects. In the temporal uncertainty cohort, co-contraction during the stabilisation phase was significantly elevated relative to baseline in both predictable and uncertain conditions, with reliably higher levels under temporal uncertainty. This pattern is consistent with established evidence that antagonist muscle activation contributes to increased limb impedance during stabilisation [1]. In contrast, co-contraction was not significantly elevated in either the high- or low-amplitude conditions of the perturbation amplitude cohort, and no differences were observed between amplitude levels. Across both cohorts, co-contraction remained stable across task blocks, indicating that these activation patterns were rapidly established and maintained rather than progressively tuned.

The absence of significant co-contraction modulation in the amplitude cohort may reflect limited statistical power due to the smaller participant count, but it may also indicate genuine task-dependent differences in control strategy. Notably, the perturbation amplitude used in the temporally predictable cohort (0.75 Nm) lay between the two amplitudes tested in the amplitude cohort (0.5 and 1 Nm), raising the possibility that this intermediate level fell within a range in which co-contraction and, by extension, impedance-related strategies, can be most effectively deployed. At lower amplitudes, stabilisation demands may be insufficient to elicit sustained co-contraction, whereas at higher amplitudes the imposed forces may exceed the range over which sustained co-contraction remains effective or energetically efficient. The general range of peak angular displacement observed across cohorts aligns with the three perturbation amplitudes employed, lending tentative support to this interpretation. However, because these observations are drawn from distinct cohorts with independent participants, they should be interpreted with caution. Together, these considerations suggest that a more systematic exploration of perturbation amplitude, ideally spanning a finer-grained and continuous range, may be necessary to fully characterise the conditions under which co-contraction and impedance contribute meaningfully to stabilisation.

Across outcome measures and task structures, co-contraction showed a clear dissociation between trait-like (between-participant) and state-dependent (within-participant) contributions, with its functional role varying systematically across cohorts. For mechanical impedance, co-contraction did not explain stable between-participant differences in either cohort and in the temporal predictability cohort, was unrelated to impedance at the between-participant level. Within participants, increases in co-contraction were associated with modest reductions in estimated impedance, indicating a dissociation between sustained muscle activation and the perturbation-locked mechanical response. This pattern likely reflects both functional and methodological distinctions between the measures. Impedance was estimated from brief windows time-locked to the applied perturbations and therefore weighted toward stiffness- and inertia-dominated responses at disturbance onset. Co-contraction, by contrast, was quantified across the entire stabilisation phase and thus indexed a broader, sustained control strategy. From this perspective, elevated co-contraction may preferentially enhance damping and reflex-mediated energy dissipation, improving stability over time without increasing - and in some cases even reducing - the stiffness-dominated impedance captured at the perturbation instant. This dissociation

reinforces the view that co-contraction and impedance reflect overlapping but non-identical components of stabilisation control [1], [31], and that changes in estimated impedance should not be interpreted as a direct proxy for the overall stabilising contribution of muscle activation.

In contrast, behavioural outcomes showed stronger and more interpretable coupling to co-contraction. Peak angular displacement was constrained by state-dependent increases in co-contraction under temporal predictability, whereas in the amplitude cohort it was dominated by trait-like differences, with higher mean co-contraction conferring greater resistance to displacement, particularly in flexion. A parallel dissociation emerged for stabilisation time: in the predictability cohort, faster recovery was driven almost exclusively by within-participant increases in co-contraction, while in the amplitude cohort both higher average co-contraction and block-to-block increases contributed to faster stabilisation, especially under high-amplitude extension. Together, these findings indicate that co-contraction plays a flexible but non-unitary role in stabilisation, supporting rapid, state-dependent control when task timing is predictable while acting as a more trait-like protective factor when mechanical demands vary.

In summary, the postural stabilisation task reliably elicited a control state characterised by elevated mechanical impedance, confirming impedance as a central feature of the stabilisation response. This impedance elevation was rapidly established and functionally relevant yet was not reducible to changes in global muscle co-contraction. Instead, co-contraction and impedance contributed in complementary but dissociable ways, with impedance reflecting a task-level stabilisation strategy and co-contraction supporting behavioural outcomes in a state- and context-dependent manner. Together, these findings demonstrate that impedance was successfully elevated during postural stabilisation and underscore its emergence from coordinated sensorimotor processes rather than from tonic muscle activation alone.

4.6.3. Stabilisation Phase Impedance Modulation Persists into Subsequent Voluntary Movement

The central aim of this thesis was to explore whether impedance modulation induced during postural stabilisation persisted into subsequent voluntary movement, and whether such persistence facilitates movement preparation or instead interferes with execution (**Research Question 1**, **Aim 1C**). The present findings demonstrate that impedance-related control states do not fully reset at the onset of voluntary movement. Rather, stabilisation-induced motor states persist into the movement phase in a manner that is strongly shaped by task context, most notably by temporal predictability.

Across cohorts, voluntary movement was consistently preceded by elevated reaction times relative to baseline, indicating a substantial and immediate cost associated with transitioning from a stability-oriented to a movement-oriented control state. This slowing emerged from the first task block and persisted across the session, suggesting that it reflects a fundamental reconfiguration of sensorimotor control rather than transient surprise or learning effects.

Temporal predictability selectively shaped how this persistence manifested. Reaction times were reliably shorter following temporally predictable than temporally uncertain stabilisation, indicating that predictable perturbation timing reduced the degree of impairment in movement initiation associated with a stabilisation-oriented control state. This difference appeared as a stable offset rather than a learning-related change, suggesting that temporal predictability constrained the cost of transitioning to voluntary action irrespective of task familiarity. Within participants, transient increases in stabilisation phase co-contraction were associated with smaller reaction time costs under predictable timing, indicating that impedance-related activation was less disruptive to movement initiation when temporal structure was available. Under temporal uncertainty, this relationship was disrupted, likely because unpredictable perturbation timing prevented alignment between stabilisation-related activation and impending movement demands, forcing elevated impedance to serve a purely reactive stabilisation role that compounded initiation costs. Together, these findings align with models in which predictable task structure reduces the cost of adapting sensorimotor models [268], [269].

Endpoint accuracy was largely unaffected by either temporal predictability or perturbation amplitude, with no evidence of systematic learning or condition-dependent degradation across blocks. Where accuracy costs were observed, they were direction-specific and stable across the session, suggesting biomechanical or control-related asymmetries rather than impedance-related interference. These findings indicate that, within the constrained movement paradigm employed, impedance persistence did not produce gross impairments in endpoint accuracy. However, the resolution of the accuracy measure was limited by the restricted range of motion and the constraint to a single rotational axis. As a result, the present analyses may not fully capture changes in endpoint accuracy induced by exposure to postural stabilisation dynamics, which may only become evident in a less constrained experimental paradigm.

In the temporal predictability cohort, movement duration increased reliably relative to baseline in the first task block, producing a transient slowing evident in both flexion and extension and not significantly different between conditions. However, across blocks, this slowing remained significant following temporally predictable stabilisation, whereas effects following temporally uncertain stabilisation did not reach statistical significance. In contrast, the perturbation amplitude cohort showed no reliable change in movement duration from baseline, remaining stable across conditions, movement directions, and task blocks. Across cohorts, changes in movement duration were mild and mostly nonsignificant, suggesting that impedance persistence primarily impacts movement preparation, with minimal consequences for movement execution.

In the temporal predictability cohort, within-participant increases in reaction time covaried with longer movement durations, indicating the emergence of a unified, transiently slowed motor state linking preparation and execution [163]. This coupling was absent in the perturbation amplitude cohort, where reaction time and movement duration were largely dissociated. This lack of a unified response may, as with the stabilisation phase co-contraction dynamics, result from the specific perturbation amplitudes used in this cohort. The lower amplitude (0.5 Nm) may have been insufficient to induce a stabilisation state strong enough to persist into execution, whereas the higher amplitude (1 Nm) may have exceeded the range over which stabilisation-related control could be flexibly integrated into subsequent movement. In contrast, the intermediate amplitude used in the temporally predictable cohort (0.75 Nm) may have fallen within a range that supported both robust stabilisation and measurable carryover into voluntary execution, allowing a clearer coupling between preparation and movement duration to emerge. Addressing the temporally predictability results specifically, they suggest that when temporal structure is predictable, persistence of a stabilisation-oriented control state can propagate beyond movement initiation to influence execution dynamics.

Co-contraction analyses provided mechanistic support for the observed behavioural effects. Across cohorts, co-contraction showed strong and consistent carryover from the stabilisation phase into voluntary movement, both as stable inter-individual differences and as block-to-block fluctuations. This persistence indicates that muscle activation patterns established during stabilisation are not fully reset at movement onset, providing a physiological substrate for the delayed reaction times and, where present, slowed movement execution observed following stabilisation. The relative insensitivity of this carryover to condition or movement direction suggests that co-contraction reflects a general control state bridging reactive stabilisation and voluntary action, rather than a finely tuned, task-specific adjustment. This interpretation is consistent with existing literature describing co-contraction as mediating a fundamental trade-off between mechanical stability and responsiveness, in which increased robustness to perturbation is achieved at the cost of slower initiation and reduced flexibility of movement [13], [78].

Taken together, these findings demonstrate that impedance modulation during postural stabilisation persists into subsequent voluntary movement and is uniformly maladaptive for movement initiation. Across cohorts, persistence of a stabilisation-oriented motor state was associated with impaired movement initiation relative to baseline, indicating a consistent cost of carrying stabilisation-related control into voluntary action. Under predictable temporal dynamics, this impairment was reduced but not eliminated, suggesting that predictive structure constrains the magnitude of the cost incurred. When

perturbation amplitude differed between conditions, impedance persistence became less behaviourally expressive, and voluntary movement was governed primarily by baseline timing characteristics and general practice effects. Overall, these results indicate that impedance persistence reflects a context-sensitive but inherently maladaptive control state whose behavioural impact is shaped by predictive structure rather than by between-condition differences in mechanical load.

4.6.4. Temporal Predictability, Not Perturbation Amplitude, Governs the Flexibility of Impedance Release

This thesis examined whether impedance control adapts flexibly to task demands, and in particular whether such flexibility is governed primarily by the informational structure of the task or by its mechanical demands (**Research Question 3**, **Aim 3**). Across all analyses, a clear and consistent pattern emerged: alterations of temporal predictability exerted a far stronger influence on the modulation, persistence, and release of impedance than changing perturbation amplitude. This dissociation indicates that impedance control is governed primarily by predictive structure rather than by the magnitude of external mechanical load.

During postural stabilisation, impedance was strongly modulated by temporal predictability but not by perturbation amplitude. Predictable perturbations elicited higher impedance than uncertain perturbations, an effect that emerged early and remained stable across the session. In contrast, varying perturbation amplitude produced no systematic change in impedance, despite clear effects on behavioural outcomes such as peak displacement and stabilisation time. This dissociation indicates that impedance was not continuously rescaled in proportion to mechanical demand but instead reflected a task-level control policy sensitive to temporal structure rather than force amplitude.

The same pattern characterised transitions into voluntary movement. In the temporal predictability cohort, stabilisation-related control states persisted into movement initiation, producing impaired reaction times relative to baseline. Predictable timing consistently reduced but did not eliminate this impairment, indicating greater flexibility in how impedance-related control was released when temporal structure was available. Under temporal uncertainty, this flexibility was diminished: reaction times were longer, co-contraction carried over more strongly into movement, and preparation and execution became coupled within a transiently slowed motor state. These findings suggest that uncertainty limits the system's ability to disengage stabilisation-oriented control, amplifying the cost of impedance persistence.

By contrast, when perturbation amplitude differed between conditions, impedance persistence was less behaviourally expressive. Reaction time and execution measures were largely insensitive to stabilisation phase impedance or co-contraction, and voluntary movement was governed primarily by baseline timing characteristics and general practice effects. Although co-contraction persisted across task phases, this carryover had minimal impact on voluntary behaviour, indicating that mechanical load reduced the functional relevance of impedance persistence without enhancing its flexibility.

Together, these results offer a novel characterisation of impedance control as a stabilisation-oriented motor state whose persistence across stability–movement transitions is governed by predictive structure rather than by mechanical demand. Rather than scaling continuously with force, impedance was flexibly engaged and released according to the temporal organisation of the task, with predictability determining how readily this state could be attenuated during transitions to voluntary movement and, in turn, the size of the associated behavioural cost. Mechanical load shaped overt performance but exerted little influence on the regulation or release of impedance itself. This dissociation provides new evidence that impedance regulation operates primarily as an uncertainty-management strategy, highlighting predictive information, not force magnitude, as the key driver of sensorimotor flexibility across stability–movement transitions.

4.6.5. Extension Movements Are More Sensitive to Impedance Dynamics Than Flexion Movements

Across behavioural, mechanical, and muscular measures, extension movements consistently exhibited greater sensitivity to impedance-related control dynamics than flexion movements. This asymmetry was evident during postural stabilisation, persisted into voluntary movement, and was expressed across both trait-like and state-dependent timescales. Together, these findings indicate that impedance modulation and its carryover across stability–movement transitions are directionally structured, addressing **Research Question 1** and informing **Aims 1** and **3**.

During postural stabilisation, impedance levels were generally higher for extension than flexion, and condition-dependent effects of temporal predictability were more pronounced in extension. Impedance differences between predictable and uncertain perturbations were strongest for extension, while flexion effects were weaker or only trend-level. Behaviourally, extension perturbations also showed stronger coupling between displacement and stabilisation time, indicating that extension movements were more tightly governed by impedance-mediated mechanical constraints. These findings suggest that extension movements rely more heavily on impedance regulation to resist perturbations, consistent with prior work showing direction-dependent differences in wrist biomechanics and reflex gains [2], [80].

This directional sensitivity carried forward into voluntary movement. Reaction time, movement duration, and co-contraction measures repeatedly showed stronger impedance-linked effects in extension than flexion. In the temporal predictability cohort, within-participant increases in impedance and co-contraction were more consistently associated with faster stabilisation, shorter reaction times, and tighter coupling between preparation and execution during extension. Similarly, co-contraction during the stabilisation phase predicted subsequent movement-phase co-contraction more robustly in extension across both cohorts, indicating stronger persistence of stabilisation-related motor states along this direction.

Importantly, these effects were not simply attributable to greater task difficulty in extension. Accuracy during voluntary movement did not show systematic impairment for extension, and in some cases, flexion exhibited larger accuracy reductions. Instead, the heightened sensitivity of extension appears to reflect greater integration of impedance-related control into both reactive and voluntary phases of behaviour. This dissociation suggests that extension movements may prioritise mechanical stability and impedance regulation, whereas flexion movements may rely more on kinematic or feedforward control strategies.

Condition manipulations further clarified this asymmetry. Modulation of temporal predictability selectively amplified extension sensitivity: temporal uncertainty increased stabilisation phase co-contraction during extension, strengthened carryover into movement, and enhanced coupling between impedance-related states and voluntary timing. In contrast, varying perturbation amplitude produced comparatively weak and fragmented direction-dependent effects, indicating that extension sensitivity is more strongly engaged by informational structure than by mechanical load. This pattern directly informs **Research Question 3**, showing that directional biases in impedance control are stable and not readily reshaped by short-term exposure to varying torque demands.

From a mechanistic perspective, these findings align with models of impedance control in which limb dynamics emerge from the interaction of musculoskeletal geometry, neural gain modulation, and task-level objectives. Wrist extension involves larger extensor muscle groups with higher passive stiffness and stronger stretch reflexes [8], [77], [270], which may amplify the behavioural consequences of impedance modulation. As a result, changes in impedance state, whether induced by predictability, uncertainty, or co-contraction, are more readily expressed in extension than flexion.

In the context of stability–movement transitions, this directional asymmetry has important implications. Extension movements appear more susceptible to both the benefits and costs of impedance persistence: stabilisation-related control states are more likely to carry over, shape voluntary preparation, and influence execution dynamics. Flexion movements, by contrast, showed weaker and

more context-specific sensitivity, suggesting greater flexibility or more effective release of impedance during the transition to voluntary action.

Overall, these results reveal a novel directional asymmetry in how impedance dynamics persist across stability–movement transitions, with extension movements showing heightened sensitivity to stabilisation history compared with flexion. This effect was robust across cohorts and selectively shaped by temporal predictability rather than perturbation amplitude, demonstrating that the persistence and release of impedance are constrained not only by task structure but also by movement direction. These findings refine the interpretation of impedance persistence in **Research Question 1**, highlight directional constraints on adaptability in **Research Question 3**, and provide an important consideration for examining neural signatures of impedance control (**Research Question 2**) and clinical populations with impaired impedance regulation. By identifying extension as a locus of reduced flexibility in transitioning out of a stability-oriented control state, these findings advance current accounts of impedance regulation beyond static or single-phase paradigms and underscore the importance of considering direction-specific constraints when interpreting neural and behavioural signatures of sensorimotor control.

4.6.6. Levels of Beta Corticomuscular Coherence Reflect Changes in Impedance State and Motor Context

This thesis sought to determine whether beta-band neural dynamics provide a meaningful index of impedance control and its evolution across stabilisation–movement transitions (**Aim 2**, **Research Question 2**). Prevailing accounts interpret sensorimotor beta power as indexing the maintenance of the current motor state [150], with elevated beta reflecting reduced readiness to change. On this basis, increased beta power relative to baseline was expected during the stabilisation phase, reflecting heightened efforts to preserve posture under perturbation [148], [271]. Contrary to this expectation, no reliable increase in beta power was observed during postural stabilisation in either cohort.

One plausible explanation is that the involuntary movements induced by the perturbations were of sufficient magnitude to disrupt postural maintenance, eliciting beta desynchronisation associated with movement or corrective responses [272], [273]. This interpretation is supported by the fact that participants were unable to fully suppress the angular displacement induced by the applied perturbations, indicating a failure to preserve the current motor state and necessitating corrective action. From this perspective, the absence of elevated beta power during stabilisation may reflect a dynamic competition between the intention to maintain posture and the disruptive effects of externally imposed motion. Future work could address this ambiguity by incorporating control trials in which participants anticipate postural challenge without experiencing actual perturbations, allowing a clearer dissociation between beta dynamics associated with motor state preservation and those driven by perturbation-induced movement.

While direct measurements of beta power failed to encapsulate the impedance dynamics observed, beta corticomuscular coherence (β-CMC) was far more robustly coupled with impedance dynamics. Across task phases and cohorts, β-CMC tracked whether the system was engaged in a stability-oriented or movement-oriented control state and how flexibly that state could be adjusted.

During the postural stabilisation phase, β-CMC showed a large and immediate reduction from baseline in both cohorts. This effect emerged from the first exposure and remained stable across task blocks, mirroring the rapid establishment and maintenance of elevated mechanical impedance. This may reflect a decoupling of cortical contributions to impedance control [274], [275] as participants fall back on more peripheral and reflexive control strategies [58], [68]. This interpretation is supported by the general increase in co-contraction seen within the temporal predictability cohort but has unclear associations within the perturbation amplitude cohort. The absence of block-wise change argues against a learning-driven interpretation and instead supports the view that suppression of β-CMC is a defining feature of the impedance-dominated stabilisation state. Critically, this reduction was largely

insensitive to perturbation amplitude, demonstrating that corticospinal beta coupling does not scale with mechanical load. Instead, β-CMC appears to reflect a shift in control mode, consistent with accounts that associate reduced beta coupling with increased reliance on peripheral mechanisms and reduced moment-to-moment cortical regulation during postural maintenance [214], [274].

Although broadly similar across cohorts, stabilisation phase β-CMC retained sensitivity to temporal structure. In the temporal predictability cohort, suppression of β-CMC was reliably greater under predictable than uncertain perturbations. This dissociation parallels the impedance results, in which predictable timing supported higher and more stable impedance levels, whereas uncertainty led to reduced impedance. Together, these findings suggest that β-CMC indexes the degree to which impedance is set proactively within a predictable context, rather than reflecting the absolute magnitude of stabilising force or stiffness. Temporal uncertainty appears to preserve a greater degree of corticospinal coupling, potentially supporting flexibility and responsiveness when perturbation timing cannot be anticipated.

The functional relevance of β-CMC was further supported by its relationship to behaviour across task phases. During stabilisation, within-participant increases in co-contraction were associated with transient increases in β-CMC, particularly under temporal uncertainty or high mechanical load. This indicates that β-CMC is sensitive to momentary engagement of stabilising control rather than tonic muscle activation, aligning with interpretations of beta coupling as reflecting active sensorimotor integration. Mean co-contraction levels, by contrast, were unrelated to β-CMC, reinforcing the dissociation between trait-like muscle activation strategies and state-dependent neural engagement.

Across the transition into voluntary movement, β-CMC showed a different profile. Mean levels during movement were not shifted relative to baseline and did not adapt across blocks, indicating that the stabilisation-related suppression of β-CMC was released rather than persistently carried forward. However, β-CMC during movement was selectively shaped by task context and movement direction. In both cohorts, condition-dependent modulation was expressed primarily during extension movements, with temporal predictability and perturbation amplitude altering the directional profile of coupling rather than its overall level. This pattern mirrors the behavioural and impedance findings, in which extension movements were more sensitive to stabilisation history and control context than flexion movements.

Importantly, stabilisation phase β-CMC carried over into movement β-CMC primarily at the between-participant level and almost exclusively during extension. Individuals with higher corticospinal coupling during stabilisation tended to retain higher coupling during movement, indicating a trait-like continuity of neural control strategy rather than a block-to-block persistence of state. This carryover was largely independent of task condition, suggesting that while β-CMC is sensitive to motor context, individual differences in corticospinal engagement remain stable across task phases.

Finally, the behavioural correlates of β-CMC further clarify its role. In the temporal predictability cohort, higher stabilisation phase β-CMC predicted faster reaction times at both the between- and within-participant levels, particularly under predictable timing. This indicates that stronger corticospinal coupling during stabilisation may facilitate more efficient movement initiation when upcoming demands are known. Comparable effects were absent when perturbation amplitude varied, underscoring that the behavioural relevance of β-CMC is gated by temporal structure rather than mechanical intensity. Associations with movement duration were weaker and highly context dependent, reinforcing the interpretation that β-CMC primarily indexes readiness and control state rather than kinematic execution directly.

Taken together, these findings provide novel evidence that β-CMC indexes changes in impedance state and motor context rather than scaling with mechanical load. Suppression of β-CMC reliably characterised the stabilisation phase and accompanied elevated impedance, while its partial release and direction-specific modulation during movement reflected reconfiguration of control priorities across task phases. Crucially, the flexibility of this neural signature was governed by temporal predictability rather than perturbation amplitude, demonstrating that corticospinal beta coupling tracks context-dependent control states across stability–movement transitions. This positions β-CMC as a principled

neural marker of impedance regulation dynamics, extending its interpretation beyond movement execution to the organisation and release of stabilisation-oriented motor states (**Research Question 2**, **Aim 4**).

4.6.7. Post-Movement Beta Rebound Indexes Context-Dependent State Updating Rather Than Voluntary Movement Dynamics

Post-movement beta rebound (PMBR) has been widely interpreted as reflecting processes related to movement speed [165], accuracy [164], and force generation [152], [166]. In the present thesis, PMBR served as a complementary neural marker to β-CMC and co-contraction, providing insight into how control states are resolved following stability–movement transitions (**Aim 2**, **Research Question 2**). Contrary to prevailing interpretations, the results suggest that PMBR did not encode specific movement parameters but rather reflected context-dependent state updating associated with the persistence and release of impedance-related control.

Across both cohorts, PMBR exhibited a robust and stereotyped temporal profile following movement termination, with clear suppression relative to baseline and a well-defined rebound within the post-movement window. This consistency confirms PMBR as a reliable marker of post-movement cortical processing in the present paradigm. However, the amplitude of PMBR was not shaped by movement dynamics in any systematic way. Neither reaction time nor movement duration reliably predicted PMBR at the between-participant level, and only highly selective within-participant effects were observed. This dissociation argues against an interpretation of PMBR as a direct consequence of movement effort [152], [166] or execution quality [164], [165].

Instead, PMBR amplitude was strongly modulated by task context, particularly temporal predictability, and by movement direction. In the temporal predictability cohort, PMBR was consistently suppressed following temporally uncertain stabilisation compared with predictable stabilisation, with the effect most pronounced during extension movements. This modulation emerged robustly across the session and showed no evidence of learning or block-wise adaptation, indicating that PMBR reflected an ongoing contextual influence rather than transient novelty or fatigue. In contrast, when perturbation amplitude was manipulated, PMBR showed no reliable condition-dependent modulation, despite clear mechanical differences between conditions. Together, these findings mirror those observed for impedance and beta corticomuscular coherence, reinforcing the conclusion that beta-band dynamics are more sensitive to informational structure than to mechanical load.

The relationship between PMBR and impedance-related control becomes clearer when considered alongside evidence for impedance carryover. Stabilisation induced a persistent motor state characterised by elevated impedance, altered co-contraction, and suppressed β-CMC, which biased subsequent movement preparation. PMBR appears to index how this persistent state is resolved following movement completion. Following temporally predictable stabilisation, where impedance was elevated and more proactively set, PMBR was larger, suggesting a more complete or efficient post-movement state update. Following temporally uncertain stabilisation, where impedance was reduced and control remained more flexible, PMBR was attenuated, consistent with a less definitive resolution of the preceding control state.

Selective within-participant associations further support this interpretation. Under predictable timing for flexion movements, longer reaction times and movement durations were associated with larger PMBR amplitude. Rather than reflecting slower execution, this pattern suggests increased evaluative or updating demands when movement unfolds more slowly within a predictable context. The absence of these effects under temporal uncertainty implies that PMBR engagement depends on the availability of predictive structure that allows comparison between expected and realised outcomes. When such structure is lacking, as under temporal uncertainty, PMBR is uniformly suppressed and decoupled from fine-grained behavioural variability.

Taken together, these findings offer a novel interpretation of PMBR as a neural signature of context-dependent state updating that is tightly coupled to impedance control rather than to movement mechanics. PMBR amplitude indexed how definitively the sensorimotor system disengaged from a stability-oriented control regime following movement, with larger rebounds under predictable conditions indicating more complete resolution of the stabilisation state. By demonstrating that PMBR tracks the release of impedance in a manner governed by temporal predictability and not by force magnitude, these results extend prevailing accounts of PMBR beyond post-movement evaluation to encompass the final stage of impedance regulation across stability–movement transitions.

4.6.8. Cross-Phase Neural Dynamics of Impedance Control and Their Translational Relevance

Together, the neural findings demonstrate that impedance control is supported by dissociable beta-band signatures that map onto distinct phases of the stabilisation–movement sequence, rather than by a unitary oscillatory mechanism. β-CMC and PMBR captured complementary aspects of how the sensorimotor system engages, maintains, and resolves stabilisation-oriented control (**Aim 2**, **Research Question 2**). This phase-specific organisation clarifies why different beta measures showed differential sensitivity to task context and constrains interpretations that treat beta activity as a single marker of motor state.

β-CMC emerged as a neural signature of the stabilisation-oriented control regime itself. Its robust suppression during postural stabilisation coincided with elevated impedance and increased co-contraction, indicating reduced reliance on moment-to-moment corticospinal coupling during impedance-dominated control. Sensitivity of β-CMC to temporal predictability, but not to perturbation amplitude, mirrored behavioural and mechanical findings, reinforcing the interpretation that β-CMC indexes motor context and control mode rather than mechanical load. Partial carryover of β-CMC into voluntary movement at the between-participant level further suggests that it reflects stable individual strategies for organising transitions between stabilisation and movement, biasing how control states are reconfigured rather than persisting rigidly on a trial-by-trial basis.

In contrast, PMBR indexed a later and functionally distinct stage of control: the resolution and updating of the motor state following movement termination (**Aim 4**). PMBR showed minimal coupling to movement kinematics and no systematic sensitivity to force magnitude, arguing against interpretations based on execution effort or accuracy. Instead, its strong modulation by temporal predictability and movement direction positions PMBR as a marker of contextual evaluation - reflecting how definitively the sensorimotor system disengages from a stabilisation-oriented control state. Larger PMBR following predictable stabilisation suggests more complete or efficient state resolution, whereas attenuated PMBR under uncertainty indicates prolonged or incomplete disengagement of stabilisation-related control.

Crucially, mean beta power showed no reliable modulation across task phases or conditions, ruling out explanations based on global changes in cortical excitability or arousal. Instead, impedance-related neural dynamics were expressed through interactional and temporally specific measures - β-CMC during stabilisation and PMBR following movement - highlighting the importance of phase-sensitive analyses when interpreting beta-band activity in motor control.

This cross-phase organisation of beta-band dynamics has important implications for understanding sensorimotor flexibility and its impairment. Effective motor behaviour requires not only the ability to elevate impedance under stability demands, but also the capacity to flexibly resolve and release that impedance when task goals shift. The present findings indicate that temporal predictability supports this flexibility by enabling clearer engagement and resolution of stabilisation-related neural states, whereas uncertainty compromises both commitment to, and disengagement from, impedance-dominated control. In this framework, impaired movement initiation arises not from excessive impedance directly, but from difficulty resolving stabilisation-oriented control when predictive structure is lacking.

These dynamics resonate with clinical accounts of rigidity and bradykinesia in Parkinson's disease, where abnormal beta synchrony [26], [41], reduced beta flexibility [27], and altered β-CMC [276], [277] have been proposed as core pathophysiological features. Although the present work examined healthy participants, the association between reduced PMBR, altered β-CMC, and delayed movement initiation provides a mechanistic bridge to these clinical phenomena. From this perspective, motor impairment may reflect a failure of state resolution rather than an inability to generate or suppress impedance alone.

Overall, the combined neural evidence supports a new view of impedance control as a temporally structured, context-sensitive process supported by dissociable beta-band mechanisms. β-CMC reflects engagement of a stabilisation-oriented control regime, while PMBR captures its resolution following movement. Together, these measures provide a principled framework for linking stabilisation, movement initiation, and post-movement updating, and offer promising neural markers for assessing sensorimotor flexibility and its disruption in both experimental and clinical contexts (**Aim 2**, **Aim 4**).

4.6.9. Limitations and Future Directions

The main limitations of the present study relate to constraints on data quantity, experimental design, and technical implementation. To maintain a reasonable session duration, the number of trials per block was necessarily limited. While this trial count was sufficient for most outcome measures, a greater number of repetitions would strengthen robustness, particularly for neural analyses. Session time constraints also motivated suboptimal trial-level design choices, most notably the restriction of the post-movement analysis window to 1 s. Although this window was generally sufficient for identifying reliable PMBR peaks following voluntary movement, it may have reduced sensitivity to slower post-movement dynamics. Future studies of a similar nature would benefit from incorporating a longer post-movement window and less modest trial counts.

Beyond modifications to individual task elements, the overall session design could be improved. Across outcome measures, there was little evidence of adaptation or learning across the repeated task blocks (**Aim 3**). A major contributor to the extended session duration was the inclusion of multiple blocks intended to track temporal development of the measured features; however, as these effects proved largely nonsignificant, this structure offered limited benefit. Redesigning the protocol to reduce or eliminate repeated blocks would provide greater flexibility to increase trial count and optimise statistical power. Moreover, the current hierarchy of conditions, blocks, and trials constrained exploration of trial-by-trial variability, as inclusion of trial-level terms in mixed-effects models would have substantially increased model complexity and risked statistical underpowering. This was of particular concern for the perturbation amplitude cohort due to being limited to only 14 participants. Adopting a more flexible, trial-centric design would facilitate finer-grained analyses and allow multiple experimental manipulations to be combined within a single session, addressing the cohort-level separation in the current implementation. Additionally, the current design was repetitive and unengaging meaning mental fatigue and reduced attention could have impacted results [278], [279]. The proposed trial-centric design would remove the long, repetitive sections of the current design, reducing the potential impact of reduced task engagement.

Beyond design considerations, technical limitations also affected data acquisition. Principal amongst these was the limited sampling rate of the manipulandum, which was constrained by the MATLAB API for the HRX-1 and could not be executed on a background thread. As a result, data acquisition was locked to the 60 Hz screen refresh cycle, reducing temporal precision. This limitation directly impacted analyses such as β-CMC, where low sampling rates hindered precise moment-to-moment characterisation of this highly transient feature [280]. More generally, insufficient temporal precision prevented highly accurate timestamping of motor events, limiting exploration of fast neural dynamics, such as the examination of beta bursting activity, which has established relevance to movement dynamics in both healthy individuals and those with Parkinson's disease [25], [149], [190]. Addressing this technical constraint in future work would enable more detailed analysis of beta-band activity and

extension to higher-frequency dynamics, such as gamma-band activity, providing a more comprehensive understanding of impedance regulation and sensorimotor integration [210], [211].

An additional technical limitation concerns the use of single bipolar EMG recordings to index muscle activity. While this approach provided a reliable measure of overall muscle activation and co-contraction, it offers limited insight into the spatial organisation and heterogeneity of motor unit recruitment within and across muscles. High-density EMG would enable more detailed characterisation of muscle coordination, including regional activation patterns, changes in motor unit synchronisation, and muscle–muscle coupling, which are not accessible with bipolar recordings [281], [282]. This limitation is particularly relevant in the context of impedance control, where stabilisation may be achieved through nuanced, spatially distributed recruitment strategies rather than uniform increases in activation. Future studies incorporating high-density EMG could therefore provide a more mechanistic understanding of how muscle coordination supports impedance modulation and its persistence across stabilisation–movement transitions. This could be further enhanced by translating the protocol from the current one-degree-of-freedom (1-DOF) system to a two-degree-of-freedom (2-DOF) implementation. This would allow for the expression of more complex impedance dynamics and improve the ecological validity of the movements performed.

Finally, extending the present protocol to clinical populations, particularly individuals with Parkinson's disease, represents an important direction for future work. PD is characterised by abnormal beta-band dynamics, impaired modulation of corticomuscular coupling, and altered use of co-contraction during movement and postural control. Applying the current stabilisation–movement paradigm in this population would allow direct examination of how pathological beta activity and impaired impedance regulation interact during transitions between stability and voluntary action. Such an approach could clarify whether the persistence of stabilisation-oriented control states observed in healthy participants is exaggerated or inflexible in Parkinson's disease, potentially contributing to bradykinesia and impaired movement initiation. This extension would also provide a clinically relevant test of the proposed links between impedance control, predictive structure, and beta-band neural dynamics.

4.6.10. Summary

Across the preceding discussion sections, the findings converge on an integrative sensorimotor account of how impedance is regulated across transitions from postural stability to voluntary movement (**Aim 4**). Impedance emerged not as a static mechanical parameter, but as a temporally structured control state supported by coordinated interactions between limb mechanics, muscle co-contraction, and dissociable beta-band neural dynamics. A central and novel insight of this work is that the engagement, persistence, and release of impedance are governed primarily by the informational structure of the stabilisation task - particularly temporal predictability - rather than by the magnitude of mechanical load (**Research Question 3**). Predictable stabilisation dynamics supported higher and more stable impedance, stronger suppression of β-CMC, and larger PMBR, indicating clearer commitment to and resolution of a stabilisation-oriented control state. In contrast, varying perturbation amplitude between conditions had little effect on impedance regulation or its neural signatures, despite robust effects on behavioural outcomes.

Stabilisation-related control states persisted into voluntary movement, producing consistent costs for movement initiation that were uniformly maladaptive relative to baseline (**Research Question 1**). However, the magnitude of this impairment was constrained by modulation of temporal predictability: when perturbation timing was predictable, the cost of carrying stabilisation-related control into movement was reduced, whereas temporal uncertainty exacerbated delayed initiation and impaired state resolution. These effects were not mirrored by changes in mechanical load, underscoring that impedance control is tuned to managing uncertainty rather than scaling force. PMBR further revealed that release of stabilisation-related control is an active, context-dependent process, with attenuated rebound under uncertainty indicating incomplete disengagement of the stabilisation state (**Aim 2**, **Research Question 2**).

The novelty of these results lies in demonstrating that impedance control is organised specifically around the stability–movement transition, rather than being confined to either postural maintenance or movement execution alone. The findings show that stabilisation establishes a distinct motor state that persists across the transition into voluntary action and must be actively reconfigured or released for efficient movement to occur. Critically, this transition is governed by dissociable neural mechanisms that map onto stabilisation, transition, and post-movement resolution, revealing impedance regulation as a dynamic, cross-phase process.

By showing that the flexibility of this transition depends on predictive structure rather than mechanical demand, the results reframe impedance control as a problem of managing competing stability and movement requirements under uncertainty. The integration of behavioural costs, muscular activation, and beta-band neural dynamics clarifies how stabilisation-oriented states bias subsequent movement preparation and execution, resolving ambiguities in the interpretation of beta activity during motor tasks. This stability–movement transition perspective advances current models of sensorimotor control by explicitly linking impedance persistence and release to task structure and provides a principled framework for understanding impaired motor flexibility when predictive information is degraded.

V. Passive Wrist Stiffness in Healthy Motor Control Following Stability–Movement Transitions and at Baseline in Parkinson's Disease

5.1. Introduction

Mechanical impedance of the wrist plays a central role in human motor control, with stiffness constituting its largest and most influential component [77]. Accurate assessment of wrist stiffness requires the application of stable low-amplitude torques that minimally engage voluntary motor responses [58], [283]. In clinical practice for Parkinson's disease (PD), such assessments are commonly performed using the rigidity item of the Unified Parkinson's Disease Rating Scale (UPDRS) [120], in which a clinician applies sustained, external manipulations to the patient's wrist. While widely adopted, this approach is inherently subjective and suffers from substantial inter- and intra-rater variability [123], [124], [125], limiting its sensitivity and reproducibility.

These limitations motivate the development of automated, objective approaches capable of delivering precise and repeatable measurements of passive stiffness. The HRX-1 manipulandum presented an opportunity to address this need by enabling controlled torque application and high-resolution measurement of wrist responses, allowing rigidity to be quantified in a standardised manner. Importantly, this assessment was integrated with the primary experimental paradigm, permitting evaluation of how prior perturbation exposure influenced stiffness. In this context, passive wrist stiffness serves not only as a clinically relevant metric but also as a tool for probing more subtle and persistent changes in sensorimotor control and impedance carryover following stability–movement transitions.

5.2. Methods

5.2.1. Apparatus

All data presented within this section was collected using the HRX-1 device. Participants for the main paradigm completed blocks of passive assessment as part of their pre-condition baselines and following each task block (**Figure 4.5**). These participants engaged with the full experimental configuration, including the DSI-24 EEG headset and auxiliary EMG sensors. A full description of the configuration can be found in the **Apparatus** section of the previous chapter.

Participants with PD completed a single block of passive assessment in isolation. Visual feedback was minimal and was used only to assist participants in aligning the handle to a neutral position prior to torque application. This visualisation was identical to that used in the main paradigm, comprising a white crosshair indicating handle position and a red target circle. These visual elements were removed at trial onset, thereby eliminating the potential confound of participants tracking their position via visual feedback. Clinical participants interacted with the manipulandum without supplementary EEG or EMG instrumentation.

Aside from the exclusion of supplementary equipment, participants engaged with the passive assessment task in a manner identical to the main paradigm. Interaction with the device was achieved via a rubber-coated, bicycle-style handle grip, while the manipulandum supported the arm from the wrist to the elbow (**Figure 4.1**). Participants were secured with Velcro straps at the wrist and forearm to minimise compensatory elbow movement during assessment. Participants were seated facing a

computer monitor, and chair height was adjusted to ensure a comfortable posture, with approximately 40° of shoulder abduction and 20° of shoulder flexion.

5.2.2. Participants

The participants who completed the passive assessment analyses formed several distinct cohorts. Regardless of cohort, each participant provided informed consent prior to participation. The study was approved by the Imperial College Research Ethics Committee (ICREC) and performed in accordance with the Declaration of Helsinki.

Healthy participants were those who completed the main paradigm (**Participants**). They were recruited via college wide invitation and had no known physical impairment of their dominant arm or any diagnosed neurological conditions. These participants were divided into two cohorts (**Table 5.1**), defined by the perturbation feature manipulated as part of the **Main Task Design**.

Table 5.1. Healthy participant demographic breakdown. Replication of Table 4.1 , included here for completeness.

Cohort	Count	Age - Mean (SD)	Age - Median (IQR)	Sex (M/F)	Dominant Hand (R/L)
Perturbation Amplitude	14	26.2(6.51)	24 (22.00 - 30.25)	8/6	11/3
Temporal Predictability	24	25.7(5.51)	24 (22.00 - 29.00)	12/12	22/2

Participants with PD were recruited across multiple cohorts (**Table 5.2**). These cohorts were defined by both the data collection context and the contrasts available within each dataset. Passive assessment data collection was frequently embedded within other laboratory protocols, resulting in several distinct comparison sets. The first two PD cohorts were collected specifically for the present study. All participants were assessed while adhering to their usual pharmacological treatment regimen, and testing was conducted exclusively in this medicated state. Wrist rigidity was evaluated using the UPDRS prior to experimental testing, and these clinical ratings were used in the present analyses. UPDRS assessments were conducted by two clinicians without overlap, producing two cohorts defined by clinical assessor (Clinic A and Clinic B). Two additional PD cohorts were collected to enable contrasts between treatment states. In the first cohort, participants were tested both ON- and OFF-medication. In the second cohort, participants had implanted deep brain stimulators and were tested initially under their usual stimulation parameters (ON) and subsequently without stimulation (OFF). Participants in both cohorts underwent UPDRS assessments of wrist rigidity in each treatment state, enabling direct within-participant comparisons across states. The clinical assessor for the stimulation cohort was the same assessor from the Clinic A cohort, whereas the medication cohort was evaluated by a new clinician.

Table 5.2. Parkinson's disease participant demographic breakdown.

Cohort	Count	Age - Mean (SD)	Age - Median (IQR)	Sex (M/F)	Affected Side (R/L)	ON/OFF	Clinician
Clinic A	10	72.90 (7.23)	71 (70.00 - 77.00)	5/5	8/2	No	A
Clinic B	5	57.00 (4.53)	59 (53.75 - 60.25)	4/1	3/2	No	B
Medication	6	69.50 (6.32)	68 (65.00 - 71.00)	4/2	1/5	Yes	C
Stimulation	10	58.70 (8.39)	59 (55.50 – 62.00)	8/2	3/7	Yes	A

5.2.3. Passive Assessment Task Design

A custom MATLAB script implemented using the Psychtoolbox package and interfaced with the HRX-1 manipulandum was used to conduct the passive stiffness assessment. Minimal visual feedback was provided to assist participants in aligning the handle with the neutral wrist position. The HRX-1 was operated in current-control mode, allowing precise motor torque generation via selective application of motor current. Motor position and torque were sampled at 60 Hz throughout the assessment.

Participants were instructed to align their wrist with a centrally presented target and to then remain relaxed, allowing the manipulandum to move them freely. Following a 3 s countdown, four passive trials were delivered. In each trial, the motor applied a predefined low-amplitude trapezoidal current waveform comprising smooth ramp-up, hold, and ramp-down phases, followed by a mirrored sequence in the opposite direction (**Figure 5.1**). Torque hold phases were 0.5 s in duration and were included to minimise jerk during direction reversal, consistent with established protocols [261]. Each trial lasted 21 s, after which participants realigned the handle to the neutral position using simple target and crosshair visualisation. Trials were equally divided between flexion-first and extension-first sequences and presented in a randomised order. Torque was capped at 1 Nm in either direction with linear ramping. The waveform was designed to elicit passive wrist motion while minimising voluntary muscle engagement, with visual feedback restricted to alignment cues.

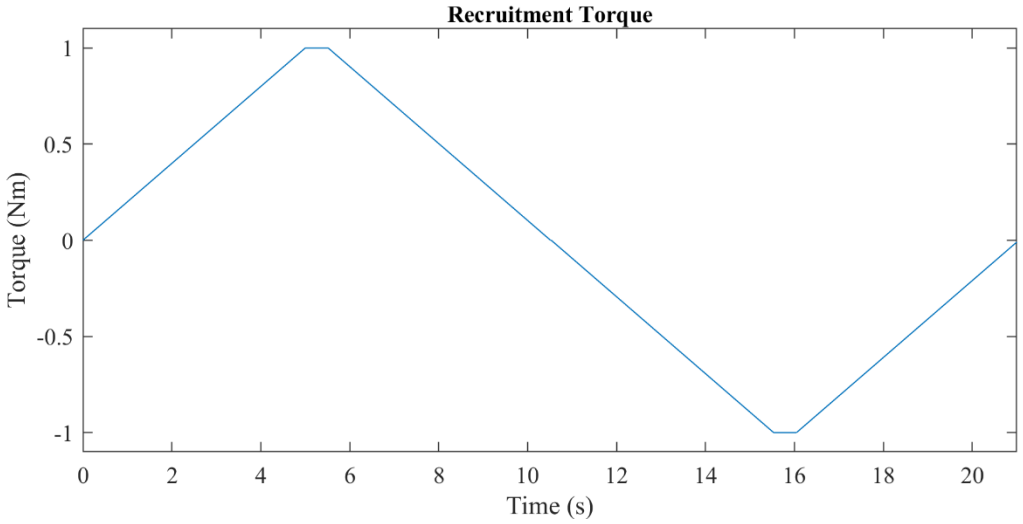

Figure 5.1. Example recruitment torque waveform used for passive stiffness assessment. The trapezoidal profile comprises smooth ramp-up, hold, and ramp-down phases, followed by a mirrored sequence in the opposite direction, with torque capped at ±1 Nm. This waveform was designed to elicit passive wrist motion while minimising voluntary muscle engagement and reducing jerk at direction reversals.

5.2.4. Stiffness Computation

Passive assessment data were analysed offline using custom MATLAB code to quantify torque–angle stiffness during flexion and extension. Motor position signals were converted to joint angle in radians and corrected for hand orientation to ensure consistent kinematic direction across participants. Trials with known acquisition or compliance issues, identified a priori for specific participants, were excluded. To confirm valid passive torque delivery, the recorded torque signal was compared with an expected reference waveform, and the root-mean-square error (RMSE) between recorded and reference torque was normalised by the reference torque range. Sweeps with a normalised error greater than 0.05 were rejected, resulting in retention of more than 98% of trials across cohorts.

Within each trial, flexion and extension phases were identified using the maximum and minimum torque values. Zero crossings of joint angle were detected and combined with torque extrema and hand-specific sign conventions to define candidate flexion and extension regions. Torque–angle stiffness was estimated separately for each direction by identifying the optimal linear segment within each phase (**Figure 5.2**). A sliding-window search was performed across candidate segments meeting predefined criteria: a minimum angular span of either 50% of the total sweep range or 20°, whichever was larger, and a segment start within 5° of neutral position for the first movement or zero-crossing for the second. Ordinary least-squares regression was applied to each candidate segment to compute the slope and coefficient of determination (R^2). The optimal segment was selected by maximising R^2, with secondary preference given to longer angular spans. Stiffness estimates with $R^2 < 0.5$ were excluded, and remaining values were averaged across trials within each block to yield final stiffness estimates in N·m/rad for flexion and extension.

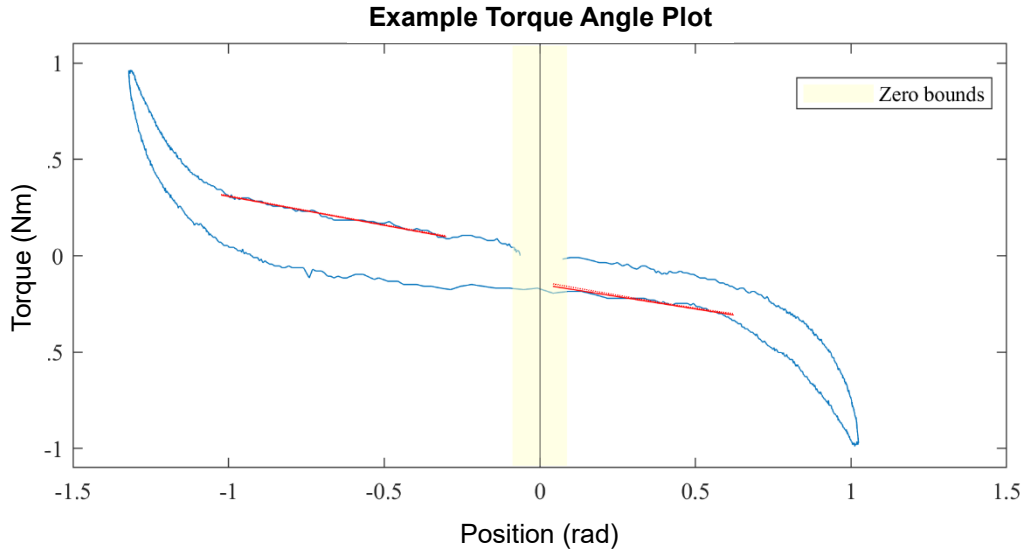

Figure 5.2. Representative torque–angle trajectory from a passive stiffness assessment trial. Blue traces show the recorded torque–angle relationship across flexion and extension, with hysteresis reflecting passive viscoelastic properties. The shaded region denotes the zero-crossing bounds used to identify neutral position. Red lines indicate the optimal linear segments selected within each movement direction for stiffness estimation based on the sliding-window regression procedure.

5.2.5. Statistical Analysis

Passive assessments conducted on healthy control participants as part of the main experimental paradigm were analysed using the same approach as the stabilisation phase and voluntary movement dynamics analyses in the previous chapter. Single-outcome measures were fitted using two complementary mixed-effects models. The first model examined block count within each condition, while the second assessed block count across the entire session. This approach enabled evaluation of the effects of repeated task exposure both within experimental conditions and at the level of overall fatigue or learning. The models included condition, block count, and movement direction as fixed effects, while controlling for inter-individual variability between participants. The full model specification and the rationale for this analytical design are provided in the **Single-Outcome Statistical Analysis** chapter. Similarly, correlations between outcome measures were assessed using a mixed-effects model that included each participant's mean predictor value per condition, together with the per-block deviation from this mean, while controlling for condition and block count. This approach enabled separation of between-participant and within-participant contributions, allowing assessment of the predictive value of both overall relationships between outcomes and participant-specific deviations.

The full model specification and analytical rationale can be found in the **Correlation-Based Statistical Analysis** chapter. Results from each analysis are reported in terms of effect sizes (β), 95% confidence intervals, and p-values (p).

For the passive assessment data from participants with PD, the statistical analysis addressed two distinct objectives. The first was to determine whether the measured outcomes discriminated between levels of clinical severity as assessed using the UPDRS wrist rigidity item. Accordingly, data were labelled and grouped according to the corresponding clinical scores. Kruskal–Wallis tests were used to evaluate overall differences between groups, followed by Dunn's post hoc tests with Bonferroni correction to identify which group pairs were distinguishable. Given the modest sample size and the ordinal nature of the clinical severity scale, this analysis was supplemented by calculation of Spearman's rank correlation coefficient to assess monotonic trends across UPDRS scores.

The second objective concerned comparative analyses between participants in different treatment states, including ON and OFF conditions for medication or brain stimulation, as well as comparisons between healthy control participants and clinical patients. For within-subject clinical comparisons, Wilcoxon signed-rank tests were used. For independent comparisons between clinical and control groups, Mann–Whitney U tests were applied. These non-parametric tests enabled evaluation of group differences without reliance on distributional assumptions required by equivalent parametric tests and were appropriate given the limited sample sizes.

5.2.6. Summary

In summary, this section introduces an objective, automated framework for assessing passive wrist stiffness that addresses key limitations of existing clinical measures. By leveraging the precise torque control and high-resolution sensing capabilities of the HRX-1 manipulandum, the protocol enables standardised quantification of torque–angle stiffness under conditions designed to minimise voluntary motor engagement. Integrating this passive assessment within the main experimental paradigm allows stiffness to be examined not only as a clinically relevant marker for PD but also as a sensitive probe of how prior stabilisation and perturbation exposure influences sensorimotor state and impedance carryover in healthy motor control. Together, this task design and analytical approach establish a robust methodological foundation for linking passive mechanical properties to broader questions of impedance regulation across stability–movement transitions.

5.3. Passive Stiffness Modulation Following the Stability–movement Transition in Healthy Motor Control

5.3.1. Introduction

The main experimental paradigm examined transitions between stability- and movement-oriented motor states, focusing on reactive impedance modulation in response to environmental instability and its subsequent release during voluntary reaching. Although stiffness is a dominant contributor to impedance regulation [77], the high-activity nature of the main task precluded reliable characterisation of stiffness dynamics, as accurate stiffness estimation requires slow, low-amplitude torques that minimise active and reflexive responses. To address this limitation, the passive assessment paradigm modelled on clinical evaluation of wrist rigidity was incorporated into the protocol.

Healthy participants completing the main task underwent passive assessments in which they remained compliant with slow, low-amplitude external manipulation, enabling estimation of mechanical stiffness with minimal voluntary contribution. Consistent with prior work, passive movements in both flexion and extension were elicited using a low-amplitude trapezoidal torque profile [8], [261]. While passive stiffness was the primary outcome, antagonist muscle co-contraction (CCI) and beta-band corticomuscular coherence (β-CMC) were quantified over the same time windows, extending beyond measures previously reported in the literature [8], [127], [261] and enabling concurrent assessment of mechanical, muscular, and neural factors.

These measures were compared with baseline assessments obtained prior to stabilisation task exposure, allowing identification of changes induced by manipulation of perturbation amplitude and temporal predictability. Because the passive assessments followed completion of the active task blocks, they captured more persistent, low-level modulations of sensorimotor impedance that endured for minutes after exposure, rather than transient effects confined to the immediate stabilisation period.

5.3.2. Passive Stiffness

Although changes in passive stiffness from baseline were not significant in either movement direction following the temporally predictable ($p \geq .058$) or uncertain ($p \geq .478$) conditions, the change in passive stiffness differed significantly between the two conditions ($\beta = 4.60 \times 10^{-4}$, 95% CI = [$8.02 \times 10^{-5}$, 8.40×10^{-4}], $p = .018$, **Figure 5.3**). This divergence was most clearly reflected in the direction of change: passive stiffness increased following the temporally predictable condition ($\beta = 1.72 \times 10^{-4}$) and decreased following the temporally uncertain condition ($\beta = -7.04 \times 10^{-5}$). This effect was comparable for flexion and extension, with no overall directional bias ($p = .184$) and no evidence that the effect of temporal predictability differed by movement direction ($p = .577$). Passive stiffness did not change significantly across task blocks in most conditions ($p \geq .451$). However, flexion movements following the temporally uncertain condition exhibited a gradual decrease in passive stiffness that approached significance ($\beta = -3.63 \times 10^{-4}$, 95% CI = [$-7.50 \times 10^{-4}$, 2.43×10^{-5}], $p = .066$). Despite this trend, no significant divergence in either the rate of change or overall stiffness level was detected between conditions ($p \geq .155$).

Nonparametric testing of the initial task block indicated that flexion stiffness following the temporally predictable condition increased significantly from baseline to the first assessment ($p = .046$, $z = 2.00$, $r = 0.43$), whereas no baseline change was observed under temporal uncertainty ($p = .715$). Extension movements showed a similar pattern but did not reach statistical significance: stiffness following the temporally predictable condition increased at a trend level ($p = .077$, $z = 1.77$, $r = 0.38$), while no meaningful change was observed following the temporally uncertain condition ($p = .520$).

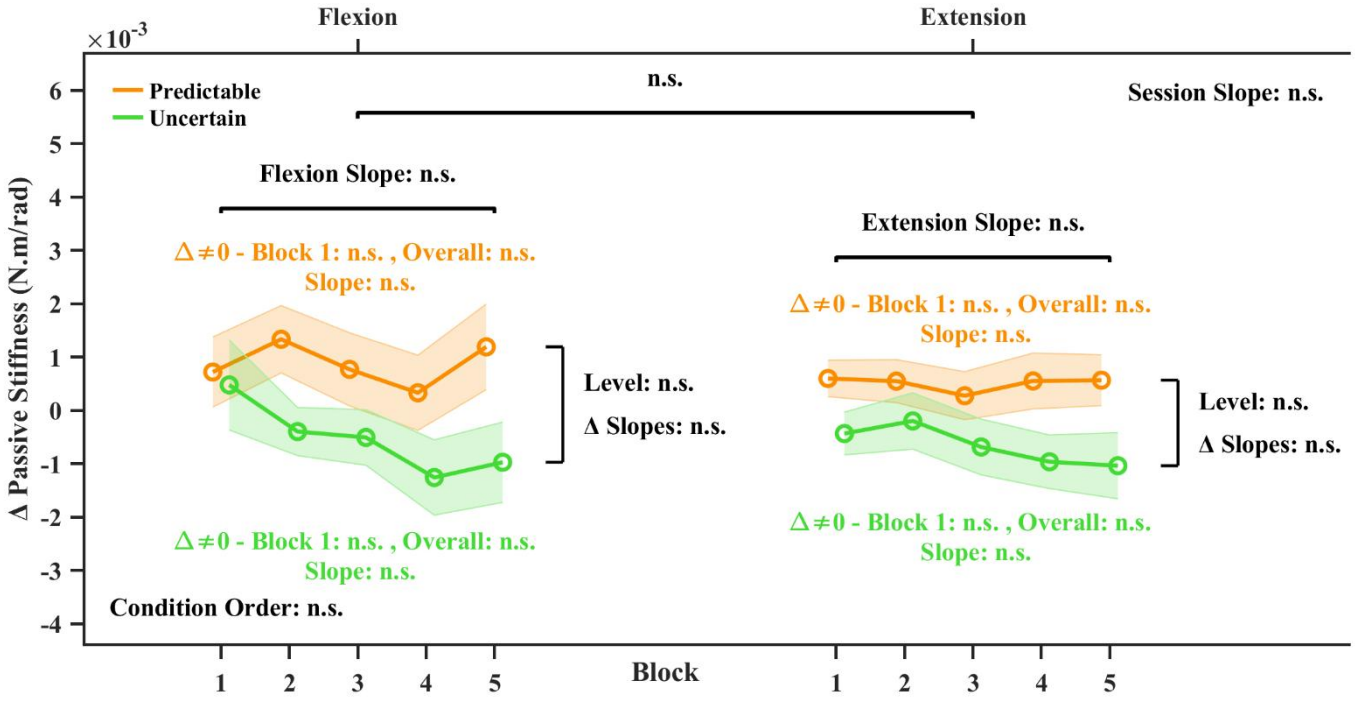

Figure 5.3. Passive Stiffness (N·m/rad) across experimental blocks for flexion (left) and extension (right) following temporally predictable (orange) and uncertain (green) perturbation conditions. Circles denote block-wise means and shaded regions represent variability (±SEM). For each condition-direction combination, stiffness was tested for statistical divergence from baseline levels (Δ ≠ 0) at the initial task block and the combination overall. Level effects indicate overall differences in passive stiffness, whereas Slope effects indicate linear trends across repeated blocks. Significance codes: * p < 0.05, ** p < 0.01, *** p < 0.001; n.s., not significant.

Passive stiffness responses differed modestly as a function of perturbation amplitude, with effects dominated by overall directional and temporal factors rather than consistent amplitude-dependent differences. Across conditions, stiffness change was biased toward greater reductions in flexion than extension ($\beta = -2.53 \times 10^{-4}$, 95% CI = [$-4.71 \times 10^{-4}$, -3.53×10^{-5}], p = .023). In addition, stiffness decreased markedly over the course of the session, with a strong overall effect indicating lower stiffness in the second task condition completed ($\beta = -1.41 \times 10^{-3}$, 95% CI = [$-1.95 \times 10^{-3}$, -8.68×10^{-4}], p < .001), alongside a smaller contribution of task order ($\beta = -2.78 \times 10^{-4}$, 95% CI = [$-5.17 \times 10^{-4}$, -3.82×10^{-5}], p = .023). Perturbation amplitude itself showed limited influence. At the global level, the contrast between 1 Nm and 0.5 Nm did not reach significance ($\beta = -4.00 \times 10^{-4}$, 95% CI = [$-8.43 \times 10^{-4}$, 4.29×10^{-5}], p = .077), and amplitude effects did not differ reliably between flexion and extension (p = .354). Within-condition analyses indicated a significant deviation from baseline only for the 1 Nm condition when collapsing across directions ($\beta = -3.57 \times 10^{-4}$, 95% CI = [$-6.88 \times 10^{-4}$, -2.55×10^{-5}], p = .035), whereas the 0.5 Nm condition showed no such effect (p = .379). Direction-specific estimates similarly indicated a reduction in flexion stiffness at 1 Nm ($\beta = -9.56 \times 10^{-4}$, 95% CI = [$-1.85 \times 10^{-3}$, -5.86×10^{-5}], p = .037), with no corresponding effect at 0.5 Nm (p = .920).

Nonparametric comparisons of the first stabilisation block relative to baseline did not reveal robust amplitude-dependent differences. No within-condition baseline change reached significance for either amplitude in flexion or extension (p ≥ .064), and baseline-corrected changes did not differ between 1 Nm and 0.5 Nm in either direction (flexion: p = .552; extension: p = .917).

Across cohorts, temporal predictability and perturbation amplitude produced qualitatively different patterns of passive stiffness modulation. Manipulating temporal predictability led to a small but reliable increase in stiffness relative to baseline, most evident in early assessments and expressed similarly in flexion and extension. This suggests that temporal predictability engages a global adjustment in passive stiffness, consistent with anticipatory or state-dependent tuning that emerges rapidly and does not require prolonged exposure. In contrast, manipulating perturbation amplitude did not yield a

comparably robust or sustained effect. Although higher-amplitude perturbations were associated with localized reductions in stiffness in some analyses, these effects were weak, inconsistent across directions, and largely overshadowed by strong session-wide decreases and order effects. The absence of clear between-condition differences at the first block further indicates that stiffness was not systematically scaled to perturbation amplitude.

Taken together, these results point to temporal predictability as a more potent driver of passive stiffness modulation than perturbation amplitude. Whereas predictability appears to bias the system toward a stiffer baseline state, changes in physical load amplitude are either insufficient to elicit a consistent passive response or are rapidly compensated by broader temporal dynamics such as adaptation, fatigue, or drift. This dissociation suggests that passive stiffness is more sensitive to higher-order task structure than to the absolute size of external perturbations.

5.3.3. Co-Contraction During Passive Mobilisation

Co-contraction showed little sensitivity to temporal predictability. Overall levels did not differ reliably between predictable and uncertain conditions ($p = .579$), nor did co-contraction change systematically over blocks or across the session ($p \geq .272$). The only consistent effect was lower co-contraction in flexion compared with extension ($\beta = -0.02$, 95% CI = [−0.03, −0.01], $p = .001$). Nonparametric comparisons confirmed that co-contraction in the first assessment block did not differ from baseline in any condition or direction ($p \geq .338$), and baseline changes did not differ between predictable and uncertain conditions ($p \geq .765$).

In the perturbation amplitude cohort, co-contraction during passive assessment was clearly modulated by perturbation amplitude and movement direction, with weaker evidence for block-wise adaptation. Overall co-contraction was lower in flexion than extension ($\beta = -0.02$, 95% CI = [−0.03, −0.01], $p < .001$). In contrast to the temporal predictability cohort, perturbation amplitude exerted a robust effect: co-contraction was consistently lower following the 1 Nm condition compared with 0.5 Nm ($\beta = -0.03$, 95% CI = [−0.05, −0.01], $p < .001$, **Figure 5.4**). This amplitude effect was direction-dependent. In extension, co-contraction was substantially reduced following the 1 Nm condition relative to 0.5 Nm ($\beta = -0.04$, 95% CI = [−0.06, −0.01], $p = .003$), whereas in flexion the same contrast showed only a trend ($p = .052$). Cell-wise estimates were consistent with this pattern, showing reduced co-contraction in flexion at 1 Nm ($\beta = -0.04$, 95% CI=[-0.08, -0.01], $p = .015$) and elevated co-contraction in extension at 0.5 Nm ($\beta = 0.05$, 95% CI=[0.02, 0.09], $p = .004$). Despite these level differences, co-contraction did not change reliably across blocks, and rates of change over time were similar between amplitudes and directions ($p \geq .230$).

Nonparametric comparisons confirmed the absence of reliable early baseline shifts. Co-contraction at the first stabilisation block did not differ from baseline in either amplitude or direction ($p \geq .363$), and baseline-corrected changes were comparable between 1 Nm and 0.5 Nm for both flexion and extension ($p \geq .221$).

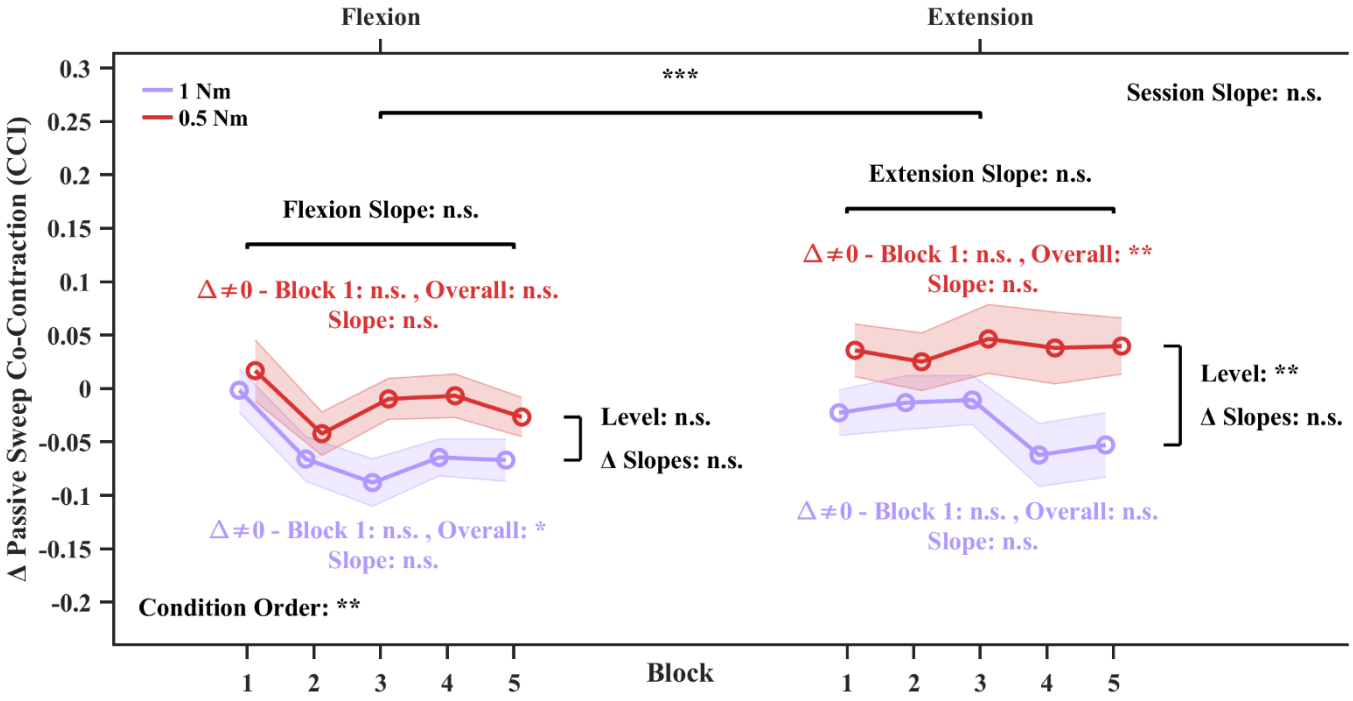

Figure 5.4. Passive Co-contraction (CCI) across experimental blocks for flexion (left) and extension (right) following high-amplitude (purple) and low-amplitude (red) perturbation conditions. Full plot description - Figure 5.3.

Across cohorts, co-contraction showed limited modulation and no evidence of baseline shifts or block-wise adaptation, contrasting with the more consistent effects observed for passive stiffness. In the first cohort, co-contraction was largely insensitive to temporal predictability, aside from a small modulation of flexion–extension asymmetry, indicating that predictability-related mechanical changes were not accompanied by sustained alterations in antagonist activation. In the second cohort, co-contraction varied systematically with perturbation amplitude, with higher loads associated with reduced antagonist activation, particularly in extension, but again showed little evidence of adaptation over time. Despite differing task manipulations, both cohorts exhibited stable co-contraction profiles, suggesting that co-contraction primarily reflects tonic, load-dependent neural strategies rather than sensitivity to higher-order temporal structure.

5.3.4. Beta-Band Corticomuscular Coherence

In the temporal predictability cohort, beta-band corticomuscular coherence (β-CMC) showed limited sensitivity to previous task condition, with effects dominated by direction and broad session-level changes rather than condition-specific modulation. Overall coherence was higher in flexion than extension ($\beta = 4.2 \times 10^{-3}$, 95% CI = [$1.1 \times 10^{-3}$, 1.0×10^{-2}], $p = .008$), indicating a consistent directional bias independent of predictability.

Evidence for predictability-related effects was weak and inconsistent. When collapsing across directions, coherence differed from baseline only following the uncertain condition ($\beta = 0.01$, 95% CI = [6.5×10^{-4}, 1.0×10^{-2}], $p = .025$), whereas the predictable condition produced no reliable baseline deviation ($p = .130$). However, direct comparisons between predictable and uncertain conditions within either flexion or extension were nonsignificant (flexion $p = .290$; extension $p = .530$), and there was no evidence that predictability altered rates of change across blocks ($p \geq .788$).

There was a minor increase in β-CMC during assessment following the second condition ($\beta = 1 \times 10^{-3}$, 95% CI = [3.5×10^{-4}, 0.01], $p = .040$), suggesting a non-condition-specific increase. This temporal

increase did not interact reliably with predictability or direction ($p \geq .059$). Cell-wise analyses and nonparametric comparisons confirmed the absence of robust early effects: coherence during the first assessment block did not differ from baseline in any condition or direction ($p \geq .170$), and baseline-to-assessment changes were comparable between predictable and uncertain conditions ($p \geq .218$).

In the perturbation amplitude cohort, β-CMC during passive assessment demonstrated specific modulation based on amplitude condition and movement direction, with little evidence for block-wise adaptation. Overall coherence was higher in flexion than extension ($\beta = 4.7 \times 10^{-3}$, 95% CI = [$1.0 \times 10^{-3}$, 1.0×10^{-2}], $p = .013$, **Figure 5.5**), indicating a robust directional bias like that observed in the temporal predictability cohort. Perturbation amplitude selectively modulated coherence – β-CMC differed from baseline only in the 0.5 Nm condition ($\beta = 0.01$, 95% CI = [3.7×10^{-3}, 2.0×10^{-2}], $p = .001$), whereas the 1 Nm condition showed no deviation from baseline ($p = .995$). Direct comparisons revealed a amplitude-dependent difference in flexion, with lower β-CMC following 1 Nm than 0.5 Nm perturbations ($\beta = -0.01$, 95% CI = [-0.02, -3×10^{-5}], $p = .049$). This effect was absent in extension ($p = .928$). Cell-wise estimates were consistent with this pattern, showing elevated flexion coherence at 0.5 Nm both at the first block ($p = .036$) and at the centred block ($p = .004$), with no corresponding effects following the 1 Nm condition. The was a significant increase in β-CMC during assessments following the second condition ($\beta = 0.01$, 95% CI = [2.23×10^{-3}, 0.01], $p = .005$) but this did not interact with perturbation amplitude or direction ($p \geq .759$). Learning-related slopes and block-wise changes were uniformly nonsignificant ($p \geq .181$), indicating stable coherence levels across assessments. Nonparametric comparisons confirmed the absence of reliable early shifts: coherence during the first assessment block did not differ from baseline in any condition or direction ($p \geq .152$), and changes were comparable between 1 Nm and 0.5 Nm in both flexion and extension ($p \geq .196$).

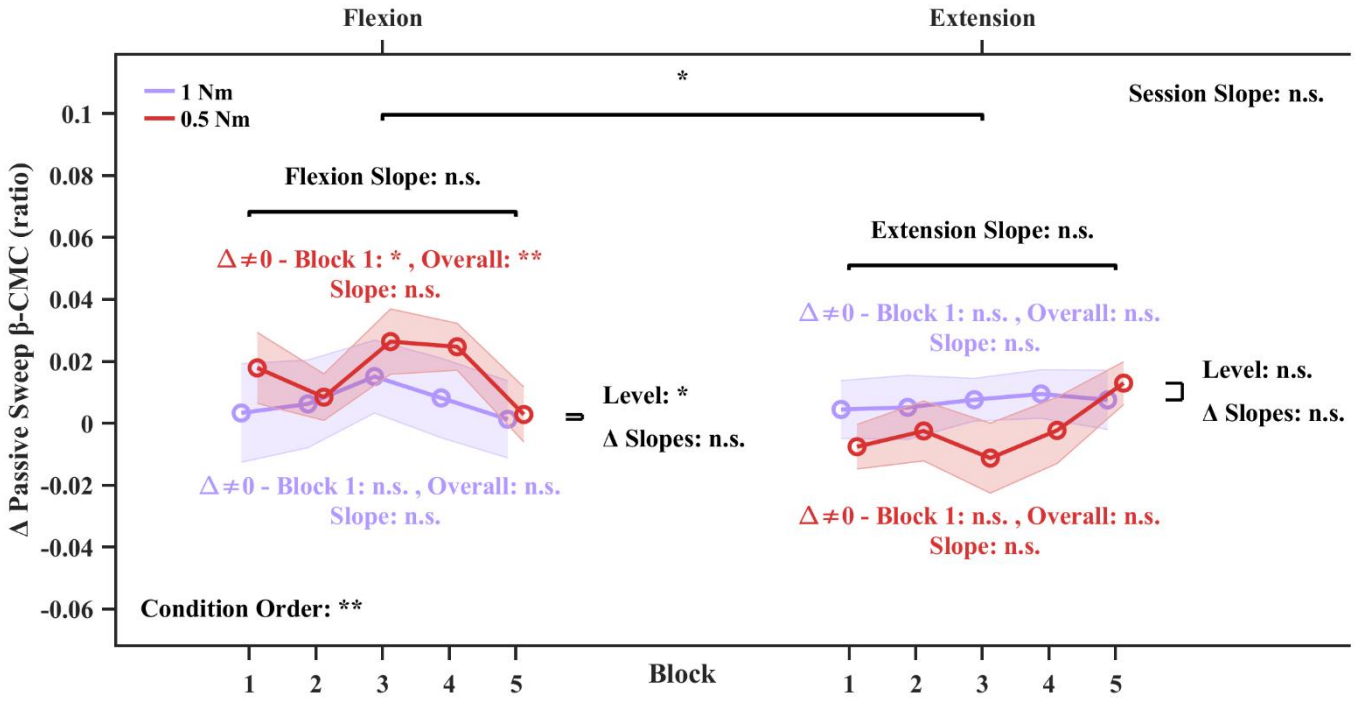

Figure 5.5. Passive beta-band corticomuscular coherence (βCMC) across experimental blocks for flexion (left) and extension (right) following high-amplitude (purple) and low-amplitude (red) perturbation conditions. Full plot description - Figure 5.3.

In the temporal predictability cohort, β-CMC exhibited a stable flexion–extension asymmetry and a gradual session-level increase, with little evidence that temporal predictability modulated coherence at task onset or across learning. β-CMC did not differ reliably between predictable and uncertain conditions, showed no consistent baseline shifts, and exhibited no condition-dependent block-wise

changes, indicating that predictability-related effects on passive mechanics were not accompanied by parallel changes in beta-band coupling.

In the perturbation amplitude cohort, β-CMC varied with perturbation amplitude rather than evolving dynamically over time. Lower-amplitude perturbations were associated with higher βCMC, particularly in flexion, whereas higher loads were accompanied by reduced βCMC. These amplitude-dependent differences reflected stable level shifts rather than learning or adaptation, with minimal evidence for baseline or block-wise effects.

Despite differing task manipulations, both cohorts showed a consistent flexion-dominant pattern of β-CMC that was largely independent of experimental context. Together, these findings indicate that β-CMC during passive assessment was largely insensitive to prior temporal structure but selectively responsive to physical load, supporting the interpretation that β-CMC primarily reflects load-dependent neural engagement rather than anticipatory or contextual tuning.

5.3.5. Does Co-Contraction Account for Variability in Passive Assessment Stiffness?

In the temporal predictability cohort, co-contraction (CCI) showed clear associations with passive stiffness at both the between- and within-participant levels. Overall, the mean level of CCI demonstrated a clear trend of greater CCI leading to greater stiffness during passive assessment ($\beta = 3.27 \times 10^{-3}$, 95% CI = $[-2.70 \times 10^{-4}, 6.80 \times 10^{-3}]$, $p = .070$). This relationship was strongly modulated by condition, with passive assessments following the temporally predictable task showing a much stronger association ($\beta = 2.80 \times 10^{-3}$, 95% CI = $[1.31 \times 10^{-3}, 4.30 \times 10^{-3}]$, $p < .001$). This pattern was consistent across both movement directions, with significant associations in each direction following the predictable condition ($p \leq .044$, **Figure 5.6**) and nonsignificant relationships following the uncertain condition ($p \geq .719$). Within-participant changes in CCI were also associated with increased stiffness overall ($\beta = 3.73 \times 10^{-3}$, 95% CI = $[8.50 \times 10^{-4}, 6.61 \times 10^{-3}]$, $p = .011$), driven primarily by flexion ($\beta = 5.09 \times 10^{-3}$, 95% CI = $[2.25 \times 10^{-3}, 7.94 \times 10^{-3}]$, $p < .001$). Positive within-participant associations were observed in flexion for both predictable and uncertain conditions ($p \leq .019$), with no significant effects in extension ($p \geq .658$).

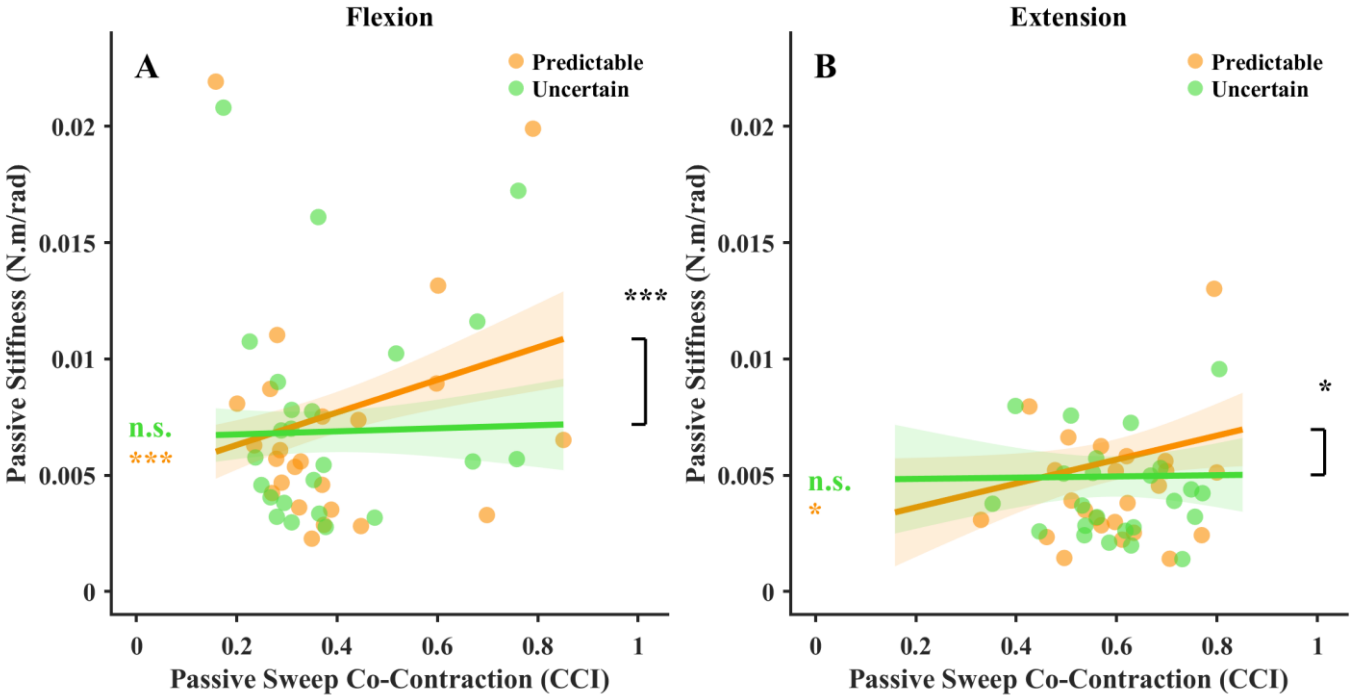

Figure 5.6. Between-participant relationship between co-contraction during passive assessment (CCI) and stiffness during passive assessment (N·m/rad) for (A) flexion and (B) extension. Each point represents an individual participant's mean level for a given condition (predictable, orange; uncertain, green). Solid lines depict condition-specific model fits, with shaded bands indicating the corresponding 95% confidence intervals. Asterisks adjacent to the axes denote the statistical significance of the respective model fits, while brackets indicate comparisons between fits. Scatter points reflect raw between-participant means and do not account for additional model coefficients, which may result in a visual mismatch between the fitted lines and the distribution of points. Significance codes: * p < 0.05, ** p < 0.01, *** p < 0.001; n.s., not significant.

In contrast, the perturbation amplitude cohort showed minimal coupling between CCI and stiffness during passive assessment. Average CCI was not associated with stiffness overall ($p = .756$), nor did this relationship differ reliably by amplitude condition ($p = .264$). A single exception was a modest negative between-participant association in extension at the higher perturbation amplitude ($\beta = -3.86 \times 10^{-3}$, 95% CI = [$-7.58 \times 10^{-3}$, -1.39×10^{-4}], $p = .042$), which was absent at 0.5 Nm and did not differ significantly between amplitudes ($p = .071$). Within-participant co-contraction fluctuations did not predict stiffness in any condition ($p \geq .166$).

Overall, stiffness was tightly coupled to co-contraction under temporal predictability, particularly in flexion and at the between-participant level, whereas in the amplitude cohort stiffness showed little dependence on either baseline or alterations in co-contraction.

5.3.6. Does Passive Assessment Stiffness Correlate with Beta-Band Corticomuscular Coherence?

In the temporal predictability cohort, passive stiffness was strongly and consistently related to beta-band corticomuscular cohere (βCMC) at both the between- and within-participant levels, with predominantly negative associations. Across participants, higher β-CMC was associated with lower stiffness overall (β = -0.07, 95% CI = [-0.09, -0.05], $p < .001$). This inverse relationship was present in both directions but varied by condition. In flexion, negative associations of similar amplitude were observed under both predictable and uncertain conditions ($p < .001$), with no reliable difference between them ($p = .143$). In extension, β-CMC predicted lower stiffness under predictable conditions (β = -0.06, 95% CI = [-0.09, -0.03], $p < .001$) but not under uncertain conditions ($p = .472$), with a significant divergence between conditions ($p = .007$). Within-participant deviations in β-CMC were also

associated with reduced stiffness (β = -0.03, 95% CI = [-0.04, -0.02], p < .001). These within-participant effects were evident in both directions and conditions but were strongest in flexion under uncertain conditions (β = -0.05, 95% CI = [-0.06, -0.04], p < .001, **Figure 5.7A**).

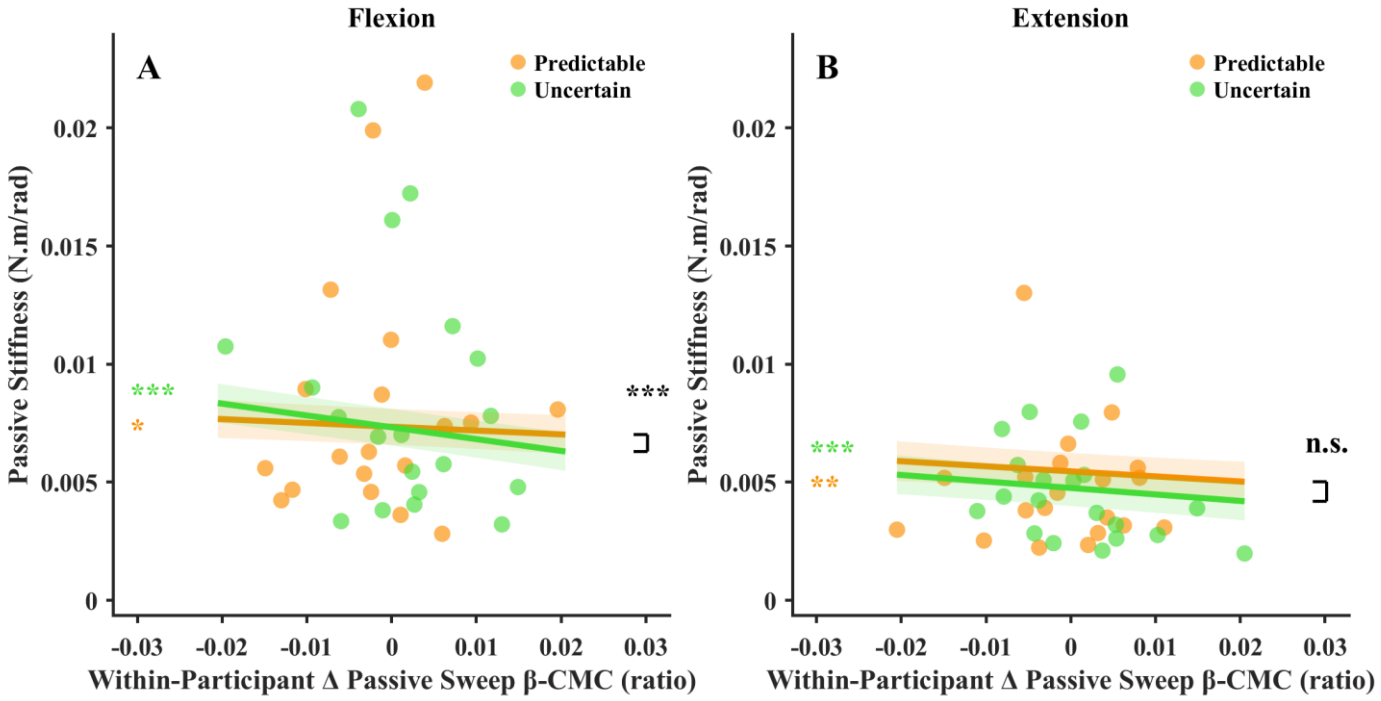

Figure 5.7. With-participant relationship between change in beta-band corticomuscular coherence during passive assessment (β-CMC) and stiffness during passive assessment (N·m/rad) for (A) flexion and (B) extension. Each point represents an individual participant's mean level for a given condition (predictable, orange; uncertain, green). Full plot description - Figure 5.6.

In the perturbation amplitude cohort, passive stiffness likewise showed robust inverse associations with β-CMC at both the between- and within-participant levels, with these relationships modulated by perturbation amplitude. Across participants, higher β-CMC predicted lower stiffness overall (β = −0.04, 95% CI = [−0.07, -6.48×10^{-3}], p = .017). This negative association was present following the low-amplitude condition (0.5 Nm) for both flexion (β = −0.03, 95% CI = [−0.06, -7.73×10^{-3}], p = .012, **Figure 5.8A**) and extension (β = −0.07, 95% CI = [−0.12, −0.03], p = .002, **Figure 5.8B**) but was nonsignificant following the high-amplitude condition (1 Nm) in both directions (p ≥ .093). Within participants, transient increases in β-CMC were associated with lower stiffness in both flexion and extension following both amplitude conditions (p ≤ .018), with no reliable differences between effect sizes (p ≥ .213).

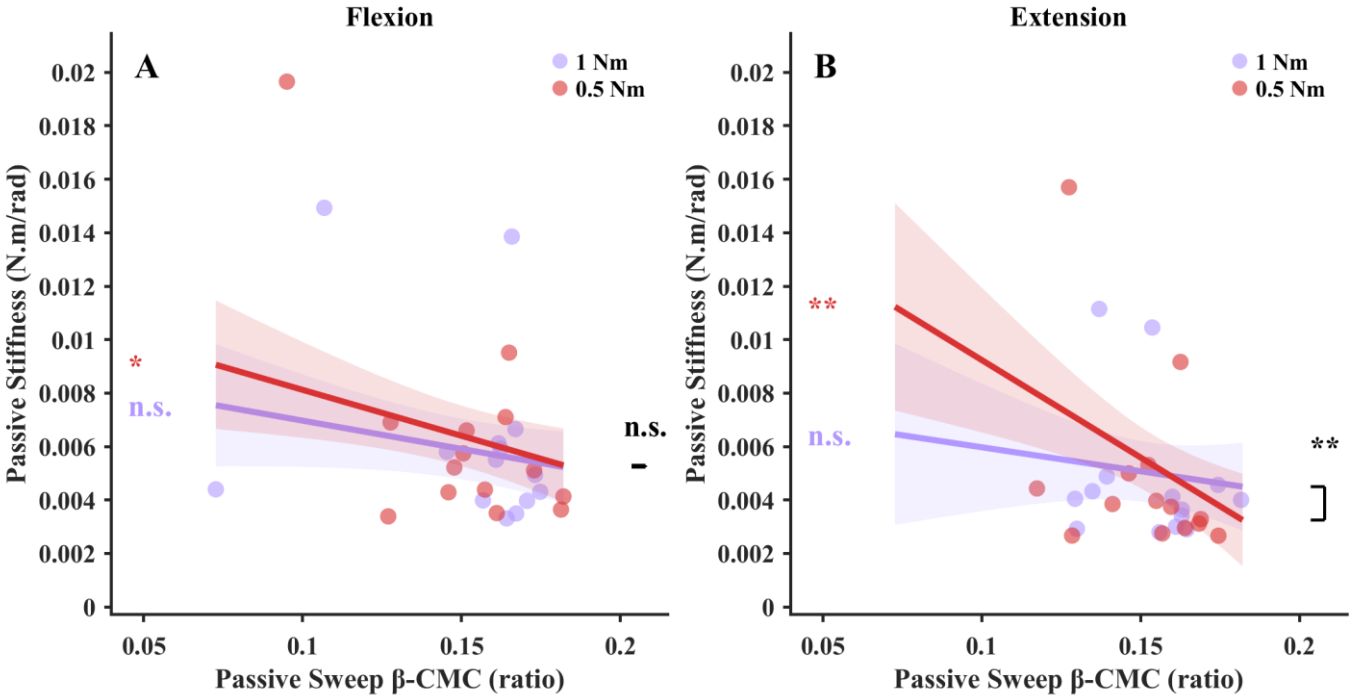

Figure 5.8. Between-participant relationship between beta-band corticomuscular coherence during passive assessment (β-CMC) and stiffness during passive assessment (N·m/rad) for (A) flexion and (B) extension. Each point represents an individual participant's mean level for a given condition (high-amplitude, purple; low-amplitude, red). Full plot description - Figure 5.6.

Across cohorts, passive stiffness showed a robust inverse relationship with beta-band corticomuscular coherence. In the perturbation amplitude cohort, higher β-CMC was associated with lower stiffness both across and within participants, with between-participant effects strongest at lower perturbation amplitudes and within-participant effects present regardless of load or direction. In the temporal predictability cohort, β-CMC likewise predicted reduced stiffness at both levels of analysis, with consistent effects in flexion across conditions and condition-dependent effects in extension. Together, these findings indicate that increased corticospinal coupling is reliably associated with a more compliant mechanical state, while task demands such as load amplitude and predictability modulate the strength, but not the direction, of this relationship.

5.3.7. Does Passive Assessment Co-Contraction Correlate with Beta-Band Corticomuscular Coherence?

In the temporal predictability cohort, associations between co-contraction (CCI) and beta-band corticomuscular coherence (βCMC) were weak and selective. Between participants, average task CCI showed a modest negative association with β-CMC that did not reach significance overall ($p = .090$), but a significant negative relationship emerged in flexion under predictable conditions ($\beta = -0.05$, 95% CI = $[-0.10, -9.89 \times 10^{-3}]$, $p = .016$). No corresponding effects were observed in flexion under uncertain conditions ($p = .730$) or in extension ($p \geq .105$), and the difference in flexion slopes between conditions approached but did not reach significance ($p = .057$). Within-participant variation did not predict β-CMC overall ($p = .951$) or within any condition or direction ($p \geq .096$).

In the amplitude cohort, CCI again showed no overall association with β-CMC at either the between- or within-participant level. Mean CCI was not significant when averaged across directions and amplitudes ($p = .257$), but a significant negative association was observed in flexion following the higher perturbation amplitude condition ($\beta = -0.07$, 95% CI = [-0.11, -0.02], $p = .007$), with no effect at 0.5 Nm ($p = .627$). The difference between amplitudes in flexion approached significance ($p = .053$), and no

effects were present in extension (p ≥ .745). Within-participant effects were nonsignificant overall (p = .156) and within all amplitude and direction combinations (p ≥ .292).

Overall, in both cohorts, only between-participant differences in co-contraction showed limited associations with βCMC, confined to flexion under specific task conditions, while within-participant fluctuations in co-contraction did not predict corticomuscular coherence.

5.3.8. Is Co-Contraction Coupled Between Stabilisation and Passive Assessment Phases?

In the temporal predictability cohort, coupling between stabilisation phase and passive co-contraction was evident primarily within participants and depended on both direction and temporal structure, whereas between-participant associations were weak. Average task co-contraction did not predict passive co-contraction overall or when stratified by condition or direction (p ≥ .086). In contrast, clear within-participant coupling emerged under predictable timing. In flexion, increases in stabilisation phase co-contraction were associated with higher passive co-contraction following the predictable condition (β = 0.55, 95% CI = [0.18, 0.93], p = .004, **Figure 5.9A**), an effect absent following the uncertain condition (p = .581). In extension, the relationship reversed under predictable timing, with higher task co-contraction predicting lower passive co-contraction (β = -0.56, 95% CI = [-0.93, -0.18], p = .004, **Figure 5.9B**), and no association under uncertainty (p = .420). These effects were supported by a significant interaction showing that within-participant coupling was modulated by direction (β = 0.27, 95% CI = [0.10, 0.44], p = .002). Overall, task and passive co-contraction were dynamically linked within individuals only under predictable temporal structure, in a direction-specific manner, and did not generalise across participants.

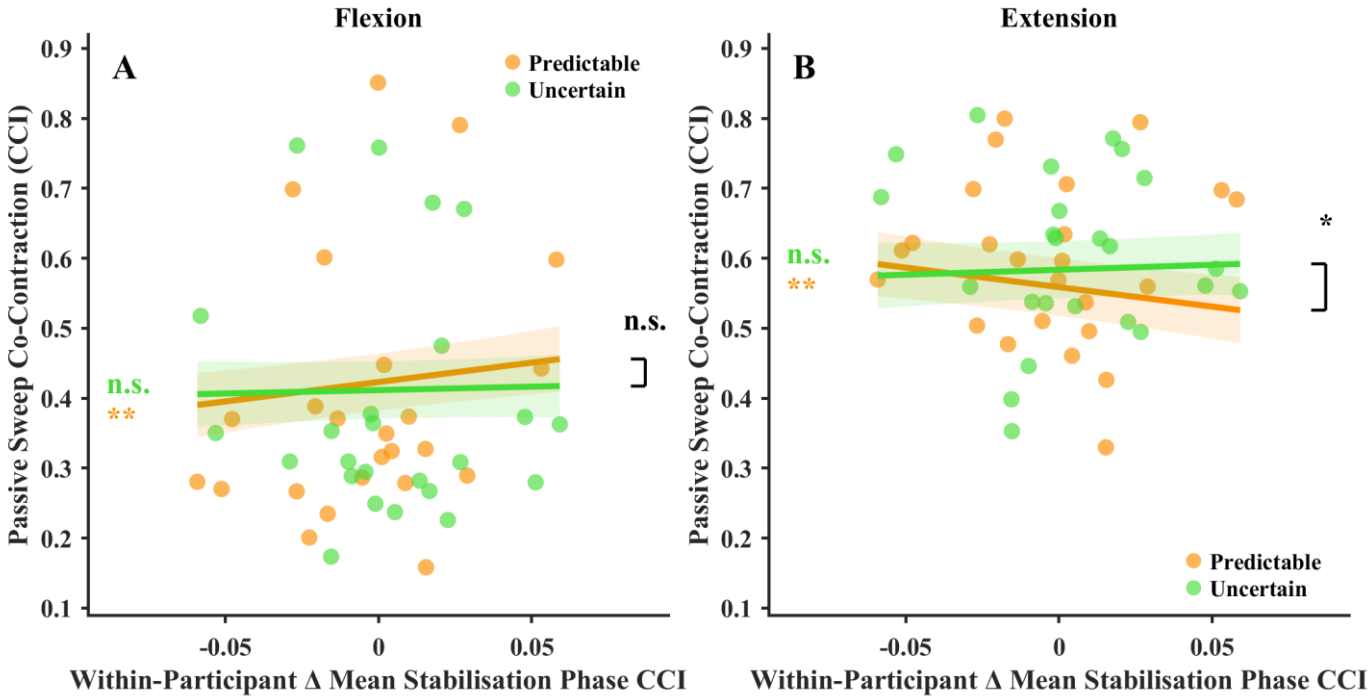

Figure 5.9. Within-participant relationship between change in co-contraction during the stabilisation phase (CCI) and co-contraction during passive assessment (CCI) for (A) flexion and (B) extension. Each point represents an individual participant's mean level for a given condition (high-amplitude, purple; low-amplitude, red). Full plot description - Figure 5.6.

In the amplitude cohort, no systematic coupling was observed between stabilisation phase and passive co-contraction at either the between- (p = .597) or within-participant level (p = .201). Average task co-

contraction did not predict passive co-contraction overall or within any combination of direction and perturbation amplitude ($p \geq .187$), and within-participant fluctuations likewise showed no reliable associations ($p \geq .313$) . Together, these results indicate that task-passive co-contraction coupling reflects context-specific state modulation rather than a stable or load-dependent trait.

5.3.9. Is Beta-Band Corticomuscular Coherence Coupled Between Stabilisation and Passive Assessment Phases?

In the temporal predictability cohort, relationships between task-related and passive-assessment β-CMC were weak, with only limited direction-specific coupling. Neither average nor within-participant changes in task β-CMC predicted passive β-CMC overall ($p \geq .322$), and no significant between-participant effects were observed for any direction or condition ($p \geq .096$), nor did these relationships differ reliably across conditions ($p \geq .572$). The only significant within-participant association was observed in extension following the temporally predictable condition ($\beta = 0.98$, 95% CI = [0.01, 1.95], $p = .047$).

In the amplitude cohort, there was no evidence for coupling between task-related and passive β-CMC at either the between- or within-participant level. Average task β-CMC did not predict passive β-CMC overall ($p = .427$), and this null effect was consistent across perturbation amplitudes and movement directions ($p \geq .434$). Within-participant fluctuations in task β-CMC likewise showed no association with passive β-CMC ($p = .595$), with no effects emerging in any direction or amplitude ($p \geq .423$).

Overall, task-to-passive β-CMC coupling was largely absent, and the single significant effect observed was isolated and not indicative of a general relationship.

5.3.10. Summary

Across cohorts, temporal predictability and perturbation amplitude dissociated in their influence on passive stiffness and associated neural measures. Manipulating temporal predictability produced divergent stiffness biases: temporally predictable stabilisation was followed by increased passive stiffness, whereas temporally uncertain stabilisation was associated with reduced stiffness relative to baseline. In contrast, changes in perturbation amplitude did not yield a stable or systematic scaling of stiffness, with weak and directionally inconsistent effects that were overshadowed by broader session-level dynamics. This dissociation indicates that passive stiffness is more sensitive to higher-order temporal structure than to absolute perturbation size.

Co-contraction during passive assessment showed a complementary pattern. It was largely insensitive to temporal predictability and exhibited no baseline shifts or adaptive dynamics, whereas perturbation amplitude modulated co-contraction tonically, with higher loads associated with reduced antagonist activation. This stability across time and conditions suggests that co-contraction during passive mobilisation primarily reflects load-dependent neural strategies rather than anticipatory or contextual tuning. Consistent with this interpretation, stiffness was tightly coupled to co-contraction only under temporal predictability, with little coupling evident in the amplitude cohort.

Beta-band corticomuscular coherence (β-CMC) displayed a distinct profile. Across cohorts, passive stiffness was robustly and inversely related to β-CMC at both the between- and within-participant levels, indicating that stronger corticospinal coupling was associated with a more compliant mechanical state. Although the strength of this relationship was modulated by task demands—being most pronounced at lower loads and under predictable timing—its direction was preserved across contexts. In contrast, coupling between task-related and passive β-CMC was largely absent, and associations between co-contraction and β-CMC were weak and condition specific.

Together, these findings support a functional dissociation between passive stiffness, co-contraction, and β-CMC. Passive stiffness is preferentially shaped by higher-order temporal structure, co-contraction reflects tonic, load-dependent control, and β-CMC indexes neural engagement linked to mechanical compliance. Their partial independence indicates that anticipatory tuning, load-dependent activation, and corticospinal coupling contribute to limb mechanics through distinct but interacting sensorimotor control processes.

5.4. Passive Stiffness in Parkinson's Disease

5.4.1. Introduction

The HRX-1 manipulandum is well suited to the automated assessment of rigidity in Parkinson's disease, addressing a motor symptom that has historically received far less attention in automated diagnostic research than tremor and bradykinesia. This imbalance largely reflects practical limitations: unlike tremor or slowness of movement, rigidity assessment requires the active application of external torque, a requirement that is incompatible with most wearable systems designed for passive measurement. By generating slow, controlled flexion and extension movements at the wrist, however, it is possible to approximate key elements of the clinical examination used by neurologists to assess rigidity. Building on this principle, a small proof-of-concept study was undertaken to investigate whether quantitative measures of stiffness derived from the system align with clinician-rated rigidity, whether changes between on and off treatment states - both pharmacological and neural stimulation - can be detected, and whether these measures can distinguish individuals with Parkinson's disease from healthy controls.

5.4.2. Do Passive Assessments Correlate with Clinician's UPDRS Scores?

The primary evaluation of the clinical utility of the passive assessment was to determine whether it could reliably reproduce clinician-rated rigidity as quantified by UPDRS-III scores. Parkinson's disease data were therefore stratified into ON-treatment and OFF-treatment conditions, and the relationship between the derived stiffness measures and the corresponding clinical labels was systematically examined. Analyses were performed separately for each movement direction, as well as for the mean stiffness across each trial. Separating ON- and OFF-treatment data both avoided bias arising from repeated measures within the same participant and enabled assessment of whether the association between passive stiffness measures and clinical rigidity ratings remained robust across changes in treatment state.

When assessing the ON-treatment condition, Kruskal–Wallis tests demonstrated a significant separation by UPDRS rigidity scores for both direction-specific and averaged stiffness measures ($p \leq .009$). The strongest effect was observed for flexion stiffness ($H = 13.840$, $\eta^2 = 0.452$, $\varepsilon^2 = 0.402$, $p = .003$). Pairwise comparisons indicated that this overall significance was driven primarily by contrasts between the lowest UPDRS scores and the highest (**Table 5.3**), a pattern that was consistent for extension and mean stiffness measures. Complementary Spearman correlation analyses supported these findings, with flexion stiffness showing the strongest association with clinical rigidity ratings ($\rho = 0.693$, $\rho^2 = 0.481$, 95% CI = [0.475, 0.830], $p < .001$), while all stiffness measures exhibited a highly significant monotonic relationship with UPDRS scores ($p \leq .001$, **Figure 5.4**).

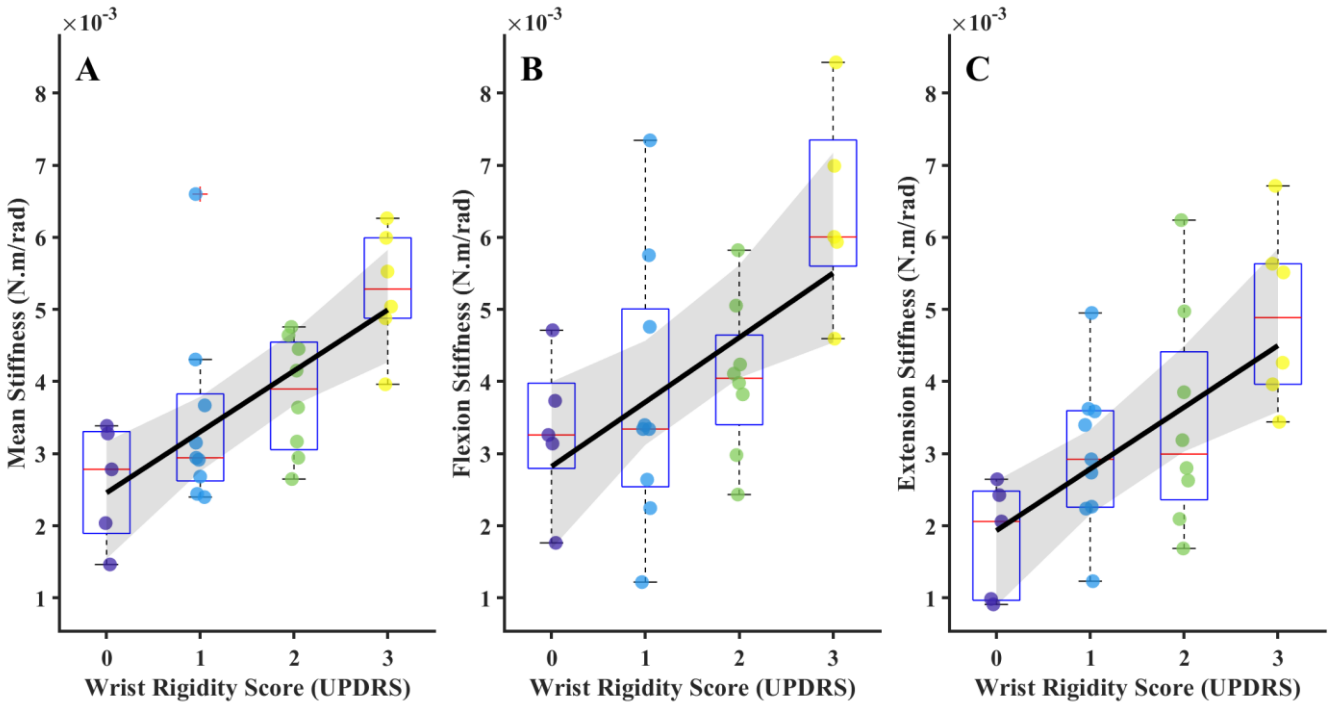

Figure 5.10. Boxplots showing the mean stiffness estimate (N·m/rad) grouped by clinical UPDRS wrist rigidity score for (A) mean across both movement directions, (B) flexion movements and (C) extension movements when participants were ON-treatment. Fitted black line represents the spearman correlation with the shaded area indication 95% confidence interval.

Table 5.3. Table showing the pairwise breakdown of mean stiffness estimates (N·m/rad) following Kruskal-Wallis testing.

UPDRS A	UPDRS B	Estimate	Lower CI	Upper CI	pValue
0	1	-1.644	-13.749	10.460	1.000
0	2	-10.950	-23.322	1.422	0.117
0	3	-14.200	-27.341	-1.059	0.026
1	2	-9.306	-19.851	1.240	0.119
1	3	-12.556	-23.994	-1.118	0.023
2	3	-3.250	-14.971	8.471	1.000

When evaluating the relationship between stiffness measures and clinical UPDRS rigidity scores in the OFF-treatment condition, the previously observed association was largely absent. Neither the Kruskal–Wallis tests nor the correlation analyses reached statistical significance for either movement direction or for the averaged stiffness values ($p \geq .189$, **Figure 5.11**). This lack of differentiation was further supported by the pairwise comparisons, in which p-values were almost uniformly equal to 1, indicating no detectable separation between UPDRS score groups under OFF-treatment conditions. While this pattern of null results may initially suggest a disrupted relationship between passive assessment and OFF-treatment clinical scores, it is important to consider the sparsity of the data, with only 16 total samples distributed across four bins and assessed by two different clinicians. As such, although these findings are suggestive, they should be interpreted with appropriate caution.

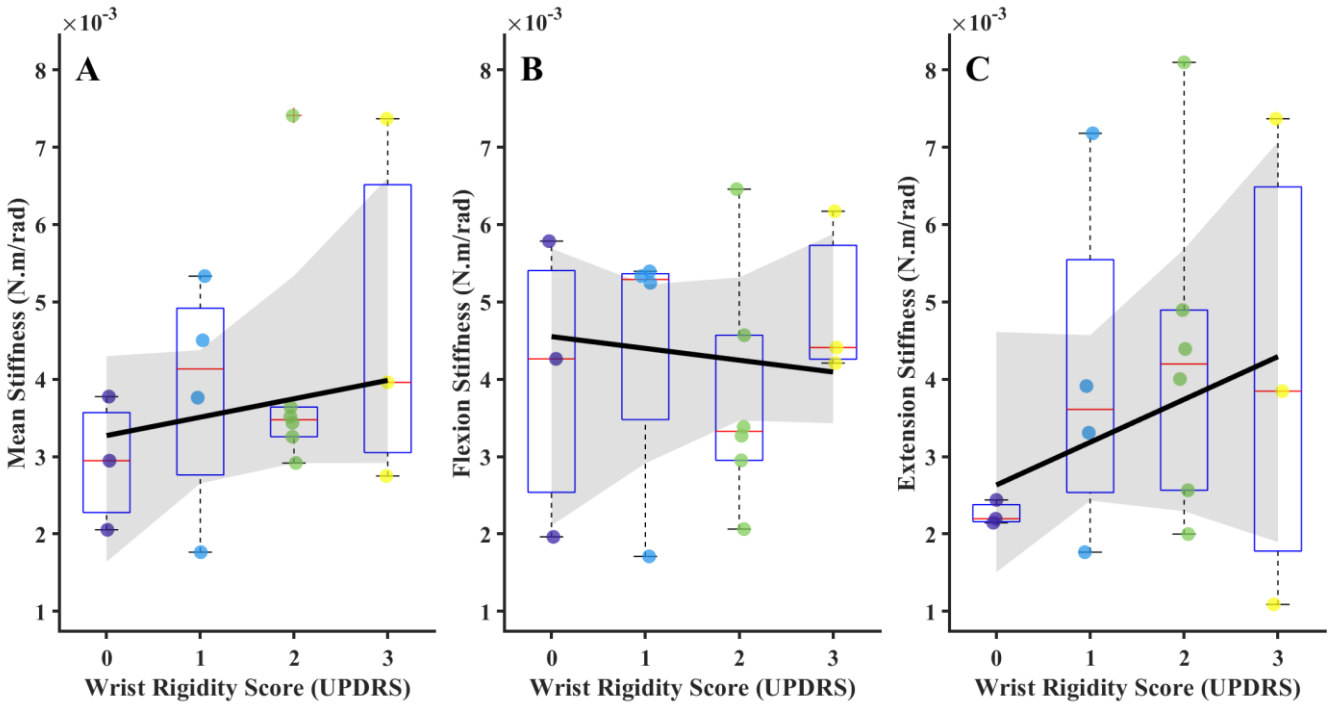

Figure 5.11. Boxplots showing the mean stiffness estimate (N·m/rad) grouped by clinical UPDRS wrist rigidity score for (A) mean across both movement directions, (B) flexion movements and (C) extension movements when participants were OFF-treatment. Fitted black line represents the spearman correlation with the shaded area indication 95% confidence interval.

Across the dataset as a whole, data sparsity represents an important limitation, but this issue is substantially more pronounced in the OFF-treatment condition. In the ON-treatment analyses, despite limited sample sizes, the observed relationships between passive stiffness measures and UPDRS rigidity scores remained robust, even when clinical ratings were provided by three different clinicians. This consistency suggests a degree of generalisability in the passive assessment that persists despite well-documented inter-rater variability in UPDRS scoring. By contrast, the combination of fewer samples and fewer raters in the OFF-treatment condition likely amplified variability and reduced statistical power, making it difficult to draw firm conclusions regarding the absence of observed associations. As such, the contrasting results between ON and OFF conditions should be interpreted in the context of uneven data density rather than as definitive evidence of treatment-specific failure of the passive assessment.

5.4.3. Differentiation of ON and OFF Medication States

Wilcoxon signed-rank testing indicated no statistically significant differences between ON- and OFF-medication states across any of the directional stiffness estimates ($p \geq .438$, **Figure 5.12**), nor were meaningful differences observed between flexion and extension assessments. It should be noted, however, that this analysis was based on only six participants, substantially limiting statistical power and rendering the robustness of these inferential results questionable. As such, qualitative examination of individual trajectories provides valuable additional context. Notably, one participant was clinically rated as having reduced wrist rigidity in the OFF-medication state relative to ON-medication. Although counterintuitive, the corresponding stiffness estimates closely mirrored this clinical assessment, suggesting that this trajectory is unlikely to reflect measurement error and may instead improvement in task compliance underscoring known limitations in the sensitivity and reliability of UPDRS-III rigidity scoring. Consistent with this interpretation, most participants who exhibited a change in clinical rigidity score also demonstrated concordant changes in stiffness quantification. In contrast, cases in which no change in UPDRS score was recorded showed less consistent stiffness trajectories, with changes that

were often larger in amplitude than those observed when clinical scores did change. These discrepancies may reflect the limits of precision of the passive assessment; alternatively, they may indicate that the continuous stiffness measures are capturing subtle variations in rigidity that are not resolved by the coarse, ordinal structure of the UPDRS-III scale.

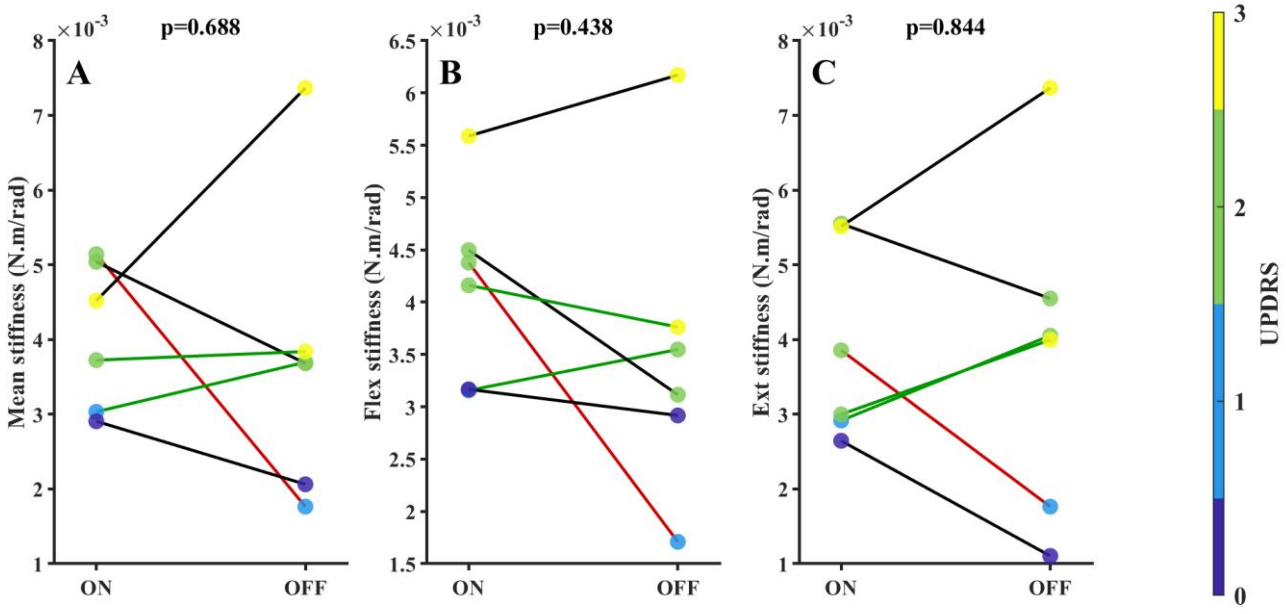

Figure 5.12. Visualisation of the paired ON- vs. OFF-medication mean stiffness estimates (N·m/rad) for (A) mean across both movement directions, (B) flexion movements and (C) extension movements. Pairs are linked, the colour of the line indicating an increase in UPDRS score (green), a decrease (red) or no change (black). UPDRS scores for each assessment are colour-coded based on the colourmap on the right of the figure. Wilcoxon sign rank p-value listed in the title of each plot.

5.4.4. Differentiation of ON and OFF Stimulation States

This analysis highlights a fundamental tension between group-level inference and individual-level behaviour in the ON–OFF stimulation comparison. Although none of the stiffness metrics reach statistical significance ($p \leq .096$, **Figure 5.13**), the near-threshold p-values suggest that the absence of significance is more likely driven by limited sample size and high inter-individual variability than by a true lack of stimulation effect. The wide dispersion of trajectories indicates that stimulation does not exert a uniform influence on passive wrist stiffness but instead modulates rigidity in a highly participant-specific manner. This effect is additionally modulated by heterogeneous parameterisation of stimulation and associated divergence in symptomatic impact. Importantly, where clinical UPDRS rigidity scores change between ON and OFF states, the direction of stiffness change is generally concordant, supporting the physiological relevance of the passive measures. In contrast, participants with unchanged UPDRS scores often show stiffness fluctuations of similar or greater amplitude but without consistent direction, implying that the UPDRS-III scale may be insufficiently sensitive to capture more subtle or continuous changes in rigidity. This pattern suggests that the passive assessment may be detecting underlying mechanical changes that are either masked by the ordinal nature of the clinical scale or averaged out by clinician judgement. Taken together, the results argue against interpreting the null statistical findings as evidence of insensitivity of the passive method and instead point to data sparsity and heterogeneity of stimulation response as the dominant limiting factors.

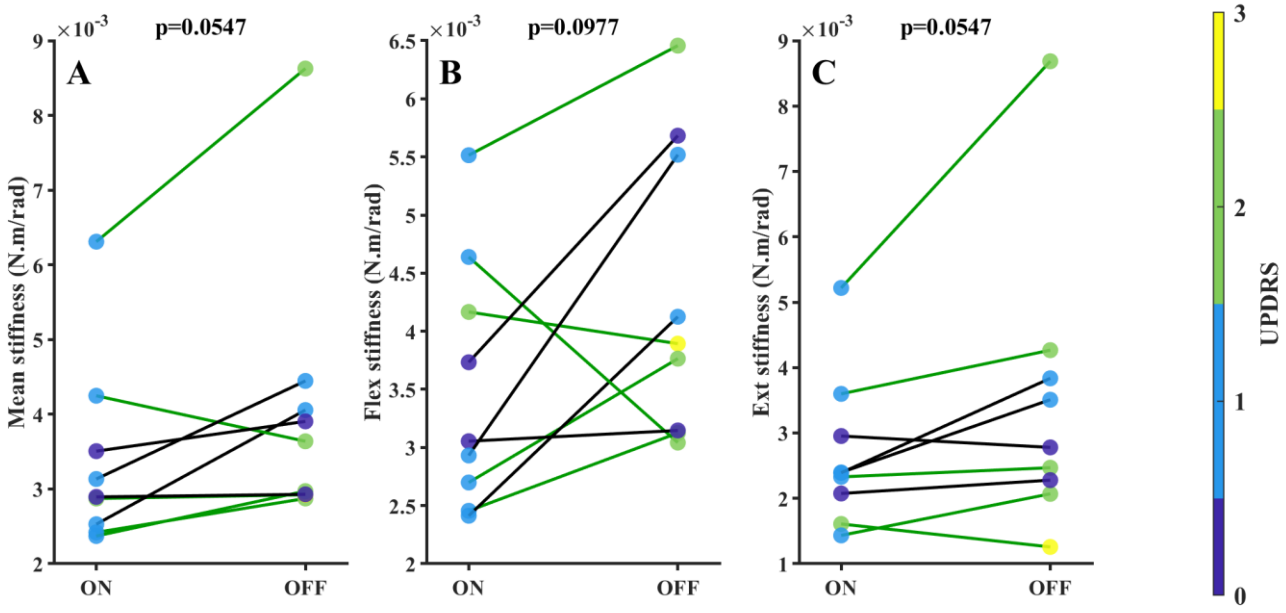

Figure 5.13. Visualisation of the paired ON- vs. OFF-stimulation mean stiffness estimates (N·m/rad) for (A) mean across both movement directions, (B) flexion movements and (C) extension movements. Pairs are linked, the colour of the line indicating an increase in UPDRS score (green), a decrease (red) or no change (black). UPDRS scores for each assessment are colour-coded based on the colourmap on the right of the figure. Wilcoxon sign rank p-value listed in the title of each plot.

5.4.5. Differentiation of Healthy Controls and Parkinson's Disease

The analysis demonstrates that healthy controls exhibit higher passive wrist stiffness than individuals with Parkinson's disease in the ON-treatment state, with the clearest separation observed in flexion stiffness, which reached statistical significance ($p = 0.02$, $z = 2.30$, $r = 0.30$, **Figure 5.14A**). Mean and extension stiffness show similar trends but do not attain significance ($p \geq .069$, **Figure 5.14C**), reflecting substantial overlap between groups and considerable inter-individual variability. Importantly, the observation of greater stiffness in healthy controls should be interpreted with caution, as the control cohort was not age matched to the Parkinson's disease group. Increased stiffness in the healthy cohort may therefore reflect greater baseline muscle tone associated with a younger population rather than disease-related differences in rigidity. Within the Parkinson's disease group, higher stiffness values generally coincide with higher UPDRS rigidity scores, supporting the physiological relevance of the passive measures despite incomplete group separation. Overall, the results suggest that passive stiffness assessment can capture systematic differences between groups, particularly in flexion, but that demographic mismatches and biological variability limit the extent to which these differences can be directly attributed to pathology.

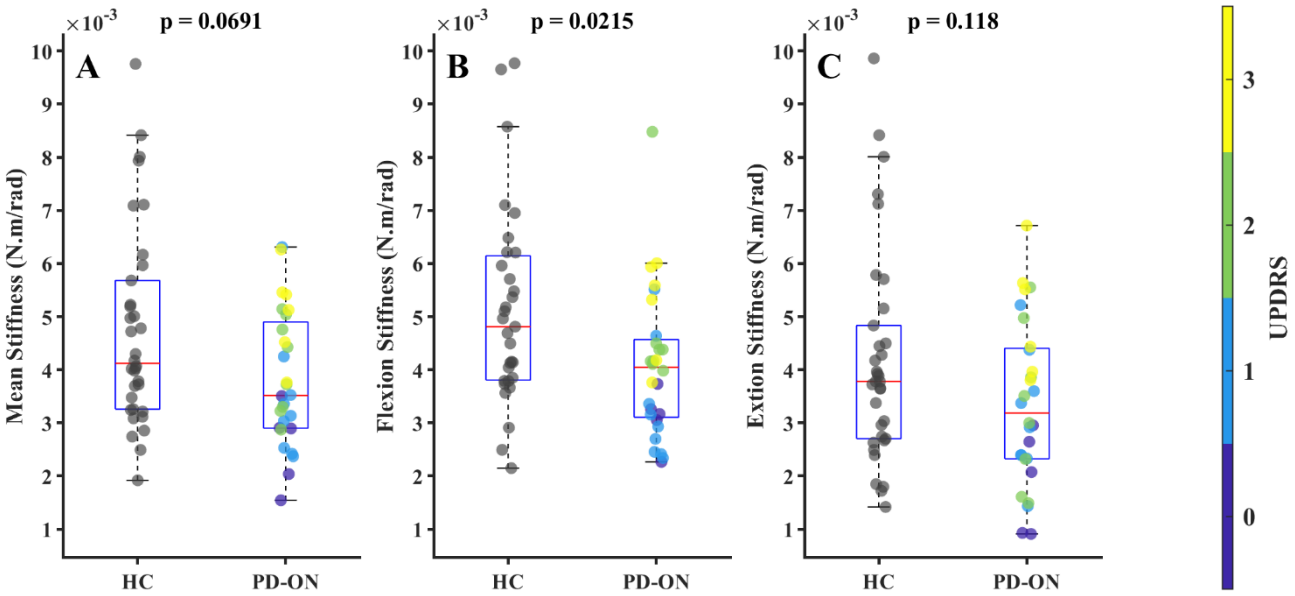

Figure 5.14. Boxplots showing the distribution of mean stiffness estimates (N·m/rad) split between healthy control participants and Parkinson's disease participants ON-treatment for (A) mean across both movement directions, (B) flexion movements and (C) extension movements. UPDRS scores for PD participants is colour-coded based on the colourmap on the right of the figure.

5.4.6. Summary

Taken together, the UPDRS association analyses, ON–OFF treatment comparisons, and healthy control versus PD evaluations position this work as an initial exploratory investigation into the feasibility of using the HRX-1 manipulandum for clinical assessment of Parkinsonian rigidity. Across ON-treatment conditions, passive stiffness measures, particularly in flexion, showed strong and consistent associations with clinician-rated UPDRS rigidity scores, including large effect sizes and robust monotonic relationships that persisted despite known inter-rater variability. These findings provide initial evidence that the passive assessment protocol deployed on the HRX-1 can capture biomechanical signatures that align meaningfully with established clinical assessments. In contrast, OFF-treatment analyses were inconclusive, with disrupted group-level relationships and substantial variability, a pattern likely driven by pronounced data sparsity, uneven rater contributions, and increased physiological heterogeneity rather than a definitive failure of the passive assessment approach. Comparisons between healthy controls and PD participants further demonstrated that the HRX-1 is sensitive to systematic differences in passive stiffness, although the unexpected observation of greater stiffness in healthy controls underscores the importance of cohort matching, as this effect may reflect age-related differences in baseline muscle tone rather than pathology. Collectively, these results should not be interpreted as definitive validation of the approach taken, but rather as supportive proof-of-concept evidence that controlled, passive wrist manipulation can yield clinically relevant information about rigidity. The consistency of findings in the ON-treatment and UPDRS-correlated analyses, despite small sample sizes and methodological constraints, suggests sufficient promise to justify more comprehensive, adequately powered studies with matched cohorts and standardised clinical scoring to fully establish clinical utility.

5.5. Discussion

5.5.1. Introduction

This chapter investigated whether exposure to the stability–movement transition paradigm produced sustained changes in passive wrist stiffness, extending beyond the immediate period of active stabilisation and voluntary movement. The primary purpose of this investigation was to evaluate whether repeated engagement of stabilisation-oriented control induced longer-lasting modulation of mechanical stiffness that can be detected under passive conditions, where voluntary and reflexive contributions are minimised. By focusing on stiffness - a dominant component of mechanical impedance - this assessment targeted residual sensorimotor effects that persist for minutes following task exposure, providing a complementary perspective to the transient dynamics observed during the main experimental paradigm.

In parallel, application of the passive assessment to participants with Parkinson's disease served a dual purpose. First, it allowed exploration of the protocol's clinical relevance as an objective, standardised measure of wrist rigidity. Second, it provided validation of the assessment's sensitivity and interpretability by situating healthy control measurements within a broader clinical context. Together, these aims position the passive stiffness analysis as both a mechanistic extension of the stability–movement framework and a translational step toward objective quantification of impaired impedance regulation.

5.5.2. Temporal Predictability, Not Perturbation Amplitude, Drives Passive Stiffness Modulation

The passive assessment results reinforce and extend the central finding of the main paradigm: impedance control is driven more by the informational structure of the task than by the magnitude of mechanical load. Temporally predictable stabilisation challenges produced a reliable bias toward increased passive wrist stiffness relative to baseline, emerging early and expressed similarly across flexion and extension. In contrast, temporal uncertainty failed to elicit a comparable increase and in some analyses was associated with a gradual reduction in stiffness. Notably, these effects were expressed primarily as relative differences between conditions rather than large within-condition shifts, indicating that predictability modulates the set-point of passive impedance rather than inducing uniform stiffness changes. The close correspondence with the main task results suggests that predictable timing promotes a common impedance state that generalises across active and passive contexts and persists beyond the stability–movement transition.

By contrast, perturbation amplitude exerted little influence on subsequent passive stiffness. Although higher-amplitude perturbations were occasionally associated with reduced stiffness, particularly in flexion, these effects were weak, inconsistent, and overshadowed by strong session-level and order-related decreases. The absence of reliable differences at the initial post-task assessment further indicates that passive stiffness was not systematically scaled to perturbation amplitude. This mirrors the main task findings, in which impedance estimates were largely insensitive to perturbation amplitude despite clear effects on movement dynamics. Together, these results challenge gain-scheduling accounts in which impedance is continuously tuned to force demands [4], [82], [267] and instead support models in which impedance reflects a context-dependent control policy [1], [268].

Within the broader motor control literature, these findings align with frameworks that emphasise prediction and uncertainty as central determinants of control strategy selection [83], [179]. From this perspective, impedance is not simply scaled to mechanical load, but is deployed to manage uncertainty, increasing robustness when disturbances are predictable while preserving flexibility when they are not. This interpretation is supported by the stabilisation phase of the main task, in which temporally

predictable perturbations elicited elevated responsive impedance despite reduced co-contraction across perturbation windows when compared with temporally uncertain perturbation conditions, indicating more efficient, state-dependent control rather than increased muscular co-activation. The passive results extend this account by showing that predictable temporal structure biases the system toward a persistently stiffer mechanical state, whereas temporal uncertainty discourages sustained stiffening even after stabilisation demands have ended. In contrast, perturbation amplitude provided limited informational value for selecting or retaining an impedance state, aligning with the weak and inconsistent amplitude effects observed. Together, these findings support the view that impedance modulation reflects a context-sensitive control policy shaped by task predictability rather than a simple response to force magnitude.

These results directly address **Research Question 1** by showing that predictability-induced modulation of impedance is not transient but persists into subsequent motor states when voluntary control is minimised. They also speak to **Research Question 3** by demonstrating that repeated exposure to higher mechanical loads does not produce systematic adaptation of passive stiffness within the tested range. Taken together, the passive assessments provide converging evidence that higher-order temporal structure, rather than force magnitude, governs how impedance-related states are established and retained, reinforcing the view that impedance regulation reflects strategic, context-sensitive control rather than simple force-dependent scaling.

5.5.3. Differential Contributions of Muscular Co-Contraction and Corticospinal Coupling Do Not Uniformly Explain Passive Stiffness

The passive assessment results showed that sustained passive stiffness could not be uniformly explained by either muscular co-contraction or corticospinal coupling alone. Instead, these measures related to passive mechanical state in dissociable and context-dependent ways, clarifying which components of stabilisation-induced control persisted beyond the stability–movement transition and how they aligned with the broader aims of the thesis.

Passive stiffness was systematically biased by temporal predictability, with predictable stabilisation followed by increased stiffness and uncertain stabilisation followed by reduced stiffness, despite minimal baseline shifts within individual conditions. Co-contraction during passive mobilisation did not mirror this effect, showing no reliable sensitivity to temporal structure and no evidence of adaptive change across blocks. This dissociation indicated that the persistence of impedance into a low-activity context was not driven by sustained antagonist activation, directly addressing the question of whether stabilisation-induced impedance modulation persists across transitions into subsequent motor states, as posed in **Research Question 1**.

This pattern was consistent with findings from the main task stabilisation phase. Temporally predictable perturbations elicited elevated responsive impedance despite reduced co-contraction across stabilisation windows when compared to temporally uncertainty conditions, indicating that robust stabilisation under predictable timing did not rely solely on sustained muscular co-activation. The passive assessment extended this observation by demonstrating that predictability-related mechanical bias remained evident even when co-contraction was not elevated, supporting the interpretation that persistence reflected centrally organised state modulation rather than tonic muscle activation.

Perturbation amplitude showed a contrasting profile. Passive co-contraction was strongly modulated by amplitude, with higher-amplitude perturbations followed by reduced co-contraction during passive assessment, particularly in extension. However, passive stiffness showed weak and inconsistent amplitude scaling and was dominated by broader session-level decreases. This dissociation indicated limited short-term adaptation of sustained passive impedance to perturbation amplitude, aligning with the broader objective of examining flexibility and adaptation of impedance control and informing **Research Question 3**.

Beta-band corticomuscular coherence (β-CMC) provided complementary neural insight. Mean β-CMC levels showed limited sensitivity to temporal predictability, yet passive stiffness was robustly and inversely related to β-CMC at both between- and within-participant levels across cohorts. Stronger corticospinal coupling consistently accompanied a more compliant mechanical state, identifying β-CMC as a neural correlate of sustained impedance variability even when condition-level differences were weak. Amplitude-related effects on β-CMC were expressed as stable level shifts rather than adaptive changes, further distinguishing load-dependent neural engagement from context-dependent stiffness persistence (**Aim 2**, **Research Question 2**)

Taken together, these findings demonstrate that passive stiffness did not arise from a single muscular or neural mechanism. Co-contraction primarily reflected tonic, load- and direction-dependent activation, whereas corticospinal coupling indexed a neural state linked to mechanical compliance. Temporal predictability selectively biased the retained mechanical state without necessitating sustained changes in either co-contraction or corticospinal coupling levels. This pattern reinforces the broader conclusion of the thesis that impedance regulation across stability–movement transitions is governed primarily by higher-order task structure rather than by perturbation amplitude or tonic muscle activation alone.

5.5.4. Passive Stiffness Indexes Sustained Sensorimotor Adaptation Beyond the Stability–Movement Transition

Passive stiffness measured following task exposure reflected a sustained sensorimotor adaptation rather than a transient mechanical after-effect of prior force application. Although the passive assessment was designed to minimise voluntary engagement, stiffness was systematically shaped by the structure of the preceding stabilisation task. This dependence on prior task context indicates that limb mechanics were governed by retained sensorimotor state rather than by residual loading alone. In this way, the passive results directly addressed the core issue of persistence raised in **Research Question 1** by testing whether stabilisation-induced impedance modulation survived the transition into a subsequent, low-activity motor context.

Temporal predictability emerged as the dominant factor governing this sustained mechanical bias. Passive stiffness was reliably elevated following temporally predictable stabilisation, despite the absence of high torques or ongoing control demands during the passive assessment. This pattern mirrored the main task, where predictable perturbations elicited higher and more stable impedance during stabilisation, and demonstrates that predictability promoted anticipatory tuning of the sensorimotor system that persisted beyond the stability–movement transition. By contrast, varying perturbation amplitude produced weak and inconsistent effects on passive stiffness, even though amplitude strongly influenced behaviour and muscle activation during the task itself. This dissociation indicates that exposure to larger forces did not, by itself, induce a durable change in baseline mechanical state, directly informing **Research Question 3** by showing that short-term adaptation of sustained impedance was governed more by temporal structure than by perturbation amplitude.

Importantly, these persistent stiffness biases were not uniformly accompanied by elevated co-contraction or increased corticospinal engagement during passive assessment. Co-contraction showed little evidence of baseline shifts, and beta-band corticomuscular coherence was often inversely related to stiffness. These findings argue against explanations based on residual muscle activation or prolonged cortical drive and instead suggest that passive stiffness reflected a retained configuration of the sensorimotor system, potentially involving altered reflex gains, intrinsic muscle properties, or spinal circuitry. This interpretation aligns with **Aim 2** by clarifying how neural signatures relate to sustained mechanical state without requiring ongoing voluntary control.

Taken together, these findings extend the main task results by demonstrating that stabilisation-related control states left a measurable imprint on passive limb mechanics minutes after active interaction had ceased. While prior work has primarily characterised impedance modulation during ongoing interaction,

perturbation response, or steady-state posture [1], [216], the present results show that task-induced impedance states can persist into a subsequent, low-activity context in which voluntary control demands are minimised. Passive stiffness therefore provided a novel and complementary window onto impedance regulation, revealing longer-lasting, state-dependent effects that were not evident from active behaviour or muscle activation alone.

This persistence directly advances existing accounts of impedance control by showing that stabilisation-related modulation is not confined to the immediate stabilisation epoch nor fully released at the transition to a new motor context. Instead, impedance appears to operate across multiple timescales, consistent with frameworks that describe motor control as the selection and maintenance of context-dependent control policies rather than continuous force-scaled tuning [83]. By linking predictable task structure to durable changes in baseline mechanical state, these findings extend classical views of impedance as an online, reactive mechanism and demonstrate that higher-order task structure can shape not only immediate stabilisation responses [284] but also the mechanical state to which the system returns following stability–movement transitions. In this way, the passive assessment provides novel empirical support for the persistence of impedance-related control beyond active task engagement, directly addressing the central aim of characterising short-term impedance persistence induced by externally imposed stability demands

5.5.5. Passive Robotic Assessment as an Objective Complement to Clinical Rigidity Scoring

The passive assessment results provided preliminary but compelling evidence that the HRX-1 manipulandum and passive assessment protocol captured biomechanical signatures of wrist rigidity that aligned meaningfully with established clinical ratings. In ON-treatment Parkinson's disease (PD) participants, passive stiffness showed strong monotonic associations with clinician-rated rigidity scores, with the clearest and most robust relationships observed in flexion. These associations were evident for both direction-specific and averaged stiffness estimates and persisted despite the known inter-rater variability inherent to clinical rigidity scoring. This pattern indicated that the robotic assessment captured a physiologically relevant component of rigidity.

The selective sensitivity of flexion stiffness was consistent with broader findings in this thesis showing direction-dependent expression of impedance-related control and persistence. This convergence supports the interpretation that passive stiffness was not an arbitrary mechanical measure but reflected underlying biomechanical and control asymmetries that were also evident during stabilisation and stability–movement transitions. Importantly, the use of continuous mechanical measurements allowed differentiation between higher and lower rigidity scores in a manner that may not be achievable with ordinal clinical scales, which necessarily compress variability and may obscure subtle but functionally meaningful differences. In this sense, the passive assessment directly aligned with the translational objectives of the thesis by linking experimentally derived impedance measures to clinically relevant motor impairment.

OFF-treatment analyses did not reveal reliable group-level associations between passive stiffness and clinical rigidity scores. However, this absence was interpreted cautiously. The OFF-treatment dataset was sparse and unevenly distributed across rigidity ratings, limiting statistical sensitivity. Qualitative inspection suggested that when clinical rigidity ratings changed between ON and OFF states, passive stiffness estimates often changed concordantly, whereas cases with unchanged clinical scores showed heterogeneous stiffness fluctuations. This pattern raised the possibility that the passive robotic assessment was sensitive to mechanical changes that fell below the resolution of clinical scoring, rather than being insensitive to medication-related effects. Such sensitivity would be consistent with the thesis aim of developing objective tools capable of detecting graded changes in sensorimotor state.

Comparisons between healthy controls and PD participants further illustrated both the promise and the limitations of the approach. While flexion stiffness differentiated groups, the direction of the effect was inverted by age differences between cohorts, underscoring the importance of demographic matching

in future validation studies. Nevertheless, within the Parkinson's disease cohort, higher passive stiffness consistently aligned with higher clinical rigidity scores, supporting the internal validity of the robotic measure despite between-group confounds.

Taken together, these findings positioned the passive assessment protocol as a promising objective complement to clinician-rated rigidity scoring rather than a replacement (**Aim 5**). The results suggested that controlled robotic manipulation could yield reproducible, continuous measures of stiffness that reflected clinically meaningful aspects of rigidity while also revealing variability and state dependence that may be masked by ordinal clinical scales. Although necessarily exploratory, these analyses provided proof-of-concept support for the use of robotic passive assessment as a tool for improving the precision, sensitivity, and interpretability of rigidity evaluation in Parkinson's disease, directly advancing the translational aims of the thesis and motivating further investigation in larger, carefully matched clinical cohorts.

5.5.6. Limitations and Future Directions

Across both groups, the limited number of trials per condition reduced statistical confidence in stiffness estimates and constrained characterisation of intra-individual variability, which is likely to be clinically meaningful. Low trial counts also prevented systematic exclusion of early trials that may reflect startle, anxiety, or familiarisation effects - factors particularly relevant in clinical populations. In addition, modest participant numbers, especially in the perturbation amplitude and PD cohorts, limited generalisability and reduced sensitivity for subgroup comparisons, including medication state effects.

Methodological constraints further influenced interpretability. Feature extraction focused on stationary, single-value metrics within restricted temporal windows, which may have reduced sensitivity to clinically relevant non-stationary dynamics. Device-level limitations also played a role: the position-unaware passive control mode of the HRX-1 resulted in unconstrained movement ranges that may have altered measured stiffness, reducing physiological specificity despite torques remaining well within safe limits.

Future work should prioritise increasing trial counts, enabling more robust estimation of stiffness and intra-individual variability, and expanding participant numbers to establish normative ranges and clinically meaningful effect sizes. Methodological extensions to incorporate non-stationary analyses would improve sensitivity to disease-relevant dynamics, while refinement of the HRX-1 control architecture to support position-aware passive assessment would enhance safety, comfort, and measurement specificity. For PD-focused investigations, fully standardised clinical protocols - including age-matched controls and harmonised clinical ratings - will be essential to validate passive stiffness as an objective complement to existing rigidity measures.

5.5.7. Summary

Across cohorts, passive wrist stiffness was modulated more strongly by temporal predictability than by perturbation amplitude, providing novel evidence that impedance persistence is governed primarily by higher-order task structure rather than by mechanical load alone. Temporally predictable stabilisation produced a small but reliable increase in subsequent passive stiffness that emerged early and was expressed similarly across movement directions, whereas manipulations of perturbation amplitude yielded weak and inconsistent effects that were overshadowed by session-level drift. This dissociation demonstrates that sustained mechanical state is not a simple after-effect of force exposure but reflects how stabilisation demands are structured in time.

Passive co-contraction exhibited a clearly dissociable profile. It was largely insensitive to temporal predictability and showed no baseline shifts or adaptive dynamics, while perturbation amplitude modulated co-contraction tonically, particularly in extension. The divergence between stiffness and co-

contraction establishes that predictability-related stiffness biases cannot be attributed to sustained antagonist activation and instead reflect state-dependent modulation of impedance that is not reducible to tonic muscle activity. This distinction advances current interpretations of impedance control by separating persistent mechanical state from overt muscular activation.

A further novel contribution was the identification of a robust inverse relationship between passive stiffness and β-CMC across cohorts. Stronger corticospinal coupling was consistently associated with a more compliant mechanical state, independent of task condition, whereas associations between co-contraction and beta-band coherence were weak and selective. This dissociation positions beta-band coupling as a neural marker of active impedance regulation rather than a proxy for tonic muscle activation, extending prior work that has primarily examined beta dynamics during active movement or stabilisation.

Critically, carryover from the stability–movement transition into passive assessment was observed only under predictable temporal structure. Stabilisation-phase co-contraction predicted passive stiffness and passive co-contraction in a direction-specific manner following predictable stabilisation, whereas such couplings were largely absent when perturbation amplitude was manipulated. This pattern provides direct evidence that temporal predictability enables stabilisation-related motor states to persist beyond active engagement, demonstrating that impedance-related control can be retained across task phases rather than being reset at the cessation of stabilisation demands.

Finally, exploratory clinical analyses showed that passive stiffness, particularly in flexion, aligned strongly with clinician-rated rigidity in ON-treatment Parkinson's disease participants. Although necessarily preliminary, these results establish the physiological relevance of the passive measures and highlight their potential translational value. Taken together, the findings demonstrate that passive stiffness provides a sensitive and theoretically informative marker of a persistent, context-dependent impedance state, linking task history, neural coupling, and clinical relevance, and identifying predictability as a dominant driver of sustained impedance modulation across stability–movement transitions.

VI. Conclusion and Final Remarks

6.1. Summary of Findings

This thesis set out to characterise how the human sensorimotor system modulates, maintains, and releases mechanical impedance across transitions between stability-oriented and movement-oriented control states. By integrating behavioural, muscular, and neural measures within a unified experimental framework, the work demonstrates that impedance regulation is a flexible yet persistent control strategy that is shaped primarily by higher-order task structure - particularly temporal predictability - rather than by mechanical load alone.

Across experiments, externally imposed postural instability reliably induced a stability-oriented motor state characterised by elevated impedance. This state emerged rapidly, was expressed from the earliest task exposure, and showed little evidence of gradual learning, consistent with anticipatory and context-sensitive regulation rather than slow optimisation. Behaviourally, elevated impedance constrained perturbation-induced displacement and supported faster post-perturbation stabilisation, confirming its functional relevance for mechanical stability.

Temporal predictability emerged as a dominant factor shaping impedance control. Predictable perturbation timing was associated with increased reactive impedance during stabilisation despite reduced co-contraction relative to temporally uncertain conditions, alongside tighter coupling between displacement and recovery and reduced costs during the transition to voluntary movement. In contrast, temporal uncertainty attenuated stabilisation-phase co-contraction, delayed movement initiation, and promoted persistence of stabilisation-related motor states into the movement phase. By comparison, varying perturbation amplitude exerted surprisingly limited influence on impedance magnitude, learning dynamics, or voluntary movement performance, indicating that the sensorimotor system prioritises informational structure over physical load when regulating impedance within the tested range.

Neural findings reinforced this interpretation. Beta-band corticomuscular coherence was consistently suppressed during stabilisation, reflecting engagement of an impedance-dominated control regime. Its magnitude tracked transient, within-participant fluctuations in stabilising muscle activity rather than stable individual differences, suggesting sensitivity to momentary control state rather than tonic activation. During voluntary movement, beta-band measures showed little evidence of learning-related change but were selectively modulated by task context and movement direction. Stabilisation-phase beta-band coherence predicted subsequent reaction time and movement duration primarily at the between-participant level and only under predictable temporal structure, indicating that beta-band coupling indexed individual efficiency of sensorimotor integration whose behavioural relevance was gated by predictability. Post-movement beta rebound further supported this view, acting as a marker of context-dependent state updating rather than movement execution, with attenuation under temporal uncertainty consistent with prolonged engagement of stabilisation-related control.

Across analyses, movement direction emerged as a consistent organising factor. Extension movements were more sensitive to impedance modulation, corticomuscular coupling, and carryover effects than flexion, suggesting inherent biomechanical or control asymmetries in how stability and movement demands are negotiated at the wrist.

Passive assessment results extended these findings beyond active task performance. Passive wrist stiffness was modulated more strongly by temporal predictability than by perturbation amplitude, exhibited robust inverse relationships with beta-band corticomuscular coherence, and showed context-dependent carryover from prior stabilisation. These findings indicate that impedance-related control states can leave a measurable imprint on baseline mechanical properties even in the absence of active engagement. Importantly, passive stiffness measures aligned with clinician-rated rigidity scores in Parkinson’s disease under ON-treatment conditions, providing proof-of-concept evidence that robotic

passive assessment can capture clinically meaningful aspects of impedance in a continuous and objective manner.

Taken together, the findings support a unified interpretation of impedance as a persistent sensorimotor state that biases subsequent movement preparation and execution. This state is rapidly established, selectively maintained, and flexibly released depending on temporal structure and task demands. Rather than reflecting a unitary stiffness-setting mechanism, impedance control emerged as an integrated control strategy spanning muscular activation, corticospinal coupling, and behaviour. By linking experimental manipulation, neural dynamics, and preliminary clinical relevance, this thesis advances an integrative framework for understanding how the sensorimotor system negotiates stability–movement trade-offs and provides a foundation for future translational work targeting disorders of impaired impedance regulation.

6.2. Overall Conclusions

This thesis advances a conceptual redefinition of mechanical impedance in human motor control. Rather than emerging as a transient, reactive response to perturbation or a parameter continuously scaled to mechanical load, impedance is shown to operate as a structured, context-dependent control state that persists across stability–movement transitions. This state is rapidly engaged, selectively maintained, and flexibly released in accordance with task structure, indicating that impedance regulation reflects higher-level control policies rather than low-level mechanical tuning.

A central conclusion is that informational structure, specifically temporal predictability, plays a decisive role in shaping how impedance-related control states are organised. Predictability enabled more efficient stabilisation strategies and more flexible disengagement of stabilising control during transitions to voluntary movement, whereas uncertainty promoted persistence of stabilisation-oriented control at the expense of movement initiation. The relative insensitivity of impedance to perturbation amplitude within the tested range underscores that the sensorimotor system prioritises prediction and uncertainty management over force magnitude when resolving competing demands for stability and movement.

The results further clarify how impedance can be both persistent and adaptable without requiring continuous recalibration. Stable, trait-like differences in control strategy coexisted with transient, state-dependent modulation, revealing a layered organisation in which enduring individual tendencies shape performance while momentary adjustments support online stability. This distinction resolves apparent tensions in the literature between views of impedance as either fixed or highly flexible, showing instead that persistence and adaptability operate at different timescales and levels of control.

Neural findings strengthen this interpretation by identifying beta-band corticomuscular coherence as a marker of control state rather than movement execution or tonic activation. Suppression and selective carryover of coherence indexed engagement and release of impedance-dominated control, while post-movement beta rebound reflected context-dependent resolution of stabilisation states. Together, these dynamics demonstrate that impedance regulation is supported by dissociable neural processes aligned to stabilisation, transition, and state updating, rather than by a single oscillatory mechanism.

Finally, by extending analysis beyond active task performance, the thesis shows that stabilisation-related control states can leave a measurable imprint on passive limb mechanics and that these mechanical signatures align with clinically relevant features of rigidity in Parkinson’s disease. This establishes impedance persistence as not only a theoretical construct but a measurable property with translational relevance.

In summary, this work reframes impedance control as a temporally extended, prediction-sensitive motor state that governs how the sensorimotor system negotiates the fundamental trade-off between stability and movement. By integrating behaviour, muscle activity, neural coupling, and passive mechanics, the thesis provides a coherent framework for understanding stability–movement transitions and offers a principled basis for future investigation of impaired sensorimotor flexibility in neurological disease.

6.3. Future Directions

The findings of this thesis open several clear avenues for further investigation into impedance control, sensorimotor state transitions, and their neural and translational significance.

Future work would benefit from explicitly manipulating stability–movement transitions rather than inferring them from sequential task phases. In the present work, persistence of impedance-related motor states was inferred from carryover into voluntary movement and passive assessment. Parametrically varying the delay between stabilisation and movement initiation, introducing explicit cues to release stiffness, or imposing competing movement demands immediately following stabilisation would allow direct testing of how rapidly impedance is disengaged, whether delayed release interferes with movement preparation or execution, and how these dynamics depend on temporal predictability.

Further insight into the neural mechanisms supporting impedance engagement and release could be gained using methods with greater spatial or causal resolution. While beta-band corticomuscular coherence and post-movement beta rebound provided informative markers of control state and context-dependent updating, they cannot fully specify the cortical or subcortical circuits involved. Although the present work employed CSD EEG to improve spatial specificity at the sensor level, future studies could combine the paradigm with source-localised cortical recordings or subcortical recordings to more directly interrogate the neural circuits supporting impedance engagement and release. Source-localised EEG or MEG would allow identification of cortical generators of impedance-related beta dynamics, while subcortical recordings would be necessary to test the contribution of basal ganglia and brainstem circuits that are likely critical for regulating stabilisation-oriented control states.

The limited evidence for learning across repeated task exposure suggests that impedance regulation may rely primarily on rapid state selection rather than gradual adaptation within a session. This distinction could be probed by manipulating perturbation structure across multiple sessions, increasing variability or uncertainty over longer timescales, or explicitly training participants to release impedance more efficiently. Such approaches would help determine whether impedance control adapts over extended experience in ways not captured by the present design.

The passive assessment findings highlight the importance of further disentangling active and passive contributors to impedance. Integrating high-density EMG, reflex probing, or pharmacological manipulation would help separate neural, muscular, and connective tissue contributions to sustained stiffness. In particular, concurrent assessment of reflex gains alongside passive stiffness could clarify whether predictability-related stiffness biases primarily reflect altered spinal feedback, intrinsic muscle properties, or supraspinal control.

An important extension of this work will be the application of the full stabilisation–movement paradigm to individuals with Parkinson's disease. While the present thesis examined passive stiffness in Parkinson's disease in isolation, applying the main task would allow direct investigation of how stabilisation-induced control states are engaged, persist, and are released in a population characterised by impaired motor flexibility. Given well-documented abnormalities in beta-band dynamics, co-contraction, and rigidity, this paradigm provides a principled framework for testing whether motor impairment arises from exaggerated engagement of stabilisation-oriented control, impaired release of impedance during transitions to voluntary movement, or both. Manipulating temporal predictability in this population would be particularly informative, as deficits in predictive processing may amplify persistence of stabilisation-related control states and exacerbate bradykinesia or delayed movement initiation.

Finally, the translational potential of the HRX-1 platform warrants dedicated investigation. The observed alignment between passive stiffness and clinician-rated rigidity under ON-treatment conditions provides proof-of-concept support for objective rigidity assessment, but larger, age-matched cohorts and standardised clinical protocols are required. Future studies should examine test–retest reliability,

sensitivity to disease progression, and responsiveness to therapeutic interventions, and extend the approach to other movement disorders characterised by abnormal impedance regulation.

Together, these directions outline a coherent programme of work that builds directly on the present findings. By refining behavioural paradigms, incorporating targeted neural measurements, and pursuing systematic clinical validation, future studies can further elucidate how impedance is regulated, released, and disrupted across motor contexts and disease states, extending both the theoretical and translational impact of this thesis.

Bibliography

[1] N. Hogan, “Impedance control: An approach to manipulation: Part I-theory,” *Journal of Dynamic Systems, Measurement and Control, Transactions of the ASME*, vol. 107, no. 1, 1985, doi: 10.1115/1.3140702.

[2] A. Kadiallah, G. Liaw, M. Kawato, D. W. Franklin, and E. Burdet, “Impedance control is selectively tuned to multiple directions of movement,” *J. Neurophysiol.*, vol. 106, no. 5, 2011, doi: 10.1152/jn.00079.2011.

[3] M. Darainy, A. A. G. Mattar, and D. J. Ostry, “Effects of human arm impedance on dynamics learning and generalization,” *J. Neurophysiol.*, vol. 101, no. 6, pp. 3158–3168, Jun. 2009, doi: 10.1152/jn.91336.2008.

[4] L. P. J. Selen, D. W. Franklin, and D. M. Wolpert, “Impedance control reduces instability that arises from motor noise,” *Journal of Neuroscience*, vol. 29, no. 40, 2009, doi: 10.1523/JNEUROSCI.2826-09.2009.

[5] X. Lv, C. Xiong, and Q. Zhang, “A simplified impedance estimation method inspired by the independent effect of arm posture and muscle co-contraction,” *Biomed. Signal Process. Control*, vol. 95, p. 106469, Sep. 2024, doi: 10.1016/J.BSPC.2024.106469.

[6] H. K. Kim, J. M. Carmena, S. J. Biggs, T. L. Hanson, M. A. L. Nicolelis, and M. A. Srinivasan, “The muscle activation method: An approach to impedance control of brain-machine interfaces through a musculoskeletal model of the arm,” *IEEE Trans. Biomed. Eng.*, vol. 54, no. 8, pp. 1520–1529, Aug. 2007, doi: 10.1109/TBME.2007.900818.

[7] M. B. Carpenter, “The Co-ordination and Regulation of Movements,” *J. Neuropathol. Exp. Neurol.*, vol. 27, no. 2, 1968, doi: 10.1097/00005072-196804000-00011.

[8] D. Formica, S. K. Charles, L. Zollo, E. Guglielmelli, N. Hogan, and H. I. Krebs, “The passive stiffness of the wrist and forearm,” *J. Neurophysiol.*, vol. 108, no. 4, 2012, doi: 10.1152/jn.01014.2011.

[9] M. Lakie, E. G. Walsh, and G. W. Wright, “Passive mechanical properties of the wrist and physiological tremor,” *J. Neurol. Neurosurg. Psychiatry*, vol. 49, no. 6, 1986, doi: 10.1136/jnnp.49.6.669.

[10] T. G. Simpson *et al.*, “Cortical beta oscillations help synchronise muscles during static posture holding in healthy motor control,” *Neuroimage*, vol. 298, p. 120774, Sep. 2024, doi: 10.1016/J.NEUROIMAGE.2024.120774.

[11] H. Ohtsuka, T. Nakajima, T. Komiyama, S. Suzuki, S. Irie, and R. Ariyasu, “Execution of natural manipulation in the air enhances the beta-rhythm intermuscular coherences of the human arm depending on muscle pairs,” *J. Neurophysiol.*, vol. 127, no. 4, pp. 946–957, Apr. 2022, doi: 10.1152/jn.00421.2021.

[12] K. P. Granata, K. F. Orishimo, and A. H. Sanford, “Trunk muscle coactivation in preparation for sudden load,” *Journal of Electromyography and Kinesiology*, vol. 11, no. 4, pp. 247–254, Aug. 2001, doi: 10.1016/S1050-6411(01)00003-7.

[13] D. W. Franklin and T. E. Milner, “Adaptive control of stiffness to stabilize hand position with large loads,” *Exp. Brain Res.*, vol. 152, no. 2, 2003, doi: 10.1007/s00221-003-1540-3.

[14] S. J. De Serres and T. E. Milner, “Wrist muscle activation patterns and stiffness associated with stable and unstable mechanical loads,” *Exp. Brain Res.*, vol. 86, no. 2, 1991, doi: 10.1007/BF00228972.

[15] P. Haggard and A. Wing, “Coordinated responses following mechanical perturbation of the arm during prehension,” 1995.

[16] W. Karwowski, J. De Havas, L. Simon, H. Börner, S. Endo, and S. Hirche, “Estimation of Involuntary Components of Human Arm Impedance in Multi-Joint Movements via Feedback Jerk Isolation,” *Frontiers in Neuroscience | www.frontiersin.org*, vol. 1, p. 459, 2020, doi: 10.3389/fnins.2020.00459.

[17] J. Buchli, F. Stulp, E. Theodorou, and S. Schaal, “Learning Variable Impedance Control,” 2011.

[18] M. Darainy, N. Malfait, P. L. Gribble, F. Towhidkhah, and D. J. Ostry, “Learning to control arm stiffness under static conditions,” *J. Neurophysiol.*, vol. 92, no. 6, 2004, doi: 10.1152/jn.00596.2004.

[19] I. W. Hunter and R. E. Kearney, “Dynamics of human ankle stiffness: Variation with mean ankle torque,” *J. Biomech.*, vol. 15, no. 10, 1982, doi: 10.1016/0021-9290(82)90089-6.

[20] S. Hansen, N. L. Hansen, · L O D Christensen, · N T Petersen, and J. B. Nielsen, “Coupling of antagonistic ankle muscles during co-contraction in humans,” *Exp Brain Res*, vol. 146, pp. 282–292, 2002, doi: 10.1007/s00221-002-1152-3.

[21] T. Igawa, J. Katsuhira, and S. Yamamoto, “Electromyographic analysis of agonist-antagonist muscular activation during gait, and stair ascent and descent elderly adults,” *Rigakuryoho Kagaku*, vol. 28, no. 1, 2013, doi: 10.1589/rika.28.35.

[22] A. Berardelli, A. F. Sabra, M. Hallett, and M. Hallett, “Physiological mechanisms of rigidity in Parkinson’s disease,” 1983.

[23] B. K. Park *et al.*, “Analysis of viscoelastic properties of wrist joint for quantification of parkinsonian rigidity,” *IEEE Transactions on Neural Systems and Rehabilitation Engineering*, vol. 19, no. 2, 2011, doi: 10.1109/TNSRE.2010.2091149.

[24] H. S. Markus, M. Cox, and A. M. Tomkins, “Raised resting energy expenditure in Parkinson’s disease and its relationship to muscle rigidity,” *Clin. Sci.*, vol. 83, no. 2, 1992, doi: 10.1042/cs0830199.

[25] Y. Yu *et al.*, “Parkinsonism alters beta burst dynamics across the basal ganglia-motor cortical network,” *Journal of Neuroscience*, vol. 41, no. 10, 2021, doi: 10.1523/JNEUROSCI.1591-20.2021.

[26] A. Eusebio and P. Brown, “Synchronisation in the beta frequency-band - The bad boy of parkinsonism or an innocent bystander?,” 2009. doi: 10.1016/j.expneurol.2009.02.003.

[27] S. Little, A. Pogosyan, A. A. Kuhn, and P. Brown, “Beta band stability over time correlates with Parkinsonian rigidity and bradykinesia,” *Exp. Neurol.*, vol. 236, no. 2, pp. 383–388, Aug. 2012, doi: 10.1016/j.expneurol.2012.04.024.
[28] S. Little and P. Brown, “The functional role of beta oscillations in Parkinson’s disease,” *Parkinsonism Relat. Disord.*, vol. 20, no. SUPPL.1, 2014, doi: 10.1016/S1353-8020(13)70013-0.
[29] T. Tsuji, P. G. Morasso, K. Goto, and K. Ito, “Human hand impedance characteristics during maintained posture,” *Biol. Cybern.*, vol. 72, no. 6, 1995, doi: 10.1007/BF00199890.
[30] A. J. Suminski, S. M. Rao, K. M. Mosier, and R. A. Scheidt, “Neural and electromyographic correlates of wrist posture control,” *J. Neurophysiol.*, vol. 97, no. 2, 2007, doi: 10.1152/jn.01160.2006.
[31] E. Burdet, R. Osu, D. W. Franklin, T. E. Milner, and M. Kawato, “The central nervous system stabilizes unstable dynamics by learning optimal impedance,” *Nature*, vol. 414, no. 6862, 2001, doi: 10.1038/35106566.
[32] N. Saijo and H. Gomi, “Multiple motor learning strategies in visuomotor rotation,” *PLoS One*, vol. 5, no. 2, 2010, doi: 10.1371/journal.pone.0009399.
[33] J. W. Krakauer, “Motor learning and consolidation: The case of visuomotor rotation,” *Adv. Exp. Med. Biol.*, vol. 629, 2009, doi: 10.1007/978-0-387-77064-2_21.
[34] D. W. Franklin, U. So, M. Kawato, and T. E. Milner, “Impedance control balances stability with metabolically costly muscle activation,” *J. Neurophysiol.*, vol. 92, no. 5, 2004, doi: 10.1152/jn.00364.2004.
[35] Z. Hasan, “The human motor control system’s response to mechanical perturbation: Should it, can it, and does it ensure stability?,” 2005. doi: 10.3200/JMBR.37.6.484-493.
[36] M. Macht *et al.*, “Predictors of freezing in Parkinson’s disease: A survey of 6,620 patients,” *Movement Disorders*, vol. 22, no. 7, 2007, doi: 10.1002/mds.21458.
[37] C. Gao, J. Liu, Y. Tan, and S. Chen, “Freezing of gait in Parkinson’s disease: Pathophysiology, risk factors and treatments,” 2020. doi: 10.1186/s40035-020-00191-5.
[38] M. C. Vinding *et al.*, “Attenuated beta rebound to proprioceptive afferent feedback in Parkinson’s disease,” *Sci. Rep.*, vol. 9, no. 1, 2019, doi: 10.1038/s41598-019-39204-3.
[39] N. Baradaran *et al.*, “Parkinson’s disease rigidity: Relation to brain connectivity and motor performance,” *Front. Neurol.*, vol. 4 JUN, 2013, doi: 10.3389/fneur.2013.00067.
[40] H. Bergman *et al.*, “Physiological aspects of information processing in the basal ganglia of normal and parkinsonian primates,” *Trends Neurosci.*, vol. 21, no. 1, 1998, doi: 10.1016/S0166-2236(97)01151-X.
[41] R. Levy, W. D. Hutchison, A. M. Lozano, and J. O. Dostrovsky, “Synchronized Neuronal Discharge in the Basal Ganglia of Parkinsonian Patients Is Limited to Oscillatory Activity,” *Journal of Neuroscience*, vol. 22, no. 7, 2002, doi: 10.1523/jneurosci.22-07-02855.2002.
[42] M. F. Dirkx, H. Zach, B. R. Bloem, M. Hallett, and R. C. Helmich, “The nature of postural tremor in Parkinson disease,” *Neurology*, vol. 90, no. 13, pp. e1095–e1102, Mar. 2018, doi: 10.1212/WNL.0000000000005215.
[43] N. P. Connor and J. H. Abbs, “Task-dependent variations in parkinsonian motor impairments,” *Brain*, vol. 114A, no. 1, 1991, doi: 10.1093/oxfordjournals.brain.a101865.
[44] S. M. Keloth, S. P. Arjunan, S. Raghav, and D. K. Kumar, “Muscle activation strategies of people with early-stage Parkinson’s during walking,” *J. Neuroeng. Rehabil.*, vol. 18, no. 1, 2021, doi: 10.1186/s12984-021-00932-1.
[45] H. J. Groenewegen, “The basal ganglia and motor control.,” 2003. doi: 10.1155/NP.2003.107.
[46] M. Jahanshahi, I. Obeso, J. C. Rothwell, and J. A. Obeso, “A fronto-striato-subthalamic-pallidal network for goal-directed and habitual inhibition,” 2015. doi: 10.1038/nrn4038.
[47] S. N. Haber, “Corticostriatal circuitry,” *Dialogues Clin. Neurosci.*, vol. 18, no. 1, 2016, doi: 10.31887/dcns.2016.18.1/shaber.
[48] M. G. Packard and B. J. Knowlton, “Learning and memory functions of the basal ganglia,” 2002. doi: 10.1146/annurev.neuro.25.112701.142937.
[49] J. Song, H. Lin, and S. Liu, “Basal ganglia network dynamics and function: Role of direct, indirect and hyper-direct pathways in action selection,” *Network: Computation in Neural Systems*, vol. 34, no. 1–2, 2023, doi: 10.1080/0954898X.2023.2173816.
[50] H. Schroll and F. H. Hamker, “Computational models of basal-ganglia pathway functions: Focus on functional neuroanatomy,” 2013. doi: 10.3389/fnsys.2013.00122.
[51] N. Giladi and A. Nieuwboer, “Understanding and treating freezing of gait in Parkinsonism, proposed working definition, and setting the stage,” 2008. doi: 10.1002/mds.21927.
[52] L. di Biase *et al.*, “Quantitative analysis of bradykinesia and rigidity in Parkinson’s disease,” *Front. Neurol.*, vol. 9, no. MAR, Mar. 2018, doi: 10.3389/fneur.2018.00121.
[53] B. E. Kilavik, M. Zaepffel, A. Brovelli, W. A. MacKay, and A. Riehle, “The ups and downs of beta oscillations in sensorimotor cortex,” *Exp. Neurol.*, vol. 245, pp. 15–26, Jul. 2013, doi: 10.1016/J.EXPNEUROL.2012.09.014.
[54] A. M. Smith, “The coactivation of antagonist muscles,” 1981. doi: 10.1139/y81-110.
[55] N. Hogan, “Adaptive Control of Mechanical Impedance by Coactivation of Antagonist Muscles,” *IEEE Trans. Automat. Contr.*, vol. 29, no. 8, 1984, doi: 10.1109/TAC.1984.1103644.
[56] B. Huang *et al.*, “Wearable stretch sensors for motion measurement of the wrist joint based on dielectric elastomers,” *Sensors (Switzerland)*, vol. 17, no. 12, 2017, doi: 10.3390/s17122708.

[57] H. Nishimaru and M. Kakizaki, “The role of inhibitory neurotransmission in locomotor circuits of the developing mammalian spinal cord,” 2009. doi: 10.1111/j.1748-1716.2009.02020.x.
[58] T. Sinkjær and R. Hayashi, “Regulation of wrist stiffness by the stretch reflex,” *J. Biomech.*, vol. 22, no. 11–12, pp. 1133–1140, Jan. 1989, doi: 10.1016/0021-9290(89)90215-7.
[59] R. Osu *et al.*, “Short- and long-term changes in joint co-contraction associated with motor learning as revealed from surface EMG,” *J. Neurophysiol.*, vol. 88, no. 2, 2002, doi: 10.1152/jn.2002.88.2.991.
[60] C. Crone, “Reciprocal inhibition in man.,” 1993.
[61] H. Hultborn, “Spinal reflexes, mechanisms and concepts: From Eccles to Lundberg and beyond,” 2006. doi: 10.1016/j.pneurobio.2006.04.001.
[62] “Reflexes in response to stretch (myotatic reflexes),” *Proceedings of the Royal Society of London. Series B, Containing Papers of a Biological Character*, vol. 96, no. 675, 1924, doi: 10.1098/rspb.1924.0023.
[63] B. E. G T Liddell and S. Charles Sherrington, “Reflexes in Response,” 1924. [Online]. Available: https://royalsocietypublishing.org/
[64] V. G. Macefield and T. P. Knellwolf, “Functional properties of human muscle spindles,” *J Neurophysiol*, vol. 120, pp. 452–467, 2018, doi: 10.1152/jn.00071.2018.-Muscle.
[65] Hasan, “A Model of Spindle Afferent Response to Muscle Stretch,” 1983.
[66] “The structure and innervation of the nuclear bag muscle fibre system and the nuclear chain muscle fibre system in mammalian muscle spindles,” *Philos. Trans. R. Soc. Lond. B Biol. Sci.*, vol. 245, no. 720, 1962, doi: 10.1098/rstb.1962.0007.
[67] I. A. Boyd, M. H. Gladden, P. N. McWilliam, and J. Ward, “Control of dynamic and static nuclear bag fibres and nuclear chain fibres by gamma and beta axons in isolated cat muscle spindels.,” *J. Physiol.*, vol. 265, no. 1, 1977, doi: 10.1113/jphysiol.1977.sp011709.
[68] P. B. C. Matthews, “The human stretch reflex and the motor cortex,” *Trends Neurosci.*, vol. 14, no. 3, pp. 87–91, Mar. 1991, doi: 10.1016/0166-2236(91)90064-2.
[69] J. A. Pruszynski and S. H. Scott, “Optimal feedback control and the long-latency stretch response,” 2012. doi: 10.1007/s00221-012-3041-8.
[70] C. Rossi-Durand, “The influence of increased muscle spindle sensitivity on Achilles tendon jerk and H-reflex in relaxed human subjects,” *Somatosens. Mot. Res.*, vol. 19, no. 4, 2002, doi: 10.1080/0899022021000037755.
[71] R. Hayashi, T. Hashimoto, T. Tada, and S. Ikeda, “Relation between changes in long-latency stretch reflexes and muscle stiffness in Parkinson’s disease – comparison before and after unilateral pallidotomy,” *Clinical Neurophysiology*, vol. 112, no. 10, pp. 1814–1821, Oct. 2001, doi: 10.1016/S1388-2457(01)00642-3.
[72] P. Barrett, T. J. Quick, V. Mudera, and D. J. Player, “Generating intrafusal skeletal muscle fibres in vitro: Current state of the art and future challenges,” 2020, *SAGE Publications Ltd*. doi: 10.1177/2041731420985205.
[73] P. H. Ellaway, A. Taylor, and R. Durbaba, “Muscle spindle and fusimotor activity in locomotion,” 2015. doi: 10.1111/joa.12299.
[74] J. B. Nielsen, N. T. Petersen, C. Crone, and T. Sinkjaer, “Stretch Reflex Regulation in Healthy Subjects and Patients with Spasticity,” *Neuromodulation: Technology at the Neural Interface*, vol. 8, no. 1, pp. 49–57, Jan. 2005, doi: 10.1111/J.1094-7159.2005.05220.X.
[75] P. J. Delwaide and E. Oliver, “Short-latency autogenic inhibition (IB inhibition) in human spasticity,” *J. Neurol. Neurosurg. Psychiatry*, vol. 51, no. 12, 1988, doi: 10.1136/jnnp.51.12.1546.
[76] N. A. Al-Falahe and A. B. Vallbo, “Role of the human fusimotor system in a motor adaptation task.,” *J. Physiol.*, vol. 401, no. 1, 1988, doi: 10.1113/jphysiol.1988.sp017152.
[77] S. K. Charles and N. Hogan, “Dynamics of wrist rotations,” *J. Biomech.*, vol. 44, no. 4, pp. 614–621, Feb. 2011, doi: 10.1016/J.JBIOMECH.2010.11.016.
[78] P. L. Gribble, L. I. Mullin, N. Cothros, and A. Mattar, “Role of cocontraction in arm movement accuracy,” *J. Neurophysiol.*, vol. 89, no. 5, 2003, doi: 10.1152/jn.01020.2002.
[79] J. Wong, E. T. Wilson, N. Malfait, and P. L. Gribble, “Limb stiffness is modulated with spatial accuracy requirements during movement in the absence of destabilizing forces,” *J. Neurophysiol.*, vol. 101, no. 3, 2009, doi: 10.1152/jn.91188.2008.
[80] D. W. Franklin, G. Liaw, T. E. Milner, R. Osu, E. Burdet, and M. Kawato, “Endpoint stiffness of the arm is directionally tuned to instability in the environment,” *Journal of Neuroscience*, vol. 27, no. 29, 2007, doi: 10.1523/JNEUROSCI.0968-07.2007.
[81] C. D. Takahashi, R. A. Scheidt, and D. J. Reinkensmeyer, “Impedance Control and Internal Model Formation When Reaching in a Randomly Varying Dynamical Environment,” 2001. [Online]. Available: www.jn.org
[82] D. W. Franklin, R. Osu, E. Burdet, M. Kawato, and T. E. Milner, “Adaptation to Stable and Unstable Dynamics Achieved by Combined Impedance Control and Inverse Dynamics Model,” *J. Neurophysiol.*, vol. 90, no. 5, 2003, doi: 10.1152/jn.01112.2002.
[83] D. W. Franklin *et al.*, “CNS learns stable, accurate, and efficient movements using a simple algorithm,” *Journal of Neuroscience*, vol. 28, no. 44, pp. 11165–11173, Oct. 2008, doi: 10.1523/JNEUROSCI.3099-08.2008.
[84] F. Lacquaniti and C. Maioli, “The role of preparation in tuning anticipatory and reflex responses during catching,” *Journal of Neuroscience*, vol. 9, no. 1, 1989, doi: 10.1523/jneurosci.09-01-00134.1989.
[85] G. J. P. Savelsbergh, H. T. A. Whiting, A. M. Burden, and R. M. Bartlett, “The role of predictive visual temporal information in the coordination of muscle activity in catching,” Springer-Verlag, 1992.

[86] H. Kambara, H. Ogawa, A. Takagi, D. Shin, N. Yoshimura, and Y. Koike, “Modulation of wrist stiffness caused by adaptation to stochastic environment,” *Advanced Robotics*, vol. 35, no. 13–14, 2021, doi: 10.1080/01691864.2021.1900913.
[87] G. DeMaagd and A. Philip, “Parkinson’s disease and its management part 1: Disease entity, risk factors, pathophysiology, clinical presentation, and diagnosis,” *P and T*, vol. 40, no. 8, 2015.
[88] O. B. Tysnes and A. Storstein, “Epidemiology of Parkinson’s disease,” 2017. doi: 10.1007/s00702-017-1686-y.
[89] S. Chapuis, L. Ouchchane, O. Metz, L. Gerbaud, and F. Durif, “Impact of the motor complications of Parkinson’s disease on the quality of life,” *Movement Disorders*, vol. 20, no. 2, pp. 224–230, Feb. 2005, doi: 10.1002/mds.20279.
[90] E. Martignoni *et al.*, “Comorbid disorders and hospitalisation in Parkinson’s disease: A prospective study,” *Neurological Sciences*, vol. 25, no. 2, 2004, doi: 10.1007/s10072-004-0232-5.
[91] M. Bologna, G. Paparella, A. Fasano, M. Hallett, and A. Berardelli, “Evolving concepts on bradykinesia,” 2020. doi: 10.1093/brain/awz344.
[92] P. Ghiglione, R. Mutani, and A. Chiò, “Cogwheel rigidity,” 2005. doi: 10.1001/archneur.62.5.828.
[93] K. P. Bhatia *et al.*, “Consensus Statement on the classification of tremors. from the task force on tremor of the International Parkinson and Movement Disorder Society,” *Movement Disorders*, vol. 33, no. 1, 2018, doi: 10.1002/mds.27121.
[94] D. Aarsland, K. Andersen, J. P. Larsen, A. Lolk, H. Nielsen, and P. Kragh-Sørensen, “Risk of dementia in Parkinson’s disease: A community-based, prospective study,” *Neurology*, vol. 56, no. 6, 2001, doi: 10.1212/WNL.56.6.730.
[95] R. D. Dobkin *et al.*, “Depression in Parkinson’s disease: Symptom improvement and residual symptoms after acute pharmacologic management,” *American Journal of Geriatric Psychiatry*, vol. 19, no. 3, 2011, doi: 10.1097/JGP.0b013e3181e448f7.
[96] S. E. Starkstein, H. S. Mayberg, T. J. Preziosi, P. Andrezejewski, R. Leiguarda, and R. G. Robinson, “Reliability, validity, and clinical correlates of apathy in Parkinson’s disease,” *Journal of Neuropsychiatry and Clinical Neurosciences*, vol. 4, no. 2, 1992, doi: 10.1176/jnp.4.2.134.
[97] L. M. Allcock, K. Ullyart, R. A. Kenny, and D. J. Burn, “Frequency of orthostatic hypotension in a community based cohort of patients with Parkinson’s disease,” *J. Neurol. Neurosurg. Psychiatry*, vol. 75, no. 10, 2004, doi: 10.1136/jnnp.2003.029413.
[98] A. Berardelli, J. C. Rothwell, P. D. Thompson, and M. Hallett, “Pathophysiology of bradykinesia in Parkinson’s disease,” 2001.
[99] J. M. Shulman, P. L. De Jager, and M. B. Feany, “Parkinson’s disease: Genetics and pathogenesis,” *Annual Review of Pathology: Mechanisms of Disease*, vol. 6, 2011, doi: 10.1146/annurev-pathol-011110-130242.
[100] E. Paulėkas, T. Vanagas, S. Lagunavičius, E. Pajėdienė, K. Petrikonis, and D. Rastenytė, “Navigating the Neurobiology of Parkinson’s: The Impact and Potential of α-Synuclein,” Sep. 01, 2024, *Multidisciplinary Digital Publishing Institute (MDPI)*. doi: 10.3390/biomedicines12092121.
[101] J. Q. Trojanowski, M. Goedert, T. Iwatsubo, and V. M. Y. Lee, “Fatal attractions: Abnormal protein aggregation and neuron death in Parkinson’s disease and Lewy body dementia,” 1998. doi: 10.1038/sj.cdd.4400432.
[102] J. Q. Trojanowski and V. M. Y. Lee, “Aggregation of neurofilament and α-synuclein proteins in Lewy bodies: Implications for the pathogenesis of Parkinson disease and Lewy body dementia,” 1998. doi: 10.1001/archneur.55.2.151.
[103] H. Braak, K. Del Tredici, U. Rüb, R. A. I. De Vos, E. N. H. Jansen Steur, and E. Braak, “Staging of brain pathology related to sporadic Parkinson’s disease,” *Neurobiol. Aging*, vol. 24, no. 2, 2003, doi: 10.1016/S0197-4580(02)00065-9.
[104] N. P. Visanji, P. L. Brooks, L. N. Hazrati, and A. E. Lang, “The prion hypothesis in Parkinson’s disease: Braak to the future,” 2014. doi: 10.1186/2051-5960-1-2.
[105] B. Rossi *et al.*, “Muscle modifications in Parkinson’s disease: Myoelectric manifestations,” *Electroencephalography and Clinical Neurophysiology - Electromyography and Motor Control*, vol. 101, no. 3, 1996, doi: 10.1016/0924-980X(96)94672-X.
[106] P. J. Delwaide, J. L. Pepin, and A. M. De Noordhout, “Short-latency autogenic inhibition in patients with parkinsonian rigidity,” *Ann. Neurol.*, vol. 30, no. 1, 1991, doi: 10.1002/ana.410300115.
[107] S. Lelli, M. Panizza, and M. Hallett, “Spinal cord inhibitory mechanisms in Parkinson’s disease,” *Neurology*, vol. 41, no. 4, 1991, doi: 10.1212/wnl.41.4.553.
[108] R. Xia, J. Sun, and A. J. Threlkeld, “Analysis of interactive effect of stretch reflex and shortening reaction on rigidity in Parkinson’s disease,” *Clinical Neurophysiology*, vol. 120, no. 7, 2009, doi: 10.1016/j.clinph.2009.05.001.
[109] G. N. Lewis and W. D. Byblow, “Altered sensorimotor integration in Parkinson’s disease,” *Brain*, vol. 125, no. 9, 2002, doi: 10.1093/brain/awf200.
[110] J. Konczak *et al.*, “Parkinson’s disease accelerates age-related decline in haptic perception by altering somatosensory integration,” *Brain*, vol. 135, no. 11, 2012, doi: 10.1093/brain/aws265.

[111] J. Noth, M. Schürmann, K. Podoll, and M. Schwarz, “Reconsideration of the concept of enhanced static fusimotor drive in rigidity in patients with Parkinson’s disease,” *Neurosci. Lett.*, vol. 84, no. 2, 1988, doi: 10.1016/0304-3940(88)90415-6.
[112] C. Fearon, L. Doherty, and T. Lynch, “How Do I Examine Rigidity and Spasticity?,” 2015. doi: 10.1002/mdc3.12147.
[113] H. Zetterberg, G. E. Frykberg, J. Gäverth, and P. G. Lindberg, “Neural and nonneural contributions to wrist rigidity in parkinson’s disease: An explorative study using the neuroflexor,” *Biomed Res. Int.*, vol. 2015, 2015, doi: 10.1155/2015/276182.
[114] J. C. Rothwell, J. A. Obeso, M. M. Traub, and C. D. Marsden, “The behaviour of the long-latency stretch reflex in patients with Parkinson’s disease,” *J. Neurol. Neurosurg. Psychiatry*, vol. 46, no. 1, 1983, doi: 10.1136/jnnp.46.1.35.
[115] D. M. Herz and P. Brown, “Moving, fast and slow: behavioural insights into bradykinesia in Parkinson’s disease,” 2023. doi: 10.1093/brain/awad069.
[116] P. Brown and C. D. Marsden, “Bradykinesia and impairment of EEG desynchronization in Parkinson’s disease,” *Movement Disorders*, vol. 14, no. 3, 1999, doi: 10.1002/1531-8257(199905)14:3<423::AID-MDS1006>3.0.CO;2-V.
[117] B. Palakurthi and S. P. Burugupally, “Postural instability in parkinson’s disease: A review,” 2019. doi: 10.3390/brainsci9090239.
[118] S. D. Kim, N. E. Allen, C. G. Canning, and V. S. C. Fung, “Postural instability in patients with Parkinson’s disease: Epidemiology, pathophysiology and management,” 2013. doi: 10.1007/s40263-012-0012-3.
[119] J. J. Crouse, J. R. Phillips, M. Jahanshahi, and A. A. Moustafa, “Postural instability and falls in Parkinson’s disease,” 2016. doi: 10.1515/revneuro-2016-0002.
[120] C. G. Goetz *et al.*, “Movement Disorder Society-Sponsored Revision of the Unified Parkinson’s Disease Rating Scale (MDS-UPDRS): Scale presentation and clinimetric testing results,” *Movement Disorders*, vol. 23, no. 15, 2008, doi: 10.1002/mds.22340.
[121] C. C. Goetz, “The Unified Parkinson’s Disease Rating Scale (UPDRS): Status and recommendations,” 2003. doi: 10.1002/mds.10473.
[122] J. A. Opara, A. Małecki, E. Małecka, and T. Socha, “Motor assessment in parkinson’s disease,” 2017. doi: 10.5604/12321966.1232774.
[123] M. Richards, K. Marder, L. Cote, and R. Mayeux, “Interrater reliability of the unified Parkinson’s disease rating scale motor examination,” *Movement Disorders*, vol. 9, no. 1, 1994, doi: 10.1002/mds.870090114.
[124] A. Siderowf, M. McDermott, K. Kieburtz, K. Blindauer, S. Plumb, and I. Shoulson, “Test-retest reliability of the unified Parkinson’s disease rating scale in patients with early Parkinson’s disease: Results from a multicenter clinical trial,” *Movement Disorders*, vol. 17, no. 4, 2002, doi: 10.1002/mds.10011.
[125] J. L. Palmer, M. A. Coats, C. M. Roe, S. M. Hanko, C. Xiong, and J. C. Morris, “Unified Parkinson’s Disease Rating Scale-Motor Exam: Inter-rater reliability of advanced practice nurse and neurologist assessments,” *J. Adv. Nurs.*, vol. 66, no. 6, pp. 1382–1387, Jun. 2010, doi: 10.1111/j.1365-2648.2010.05313.x.
[126] A. Regnault, B. Boroojerdi, J. Meunier, M. Bani, T. Morel, and S. Cano, “Does the MDS-UPDRS provide the precision to assess progression in early Parkinson’s disease? Learnings from the Parkinson’s progression marker initiative cohort,” *J. Neurol.*, vol. 266, no. 8, pp. 1927–1936, Aug. 2019, doi: 10.1007/s00415-019-09348-3.
[127] Y. Kwon *et al.*, “Analysis of antagonistic co-contractions with motorized passive movement device in patients with parkinson’s disease,” in *Bio-Medical Materials and Engineering*, 2014. doi: 10.3233/BME-141042.
[128] S. Meunier, S. Pol, J. L. Houeto, and M. Vidailhet, “Abnormal reciprocal inhibition between antagonist muscles in Parkinson’s disease,” 2000.
[129] B. R. Bloem, D. J. Beckley, M. P. Remler, R. A. C. Roos, and J. Gert Van Dijk, “Postural reflexes in Parkinson’s disease during ‘resist’ and ‘yield’ tasks,” 1995.
[130] R. D. Seidler, “Neural correlates of motor learning, transfer of learning, and learning to learn,” 2010. doi: 10.1097/JES.0b013e3181c5cce7.
[131] R. H. Roth and J. B. Ding, “Cortico-basal ganglia plasticity in motor learning,” *Neuron*, vol. 112, no. 15, pp. 2486–2502, Aug. 2024, doi: 10.1016/J.NEURON.2024.06.014.
[132] J. L. Contreras-Vidal and E. R. Buch, “Effects of Parkinson’s disease on visuomotor adaptation,” *Exp. Brain Res.*, vol. 150, no. 1, 2003, doi: 10.1007/s00221-003-1403-y.
[133] L. Marinelli, A. Quartarone, M. Hallett, G. Frazzitta, and M. F. Ghilardi, “The many facets of motor learning and their relevance for Parkinson’s disease,” 2017. doi: 10.1016/j.clinph.2017.03.042.
[134] J. Cristini *et al.*, “Motor Memory Consolidation Deficits in Parkinson’s Disease: A Systematic Review with Meta-Analysis,” 2023. doi: 10.3233/JPD-230038.
[135] E. Heremans, E. Nackaerts, G. Vervoort, S. Broeder, S. P. Swinnen, and A. Nieuwboer, “Impaired retention of motor learning of writing skills in patients with Parkinson’s disease with freezing of gait,” *PLoS One*, vol. 11, no. 2, 2016, doi: 10.1371/journal.pone.0148933.
[136] R. Cools, R. A. Barker, B. J. Sahakian, and T. W. Robbins, “Mechanisms of cognitive set flexibility in Parkinson’s disease,” *Brain*, vol. 124, no. 12, 2001, doi: 10.1093/brain/124.12.2503.
[137] W. Schultz and A. Dickinson, “Neuronal coding of prediction errors,” 2000. doi: 10.1146/annurev.neuro.23.1.473.

[138] J. Diedrichsen, O. White, D. Newman, and N. Lally, “Use-dependent and error-based learning of motor behaviors,” *Journal of Neuroscience*, vol. 30, no. 15, pp. 5159–5166, Apr. 2010, doi: 10.1523/JNEUROSCI.5406-09.2010.
[139] R. Shadmehr, M. A. Smith, and J. W. Krakauer, “Error correction, sensory prediction, and adaptation in motor control,” 2010. doi: 10.1146/annurev-neuro-060909-153135.
[140] M. V. L. Bennett and R. S. Zukin, “Electrical Coupling and Neuronal Synchronization in the Mammalian Brain,” 2004. doi: 10.1016/S0896-6273(04)00043-1.
[141] C. G. Richter, R. Coppola, and S. L. Bressler, “Top-down beta oscillatory signaling conveys behavioral context in early visual cortex,” *Sci. Rep.*, vol. 8, no. 1, 2018, doi: 10.1038/s41598-018-25267-1.
[142] T. Bardouille, T. W. Picton, and B. Ross, “Attention modulates beta oscillations during prolonged tactile stimulation,” *European Journal of Neuroscience*, vol. 31, no. 4, 2010, doi: 10.1111/j.1460-9568.2010.07094.x.
[143] M. Wiener, A. Parikh, A. Krakow, and H. B. Coslett, “An intrinsic role of beta oscillations in memory for time estimation,” *Sci. Rep.*, vol. 8, no. 1, 2018, doi: 10.1038/s41598-018-26385-6.
[144] R. Schmidt, M. H. Ruiz, B. E. Kilavik, M. Lundqvist, P. A. Starr, and A. R. Aron, “Beta oscillations in working memory, executive control of movement and thought, and sensorimotor function,” in *Journal of Neuroscience*, 2019. doi: 10.1523/JNEUROSCI.1163-19.2019.
[145] E. Heinrichs-Graham, M. J. Kurz, J. E. Gehringer, and T. W. Wilson, “The functional role of post-movement beta oscillations in motor termination,” *Brain Struct. Funct.*, vol. 222, no. 7, 2017, doi: 10.1007/s00429-017-1387-1.
[146] R. Courtemanche, N. Fujii, and A. M. Graybiel, “Synchronous, Focally Modulated β-Band Oscillations Characterize Local Field Potential Activity in the Striatum of Awake Behaving Monkeys,” *Journal of Neuroscience*, vol. 23, no. 37, 2003, doi: 10.1523/jneurosci.23-37-11741.2003.
[147] A. Pogosyan *et al.*, “Parkinsonian impairment correlates with spatially extensive subthalamic oscillatory synchronization,” *Neuroscience*, vol. 171, no. 1, 2010, doi: 10.1016/j.neuroscience.2010.08.068.
[148] H. J. Luhmann, F. I. Arce-Mcshane, V. Litvak, J. Barone, and H. E. Rossiter, “Understanding the Role of Sensorimotor Beta Oscillations,” 2021, doi: 10.3389/fnsys.2021.655886.
[149] T. G. Simpson *et al.*, “The role of cortical beta oscillations in healthy motor control.”
[150] A. K. Engel and P. Fries, “Beta-band oscillations-signalling the status quo?,” 2010. doi: 10.1016/j.conb.2010.02.015.
[151] V. Chakarov, J. R. Naranjo, J. Schulte-Mönting, W. Omlor, F. Huethe, and R. Kristeva, “Beta-range EEG-EMG coherence with isometric compensation for increasing modulated low-level forces,” *J. Neurophysiol.*, vol. 102, no. 2, 2009, doi: 10.1152/jn.91095.2008.
[152] J. Gross, P. A. Tass, S. Salenius, R. Hari, H. J. Freund, and A. Schnitzler, “Cortico-muscular synchronization during isometric muscle contraction in humans as revealed by magnetoencephalography,” *Journal of Physiology*, vol. 527, no. 3, 2000, doi: 10.1111/j.1469-7793.2000.00623.x.
[153] S. Heitmann, T. Boonstra, P. Gong, M. Breakspear, and B. Ermentrout, “The rhythms of steady posture: Motor commands as spatially organized oscillation patterns,” *Neurocomputing*, vol. 170, 2015, doi: 10.1016/j.neucom.2015.01.088.
[154] A. Fry *et al.*, “Modulation of post-movement beta rebound by contraction force and rate of force development,” *Hum. Brain Mapp.*, vol. 37, no. 7, 2016, doi: 10.1002/hbm.23189.
[155] N. J. Ghosn, J. A. Palmer, M. R. Borich, L. H. Ting, and A. M. Payne, “Cortical beta oscillatory activity evoked during reactive balance recovery scales with perturbation difficulty and individual balance ability,” *Brain Sci.*, vol. 10, no. 11, 2020, doi: 10.3390/brainsci10110860.
[156] E. Heinrichs-Graham and T. W. Wilson, “Is an absolute level of cortical beta suppression required for proper movement? Magnetoencephalographic evidence from healthy aging,” *Neuroimage*, vol. 134, 2016, doi: 10.1016/j.neuroimage.2016.04.032.
[157] R. Kristeva-Feige, C. Fritsch, J. Timmer, and C. H. Lücking, “Effects of attention and precision of exerted force on beta range EEG-EMG synchronization during a maintained motor contraction task,” *Clinical Neurophysiology*, vol. 113, no. 1, 2002, doi: 10.1016/S1388-2457(01)00722-2.
[158] H. Tan, C. Wade, and P. Brown, “Post-movement beta activity in sensorimotor cortex indexes confidence in the estimations from internal models,” *Journal of Neuroscience*, vol. 36, no. 5, pp. 1516–1528, Feb. 2016, doi: 10.1523/JNEUROSCI.3204-15.2016.
[159] N. Swann *et al.*, “Intracranial EEG reveals a time- and frequency-specific role for the right inferior frontal gyrus and primary motor cortex in stopping initiated responses,” *Journal of Neuroscience*, vol. 29, no. 40, 2009, doi: 10.1523/JNEUROSCI.3359-09.2009.
[160] N. C. Swann *et al.*, “Roles for the pre-supplementary motor area and the right inferior frontal gyrus in stopping action: Electrophysiological responses and functional and structural connectivity,” *Neuroimage*, vol. 59, no. 3, 2012, doi: 10.1016/j.neuroimage.2011.09.049.
[161] S. G. Heideman, F. van Ede, and A. C. Nobre, “Temporal alignment of anticipatory motor cortical beta lateralisation in hidden visual-motor sequences,” *European Journal of Neuroscience*, vol. 48, no. 8, 2018, doi: 10.1111/ejn.13700.
[162] L. M. Parkes, M. C. M. Bastiaansen, and D. G. Norris, “Combining EEG and fMRI to investigate the post-movement beta rebound,” *Neuroimage*, vol. 29, no. 3, 2006, doi: 10.1016/j.neuroimage.2005.08.018.

[163] R. B. Leriche, N. A. Jackson, K. Peterson, Z. Aspandiar, V. Hufnagel, and N. C. Swann, “Reduced sensorimotor beta dynamics could represent a ‘slowed movement state’ in healthy individuals,” *Neuropsychologia*, vol. 172, p. 108276, Jul. 2022, doi: 10.1016/J.NEUROPSYCHOLOGIA.2022.108276.
[164] T. Gilbertson, E. Lalo, L. Doyle, V. Di Lazzaro, B. Cioni, and P. Brown, “Existing motor state is favored at the expense of new movement during 13-35 Hz oscillatory synchrony in the human corticospinal system,” *Journal of Neuroscience*, vol. 25, no. 34, 2005, doi: 10.1523/JNEUROSCI.1762-05.2005.
[165] A. Pogosyan, L. D. Gaynor, A. Eusebio, and P. Brown, “Boosting Cortical Activity at Beta-Band Frequencies Slows Movement in Humans,” *Current Biology*, vol. 19, no. 19, 2009, doi: 10.1016/j.cub.2009.07.074.
[166] B. A. Conway *et al.*, “Synchronization between motor cortex and spinal motoneuronal pool during the performance of a maintained motor task in man.,” *J. Physiol.*, vol. 489, no. 3, 1995, doi: 10.1113/jphysiol.1995.sp021104.
[167] D. J. McFarland, L. A. Miner, T. M. Vaughan, and J. R. Wolpaw, “Mu and beta rhythm topographies during motor imagery and actual movements,” *Brain Topogr.*, vol. 12, no. 3, 2000, doi: 10.1023/A:1023437823106.
[168] G. Pfurtscheller, A. Stancák, and C. Neuper, “Post-movement beta synchronization. A correlate of an idling motor area?,” *Electroencephalogr. Clin. Neurophysiol.*, vol. 98, no. 4, pp. 281–293, Apr. 1996, doi: 10.1016/0013-4694(95)00258-8.
[169] S. Little and P. Brown, “What brain signals are suitable for feedback control of deep brain stimulation in Parkinson’s disease?,” *Ann. N. Y. Acad. Sci.*, vol. 1265, no. 1, 2012, doi: 10.1111/j.1749-6632.2012.06650.x.
[170] S. Ricci *et al.*, “Beta oscillations during adaptation to inertial and velocity dependent perturbations,” in *Proceedings of the IEEE RAS and EMBS International Conference on Biomedical Robotics and Biomechatronics*, 2020. doi: 10.1109/BioRob49111.2020.9224309.
[171] A. G. Fischer, R. Nigbur, T. A. Klein, C. Danielmeier, and M. Ullsperger, “Cortical beta power reflects decision dynamics and uncovers multiple facets of post-error adaptation,” *Nat. Commun.*, vol. 9, no. 1, Dec. 2018, doi: 10.1038/s41467-018-07456-8.
[172] L. H. Arnal, “Predicting ‘when’ using the motor system’s beta-band oscillations,” *Front. Hum. Neurosci.*, no. JULY, 2012, doi: 10.3389/fnhum.2012.00225.
[173] C. E. Palmer, R. Auksztulewicz, S. Ondobaka, and J. M. Kilner, “Sensorimotor beta power reflects the precision-weighting afforded to sensory prediction errors,” *Neuroimage*, vol. 200, 2019, doi: 10.1016/j.neuroimage.2019.06.034.
[174] V. Betti, S. Della Penna, F. de Pasquale, and M. Corbetta, “Spontaneous Beta Band Rhythms in the Predictive Coding of Natural Stimuli,” 2021. doi: 10.1177/1073858420928988.
[175] B. Spitzer and S. Haegens, “Beyond the status quo: A role for beta oscillations in endogenous content (RE)activation,” Jul. 21, 2017, *Society for Neuroscience*. doi: 10.1523/ENEURO.0170-17.2017.
[176] S. Walker *et al.*, “Older Age Increases the Amplitude of Muscle Stretch-Induced Cortical Beta-Band Suppression But Does not Affect Rebound Strength,” *Front. Aging Neurosci.*, vol. 12, 2020, doi: 10.3389/fnagi.2020.00117.
[177] L. Spieser, H. B. Meziane, and M. Bonnard, “Cortical mechanisms underlying stretch reflex adaptation to intention: A combined EEG-TMS study,” *Neuroimage*, vol. 52, no. 1, 2010, doi: 10.1016/j.neuroimage.2010.04.020.
[178] R. Shadmehr and F. A. Mussa-Ivaldi, “Adaptive representation of dynamics during learning of a motor task,” *Journal of Neuroscience*, vol. 14, no. 5 II, 1994, doi: 10.1523/jneurosci.14-05-03208.1994.
[179] D. M. Wolpert, Z. Ghahramani, and M. I. Jordan, “An internal model for sensorimotor integration,” *Science (1979).*, vol. 269, no. 5232, 1995, doi: 10.1126/science.7569931.
[180] U. Halsband and R. K. Lange, “Motor learning in man: A review of functional and clinical studies,” *J. Physiol. Paris*, vol. 99, no. 4–6, 2006, doi: 10.1016/j.jphysparis.2006.03.007.
[181] K. R. Ridderinkhof, W. P. M. Van Den Wildenberg, S. J. Segalowitz, and C. S. Carter, “Neurocognitive mechanisms of cognitive control: The role of prefrontal cortex in action selection, response inhibition, performance monitoring, and reward-based learning,” *Brain Cogn.*, vol. 56, no. 2 SPEC. ISS., pp. 129–140, 2004, doi: 10.1016/j.bandc.2004.09.016.
[182] R. M. Hardwick, C. Rottschy, R. C. Miall, and S. B. Eickhoff, “A quantitative meta-analysis and review of motor learning in the human brain,” *Neuroimage*, vol. 67, 2013, doi: 10.1016/j.neuroimage.2012.11.020.
[183] T. Koelewijn, H. T. van Schie, H. Bekkering, R. Oostenveld, and O. Jensen, “Motor-cortical beta oscillations are modulated by correctness of observed action,” *Neuroimage*, vol. 40, no. 2, 2008, doi: 10.1016/j.neuroimage.2007.12.018.
[184] W. C. Gaetz *et al.*, “Brain Activity Reveals Multiple Motor-Learning Mechanisms in a Real-World Task,” 2020, doi: 10.3389/fnhum.2020.00354.
[185] S. Espenhahn *et al.*, “Sensorimotor cortex beta oscillations reflect motor skill learning ability after stroke,” *Brain Commun.*, 2020, doi: 10.1093/braincomms/fcaa161.
[186] N. Jenkinson and P. Brown, “New insights into the relationship between dopamine, beta oscillations and motor function,” 2011. doi: 10.1016/j.tins.2011.09.003.
[187] N. C. Rowland *et al.*, “Task-related activity in sensorimotor cortex in Parkinson’s disease and essential tremor: Changes in beta and gamma bands,” *Front. Hum. Neurosci.*, vol. 9, no. September, 2015, doi: 10.3389/fnhum.2015.00512.

[188] S. N. Meissner, V. Krause, M. Südmeyer, C. J. Hartmann, and B. Pollok, “The significance of brain oscillations in motor sequence learning: Insights from Parkinson’s disease,” *Neuroimage Clin.*, vol. 20, 2018, doi: 10.1016/j.nicl.2018.08.009.
[189] E. Heinrichs-Graham *et al.*, “Neuromagnetic evidence of abnormal movement-related beta desynchronization in Parkinson’s disease,” *Cerebral Cortex*, vol. 24, no. 10, 2014, doi: 10.1093/cercor/bht121.
[190] R. Lofredi *et al.*, “Beta bursts during continuous movements accompany the velocity decrement in Parkinson’s disease patients,” *Neurobiol. Dis.*, vol. 127, 2019, doi: 10.1016/j.nbd.2019.03.013.
[191] P. Brown, “Oscillatory nature of human basal ganglia activity: Relationship to the pathophysiology of parkinson’s disease,” 2003. doi: 10.1002/mds.10358.
[192] A. Schnitzler and J. Gross, “Normal and pathological oscillatory communication in the brain,” 2005. doi: 10.1038/nrn1650.
[193] A. A. Kühn, A. Kupsch, G. H. Schneider, and P. Brown, “Reduction in subthalamic 8-35 Hz oscillatory activity correlates with clinical improvement in Parkinson’s disease,” *European Journal of Neuroscience*, vol. 23, no. 7, 2006, doi: 10.1111/j.1460-9568.2006.04717.x.
[194] M. Weinberger *et al.*, “Beta oscillatory activity in the subthalamic nucleus and its relation to dopaminergic response in Parkinson’s disease,” *J. Neurophysiol.*, vol. 96, no. 6, 2006, doi: 10.1152/jn.00697.2006.
[195] H. S.D. *et al.*, “GABA-mediated changes in inter-hemispheric beta frequency activity in early-stage Parkinson’s disease,” *Neuroscience*, vol. 281, 2014.
[196] T. M. Herrington, J. J. Cheng, and E. N. Eskandar, “Mechanisms of deep brain stimulation,” 2016. doi: 10.1152/jn.00281.2015.
[197] C. H. Kuo, G. A. White-Dzuro, and A. L. Ko, “Approaches to closed-loop deep brain stimulation for movement disorders,” *Neurosurg. Focus*, vol. 45, no. 2, 2018, doi: 10.3171/2018.5.FOCUS18173.
[198] C. R. Honey *et al.*, “Deep Brain Stimulation Target Selection for Parkinson’s Disease,” in *Canadian Journal of Neurological Sciences*, 2017. doi: 10.1017/cjn.2016.22.
[199] E. Moro, R. J. A. Esselink, J. Xie, M. Hommel, A. L. Benabid, and P. Pollak, “The impact on Parkinson’s disease of electrical parameter settings in STN stimulation,” *Neurology*, vol. 59, no. 5, 2002, doi: 10.1212/WNL.59.5.706.
[200] Q. Li *et al.*, “Therapeutic Deep Brain Stimulation in Parkinsonian Rats Directly Influences Motor Cortex,” *Neuron*, vol. 76, no. 5, 2012, doi: 10.1016/j.neuron.2012.09.032.
[201] G. Tinkhauser *et al.*, “The modulatory effect of adaptive deep brain stimulation on beta bursts in Parkinson’s disease,” *Brain*, vol. 140, no. 4, 2017, doi: 10.1093/brain/awx010.
[202] M. C. Dalakas, “Stiff-person syndrome and related disorders-diagnosis, mechanisms and therapies,” *Nat. Rev. Neurol.*, vol. 20, pp. 587–601, 2024, doi: 10.1038/s41582-024-01012-3.
[203] C. Cepeda, N. Wu, V. M. André, D. M. Cummings, and M. S. Levine, “The corticostriatal pathway in Huntington’s disease,” 2007. doi: 10.1016/j.pneurobio.2006.11.001.
[204] P. McColgan and S. J. Tabrizi, “Huntington’s disease: a clinical review,” 2018. doi: 10.1111/ene.13413.
[205] A. Berardelli, J. C. Rothwell, M. Hallett, P. D. Thompson, M. Manfredi, and C. D. Marsden, “The pathophysiology of primary dystonia,” 1998. doi: 10.1093/brain/121.7.1195.
[206] S. Rona, A. Berardelli, L. Vacca, M. Inghilleri, and M. Manfredi, “Alterations of motor cortical inhibition in patients with dystonia,” *Movement Disorders*, vol. 13, no. 1, 1998, doi: 10.1002/mds.870130123.
[207] M. J. Wessel *et al.*, “Noninvasive theta-burst stimulation of the human striatum enhances striatal activity and motor skill learning,” *Nat. Neurosci.*, vol. 26, no. 11, 2023, doi: 10.1038/s41593-023-01457-7.
[208] L. Brinkman, A. Stolk, H. C. Dijkerman, F. P. De Lange, and I. Toni, “Distinct roles for alpha- and beta-band oscillations during mental simulation of goal-directed actions,” *Journal of Neuroscience*, vol. 34, no. 44, pp. 14783–14792, Oct. 2014, doi: 10.1523/JNEUROSCI.2039-14.2014.
[209] F. Budini *et al.*, “Alpha band cortico-muscular coherence occurs in healthy individuals during mechanically-induced tremor,” *PLoS One*, vol. 9, no. 12, 2014, doi: 10.1371/journal.pone.0115012.
[210] N. Kopell, G. B. Ermentrout, M. A. Whittington, and R. D. Traub, “Gamma rhythms and beta rhythms have different synchronization properties,” *Proc. Natl. Acad. Sci. U. S. A.*, vol. 97, no. 4, 2000, doi: 10.1073/pnas.97.4.1867.
[211] J. T. Gwin and D. P. Ferris, “Beta- and gamma-range human lower limb corticomuscular coherence,” *Front. Hum. Neurosci.*, no. AUGUST, 2012, doi: 10.3389/fnhum.2012.00258.
[212] J. Peng, T. Zikereya, Z. Shao, and K. Shi, “The neuromechanical of Beta-band corticomuscular coupling within the human motor system,” 2024, *Frontiers Media SA*. doi: 10.3389/fnins.2024.1441002.
[213] J. M. Kilner, S. N. Baker, S. Salenius, R. Hari, and R. N. Lemon, “Human cortical muscle coherence is directly related to specific motor parameters,” *Journal of Neuroscience*, vol. 20, no. 23, 2000, doi: 10.1523/jneurosci.20-23-08838.2000.
[214] R. Kristeva, L. Patino, and W. Omlor, “Beta-range cortical motor spectral power and corticomuscular coherence as a mechanism for effective corticospinal interaction during steady-state motor output,” *Neuroimage*, vol. 36, no. 3, pp. 785–792, Jul. 2007, doi: 10.1016/J.NEUROIMAGE.2007.03.025.
[215] A. Pogosyan, L. D. Gaynor, A. Eusebio, and P. Brown, “Boosting Cortical Activity at Beta-Band Frequencies Slows Movement in Humans,” *Current Biology*, vol. 19, no. 19, pp. 1637–1641, Oct. 2009, doi: 10.1016/J.CUB.2009.07.074.

[216] F. A. Mussa-Ivaldi, N. Hogan, and E. Bizzi, “Neural, mechanical, and geometric factors subserving arm posture in humans,” *Journal of Neuroscience*, vol. 5, no. 10, 1985, doi: 10.1523/jneurosci.05-10-02732.1985.
[217] T. Flash and F. Mussa-Ivaidi, “Human arm stiffness characteristics during the maintenance of posture,” Springer-Verlag, 1990.
[218] J. M. Dolan, “An investigation of postural and voluntary human arm impedance control,” 1991.
[219] R. E. Kearney and I. W. Hunter, “Dynamics of human ankle stiffness: Variation with displacement amplitude,” *J. Biomech.*, vol. 15, no. 10, 1982, doi: 10.1016/0021-9290(82)90090-2.
[220] K. Falconer, “Quantitative assessment of co-contraction at the ankle joint in walking,” *Electromyogr. Clin. Neurophysiol.*, vol. 25, no. 2–3, 1985.
[221] R. G. Lee and W. G. Tatton, “Long Latency Reflexes to Imposed Displacements of the Human Wrist: Dependence on Duration of Movement*,” 1982.
[222] T. E. Milner and C. Cloutier, “Damping of the wrist joint during voluntary movement,” *Exp. Brain Res.*, vol. 122, no. 3, 1998, doi: 10.1007/s002210050519.
[223] C. C. A. M. , H. J. C. Gielen, “Mathematical and computer modelling reports: A model of the motor servo: Incorporating nonlinear spindle receptor and muscle mechanical properties,” *Mathematical and Computer Modelling: An International Journal*, vol. 12, no. 3, Jan. 1989.
[224] H. Teräväinen, J. K. c. Tsui, E. Mak, and D. B. Calne, “Optimal Indices for Testing Parkinsonian Rigidity,” *Canadian Journal of Neurological Sciences / Journal Canadien des Sciences Neurologiques*, vol. 16, no. 2, 1989, doi: 10.1017/S0317167100028857.
[225] J. J. Crisco, W. M. R. Heard, R. R. Rich, D. J. Paller, and S. W. Wolfe, “The mechanical axes of the wrist are oriented obliquely to the anatomical axes,” *Journal of Bone and Joint Surgery*, vol. 93, no. 2, 2011, doi: 10.2106/JBJS.I.01222.
[226] S. Babadi, S. Vahdat, and T. E. Milner, “Neural substrates of muscle co-contraction during dynamic motor adaptation,” *Journal of Neuroscience*, vol. 41, no. 26, 2021, doi: 10.1523/JNEUROSCI.2924-19.2021.
[227] S. Beveridge, S. A. Herff, B. Buck, G. B. Madden, and H. C. Jabusch, “Expertise-Related Differences in Wrist Muscle Co-contraction in Drummers,” *Front. Psychol.*, vol. 11, 2020, doi: 10.3389/fpsyg.2020.01360.
[228] B. Berret, D. V. Id, E. B. Id, and J. Id, “Co-contraction embodies uncertainty: An optimal feedforward strategy for robust motor control,” 2024, doi: 10.1371/journal.pcbi.1012598.
[229] A. Ajoudani, N. Tsagarakis, and A. Bicchi, “Tele-impedance: Teleoperation with impedance regulation using a body-machine interface,” *International Journal of Robotics Research*, vol. 31, no. 13, 2012, doi: 10.1177/0278364912464668.
[230] T. E. Milner *et al.*, “Inability to activate muscles maximally during cocontraction and the effect on joint stiffness,” Springer-Verlag, 1995.
[231] R. J. Meara and F. W. J. Cody, “Relationship between electromyographic activity and clinically assessed rigidity studied at the wrist joint in parkinson’s disease,” *Brain*, vol. 115, no. 4, 1992, doi: 10.1093/brain/115.4.1167.
[232] R. J. Meara and F. W. J. Cody, “Stretch reflexes of individual parkinsonian patients studied during changes in clinical rigidity following medication,” *Electroencephalography and Clinical Neurophysiology/ Evoked Potentials*, vol. 89, no. 4, 1993, doi: 10.1016/0168-5597(93)90105-X.
[233] M. P. Caligiuri, “Portable device for quantifying parkinsonian wrist rigidity,” *Movement Disorders*, vol. 9, no. 1, 1994, doi: 10.1002/mds.870090109.
[234] R. Xia, K. Markopoulou, S. E. Puumala, and W. Z. Rymer, “A comparison of the effects of imposed extension and flexion movements on Parkinsonian rigidity,” *Clinical Neurophysiology*, vol. 117, no. 10, 2006, doi: 10.1016/j.clinph.2006.06.176.
[235] D. Powell, A. Joseph Threlkeld, X. Fang, A. Muthumani, and R. Xia, “Amplitude- and velocity-dependency of rigidity measured at the wrist in Parkinson’s disease,” *Clinical Neurophysiology*, vol. 123, no. 4, pp. 764–773, Apr. 2012, doi: 10.1016/J.CLINPH.2011.08.004.
[236] D. Powell, N. Hanson, A. Joseph Threlkeld, X. Fang, and R. Xia, “Enhancement of parkinsonian rigidity with contralateral hand activation,” *Clinical Neurophysiology*, vol. 122, no. 8, 2011, doi: 10.1016/j.clinph.2011.01.010.
[237] T. Rätsep and T. Asser, “Changes in viscoelastic properties of skeletal muscles induced by subthalamic stimulation in patients with Parkinson’s disease,” *Clinical Biomechanics*, vol. 26, no. 2, 2011, doi: 10.1016/j.clinbiomech.2010.09.014.
[238] P. Mazzoni, A. Hristova, and J. W. Krakauer, “Why don’t we move faster? Parkinson’s disease, movement vigor, and implicit motivation,” *Journal of Neuroscience*, vol. 27, no. 27, 2007, doi: 10.1523/JNEUROSCI.0264-07.2007.
[239] A. Fasano, A. Mazzoni, and E. Falotico, “Reaching and Grasping Movements in Parkinson’s Disease: A Review,” 2022. doi: 10.3233/JPD-213082.
[240] A. Melendez-Calderon, L. Bagutti, B. Pedrono, and E. Burdet, “Hi5: A versatile dual-wrist device to study human-human interaction and bimanual control,” in *IEEE International Conference on Intelligent Robots and Systems*, 2011. doi: 10.1109/IROS.2011.6048068.
[241] E. Ivanova, G. Carboni, J. Eden, J. Krüger, and E. Burdet, “For motion assistance humans prefer to rely on a robot rather than on an unpredictable human,” *IEEE Open J. Eng. Med. Biol.*, vol. 1, 2020, doi: 10.1109/OJEMB.2020.2987885.

[242] Y. Li, J. Eden, G. Carboni, and E. Burdet, “Improving Tracking through Human-robot Sensory Augmentation.”
[243] X. A. Takagi, S. Maxwell, X. A. Melendez-Calderon, and E. Burdet, “The dominant limb preferentially stabilizes posture in a bimanual task with physical coupling,” *J Neurophysiol*, vol. 123, pp. 2154–2160, 2020, doi: 10.1152/jn.00047.2020.-Humans.
[244] E. , M. M. , T. A. , F. I. , G. S. , & B. E. Wilhelm, “Investigating Tactile Sensation in the Hand Using a Robot-Based Tactile Assessment Tool,” *International Conference on Human Haptic Sensing and Touch Enabled Computer Applications*, pp. 17–24, Jul. 2016.
[245] D. F. Sakellariou, S. Dall’orso, E. Burdet, J.-P. Lin, M. P. Richardson, and V. M. Mcclelland, “Abnormal microscale neuronal connectivity triggered by a proprioceptive stimulus in dystonia,” *Scientific Reports* |, vol. 10, p. 20758, 123AD, doi: 10.1038/s41598-020-77533-w.
[246] N. Peña-Pérez, J. Eden, E. Ivanova, I. Farkhatdinov, and E. Burdet, “How virtual and mechanical coupling impact bimanual tracking,” *J. Neurophysiol.*, vol. 129, no. 1, pp. 102–114, Jan. 2023, doi: 10.1152/jn.00057.2022.
[247] J. Brown, A. Yurkewich, M. Zardbani, L. Cazenave, E. Burdet, and I. Farkhatdinov, “Measuring Muscle Activation with the HRX-1 Wrist Manipulation Robot,” in *IEEE International Conference on Rehabilitation Robotics*, IEEE Computer Society, 2025, pp. 1047–1052. doi: 10.1109/ICORR66766.2025.11062983.
[248] H. B€orner *et al.*, “Physically interacting humans regulate muscle coactivation to improve visuohaptic perception,” *J. Neurophysiol.*, vol. 129, no. 2, pp. 494–499, Feb. 2023, doi: 10.1152/jn.00420.2022.
[249] L. Cazenave *et al.*, “Hybrid Functional Electrical Stimulation and Robotic Assistance for Wrist Motion Training After Stroke: Preliminary Results,” in *IEEE International Conference on Rehabilitation Robotics*, IEEE Computer Society, 2023. doi: 10.1109/ICORR58425.2023.10304736.
[250] A. Dutta *et al.*, “Extended Reality Biofeedback for Functional Upper Limb Weakness: Mixed Methods Usability Evaluation,” *JMIR XR and Spatial Computing*, vol. 2, 2025, doi: 10.2196/68580.
[251] P. Angeles, Y. Tai, N. Pavese, S. Wilson, and R. Vaidyanathan, “Automated assessment of symptom severity changes during deep brain stimulation (DBS) therapy for Parkinson’s disease,” in *IEEE International Conference on Rehabilitation Robotics*, 2017. doi: 10.1109/ICORR.2017.8009462.
[252] G. Vignoud *et al.*, “Video-Based Automated Assessment of Movement Parameters Consistent with MDS-UPDRS III in Parkinson’s Disease,” *J. Parkinsons Dis.*, vol. 12, no. 7, 2022, doi: 10.3233/JPD-223445.
[253] K. S. Rudolph, M. J. Axe, and L. Snyder-Mackler, “Dynamic stability after ACL injury: Who can hop?,” *Knee Surgery, Sports Traumatology, Arthroscopy*, vol. 8, no. 5, 2000, doi: 10.1007/s001670000130.
[254] G. Li, M. S. Shourijeh, D. Ao, C. Patten, and B. J. Fregly, “How Well Do Commonly Used Co-contraction Indices Approximate Lower Limb Joint Stiffness Trends During Gait for Individuals Post-stroke?,” *Front. Bioeng. Biotechnol.*, vol. 8, 2021, doi: 10.3389/fbioe.2020.588908.
[255] V. S. C. Fung, J. A. Burne, and J. G. L. Morris, “Objective Quantification of Resting and Activated Parkinsonian Rigidity: A Comparison of Angular Impulse and Work Scores,” *Movement Disorders*, 2000, doi: 10.1002/1531-8257(200001)15:1<48::AID-MDS1009>3.0.CO;2-E.
[256] R. Cantello, M. Gianelli, D. Bettucci, C. Civardi, M. S. De Angelis, and R. Mutani, “Parkinson’s disease rigidity: Magnetic motor evoked potentials in a small hand muscle,” *Neurology*, vol. 41, no. 9, 1991, doi: 10.1212/wnl.41.9.1449.
[257] J. Levin, S. Krafzcyk, P. Valkovič, T. Eggert, J. Claassen, and K. Bötzel, “Objective measurement of muscle rigidity in Parkinsonian patients treated with subthalamic stimulation,” *Movement Disorders*, vol. 24, no. 1, 2009, doi: 10.1002/mds.22291.
[258] R. W. Angel, “Shortening reaction in normal and parkinsonian subjects,” *Neurology*, vol. 32, no. 3, 1982, doi: 10.1212/wnl.32.3.246.
[259] A. Prochazka *et al.*, “Measurement of Rigidity in Parkinson’s Disease,” *Movement Disorders*, vol. 12, no. 1, pp. 24–32, 1997, doi: 10.1002/mds.870120106.
[260] P. Costa, M. J. Rosas, R. Vaz, and J. P. Cunha, “Wrist rigidity assessment during Deep Brain Stimulation surgery,” in *Proceedings of the Annual International Conference of the IEEE Engineering in Medicine and Biology Society, EMBS*, 2015. doi: 10.1109/EMBC.2015.7319128.
[261] L. Raiano, G. Di Pino, L. Di Biase, M. Tombini, N. L. Tagliamonte, and D. Formica, “PDMeter: A Wrist Wearable Device for an at-Home Assessment of the Parkinson’s Disease Rigidity,” *IEEE Transactions on Neural Systems and Rehabilitation Engineering*, vol. 28, no. 6, 2020, doi: 10.1109/TNSRE.2020.2987020.
[262] T. Perera *et al.*, “A palm-worn device to quantify rigidity in Parkinson’s disease,” *J. Neurosci. Methods*, vol. 317, 2019, doi: 10.1016/j.jneumeth.2019.02.006.
[263] J. C. van den Noort *et al.*, “Quantification of Hand Motor Symptoms in Parkinson’s Disease: A Proof-of-Principle Study Using Inertial and Force Sensors,” *Ann. Biomed. Eng.*, vol. 45, no. 10, 2017, doi: 10.1007/s10439-017-1881-x.
[264] D. Powell, A. Joseph Threlkeld, X. Fang, A. Muthumani, and R. Xia, “Amplitude- and velocity-dependency of rigidity measured at the wrist in Parkinson’s disease,” *Clinical Neurophysiology*, vol. 123, no. 4, 2012, doi: 10.1016/j.clinph.2011.08.004.
[265] Kapandji I.A, *The Physiology of the Joints*, 5th ed., vol. 1. London: Churchill Livingstone, 1982.
[266] S. Aydore, D. Pantazis, and R. M. Leahy, “A note on the phase locking value and its properties,” *Neuroimage*, vol. 74, 2013, doi: 10.1016/j.neuroimage.2013.02.008.

[267] T. E. Milner and D. W. Franklin, “Impedance control and internal model use during the initial stage of adaptation to novel dynamics in humans,” *Journal of Physiology*, vol. 567, no. 2, 2005, doi: 10.1113/jphysiol.2005.090449.
[268] D. W. Franklin and D. M. Wolpert, “Computational mechanisms of sensorimotor control,” 2011. doi: 10.1016/j.neuron.2011.10.006.
[269] S. H. Scott, “Optimal feedback control and the neural basis of volitional motor control,” 2004. doi: 10.1038/nrn1427.
[270] J. G. Andrews and Y. Youm, “A biomechanical investigation of wrist kinematics,” *J. Biomech.*, vol. 12, no. 1, 1979, doi: 10.1016/0021-9290(79)90012-5.
[271] N. J. Davis, S. P. Tomlinson, and H. M. Morgan, “The role of beta-frequency neural oscillations in motor control,” 2012. doi: 10.1523/JNEUROSCI.5106-11.2012.
[272] J. B. De Graaf *et al.*, “Preparing for a motor perturbation: Early implication of primary motor and somatosensory cortices,” *Hum. Brain Mapp.*, vol. 30, no. 2, 2009, doi: 10.1002/hbm.20526.
[273] A. Mierau, T. Hülsdünker, H. K. Strüder, A. Gruart, A. C. De Lima-Pardini, and L. H. Ting, “Changes in cortical activity associated with adaptive behavior during repeated balance perturbation of unpredictable timing,” 2015, doi: 10.3389/fnbeh.2015.00272.
[274] R. Suzuki and J. Ushiyama, “Context-Dependent Modulation of Corticomuscular Coherence in a Series of Motor Initiation and Maintenance of Voluntary Contractions,” *Cereb. Cortex Commun.*, vol. 1, no. 1, Aug. 2020, doi: 10.1093/texcom/tgaa074.
[275] J. W. Chung, E. Ofori, G. Misra, C. W. Hess, and D. E. Vaillancourt, “Beta-band activity and connectivity in sensorimotor and parietal cortex are important for accurate motor performance,” *Neuroimage*, vol. 144, 2017, doi: 10.1016/j.neuroimage.2016.10.008.
[276] N. Zokaei, A. J. Quinn, M. T. Hu, M. Husain, F. Van Ede, and A. C. Nobre, “Reduced cortico-muscular beta coupling in Parkinson’s disease predicts motor impairment,” *Brain Commun.*, vol. 3, no. 3, 2021, doi: 10.1093/braincomms/fcab179.
[277] H. Park, J. S. Kim, S. H. Paek, B. S. Jeon, J. Y. Lee, and C. K. Chung, “Cortico-muscular coherence increases with tremor improvement after deep brain stimulation in Parkinson’s disease,” *Neuroreport*, vol. 20, no. 16, 2009, doi: 10.1097/WNR.0b013e328331a51a.
[278] G. A. Albanese, V. Falzarano, M. W. R. Holmes, P. Morasso, and J. Zenzeri, “A Dynamic Submaximal Fatigue Protocol Alters Wrist Biomechanical Properties and Proprioception,” *Front. Hum. Neurosci.*, vol. 16, 2022, doi: 10.3389/fnhum.2022.887270.
[279] K. R. Lohse and D. E. Sherwood, “Thinking about muscles: The neuromuscular effects of attentional focus on accuracy and fatigue,” *Acta Psychol. (Amst).*, vol. 140, no. 3, pp. 236–245, Jul. 2012, doi: 10.1016/J.ACTPSY.2012.05.009.
[280] C. Zich, A. J. Quinn, L. C. Mardell, N. S. Ward, and S. Bestmann, “Dissecting Transient Burst Events,” 2020. doi: 10.1016/j.tics.2020.07.004.
[281] R. Merletti, A. Holobar, and D. Farina, “Analysis of motor units with high-density surface electromyography,” 2008. doi: 10.1016/j.jelekin.2008.09.002.
[282] A. Del Vecchio, A. Holobar, D. Falla, F. Felici, R. M. Enoka, and D. Farina, “Tutorial: Analysis of motor unit discharge characteristics from high-density surface EMG signals,” *Journal of Electromyography and Kinesiology*, vol. 53, 2020, doi: 10.1016/j.jelekin.2020.102426.
[283] A. B. Leger and T. E. Milner, “Passive and active wrist joint stiffness following eccentric exercise,” *Eur. J. Appl. Physiol.*, vol. 82, no. 5–6, 2000, doi: 10.1007/s004210000227.
[284] E. Todorov and M. I. Jordan, “Optimal feedback control as a theory of motor coordination,” *Nat. Neurosci.*, vol. 5, no. 11, 2002, doi: 10.1038/nn963.